DEVOLATILISATION AND VOLATILE MATTER COMBUSTION DURING FLUIDISED-BED GASIFICATION OF LOW-RANK COAL

by

Davide ROSS

Thesis submitted for the degree of

Doctorate of Philosophy

in

The University of Adelaide

Department of Chemical Engineering

Faculty of Engineering

January 2000

DECLARATION

This work contains no material which has been accepted for the award of any other degree or diploma in any university or any other tertiary institution, and to the best of my knowledge and belief, contains no material previously published or written by any other person, except where due reference has been made in the text.

I give consent to this copy of my thesis, when deposited in the University Library, being made available for photocopying and loan.

SIGNED : ..... DATE : 10/11/2009.....

ACKNOWLEDGMENTS

I am most privileged to have had Professor Dong-ke Zhang as a supervisor and my many thanks go to him for his guidance, encouragement and faith through the hard times during the course of this project. You have provided me with a wonderful opportunity in life that I otherwise would have overlooked, for this I show my most sincere appreciation.

I would like to gratefully acknowledge the Cooperative Research Centre for New Technologies for Power Generation from Low Rank Coal for providing the financial support that enabled me to undertake this project.

I would like to extend my greatest appreciation to Dr. Hong Ming Yan for his help and patience in the task of aiding with model development. I am in truly indebted for the time and effort you have spent with me.

A number of colleagues have been invaluable to me throughout this project, for their constructive comments, insights and help. For this, I would like to thank Adam Kosminski, Dr Craig Heidenreich, Grant Schluter, Dr Hari Vuthaluru and Dr Ying-he He. A big thankyou must also go to the chemical engineering workshop staff: Brian Mulcay, Peter Kay and especially Jason Peak for their assistance during my very frequent passage to their door step and to the secretaries: Mary, Elaine and Lynette in non technical matters

Finally, I would like to thank my family for their love and on-going support with which I am eternally blessed and to the Paesano boys for the many stress relieving (?) cycling diversions during the course of the project.

SUMMARY

It is increasingly apparent that for coal to be economically competitive, integrated gasification combined cycle (IGCC) systems are the key to obtaining higher efficiency and superior environmental performance required for power generation. The influence of volatile matter evolved during devolatilisation on the performance of low-rank coal fluidised-bed combustors has been recognised. Similar interactions are expected to occur in a fluidised-bed gasifier, but data is presently lacking in the literature.

The time taken for a coal particle to devolatilise along with coal particle mixing within the bed determines the location of volatile release in the bed for subsequent mixing with oxygen and combustion. The devolatilisation times of seven coals were determined by measuring the centre temperature response for single particles held stationary in a bench scale atmospheric fluidised-bed reactor. Bed temperature, oxygen concentration, particle size, moisture content and coal rank were found to influence the devolatilisation time. It was observed that the devolatilisation time was directly proportional to the particle diameter, contrary to current theory based on heat transfer control, which defines a square law relationship. In comparing current technique with other experimental methods, discrepancies in the reported exponent parameter values n, from correlation with devolatilisation time power law relation has been resolved. The effect of coal type and coal moisture content on the variation of reported exponent parameter values has also been highlighted. A new theoretical treatment to distinguish between heat transfer and chemical-kinetically controlled regimes of coal devolatilisation has been used to derive an analogous equation to that of the empirical power-law correlation with an exponent, n, equal to 0.94. It is now possible to quantitatively define the correlation parameter A, and explain experimental observations relating to the influence of bed temperature and gas atmosphere upon the devolatilisation time. The observed effects of these variables are consistent with that of heat transfer to and within the particle as the rate controlling step for large particle devolatilisation in fluidised-beds.

The influence of the combustion of a synthetic volatile (propane) simulating the presence of coal volatiles emitted by devolatilising coal particles upon the combustion rate of Loy Yang coal was investigated. A comparison of the single particle burn-out time of char particles as a function of bed temperature found that the char burnout times increased substantially between 13 to 88% as temperature was raised from 700°C to 900°C, respectively, upon the introduction of 3% v/v propane into a fluidising gas stream containing 10% v/v oxygen and balanced by nitrogen. The increasing difference in the burnout times with increasing bed temperature is associated with the transition of over-bed to in-bed combustion of propane. At the highest bed temperature of 900°C, the rate of char combustion is diffusion controlled while the influence of kinetics is evident at the lower bed temperatures. The ash layer formed during char burn-out does not impose any additional resistance on the char combustion rate.

The axial gas concentration profiles in a laboratory scale fluidised bed gasifier at three bed temperatures of 750°C, 850°C and 950°C have been reported. At each bed temperature, four experimental conditions were evaluated: Propane pyrolysis (nitrogen/steam), Propane gasification, Char gasification and Propane/char gasification (all air/steam). The experimental results reported here are believed to provide the first comprehensive data on volatiles combustion in a fluidised-bed gasifier. For all conditions, propane conversion whether via thermal cracking or oxidation reactions, increased with increasing bed height and temperature. For the lowest bed temperature of 750°C under propane gasification condition, propane conversion is characterised by a sudden explosive reaction at the bed surface. As the bed temperature is successively increased, propane conversion occurs increasingly throughout the bed. Introduction of a char feed to simulate gasification environment results in the rapid consumption of oxygen. At the lowest bed temperature of 750°C, char combustion dominates over gasification. With rising bed temperature, gasification plays an increasing role, with associated carbon monoxide yield increasing and correspondingly higher when compared to char gasification only. Thus indicating the relative contribution of partial volatile combustion to fuel gas yields. The char bed enhanced secondary decomposition reactions.

A comprehensive non-isothermal numerical model of gas combustion under fluidised-bed coal gasification conditions was developed. The model is based on the two-phase theory of fluidisation and incorporates the 'net flow' concept as well as temperature and concentration dependent thermodynamic properties. For char gasification conditions the model results under predicted the oxygen consumption rate, primarily due to the uncertainties in the choice of the product distribution coefficient, ϕ, for the CO/CO_2 combustion products in the char partial combustion reaction scheme. The majority of oxygen consumed within the bed was by heterogenous partial combustion reactions. Sensitivity analysis on the influence of kinetic parameters found that the model predictions were most sensitive to propane pyrolysis reactions. A best-fit kinetic representation for propane combustion was determined by minimisation of the total sum-squared error applied to changes in the pre-exponential rate constant.

For co-gasification of propane and char at 750°C the model predicts a significant proportion of homogeneous combustion to occur within the bed contrary to experimental observations. However, model predictions were exceptionally good for the higher bed temperature of 950°C, associated with stable in-bed combustion of propane. Most importantly, the addition of propane resulted in an increasing proportion of oxygen to be consumed by homogeneous rather than heterogeneous partial combustion reactions. This results in an increase in carbon conversion due to char gasification reactions. Thus, the importance of increasing the in-bed combustion efficiency of volatiles upon char combustion and gasification rates and oxygen consumption distribution between volatiles and char has been successfully demonstrated.

Parametric studies have shown decreasing the bed particle size and excess fluidisation velocity favours an increase in the in-bed combustion efficiency of propane. This is in accordance with previous observations in the literature under fluidised-bed combustion conditions. However, the information regarding the measured temperature profiles of gases in the fluidised-bed coal gasifier has been neither measured in the experiments nor found in the literature, and this leads to some difficulties for the verification of the predicted temperature profiles from the model.

TABLE OF CONTENTS

LIST OF FIGURES

LIST OF TABLES

CHAPTER 1

INTRODUCTION

1.1 BACKGROUND

Since the oil crisis in the early seventies and the more recent progression of energy and chemical industries to using natural gas, it is increasingly realised that over dependence on one energy source is not a desirable long term strategy (Farina, 1996). The enormous resources of low-rank coal as an abundant fuel source around the world have become the focus for development in power generation. Their utilisation through conventional pulverised combustion technology is often problematic due to their inherently high contents of moisture and inorganic material (Zhang et al., 1997; Guruajan et al., 1992). The development of cost competitive power generation technologies from low-rank coals will be highly dependent on the ability to meet the most stringent environmental challenges facing the world including the emission of greenhouse gases. This has seen the emergence of fluidised-bed combustion and gasification as the current leading technologies for power generation from low-rank coals (Zhang et al., 1997). Fluidised-bed combustion of coal integrated with conventional steam-turbine generation has been well established in the power utility market, with significant advancements in efficiency to be made in the development of pressurised systems. However, it is increasingly apparent that for low-rank coals to be economically competitive, especially against natural gas, integrated gasification combined cycle (IGCC) systems are the key to obtaining higher efficiency and superior environmental performance required for power generation (Farina, 1996; Griffiths, 1996). Overall energy efficiency of the IGCC process based on coal is between 43-45%, well above conventional pulverised coal combustion systems. These efficiencies are expected to rise significantly with improvements in gas turbine technology and high temperature gas clean-up systems. Consequently and most importantly, carbon dioxide emissions are reduced with sulphur capture efficiency in excess of 99.5%, and NO_x and particulate emissions below 30 and 3 ppm respectively (Farina, 1996).

1.2 CRC FOR NEW TECHNOLOGIES FOR POWER GENERATION FROM LOW-RANK COAL

One third of electricity generated from coal in Australia relies on low-rank coal as the primary energy source (Zhang, 1996). Utilisation of the large reserves of low-rank coal deposits for power generation has, however, not yet reached full potential due to economical, processing and environmental constraints. Conventional boiler power plants using low rank-coals operate at efficiencies typically around 25-30 %. This is a consequence of the significant moisture contents of these coals (up to 60 wt % as mined) which significantly reduces the specific heating value to well below 10 $MJkg^{-1}$ (Brockway and Higgins, 1991). As a result, larger and more expensive boilers are required to handle the higher throughput of coal necessary and results in increased emissions of greenhouse gases.

Following the 1998 Kyoto climate conference for the reduction of greenhouse gas emissions, Australia, along with the rest of the world were set with specific targets for CO_2 emissions by 2010. It is envisioned that technological improvements of existing plants along with the development of more efficient advanced power generation cycles will be the main mitigation methods to reduce, or at least sustain emissions at the present levels (McIntosh, 1998).

The Cooperative Research Centre (CRC) for Power Generation from Low-Rank Coal was established in 1993 to conduct research into aspects of those new generation technologies and processes that have the best prospects of overcoming the principle challenges facing the future use of low-rank coal as a competitive energy source for electricity generation. The main objectives of the centre are to provide basic understanding of power generation processes and coal behaviour; provide scientific and engineering support for the development of new process technologies and their commercial application; ensure a resource of suitably trained graduates with advanced knowledge in future power generation systems for Australian companies and electricity authorities; provide the necessary technical support for the export of such technologies to developing nations.

1.3 LOW-RANK COAL RESERVES AND RESOURCES IN SOUTH AUSTRALIA AND VICTORIA

South Australia and Victoria contain some of the world's most significant deposits of low-rank coal. These are currently utilised to provide the mainstay of electrical power generation to these states' grid using conventional pulverised coal combustion technology. The coal resources in South Australia are located at Leigh Creek, Lock and in a number of small deposits in the southeast corner of the state. Leigh Creek and Lock coals are sub-bituminous in rank, while the southeastern deposits are lignites. Leigh Creek is currently the only active coal deposit utilised within the state and is mined from the Telford basin with a resource of approximately 500 million tonnes, which is used to fuel the 500 MW Northern Power Station and the 240 MW Thomas Playford B Power Station. Bowmans coal deposit is the largest known tertiary deposit of lignite in South Australia, containing 1250 million tonnes. The other major deposit located within North Vincent Basin is at Lochiel (625 million tonnes). Smaller resources are located at Beufort, Clinton and Whitwarta. Deposits of the Murray basin include Sedan (184 million tonnes), Anna (84 million tonnes) and Kingston (12 million tonnes). These lignite deposits are currently not utilised because of their high moisture, chlorine, sodium, sulphur and ash contents (Mackay, 1996).

All Victorian coals are of low-rank except for a few thin seams of bituminous coal. Brown coal deposits are located in three major basins, the Murray, Otway and Gippsland. The Gippsland Basin is one of the world's major coal and petroleum bearing basins, which occupies an area of approximately 40,000 sq km. The major economic coal deposit of the Gippsland Basin occurs in the Latrobe Valley, where three seams, namely the Yallourn, Morwell and Traralgon, make up the estimated resource of 107,847 million tonnes (Mackay, 1996) with a readily recoverable reserve of 11,630 million tonnes (Gloe and Holdgate, 1991). The Latrobe Valley contains four conventional pulverised coal fired power stations, the largest of which is Loy Yang A with four 500 MW units and the smaller Loy Yang B with two 500 MW units. Other power stations are Hazelwood (1600 MW) and Yallourn W (1450 MW) (Gloe and Holdgate, 1991).

1.4 KEY ISSUES

Gasification is a complex process whereby carbonaceous material is converted to a gaseous fuel by reaction with oxygen and steam. This simplifies the subsequent combustion process, eases handling problems and facilitates removal of sulphur and nitrogen compounds and particulates. Successful performance of an IGCC plant depends on the ability of the coal gasifier to produce fuel gas with high steam and coal conversion efficiency and low emission levels (van Liere et al., 1996; Gururajan et al., 1992). Considerable research into char gasification and combustion reactions has been undertaken. Consequently, many of the primary process and design considerations for fluidised-bed combustors and gasifiers, FBC and FBG, have focused on the optimisation of the underlying char reactions (Bastista-Margulis et al. 1996). However, the performance of low-rank coal in pilot-scale fluidised-beds has been shown to be greatly dependent on the behaviour of volatile matter evolved during coal devolatilisation, and subsequent decomposition and combustion reactions (Gururajan et al., 1992). This is not at all surprising given that up to 50% of the specific energy of the coal is released as volatile matter. The importance of volatile combustion and its influence on NO_x formation and heat distribution flux between the bed and freeboard has been acknowledged in FBC of low rank coals. Detailed experimental investigations have been conducted to elucidate factors affecting the rate and location of in-bed volatile combustion under FBC conditions. Some of the factors that play a role in this process are:

1. The rate of volatile evolution during coal devolatilisation
2. The rate of coal particle mixing on injection into the bed
3. The bed temperature
4. The rate of mixing of volatiles with oxygen

In general terms, the rate of volatile combustion in FBC is considered to be limited by the rate of mixing of volatiles and oxygen. However, the amount of over-bed burning increases rapidly as the bed temperature falls below a critical value. Therefore, the above assumption is not strictly valid at low bed temperatures.

However, for FBG of coal there are distinct differences in relation to the bed environment. Unlike FBC where the principal make up of the bed is inert sand, for FBG the proportion of reactant, that is char, is typically an order of magnitude greater (1-3 % versus 25-50 %). Furthermore, oxygen is provided in excess quantities to ensure complete combustion in FBC unlike the reducing atmosphere of a gasifier. The potential implications for FBG of coal are:

1. The reducing environment will lead to significant thermal cracking and partial combustion of volatiles to CO.
2. The high proportion of char inventory within the bed will ensure the complete consumption of oxygen well before the bed surface and possibly influence the rate and mechanism of secondary decomposition reactions of the volatiles.
3. The possible requirement of secondary air injection into the freeboard to oxidised any high molecular weight species to prevent gas turbine damage and increase fuel gas exit temperature to maximise hot gas efficiency.

The qualitative implication of considering in-bed volatile combustion phenomena as a finite rate process in char reactions in FBG has been summarised as follows by Gururajan et al. (1992). If volatile combustion is rapid within the bed, depletion in the local oxygen concentration will occur, thus resulting in a greater extent of char gasification for sufficient particle residence times. Although, if the combustion rate is slow or incomplete within the bed, more oxygen will be available for char combustion reactions and consequently reducing char gasification conversion. The importance of considering the in-bed gas phase reactions of the volatiles and its effect on char combustion reaction rates has received scant attention in the literature. Thus, there is an immediate need for experimental investigation of both the influence of volatile combustion on the char combustion rate, particularly for highly reactive chars typically derived from low-rank coals and on the gas phase reactions of volatile components in environments simulating fluidised-bed gasification. Such data is essential to the development of a suitable mathematical model with an improved predictive capability.

1.5 SCOPE AND STRUCTURE OF THESIS

The processes leading to and including volatile combustion are of vital significance to understanding fluidised-bed gasification of low-rank coals. Thus, a systematic study of large coal particle devolatilisation and subsequent decomposition and combustion of volatiles and its effect upon char combustion reaction rates, will provide much needed fundamental data for modelling of volatile combustion in a fluidised-bed gasifier. The work presented in this study operates in parallel with a number of other projects within the CRC which includes;

- Mathematical modelling of devolatilisation of large low-rank coal particles, gasification kinetics of chars with steam and carbon dioxide.
- Sulphur release and in-situ desulphurisation.
- Computational fluid dynamic models to investigate hydrodynamic behaviour.

Ultimately it is envisioned that these various fields of study are to be integrated and developed to form a comprehensive mathematical model for the hydrodynamic and kinetic behaviour of a bubbling fluidised-bed gasifier.

The literature review presented in Chapter 2 will critically analyse previously published literature with respect to in-bed volatile combustion phenomena in bubbling fluidised-beds and its subsequent modelling, with particular emphasis on devolatilisation times of mm-sized low-rank coal particles and the combustion behaviour of pre-mixed hydrocarbon gas mixtures and its influence on char combustion rates. Ultimately this review will present an in-depth background to the present status of research and introduces the specific objectives of this work with respect to previous studies.

Chapter 3 details the experimental equipment and techniques employed in the current investigations. Chapters 4 to 6 summarise the findings of the various experiments conducted. Chapter 4 discusses the effects of various process variables on the particle devolatilisation time by measuring the particle centre temperature history and the development of a new theoretical treatment for coal particle devolatilisation time.

Chapter 5 reports the results of the combustion of volatile matter, simulated by propane, and its interaction with char combustion reactions.

Chapter 6 summarises the results of combustion, gasification and decomposition reactions occurring for propane under conditions prevailing for propane pyrolysis (in a nitrogen/steam fluidised-bed) and propane gasification (in an air/steam fluidised-bed, with and without char feed) with comparison to char gasification only (in an air/steam fluidised-bed without propane).

The development of a fluidised-bed gasifier model incorporating pre-mixed propane combustion will be outlined in Chapter 7. The model results considering the kinetic sensitivity analysis will be employed in Chapter 8 to predict experimental data collected in Chapter 6, as a means of validating the model. A summary of the work presented will be given in Chapter 9 and the implications of the present work for future investigations in the areas of coal research will be discussed.

CHAPTER 2

LITERATURE REVIEW

2.1 INTRODUCTION

This chapter reviews the published literature with respect to in-bed volatile combustion phenomena in bubbling fluidised-beds and its subsequent modelling, with particular emphasis placed on devolatilisation times of mm-sized low-rank coal particles and the combustion behaviour of pre-mixed hydrocarbon gas mixtures. Ultimately this review will present an in-depth background to the present status of research, and assist in defining the objectives of this work with respect to previous studies.

2.2 COAL FUNDAMENTALS

Coal is a complex organic polymer that originates from peat, formed from the accumulation and decomposition of organic matter in vast swamps millions of years ago. The organic matter may initially be degraded by aerobic and anaerobic bacteria, but it is the deposition of sediments (sands, clays, etc) that act to bury the peat, that the process of low grade metamorphosis involving the application of heat and pressure, termed *coalification* (Mackay, 1996), transforms peat into coal. Initially these processes include dewatering via the reduction of porosity by decomposition and compaction, formation of humates and gelification (Mackay, 1996). The chemical transformation of coal occurs in a series of steps which progressively reduce the oxygen content and increase the proportion of carbon by numerous reactions including dehydration, decarboxylation and demethoxylation (Figueiredo et al., 1986). The extent of thermal maturation of the coal is dependent upon the environment and circumstance such as the depth of the overburden deposited, which determines the temperature and pressure to which the peat was exposed. The coal structure usually consists primarily of organic material with small quantities of inorganic material. The inorganic matter is distributed in a heterogenous manner both at the macroscopic and microscopic levels.

The organic structure of low-rank coals (brown coals or lignites) which are of interest to the CRC for Power Generation, are at an intermediate stage of development between peat, (which contains significant proportions of cellulose and lignin) and sub-bituminous coal (which have lost the majority of their carboxyl and methoxyl groups) (Woskobenko et al., 1991).

Coal consists of lamellae containing nuclei of aromatic or hydroaromatic ring clusters (low-rank coals typically having between one to three rings), with various substituted heteroatoms (N,O,S) and functional groups (carbonyl, carboxyl, ethers and phenols). These lamellae are crosslinked by covalent polymethylene, etheric-oxygen and sulphur bridges, non-covalent bonds, hydrogen bonds and Van der Waal forces (Figueiredo et al., 1986 and Gavalas, 1982). A proportion of weakly bonded or physically trapped material is also present. The inorganic material can take the form of discrete mineral species or chemical complexes with the coal, such as carboxylates.

With increasing rank, the coal exhibits a changing structure that includes (Derbyshire et al., 1996):

- an increase in aromaticity and a reduction in aliphatic content
- elimination of oxygen functionalities
- a decrease in the extent of hydrogen bonding and covalent linkages
- an increase in aromatic-aromatic interactions

These changes in structure with rank are broadly defined by the American Society for Testing Materials, or ASTM. The ASTM standard classification of coals is based on the amounts of fixed carbon, volatile matter, heating value and agglomerating tendency and is shown in Table 2.1. This classification shows that the fixed carbon content and heating value increase with coal rank, whereas volatile matter content decreases with rank. It is this particular aspect, volatile matter content, which can account for up to 50% of the weight loss incurred by low-rank coals and its behaviour upon evolution within the bed that is the focus of this review.

Table 2.1 ASTM Classification of Coals. (Mitchell, 1943)

Class	Group	Fixed Carbon (DAF basis) %	Volatile Matter (DAF basis) %	Heating Value (DAF basis) MJ/kg
Anthracite	Meta-anthracite	> 98	< 2%	> 32.5
	Anthracite	92 - 98	2 - 8	> 32.5
	Semi-anthracite	86 - 92	8 - 14	> 32.5
Bituminous	Low-volatile	78 - 86	14 - 22	> 32.5
	Medium-volatile	69 - 78	22 - 31	> 32.5
	High-volatile A	< 69	> 31	30.2 - 32.5***
	High volatile B			26.7 - 30.2***
	High volatile C			24.4 - 26.7**
Subbituminous	Subbituminous A			24.4 - 26.7*
	Subbituminous B			22.1 - 24.4
	Subbituminous C			19.3 - 22.1
Lignitic	Lignite			14.6 - 19.3
	Brown coal			< 14.6

* non-agglomerating
** agglomerating
*** commonly agglomerating

2.3 DEVOLATILISATION FUNDAMENTALS

Devolatilisation is an intrinsic step in coal conversion processes, accounting for up to 50% of the weight loss incurred by low-rank coals. It is a physio-chemical process dependent on the organic properties of the coal. As the particle temperature rises, the coal matrix undergoes irreversible internal transformations. Various chemical bonds undergo thermal cleavage which results in the release of low molecular weight gas species such as CO, CO_2, H_2, CH_4, C_2H_6 etc., chemical H_2O, tarry species (volatiles which condense at room temperature) along with occluded gases. The residual mass, which is enriched in carbon and depleted in oxygen and hydrogen, and still containing some nitrogen and sulphur, and most of the mineral matter, is referred to as char. The heterogeneous nature of coal and the complexity of the process has resulted in a lack of agreement on the rates and mechanisms postulated to occur. This has hindered the development of a predictive model for the devolatilisation process. The devolatilisation of coal has been extensively reviewed by numerous authors (Gavalas, 1982; van Heek and Hodek, 1994; Solomon et al., 1993; Anthony et al., 1975; Suuberg et al., 1979; Anthony and Howard, 1976; Juntgen, 1984; Solomon and Colket, 1979; Kobayashi et al., 1977). The majority of the work carried out on devolatilisation has concentrated on determining the influence of various operating parameters upon the devolatilisation rate and the product yield and distribution relevant to pulverised coal. Of these operating parameters, the most significant is the temperature. Examination of the numerous experimental devolatilisation data show that the rates, compositions and yields after a given time change significantly with increasing temperature.

Typical product evolution profiles for fluidised bed pyrolysis of Loy Yang coal is shown in Figure 2.1 (Tyler, 1979). On heating of the coal from room temperature, the first specie to evolve is water from the evaporation of coal moisture. Occluded gases such as carbon dioxide and methane also evolve. Thermal decomposition of the coal matrix commences in the temperature range between 150 to 400°C, depending on coal type. This results in the evolution of tarry species, C_1-C_4 saturated and unsaturated hydrocarbons, oxides of carbon and water.

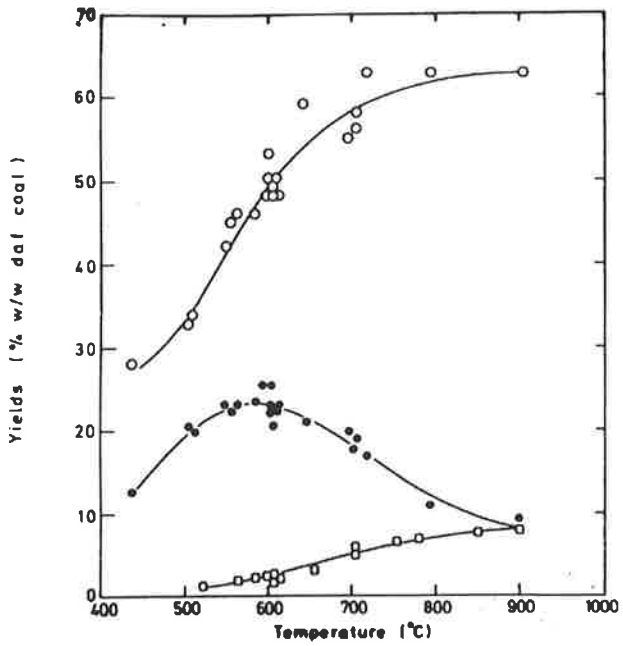

Figure 2.1 Effect of pyrolysis temperature on yields of total volatile matter (○), tar (●) and C_1-C_3 hydrocarbons (□) from Loy Yang coal (reproduced from Tyler, 1979)

Low-rank coals contain significant proportions of oxygen containing functional groups, principally carboxyl and phenolic groups. Thermal decomposition of the acid form carboxyl groups and phenolic groups have been found to commence at temperatures as low as 150°C to yield CO_2 and H_2O, and above 300°C to yield CO respectively (Caragelo et al., 1987; Scafer, 1979). At about 900°C, all carboxyl and phenolic groups have completely decomposed, with temperatures for maximum rates of evolution for CO_2, H_2O and CO for Yallourn coal occurring at 300, 350 and 500-600°C, respectively (Scafer, 1979). The evolution of C_1-C_3 saturated and unsaturated hydrocarbons commences between 400 and 500°C, which is associated with the cleavage of aliphatic bonds. Typical product yields obtained during fluidised bed pyrolysis of Loy Yang brown coal for CH_4, C_2H_2, C_2H_4, C_2H_6, C_3H_6 and C_3H_8 as a function of temperature are shown in Figure 2.2 (Tyler, 1979). The evolution of the condensable tar fraction commences between 300 and 400°C, with tar yields increasing to a maximum at 500 to 650°C. Above these temperatures, tar yields decline because of secondary decomposition reactions occurring during the diffusion through the pore network.

Primary tar species undergo thermal cracking, dehydrogenation, aromatisation and condensation reactions resulting in the formation of further light hydrocarbon gases, solid char and a subsequent increase in aromaticity of tar with increasing temperature (Collin et al., 1980). In the temperature range of 435-600°C, the aromatic portion of the tar becomes increasingly substituted, resulting in higher aliphatic hydrogen content. Beyond 600°C the aliphatic content of the tar decreases. Tyler (1979) observed that the tar atomic H/C ratio decreased from 1.35 to 0.85 over the temperature range from 435 to 900°C. The tar yield is strongly dependant on the competition between intra-particle mass transport and secondary reactions, with the balance dependent upon the time-temperature history, which in turn is dependent upon process conditions and thermo-physical properties of the coal.

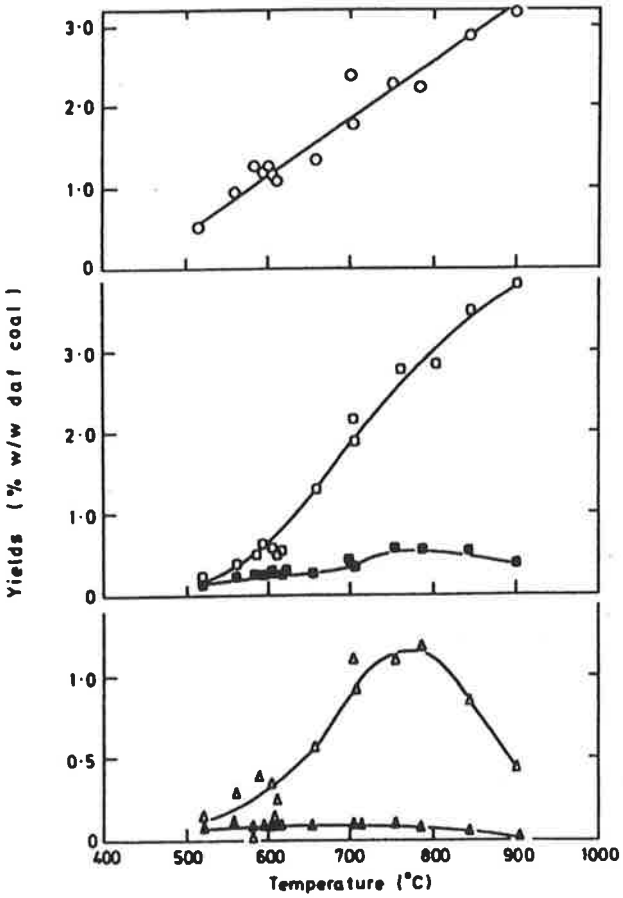

Figure 2.2 Effect of temperature on C_1 - C_3 hydrocarbon yields: CH_4 (○), C_2H_4 (□), C_2H_6 (■), C_3H_6 (Δ), C_3H_8 (▲).

2.4 GASIFICATION PRINCIPLES AND TECHNOLOGIES

Coal gasification has been utilised commercially since the early nineteenth century. The first companies were established in England and the United States and produced fuel gas for illumination by pyrolysis of coal. The convenience of a gaseous fuel as a source of heat and power has led to the increased utilisation of coal for gas generation. Coal gasification yields a wide variety of useful products for all sectors of the community as illustrated in Figure 2.3 (Figueiredo, 1986).

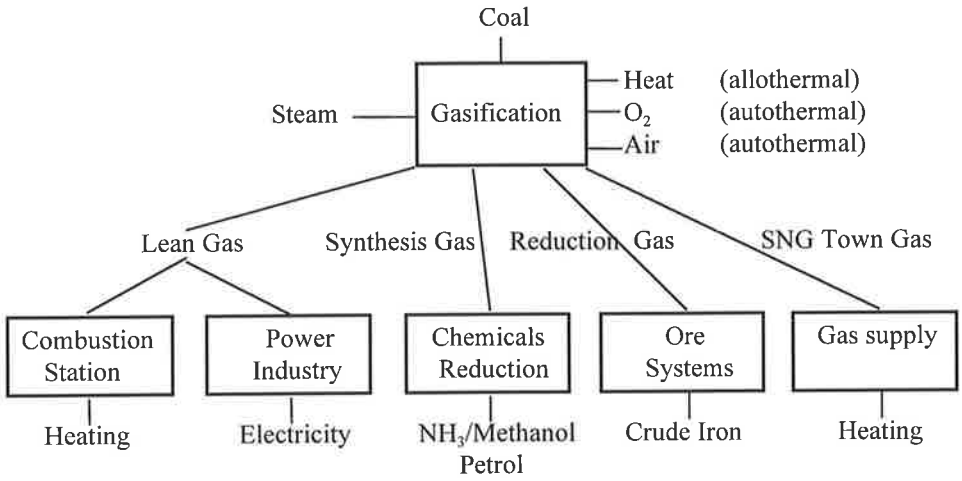

Figure 2.3 Process and application of steam gasification

The design of commercial gasifiers are controlled by the fundamental need for good contact between the solid particles and the reacting gas. The manner of contacting steam and oxygen has a major influence on the product gas composition, overall efficiency and process operability. Three types of processes have been developed for continuous gasification of coal: fixed-bed, fluidised-bed and entrained flow process (Farina, 1996). The fixed-bed and entrained flow gasifiers are more suitable to higher-rank coals while fluidised-bed gasification best accommodates lignites (Figueiredo, 1986). The best known of the classic processes being the Lurgi, Wrinkler and Koppers-Totzek gasifiers respectively. These reactors differ in the coal feed size, residence time, gas-solid contact pattern, reactant and product flow, and reaction temperature. Coal gasification developments until about 15 years ago were in the main directed to the production of town gas and syngas. Currently the main interest is for use in electricity generation (Farina, 1996).

Commercial fluidised-bed gasification of coal with steam and air began in Germany in 1922, as developed by Winkler. These units were extensively utilised throughout Germany and Japan to supply raw gas to the various synthetic chemical industries. The availability of abundant petroleum and natural gas reserves by the early 1950's resulted in the closure of many of the operating Winkler gasifiers. In order for coal gasification to be competitive both economically and environmentally, it is necessary for the development of new advanced gasification processes, as clearly the classical technologies failed to meet changing demands. Over the last two decades, many advanced processes have attained commercial maturity, such as the TEXACO (Keller, 1990) process based on entrained-flow principle and the pressurised RHEINBRAUN High-Temperature-Wrinkler (HTW) (Keller, 1990), Kellogg-Rust-Westinghouse (KRW) (Wilson et al., 1988) and U-Gas (Institute of Gas Technology) (Goyal et al., 1987) processes based on the Wrinkler fluidised-bed principle. The primary difference between the HTW and U-Gas/KRW processes is the manner in which ash is discharged from the gasifier (Gururajan et al. 1992). Unlike classical gasification processes, these advanced coal gasification technologies achieve higher energy utilisation efficiencies due to:

- increasing the gasification pressure, which simultaneously increases the gasifier capacity and minimises or eliminates the cost of gas compression downstream.
- increasing the carbon conversion rate.
- waste heat recovery through the generation of high-pressure steam.

Other important attributes are low emission levels to meet increasingly more stringent environmental regulations and high on-stream times (Keller, 1990). Importantly, gasification has the advantage of being able to accept a greater range of feed-stocks than other power plants. This enables gasification plants to respond to changing energy market prices by correspondingly changing feed stocks (Griffiths, 1996). By 1990, four commercial-scale TEXACO plants were in operation, with two more under construction. Two commercial-scale plants using Rheibraun HTW process are also in operation. Of these commercial scale plants, only one so far has been used in conjunction with combined cycle power generation (Keller, 1990).

2.5 DEVOLATILISATION OF LARGE PARTICLES

The design and operation of low-rank coal fluidised-bed combustion and gasification reactors, the location and rate of volatile release and its subsequent combustion are very important processes that require thorough understanding. Volatiles can account for up to 50% of the total heat released and depending on coal feeding system and temperature, volatile combustion may occur either in the bed or in the freeboard. If significant over-bed combustion occurs, it will contribute considerably to the freeboard excess temperature; increase heat transfer areas; lower combustion efficiency and adversely affect the emission levels of polluting SO_x and NO_x species (Stubington et al. 1997; Hadler and Saha, 1993; Prins et al., 1989).

Early published data on devolatilisation focused on the small particle size range used in conventional pulverised power stations, typically <100μm, and as such the devolatilisation rate was essentially instantaneous. However, the particle feed size range for fluidised-bed applications is much larger, typically between 1 to 10 mm, consequently transport phenomena become increasingly important and devolatilisation can no longer be assumed instantaneous. The rate of devolatilisation for large particles (> 0.5 mm) has been characterised by the total devolatilisation time, or t_v (Zhang et al., 1990).

The devolatilisation times of large coal particles pertinent to their utilisation in fluidised-bed combustion and gasification have been extensively reported in the literature (Stubington et al., 1997; Urkan and Arikol, 1994; Stubington et al., 1992; van der Honing, 1991; LaNause, 1982; Essenhigh, 1963; Stubington et al., 1990; Stubington and Linkewile, 1989; Morris and Keairns, 1979; Stubington et al., 1991; Lufei et al., 1993; Pillai, 1981; Ekinci et al., 1988; Eatough and Smoot, 1996, Hadler and Saha, 1993; Zhang et al., 1990; Pillai, 1985; Stubington and Sumaryono, 1997). Results have been typically correlated with initial particle diameter by an empirical power-law relation of the form

$$t_v = Ad_p^n. \qquad \text{....(2.1)}$$

However, there are large discrepancies in the reported values for the exponent n, with most data falling in between the range of 0.9 and 1.6. A single correlation of devolatilisation times for fluidised-beds have been reported by Stubington et al. (1992) at 850°C in air and by van der Honing (1991), for various authors (Morris and Keairns, 1979; Stubington et al., 1991; Pillai, 1981 and Zhang et al., 1990) for several coal types, bed temperatures and gas environments. The fitted constants have values for A of 1.84 and 5.77 and n of 1.5 and 1.1, respectively.

The variability of the experimental results have been attributable to the differences in the type of apparatus employed (thermogravimetric, convective tube and fluidised-beds), definition of devolatilisation time (time to 95% of final mass loss/volatiles evolution, flame period/extinction and CO/CO_2 gas analysis during combustion experiments), operating conditions (temperature and gas environment), coal type, batch size and particle fragmentation (Stubington et al., 1997; van der Honing and Stubington et al., 1991). Table 2.2 lists a summary of the experimental techniques used and influence of various experimental parameters on the observed devolatilisation times of various coals in fluidised-beds reported in the literature.

Table 2.2 Summary of the influence of various experimental parameters on the observed devolatilisation times in fluidised-beds.

Variable	Reference								
	Stubington et al. 1992	Morris & Keairns, 1979	Stubington et al. 1991	Pillai, 1981	Urkan & Arikol, 1994	Ekinci et al., 1988	Zhang et al., 1990	Eatough & Smoot, 1996	Lufei et al., 1993
*Method**	C	C	C	F	F	F	C	F	C
Temperature	Y	Y	Y	Y	Y	Y	Y	N	Y
Particle Size	Y	Y	Y	Y	Y	Y	Y	Y	Y
Gas Velocity	-	-	N	-	-	-	N	N	N
Coal Type	N	-	N	Y	Y	Y	N	Y	-
Moisture	Y	-	-	-	Y	-	-	-	-
Pressure	-	-	-	-	-	-	-	Y	-
Atmosphere	-	-	Y	-	-	-	-	-	Y
Batch Size	Y	-	-	N	-	-	-	-	-
Fragmentation	-	-	Y	-	-	-	-	-	-

** F : flame extinction time,*
** C: concentration profile 90/95% completion.*
- : not examined
N : no dependence observed.
Y : dependence observed.

2.5.1 THEORETICAL CONSIDERATIONS

It is generally acknowledged that coal devolatilisation may be controlled by three main factors, heat transfer to and within the particle, chemical kinetics of pyrolysis and mass transfer of volatile products within the particle (LaNause, 1982; Stubington and Sumaryono, 1984; Tomeczek and Kowol and Agarwal et al., 1984(a)). The parameter n as determined by equation 2.1, can distinguish the regimes of coal devolatilisation.

- A value for $n = 0$ indicates that chemical kinetics dominate.
- For a value of $n = 2$ indicates that either heat or mass transfer is controlling.
- Intermediate values for n indicate that devolatilisation is controlled by a combination of chemical kinetics and transport phenomena.

Figure 2.4 shows a column chart of the distribution of experimental results for the exponent n derived from fitting equation 2.1 to devolatilisation times reported in the literature. This chart illustrates two major peaks for the exponent n centre about values of 1.0 and 1.5.

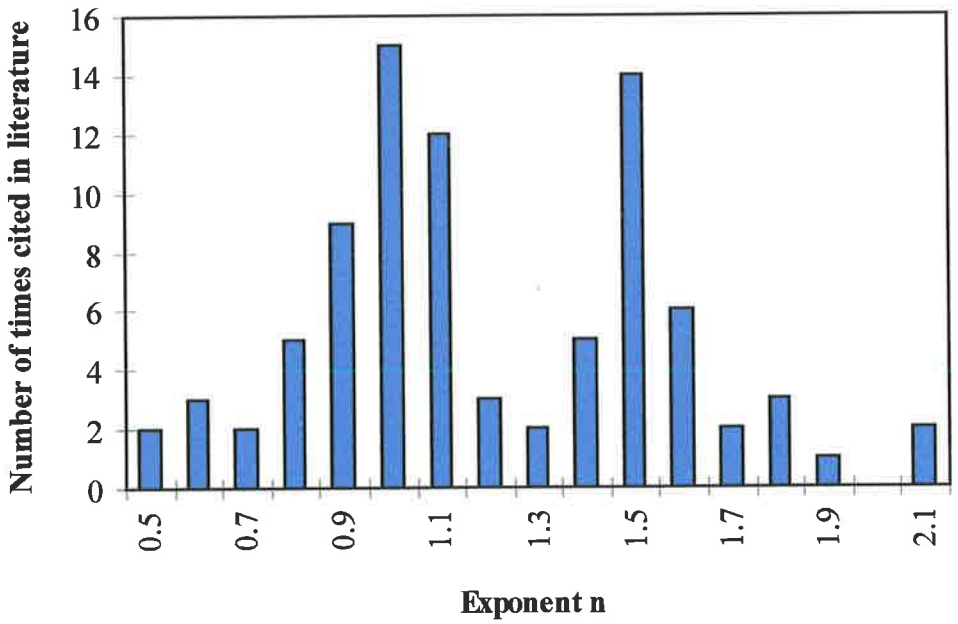

Figure 2.4 The distribution of experimental results for the exponent n derived from fitting equation 2.1 to devolatilisation times reported in the literature.

It has often been suggested that the devolatilisation time of a coal particle is proportional to the square of the particle diameter, indicative of heat or mass transfer control (LaNause, 1982; Essenhigh, 1963; Pillai, 1985; Agarwal, 1984(a); Stubington and Sumaryono, 1984; Agarwal et al., 1986). LaNause (1982) replotted the data of Morris and Keairns (1979) for the devolatilisation time against the square of the particle diameter, where it was observed that the times agree with the square law relation. The rate controlling mechanism that would result in the devolatilisation time proportional to the square of the particle diameter could thus be one or several of the following (LaNause, 1982; Pillai 1985)

(1) rate of heat transfer to the particle
(2) rate of heat transfer through the particle
(3) rate of diffusion of volatile through the particle

Early published works showed a disagreement on whether the rate controlling step was mass transfer (LaNause, 1982; Essenhigh, 1963) or heat transfer (Agarwal, 1984(a); Stubington and Sumaryono, 1984; Agarwal et al., 1986; Juntgen and van Heek, 1979). LaNause (1982) concluded that internal mass transfer must be rate limiting as calculated heating up times were approximately 40% shorter than experimental devolatilisation times. The devolatilisation time was predicted by:

$$t_V = \frac{\rho_V}{24Dc} d^2 \qquad \text{....(2.2)}$$

where ρ_v is the molar density of volatiles (g cm^{-3}), c is mean volatiles concentration (g cm^{-3}), D is the effective mass diffusivity (cm^2 s^{-1}), d particle diameter (cm) and t_v is the devolatilisation time (s). Essenhigh (1963) developed a similar expression, the difference being in the treatment of the diffusion process. However, Stubington and Sumaryono (1984), Prins et al (1989) and Heidenreich (1999) have similarly calculated the coal particle heat-up times based on the heat transfer limited mechanism and compared them with experimentally determined devolatilisation times. Calculated heating times compared favourably with experimental data, which indicates that heat transfer limits the devolatilisation mechanism under fluidised bed

conditions. This discrepancy with that of LaNause (1982) can be attributed to the fact that external heat transfer to the particle was ignored by LaNause (1982) and calculated heat-up times were based solely on internal heat transfer limitations. The relative importance of external to internal heat transfer on the heat up time of a coal particle can be deduced by calculating the Biot number. The Biot number compares the relative magnitudes of external surface-convection and internal-conduction resistances to heat transfer, as expressed below:

$$Bi = \frac{hd}{k_{eff}} \qquad \text{....(2.3)}$$

where h is the convective heat transfer coefficient ($Wm^{-2}K^{-1}$), d is the particle diameter (m) and k_{eff} is the effective thermal conductivity ($Wm^{-2}K^{-1}$). A very low Biot number, $Bi < 0.1$ (Holman, 1992) indicates that internal conduction resistance is negligible, permitting the assumption of an isothermal particle at any given time. Typical Biot numbers experienced in fluidised-bed applications are much higher, in the range of 0.5 to 10. Thus, indicating that both external and internal heat transfer must be considered in the heat transfer calculations (van der Honing, 1991; Stubington and Sumaryono, 1984; Agarwal et al., 1984(a); Prins et al., 1989; Halder and Saha, 1993).

In a parametric study by Agarwal et al. (1984(a) using a model developed for the devolatilisation of coal in fluidised-beds, the theoretical 95% devolatilisation time versus particle diameter for three distinct Biot numbers was compared. It indicated that chemical kinetics control the devolatilisation time for particle sizes less than 0.1 mm. As the particle size increased, the rate-limiting step was in a mixed regime between chemical reaction and heat transfer control.

For particle sizes greater than 1 mm, it was found that the devolatilisation rate was heat transfer controlled with $t_v \propto d_p^2$. This is illustrated in Figure 2.5 reproduced from Agarwal et al. (1984(a)). Similar findings have been reported by Juntgen and van Heek (1979) where for particle sizes below 0.6 mm, chemical kinetics are rate controlling. Agarwal et al. 1984(a) concluded that the extent of the chemical reaction regime depends upon the Biot number and bed temperature.

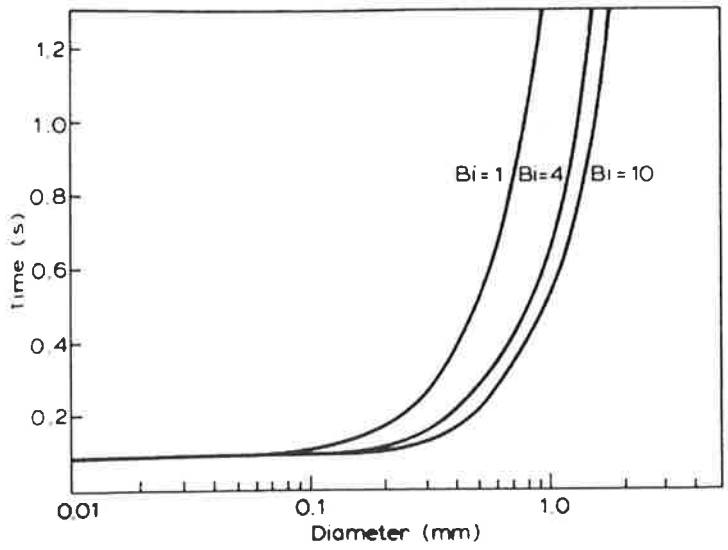

Figure 2.5 95% devolatilisation time versus diameter for smaller particle sizes, with E_o = 220 kJ mol^{-1}, σ = 20 kJ mol^{-1}, α = 0.2 mm^2 s^{-1}, T_a = 730°C (after Agarwal et al. 1984(a)).

Measurements of coal particle centre temperature for particle sizes ranging between 6.4-20 mm in fluidised-beds by Stubington and Sumaryono, 1984; Tomeczek and Kowol, 1990; Pillai, 1985; Heidenreich, 1999; Zhang et al., 1990, have shown that a time lag is exhibited before the centre of the particle reaches the bed temperature. Thus, supporting that devolatilisation time for large particles is heat transfer controlled.

However, the question still remains as to whether or not the exponent in the devolatilisation time power-law correlation should be equal to two for heat transfer controlled mechanisms. It is clearly evident that experimental results of total devolatilisation time, regardless of measurement technique, as shown in Figure 2.4, does not correlate with current theoretical square-law correlations for large coal particle devolatilisation. Simply replotting the devolatilisation time data to the square of the diameter as LaNause (1982) suggested with the data of Morris and Keairns (1979) is not plausible. The exponent *n* for the data of Morris and Keairns (1979) for a plot of devolatilisation time versus particle size is close to unity ie $t_v \propto d_p$ and similarly therefore, it can be shown to approximate the relationship of $t_v \propto d_p^2$.

Prins et al. (1989) and Agarwal (1986) recognised that in the case of external heat transfer control, the d_p^2 treatment is expected to be applicable only for an isolated coal particle in a stagnant oxidising environment. The low Reynolds number corresponding to stagnant oxidising condition results in the Nusselt number being approximately equal to 2 for all particle diameters. Thus for extreme cases of internal and external heat transfer control the particle centre temperature can be calculated respectively as (Prins et al., 1989):

$$\left(T_b - T_c\right) / \left(T_b - T_o\right) = \sum_{i=1}^{\infty} 2(-1)^{i+1} \exp\left[(-i\pi)Fo\right] \; for \; Bi > 100 \qquad ....(2.4)$$

$$\left(T_b - T_c\right) / \left(T_b - T_o\right) = \exp\left[-3BiFo\right] \; for \; Bi < 0.1 \qquad ....(2.5)$$

Realising that the Fourier number, Fo = $4\alpha(t/d^2)$ and the product of the Biot and Fourier numbers, Bi.Fo = $(2\rho c_p)/(t/d)h$, it can be seen that the heat-up time must be directly proportional to d^2 for internal heat transfer control and also for external heat transfer control in the case of stagnant conditions (Nu =2, $h \approx d^{-1}$). Furthermore, Prins et al. (1989) cited an empirical correlation for the heat transfer coefficient under fluidised-bed conditions, which predicts $h \approx d^{-0.26}$. Consequently, Prins et al. (1989) concluded that for heat transfer controlled devolatilisation, the exponent *n* would lie between a value of 2 (internal heat transfer control) and 1.26 (external heat transfer control). Model predictions and experimentally determined values for the exponent *n* were 1.6 and 1.7, respectively. Furthermore, this was supported by the estimated Biot numbers, which lie in the range between 0.7 and 4.4 (Prins et al., 1989).

Equations 2.4 and 2.5 were formulated based on the assumption of stagnant oxidising conditions so that the Nusselt number can be approximated as two, clearly not the conditions present in a fluidised-bed (LaNause, 1985). The application of an experimentally determined empirical correlation for the heat transfer coefficient collected in a bubbling fluidised-bed to Equation 2.5 is somewhat flawed. Thus, the question remains as to which mechanism(s) control the devolatilisation process.

Heidenreich (1999) established a new technique to distinguish between heat transfer and chemical kinetically controlled regimes of coal devolatilisation based on pyrolysis kinetics, particle size and heat transfer parameters. This treatment compares the ratio between the 95% evolution devolatilisation time, t_{95}, defined as when $[(V^*-V)/V^*]_{avge} = 0.05$, or $(V/V^*) = 0.95$ and the time required for 95% heating of the particle centre, T_{95}, defined as $[(T_{r=0} - T_0)/(T_\infty - T_0)] = 0.95$ versus the modified Damkholer number to Biot number ratio. If chemical kinetics are controlling the process, the particle will reach the maximum devolatilisation temperature prior to the volatiles being evolved and $t95 > T95$. Conversely, if heat transfer is the controlling mechanism, devolatilisation will take place almost instantaneously upon reaching the devolatilisation temperature and $t95 = T95$. While traditionally the Damkholer number represents the ratio of the heterogeneous reaction rate and the diffusion of a reactant gas species into the particle, devolatilisation is a unique process, in that it is a heterogeneous process that is driven by the transfer of heat into the particle. Hence, thermal diffusivity rather then gas diffusivity is considered. The modified Damkholer number, Da', is shown in equation (2.6).

$$Da' = \frac{r'\rho_o C_{p,s} d_p^2}{k_s} \qquad \text{....(2.6)}$$

In this form, the modified Damkholer number relates the ratio of the rate of solid reaction via devolatilisation to the rate of heat conduction through the particle, which is the driving force for devolatilisation. The thermal conductivity and specific heat of coal were taken as the temperature averaged values of the range of temperatures experienced by the particle. Whilst the particle density was approximated by the initial particle density and assumed constant throughout the devolatilisation process (Heidenreich, 1999). Hence, the only parameter remaining to be quantified in Equation (2.6) is the modified reaction rate term, r', which must be applicable to the situation of coal devolatilisation. Briefly (for greater detail of model refer to Heidenriech, 1999), the modified reaction rate term for a particle undergoing coal devolatilisation can be given by the following equation based on the fraction of volatiles evolved (Agarwal et. al., 1984(a)).

$$r' = -\frac{d}{dt}\left(\frac{V^* - V}{V^*}\right) = -\frac{d}{dt}\left[\int_0^{\infty} \exp\left[-k_0 \int_0^{t} \exp\left(-\frac{E}{RT}\right) dt\right] f(E) dE\right] \quad \text{....(2.7)}$$

Under normal circumstances it would be appropriate to employ the reaction activation energy, or in the case of devolatilisation, the mean activation energy. However, the 95% devolatilisation time will be better reflected by employing a value of $E_0 + 2\sigma$ as two standard deviations from the mean reflects 95% of the span of a normal distribution. Therefore, rather than considering the reaction rate calculated from an integration conducted over a range of activation energies, the reaction rate when $E = E_0 + 2\sigma$ was considered which gives :

$$r' = \frac{d}{dt}\left[\exp\left[k_0 \int_0^{t} \exp\left(-\frac{E_0 + 2\sigma}{RT}\right) dt\right] f(E_0 + 2\sigma)\right] \quad \text{....(2.8)}$$

Given that k_0 and $f(E)$ can be assumed to be constant, Equation (2.8) can be simplified to give :

$$r' = \exp\left[k_0 \exp\left(-\frac{E_0 + 2\sigma}{RT}\right)\right] f(E_0 + 2\sigma) \quad \text{....(2.9)}$$

The temperature, T, in Equation (2.9) must reflect the situation under consideration. Thus, rather than using the average particle temperature, the 95% heating temperature, $T_{95\%}$, was used and defined by :

$$\frac{T_{95\%} - T_0}{T_\infty - T_0} = 0.95 \quad \text{....(2.10)}$$

The ratio of the Biot number to modified Damkholer number was given by :

$$\frac{Bi}{Da'} = \frac{h_o}{\exp\left[k_0 \exp\left(-\frac{E_0 + 2\sigma}{RT_{95\%}}\right)\right] f(E_0 + 2\sigma) \rho_0 C_{p,c} d_p} = \frac{h_o}{r' \rho_0 C_{p,c} d_p} \quad \text{....(2.11)}$$

The heat transfer coefficient, h_O, must account for both convective and radiative heat transfers, which can be calculated by using equation (2.12). Note that as the particle surface temperature is constantly changing, the value of h_{rad} also changes so it is convenient to use the average surface temperature in Equation (2.12).

$$h_0 = h_{conv} + h_{rad} = h_{conv} + \sigma_{rad}\varepsilon_{rad}\left(T_g + T|_{r=R_0}\right)\left(T_g^{\,2} + T|_{r=R_0}{}^2\right) \quad \text{....(2.12)}$$

The ratio of dimensionless time, t_{95} / T_{95} as a function of the log(Bi/Da′) ratio is shown in Figure 2.6 (it is convenient to consider the log of the Bi/Da′ ratio due to the exponential factor present in the numerator of equation (2.11)), for various sets of model calculations performed by Heidenreich (1999), in which the particle size (0.1 - 10 mm), heat transfer parameters, and chemical kinetics were varied to yield a range of values for log(Bi/Da′). Figure 2.6 shows three distinctive regimes depending on the calculated value of log(Bi/Da′). At values of log(Bi/Da′) > 5.5, the dimensionless devolatilisation time increases with increasing log(Bi/Da′) and values of t_{95} / T_{95} >> 1 in this region suggests that chemical kinetics is the dominant mechanism. For values of log(Bi/Da′) < 4.5 the dimensionless devolatilisation time remains effectively at unity which indicates that heat transfer is the controlling mechanisms ie. the 95% evolution time is limited by the 95% heating time. In the region defined by 4.5 < log(Bi/Da′) < 5.5 there is an intermediate region where devolatilisation is controlled by a combination of chemical kinetics and heat transfer.

To validate model predictions, temperature data reported for 8-11 mm dry Bowman coal particles in a fluidised-bed and convective flow apparatus were used to estimate the 95% heating time, whilst the devolatilisation time, $t_{95\%}$, is calculated based on model predictions (Heidenreich, 1999). Similarly, using the 95% devolatilisation times for methane evolution reported by Morris and Keairns (1979) in a fluidised-bed and predictions of the model to generate the 95% heating times, $T_{95\%}$, the resulting dimensionless devolatilisation times are plotted against calculated values for the log(Bi/Da′) ratio based on the pertinent operating conditions and also shown in Figure 2.6. The fluidised-bed and convective flow devolatilisation of coal particles are in or bordering the heat transfer controlled regime.

However, for the smallest particle size employed from the data set of Morris and Keairns (1979), 0.46 mm, devolatilisation appears to occur in the kinetically controlled regime. This is consistent with previous findings of Agarwal et. al. (1984(a)) and Juntgen and van Heek (1979), both reported that for particle sizes below 0.1 mm and 0.6 mm, respectively, chemical kinetics are rate controlling.

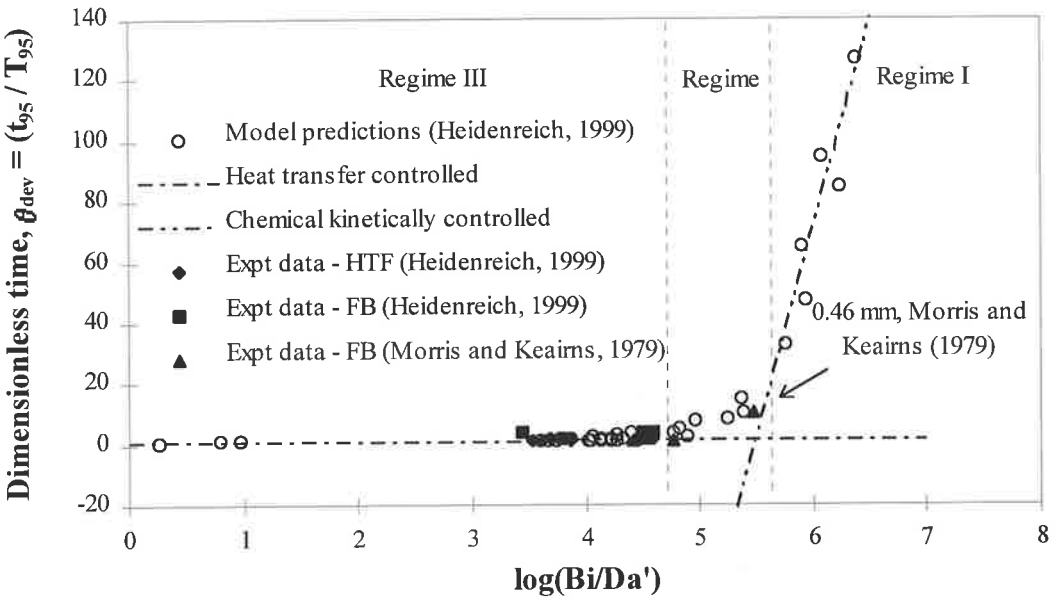

Figure 2.6 Comparison of model predictions with experimental data for the ratio of the dimensionless time as a function of the Biot to modified Damkohler number ratio.

2.5.2 EXPERIMENTAL VARIABLES

2.5.2.1 Temperature

It has been generally found amongst the various investigators that the devolatilisation time decreases with increasing temperature (Urkan and Arikol, 1994; Stubington et al. 1992; LaNause, 1982; Morris and Keairns, 1979; Stubington et al., 1991; Zhang et al., 1990; Luefei et al., 1993; Pillai, 1981; Ekinci et al., 1988). However, the degree of dependence observed varies to some extent amongst findings and may be attributed to the different experimental techniques and apparatus employed by the various authors.

The effect of temperature upon the devolatilisation time can be accounted for by the fact that the driving force, the temperature difference between the particle and bulk phase, increases with increasing bulk temperature. Hence, the initial rate of heat transfer is higher and consequently the devolatilisation time decreases. Furthermore, the contribution of radiative heat transfer to the particle increases significantly with temperature. In detailed investigations into the effect of temperature, Pillai (1981) and Ekinci et al. (1988) observed that the exponent n, increased and the correlation parameter A, decreased with increasing temperature. In an attempt to sufficiently represent the behaviour of volatile matter burnout times, Ekinci et al. (1988) conducted regression analysis to correlate the devolatilisation time with temperature and particle size in a general relationship of the form:

$$t = A + Bd + CT \tag{2.13}$$

where t is the devolatilisation time (s); A, B and C are constants, d is the particle diameter (mm), and T is the bed temperature (°C). Not surprisingly, the two-parameter regression analysis gave a better fit than the power law relation given by Equation 2.1. An attempt to also include coal type as a variable (in terms of its volatile matter content) into the regression was not successful. While this result may lead to an improvement in prediction of the estimated devolatilisation times, the correlation is still very specific to conditions of data collection and does not provide any insight into the rate controlling mechanism of the devolatilisation process.

2.5.2.2 Coal type

The most contentious variable amongst investigators is the effect of coal type on the devolatilisation time. Urkan et al. (1994), Ekinci et al. (1988), Eatough et al. (1996), Honing (1991) and Pillai (1981) reported that devolatilisation times were dependent upon coal type, while Stubington et al. (1989, 1992), Fu et al. (1987) and Agarwal (1986) did not find any dependence. Stubington et al. (1992) and Zhang et al. (1990) compared their devolatilisation times based on CO_2 evolution and flame extinction times respectively with previous work and concluded that coal type had no effect

upon the rate of devolatilisation. However, Stubington et al. (1992) made reference to comparison of only five Australian bituminous coals with a scatter of ± 30%. While the claimed good agreement between flame extinction times and gas-based 95% pyrolysis times by Zhang et al. (1990) for various coals, seems somewhat fortuitous. Especially since the oxygen concentrations were different in these studies (21 and 0 vol% O_2 respectively). Agarwal (1986) concluded negligible effect of coal type for particles > 1 mm for a single particle non-isothermal model based on kinetic parameters and the particle time-temperature history to determine the completion of devolatilisation. However, the validity of the model predictions remains questionable as comparison of kinetic parameters and thermophysical properties used by Agarwal (1986) show negligible difference between coal types.

The independence of kinetic parameters and thermophysical properties with coal type has been attributed to the inability to accurately predict the time-temperature history of coal particles during devolatilisation (Heidenreich, 1998). These parameters have been determined from inappropriate experimental data whereby heat transfer along the thermocouple to the particle results in an over estimation of the actual particle temperature. This results in unreliable estimations for kinetic and thermophysical properties and a factor leading to the suggestion that the kinetics for evolution of particular volatile species being relatively coal type independent (Heidenreich, 1998).

Characterisation of the influence of coal type on the devolatilisation time based on identifying representative coal properties to describe the dependence has proven to be difficult (Urkan and Arikol (1994). Ekinci et al. (1988) and Fu et al. (1987) unsuccessfully tried to characterise this dependence based on proximate analyses of coals. Figure 2.7 plots the volatile matter/fixed carbon (VM/FC) ratio, a measure of the coal rank, which decreases with increasing rank, versus the estimated devolatilisation time for 5 mm coal particles. This method was utilised by Urkan et al. (1994) to verify the influence of coal rank. The graph incorporates the work of Urkan et al. (1994), in addition, results form various other investigations.

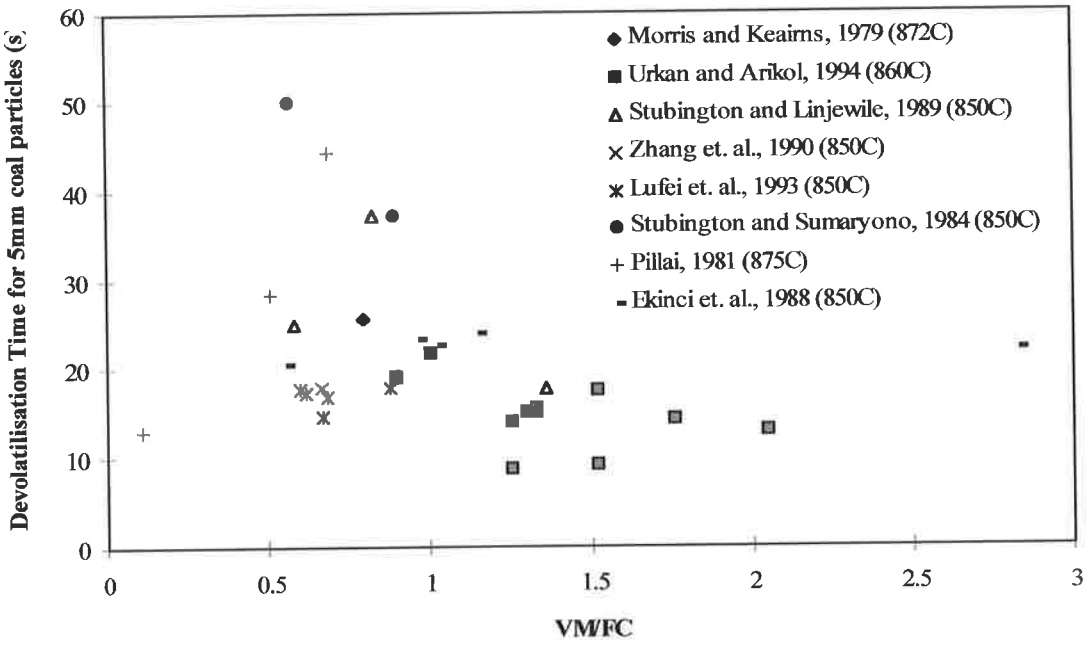

Figure 2.7 Correlation between VM/FC ratio and the devolatilisation time based on the power law relation of Equation 2.1 for a 5 mm coal particle reported in the literature.

As can been seen, there is a wide scatter amongst the reported data. Given the scatter amongst the power law parameters, A and n, for the various researchers, it is not surprising that such a distribution exists. However, the degree of variance observed may not necessarily be attributed to the different experimental techniques and apparatus employed by the various authors, but difficulty in determining the devolatilisation time for higher ranked coals. Pillai (1981) and Lufei et al. (1993) reported that for the higher ranked samples that contain little volatile matter, such as anthracite and coalite breeze samples, no visible volatile flames or any distinguishable trace of CO or CO_2 species were detectable. Thus, devolatilisation times could not be substantiated.

2.5.2.3 Moisture Content

Low-rank coals in particular contain high amounts of inherent moisture within the pore structure, which must be removed during the heating process. It has been found that as the initial moisture content of the coal increases, the total devolatilisation time

also increases (Stubington et al., 1992; Prins et al., 1989; Urkan and Arikol, 1994). The associated increase in the total devolatilisation time with moisture content is concurrent with the requirement to evaporate an increased mass of water. This suppresses the coal particle heating rate, delaying the onset of devolatilisation. Heidenreich (1999), as shown in Figure 2.8, observed the influence of evaporation of moisture on the time-temperature history of a devolatilising brown coal particle. The formation of a temperature plateau at 100°C in the temperature response is consistent with evaporation of bulk water. Thus, the delay in the onset of devolatilisation with increasing moisture content will have a significant impact upon the size of the volatile evolution region, particularly for in-bed coal feeding. Urkan and Arikol (1994) observed that the exponent n in the power law correlation decreased with decreasing moisture content. A plot of moisture content on the ratio of flame extinction times for dried and moist coals is shown in Figure 2.9 (after Urkan and Arikol, 1994). This figure clearly demonstrates the effect of moisture content on the total devolatilisation time of coal.

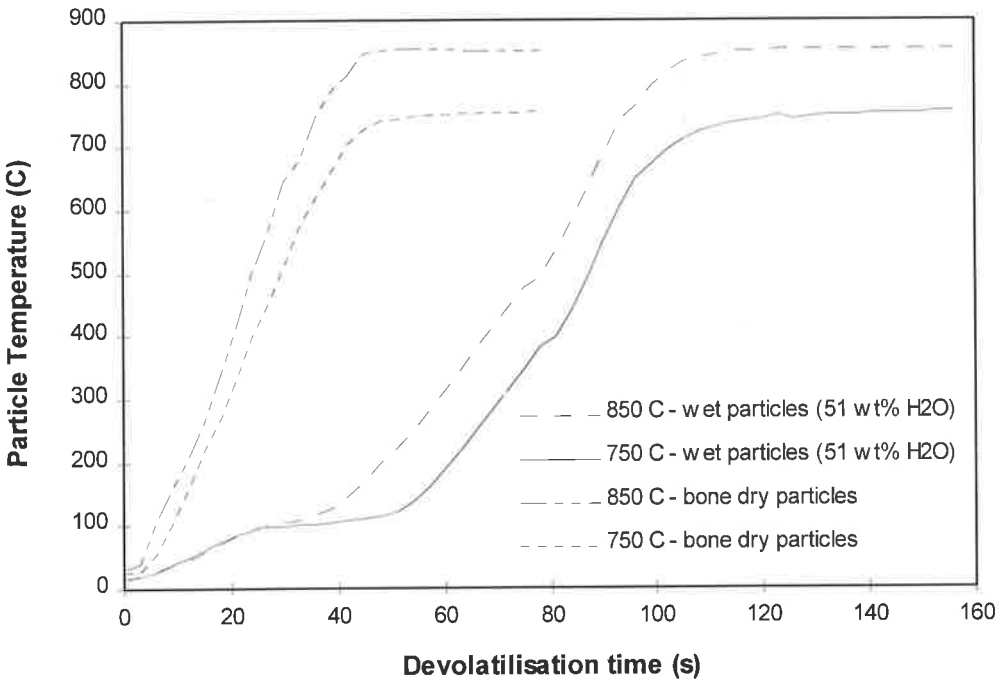

Figure 2.8 Comparison of the measured temperature response at the centre of a 10 mm wet and bone dry Bowmans coal particle in a fluidised-bed at 750°C and 850°C (reproduced from Heidenreich (1999)).

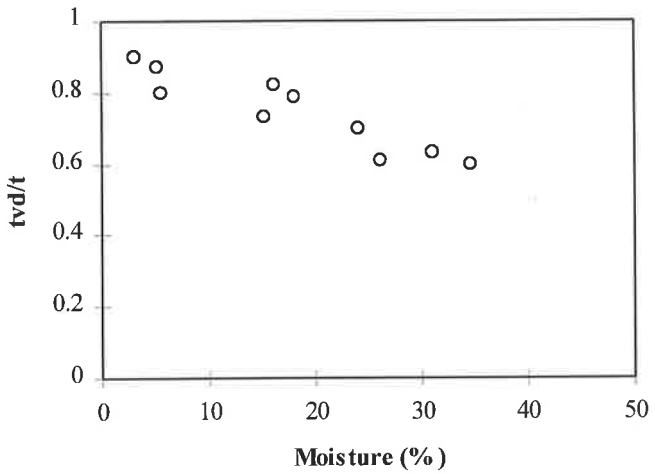

Figure 2.9 Effect of moisture content on the ratio of flame extinction times for dried and moist coals in a fluidised-bed. Bed temperature 860°C, oxygen concentration 10 vol%, particle diameter 3.35-4.00 mm (after Urkan and Arikol, 1994).

2.5.2.4 Pressure

Eatough et al. (1996) found that the devolatilisation time decreased modestly with increasing pressure and was more pronounced for the larger particles. As the pressure increases, the intra-particle transit time of the volatiles increases, consequently favouring secondary repolymerisation and condensation reactions. Overall, this will result in a reduction in volatile yield and shifts the molecular weight distribution towards lighter components that have higher molecular diffusivities. These effects may explain the decrease in devolatilisation time with increasing pressure. As the current scope of this thesis is only concerned with atmospheric pressure conditions, mass transfer limitations can therefore be ignored.

2.5.2.5 Superficial Gas Velocity

The devolatilisation times show no correlative dependence upon the superficial gas velocity (Stubington et. al., 1991; Zhang et. al., 1990 and Lufei et. al., 1993). This indicates that neither external mass or convective heat transfer limits the devolatilisation times.

2.5.2.6 Gas Atmosphere

The effect of differing atmospheres (inert, gasification and combustion) akin to a change in the oxygen concentration, on the rate of devolatilisation has been observed by Stubington et al. (1991), Pillai (1981) and Lufei et al. (1993). The decrease in devolatilisation time with increasing oxygen concentration is the result of the subsequent formation of a diffusional flame front surrounding the particle surface. The result being an enhanced rate of heat transfer experienced by the particle due to the exothermic combustion of the volatiles in the boundary layer. Panagakis (1995), Lufei et al. (1993) and Stubington et al. (1991) all reported increases in the devolatilisation time of 35%, 45% and 19% respectively when the atmosphere was changed from air to nitrogen.

2.5.3 SUMMARY

The devolatilisation time of coal has been extensively reported in the literature by numerous investigators using a myriad of coal types, techniques and definitions. Until more recently, this has resulted in conflicting conclusions over the controlling mechanism and subsequent theoretical formulations to characterise the devolatilisation time. It has been suggested that the devolatilisation time of a coal particle is proportional to the square of the particle diameter, indicative of heat or mass transfer control (LaNause, 1982; Essenhigh, 1963; Agarwal, 1984(a); Stubington and Sumaryono, 1984). However, this is contrary to the experimentally observed unity dependence reported in the literature. Heidenreich (1999) has conclusively shown that for particle sizes greater than 1.0 mm under fluidised-bed conditions, coal devolatilisation is under a heat transfer controlled regime. It has been reported in the literature that the devolatilisation time is influenced by; particle size, gas environment, moisture content, coal type and to a lesser extent pressure. However, significant variations exist between the observed degree of effect these variables have on the devolatilisation time.

2.6 VOLATILE COMBUSTION

Low-rank coals contain significant amounts of volatile matter and the subsequent combustion of the volatiles will have a significant effect on the heat released within the bed, the reaction rates of the char and the product gas composition. The behaviour of volatile matter during combustion differs completely from that of the porous coal char during combustion and gasification. This is summarised in Table 2.3, as produced by van der Honning, 1991. Volatile evolution and combustion processes occur at rates of one to two orders of magnitude faster than for char combustion, which in turn are several orders faster than for char gasification reactions. In laboratory and pilot-scale coal gasifiers, particle residence times are relatively short and it has been shown that the fast processes of coal devolatilisation and volatile combustion/decomposition control carbon conversion (Gururajan et al. 1992). A detailed understanding of the in-bed combustion behaviour of volatiles is paramount to the successful design, operation and modelling of a fluidised-bed gasifier.

Table 2.3 Comparison of the behaviour between volatiles and char within a fluidised-bed (van der Honing, 1991).

	Volatile combustion	Char gasification
Type of reaction	Homogeneous (gas-gas)	Heterogeneous (solid-gas)
Residence time in the bed	short (< 0.5 s)	long (minutes)
Distribution over the bed	dependent upon devolatilisation rate	well mixed
Carbon efficiency determined by:	incomplete reaction (mixing)	elutriation, attrition
Recycling feasibility	no	yes

The combustion of volatiles in fluidised-beds has numerous ramifications relating to their design and operation; it affects the distribution of oxygen across bed, char burn-out times, coal particle feed point spacing, NO_x formation and heat released between freeboard and bed (Stubington et al. 1997). It is desirable to achieve high in-bed combustion efficiencies in fluidised-bed combustion of coal, to maximise heat transfer through the inert emulsion phase to the steam tubes.

It has been shown that high bed temperatures (>850 °C) favour in-bed combustion of volatiles (van der Vaart 1985). However, this results in a marked increase in char burnout times due to rapid consumption of available oxygen by volatiles (Hesketh et al., 1991; Ross et al., 1999). While a dichotomy may exist for fluidised-bed combustion of coal, the exact opposite could be said for gasification conditions. The rapid depletion of oxygen in the bed by combustion of volatiles will reduce the amount of char undergoing combustion. This results in an increase in steam and carbon conversion efficiencies, as more char will be available to undergo the gasification process. Thus, there is an immediate need for experimental investigations of gas-phase reactions of volatiles in environments simulating fluidised-bed gasifiers presently lacking in the literature (Gururajan et al., 1992).

The importance of volatile combustion in fluidised-bed coal conversion processes is highlighted by taking into consideration the location of coal feed entry point. The residence time of volatile matter in the bed can be calculated by:

$$\tau = \frac{\varepsilon\,(H - H_{inj})}{u_o} \qquad \text{....2.14}$$

where ε is the bed porosity, H is the bed height, H_{inj} is the height above the distributor of coal feed injection into the bed and u_o is the superficial operating velocity. By considering a typical industrial scale bubbling fluidised-bed gasifier with a bed height H = 1.0 m, H_{inj} 0.2 m ε = 0.4 and u_o =1.0 m s^{-1}, the gas residence time is very short and the location of combustion will be in close proximity to the place of evolution. Assuming that after coal injection into the bed at a height H_{inj} above the distributor, it rises to the surface. The upward rise velocity of the coal particle may estimate the time taken for a coal particle to reach the surface. For a 3 mm coal particle, the upward rise velocity is given by Nienow et al. (1978),

$$U_s = 0.15(U-U_{mf})^{0.5} \qquad \text{....2.15}$$

Hence, the time taken for a coal particle to reach the bed surface is simply given by,

$$t = (H-H_{inj})/U_s = 5.3 \text{ s} \quad \text{....2.16}$$

From the data of Morris and Keairns (1979), the devolatilisation time for 0.5 to 4 mm coal particles is about 5-16 s. By comparing the devolatilisation time with the axial solids mixing time, this indicates that a significant fraction of the volatiles is released in the bed. Furthermore, as devolatilisation is a much faster process than radial solids mixing, the provision of adequate numbers of in-bed coal feed points will determine whether or not a uniform radial distribution of volatiles is evolved (van der Honing, 1991). The rate of combustion of volatiles is dependent on the following processes (Stubington, 1980)

- coal devolatilisation rate
- coal particle mixing rate
- rate of mixing of volatiles and oxygen

While it is generally agreed that the last process, the mixing of volatiles and oxygen controls the rate of volatile combustion, the amount of over-bed burning increases rapidly as the bed temperature falls below a critical value. Therefore, the above assumption is not strictly valid for low bed temperatures. The necessary conditions for volatile combustion are (van der Honing, 1991):

- gas temperature in excess of the ignition temperature.
- presence of oxygen
- adequately low particle concentration.

The third condition implies that volatiles are more likely to combust in the bubble and freeboard regions rather than in the emulsion phase of a fluidised-bed. However, there is lack of agreement amongst researchers as to what extent this may be the case. It is certain though that in-bed volatile combustion will not be complete even for fluidised-bed combustors with their low fuel concentrations and adequate quantities of excess air present.

A considerable fraction of the volatiles do combust in the freeboard region. The implications for fluidised-bed gasification conditions where the oxygen concentration is far lower, and the bed material consists of combustible char rather than inert sand media, presents a significant challenge that must be clarified.

This section deals with in principle, the manner in which the unique environment of a fluidised-bed affects pre-mixed gas phase combustion of volatiles. The significance of devolatilisation time and its integration with volatile combustion modelling will be briefly highlighted. However, owing to the complexities of integrating the details of volatile release and gas phase mixing into an overall system model (Srinivasan et al. 1998), further treatment in this regard remains outside the scope of current objectives. An outline of secondary decomposition of volatile matter is also reviewed, given its importance in pretext to high temperature oxidation of hydrocarbons.

2.6.1 Location Of Volatile Evolution

The location of volatile release must take into consideration the time scales for both the particle mixing and devolatilisation rates. Particle mixing in fluidised-beds involves complex hydrodynamics associated with the interactions between the gas and solid phases. In order to model the combustion of volatiles it will be necessary to identify the mixing behaviour of the fluidisation gas and the devolatilising coal particles in the bed. A useful concept in mixing is the distinction between macromixing and micromixing. Macromixing involves flow patterns and turbulence, while micromixing deals with molecular transport phenomena (Davidson et al., 1985). The rising gas bubbles in a bubbling bed governs the flow patterns of the gas and solid phases. Bed particles displace both laterally and axially by passing gas bubbles, inducing a distinct circulation pattern within the bed. Modelling this random and chaotic movement of particles with the concurrent release of volatiles within the particulate phase has required researchers to simplify the process extensively. Three different concepts for the release of volatile matter into a fluidised-bed combustor have been proposed, and are listed as summarised by Stubington et. al. (1990).

1) Volatiles released as a continuous fuel-rich region rising in plug flow through the bed as a "plume".
2) Volatiles form bubbles, which may either separate or remain attached to the coal particle.
3) A "volatile evolution region". Defined as the bed region where volatiles are released, with some of this region occupied by oxygen-rich gases and other parts by volatiles.

The plume model developed by Park et al. (1981) assumed instantaneous devolatilisation of the coal particles at the feed entry point, with the evolution of a plume of unburnt volatile matter rising in plug flow with rest of the gas. The evolved volatiles make contact with oxygen only at the circumference of the plume by radial gas mixing. In-bed combustion could be improved by increasing the bed height or gas dispersion, whereas higher superficial gas velocities and fewer coal feed points would decrease the in-bed combustion of volatiles. This was characterised by the non-dimensional Plume number:

$$Plu = \frac{D_{gr} H}{u_O L} \qquad \text{....2.17}$$

where D_{gr} is the radial gas dispersion coefficient ($m^2 s^{-1}$), H is the bed height (m), u_o is the superficial operating velocity ($m\ s^{-1}$) and L represents the radius of a coal feed point (m). The fate of the volatiles escaping into the freeboard was not elucidated.

In a similar plume model by Bywater (1980), it was also assumed that devolatilisation occurred instantaneously, but included the effect of a particle rise velocity and radial solids dispersion resulting in a time-averaged volatile release rate distribution throughout the bed. The particle and bed temperatures were assumed to be uniform, implying instantaneous heat up of the coal particle, which does not apply for large particles as commonly used in FBC. Therefore, the assumption of instantaneous devolatilisation invalidates these models for large coal particles, which exhibit a finite devolatilisation rate.

Pillai (1982) concluded from his observations of devolatilisation studies in a glass combustor that coal particles are enclosed within a volatile bubble and are only evolved as discrete bubbles when the coal particle is restrained. Yates et. al. (1981) reported that large coal particles in a fluidised-bed combustor emit volatiles as discrete bubbles rather than as plumes.

Stubington (1980) proposed that volatiles evolve within a volatile evolution region, which was that part of the bed to which devolatilising coal particles disperse from the feed injection point. The particle dispersion in the axial direction is rapid, but very slow in the radial direction. Therefore, volatile evolution confined to an axially symmetric region centred about the vertical axis through the injection point. The two main factors affecting this mixing are gas exchange between air bubbles and the particulate phase, and molecular diffusion within the particulate phase. The volatile evolution region is contained within a conical envelope about the vertical axis through the coal injector. The volatiles do not evolve uniformly throughout the particulate phase and oxygen-rich or volatile-rich regions will occupy some parts of this phase, respectively.

Van der Honing (1991) formulated a two-dimensional bubbling bed model with fast vertical particle mixing, instantaneous volatile combustion, and finite rates for devolatilisation and radial solids dispersion. The devolatilisation rate is fast when compared to radial solids mixing and slow compared to vertical solids mixing. Van der Honing (1991) modelled the coal volatiles within a volatile rich containing zone released above the coal injection point. Outside the volatile containing zone the amounts of volatiles are assumed to be negligible. The diameter of the volatile containing zone is determined by the devolatilisation time t_v, radial solids mixing coefficient D_{sr} and the radial gas mixing coefficient D_{gs}. As the axial solids mixing rate is fast, the coal feed point is modelled as a vertical line source, with the radius of the volatile containing zone r_{vz} being:

$$r_{VZ} = \sqrt{0.1 D_{SR} t_V} + \sqrt{2(D_{gr}) \frac{0.5H\left(\varepsilon_b + (1-\varepsilon_b)\varepsilon_{mf}\right)}{u_o}} \qquad \text{....2.18}$$

Recent modelling by Stubington et al. (1990a) has described particle mixing as a stochastic process with time resolution of both devolatilisation rate and particle movement during devolatilisation. The model assumes that the coal particles are stationary unless displaced radially and axially by a bubble. The particle will thus rise through the bed in a stepwise manner with a periodic upward motion dependent upon the frequency of bubble passage. The distance risen by a particle was calculated as the stationary time multiplied by the mean axial rise velocity. This particle mixing process results in the liberation of multiple discrete volatile regions within the bed, and directly into the freeboard while upon the bed surface. The size of the volatiles regions was determined from devolatilisation rates. At the bed surface, the particle will move radially to reactor wall by the action of erupting bubbles. Near the reactor wall the particle will flow downward into the bed a certain distance, before it will rise again in a stepwise manner from the passage of bubbles. The particle continuously circulates within this limited depth from the bed surface during and after its devolatilisation period.

The experimental evidence used to support this interpretation was from data collected by the use of a combined oxygen-bubble probe (Stubington et al., 1990b) along with 'simulated' coal particles (alumina particle impregnated with paraffinic oil) (Stubington et al., 1986, Stubington et al., 1990c), which eliminate the complications associated with char combustion reactions. From the analysis of the corresponding variations between the oxygen and bubble sensors, the fluctuation in oxygen concentration was not related to differences between the bubble and particulate phases. Rather, the low oxygen partial pressure regions indicate the presence of unburnt volatiles. This view was supported by the fact that the bed was operated under a cloudless or slow bubble regime. Under this regime the volatiles released assimilate into the upward gas flow, passing through both bubble and particulate phases in their path. The rapid flow of gas through both phases therefore explains why no correlation between oxygen partial pressure and phase location exists. It was also observed that numerous, small, discrete diffusion flames were burning immediately above the bed surface, unlike a single continuous flame as predicted by plume models.

Recently, Stubington et al. (1992) combined their volatile release model (Stubington 1990a), to form the new multiple discrete diffusion flame model. The volatiles were assumed to burn as discrete diffusional flames under molecular diffusion control in both particulate and bubble phases. Volatile combustion was modelled by a two-stage process:

1. Rapid consumption of oxygen initially between fuel vapour bubbles near the feed injection point.
2. A slow oxidation region which was controlled by the radial diffusion between the fuel rich volatile containing zone and surrounding oxygen rich fluidising gas flow analogous to a diffusion flame.

However, the model was not applicable for volatiles released from small particles < 0.6 mm, as a plume of volatiles forms. Preliminary results indicate the model compares favourably with combustion experiments for a laboratory-scale and a 20 MW pilot-scale fluidised-bed combustor. Importantly, a significant fraction of the volatile release occurred at the bed surface (24% and 32% respectively). This has been similarly shown by others (van der Honning, 1991; Ogada et al., 1996; Bautista-Margulis et al. 1996). Thus, the importance of accurate knowledge of the devolatilisation time in view of coal combustion modelling has been highlighted.

2.6.2 VOLATILES DECOMPOSITION

Knowledge of the role and reaction mechanisms involved during the secondary decomposition of the primary volatile matter products are important for quantifying the product yields and distributions during devolatilisation. The secondary reactions occur almost simultaneously with the primary reactions, via two principal reaction pathways.

- Thermal cracking (pyrolysis) reactions.
- Repolymerisation (condensation) reactions.

2.6.2.1 Thermal Cracking Reactions

Thermal cracking reactions involve extremely complex multiple reaction pathways, where free radicals are produced from the homolytic cleavage of C-C chemical bonds. This is usually a highly endothermic process, therefore, it is favoured by increasing temperature. These highly reactive free radicals can then undergo numerous types of reactions: hydrogen abstraction, disproportionation, β-bond scission, recombination, and hydrogen capping (Schubert, 1990). As a general rule, free radicals do not undergo isomerisation reactions to allow formation of more stable radicals. This ultimately results in the breaking down of larger molecules to form smaller molecular weight compounds, together with dehydrogenation (Petrakis et al., 1983).

2.6.2.2 Repolymerisation Reactions

Repolymerisation reactions also involve complex reaction mechanisms, where molecules adsorb or condense on internal surfaces of coal, where dehydrogenation, dealkylation and aromatisation occur, leading to formation of carbon-rich, polycyclic aromatic structures and hydrogen-rich, low molecular weight alkanes (Schobert, 1990). Adsorption can be divided into physical adsorption (Van der Waals forces) and chemisorption (active sites) (Petrakis et al., 1983). Active sites occur on the surfaces of heterogeneous catalysts, points within the coal matrix where chemically bonded mineral matter (alkali, earth-alkaline and transition metals) are located (Figueiredo et al., 1986). These sites help generate carbocations which are essential in the polymerisation of hydrocarbons.

2.6.2.3 Experimental Variables

Investigations into secondary decomposition reactions of volatile matter have primarily focused on the tar fraction, in particular, gas phase thermal cracking reactions (Calkins et al., 1984, Cliff et al., 1984, Stiles et al., 1989, Katheklakis et al., 1990, Xu et al., 1989, Hesp et al., 1970). Tar molecules are the most susceptible of the escaping volatile species to undergo secondary decomposition reactions.

This is due to their low thermal stability, high reactivity and large molecular size. The effects of cracking temperature and residence time upon the final product yields have been studied the most (Stiles et al., 1989; Katheklakis et al., 1990; Calkins et al., 1984; Xu et al., 1989; Hesp et al., 1970). The experimental rigs utilised to study tar thermal cracking reactions were either in-situ variable freeboard reactors (Stiles et al., 1989; Katheklakis et al., 1990) or a two stage system, with primary products being typically generated at 600°C, passing onto a cracking reactor (Calkins et al., 1984; Xu et al., 1989; Hesp et al., 1970). It was observed that the concentration of low molecular weight hydrocarbon gases increased, principally due to the cracking of tar vapours. A notable feature is the predominance of olefins and C_1-C_3 alkanes in the product distributions. In Figure 2.10, taken from Calkins et al. (1984), the results obtained when tar vapour are passed through a cracking reactor between 600-1100°C, with the yields expressed as a percentage of the tar produced at 600°C (29% w/w daf coal).

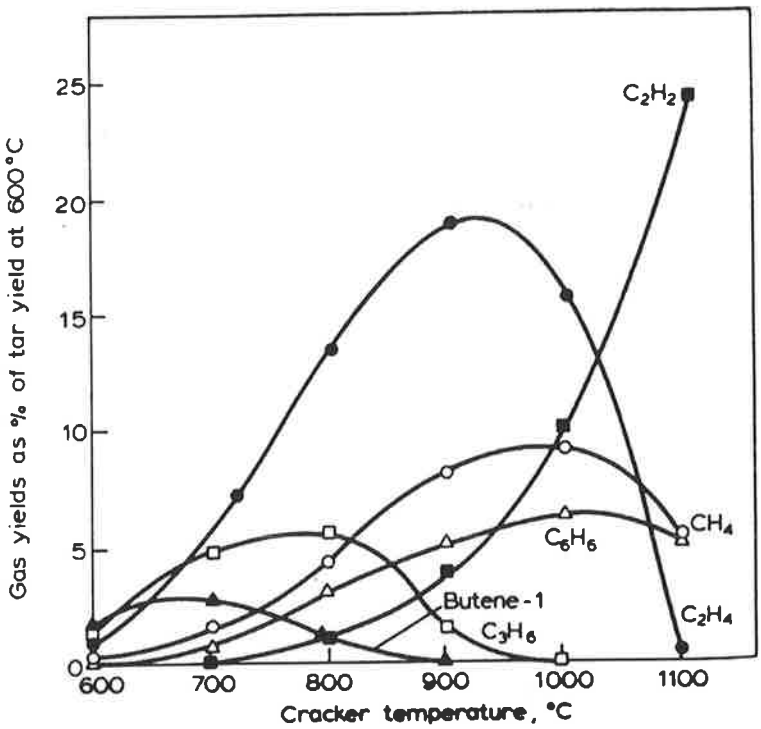

Figure 2.10 Product yields from cracking of tar vapours: CH_4 (○), C_2H_2 (■), C_2H_4 (●), C_3H_6 (□), Butene-1 (▲), C_6H_6 (Δ).

From these results, the dominant product from gas-phase secondary cracking reactions is ethylene C_2H_4, which accounts for 19% of the tar cracked at 900°C. The temperature at the maximum yield for the olefins decreases with increasing hydrocarbon chain length, with a substantial proportion of the hydrocarbons cracking themselves to produce acetylene C_2H_2. Doolan et al. (1983) similarly found a pronounced dominance in the formation of olefins as a product, in particular, ethylene, and the disfavouring of alkanes greater than C_3 chain length during the pyrolysis of n-octane. Similarly, Xu et al. (1989) presented the product yields at cracking temperatures between 500-900°C. The results indicate that the more complex hydrocarbon molecules (longer aliphatics and substituted aromatics) decompose at relatively lower temperatures, resulting in the formation of benzene and methane. The C_5-C_7 yields began to decrease above 600°C, while for C_3-C_4, the yields began to decrease above 700°C. The maximum yield of ethylene occurred at 800°C, while the yield of methane was still increasing at 900°C.

The residence time of the volatile products also plays an important role in determining the final product yield obtained. Generally, as the residence time increases at a given temperature, the greater the degree of cracking. Therefore, the tar yield decreases and the yields of light hydrocarbon gases increases (Stiles et al., 1989, Xu et al., 1989, Hesp et al., 1970). Similar profiles to that of cracking temperature are observed. Decreasing yields of C_2-C_5 aliphatics and increasing yields of CH_4 and C_2H_4 products occur. The maximum yield of C_2H_4 was reached at 800°C. This is in agreement with the fact that olefins are more thermally stable than the corresponding paraffins. Although at 900°C, the C_2 yield decreases, consistent with the decomposition of C_2H_4.

Hesp et al. (1970) used a static bed cracking reactor that was filled with -50 + 25 mm low ash coke. The use of the carbonaceous packing alters the ultimate product yields obtained, as the coke provides active sites for the adsorption and subsequent decomposition of tars. Thus altering the decomposition mechanism from homogeneous to heterogeneous reaction. Ultimately, an increase in the coke deposition or char formation results due to repolymerisation reactions and decreasing gas yields.

The following Figures 2.11 (a) and (b) from Hesp et al. (1970) shows the overall yields of products as wt% of the tar entering the cracking reactor and the composition of the gas products vol%. Over 50% of the tar entering at 1000°C forms or deposits as carbon or soot, with the rest forming gas. Only a small fraction (1 to 2 wt%) of the tar leaves the reactor unchanged. The compositions of the gas although showing similar product species have significantly differing evolution sequences when compared to gas phase thermal cracking. Methane as well as saturated and unsaturated C_2-C_4 hydrocarbons are the main products below 700°C. Olefins show a continual monotonic decline with temperature, and the maximum methane yield reached at only 700°C. Above 800°C, hydrogen became the most abundant gas.

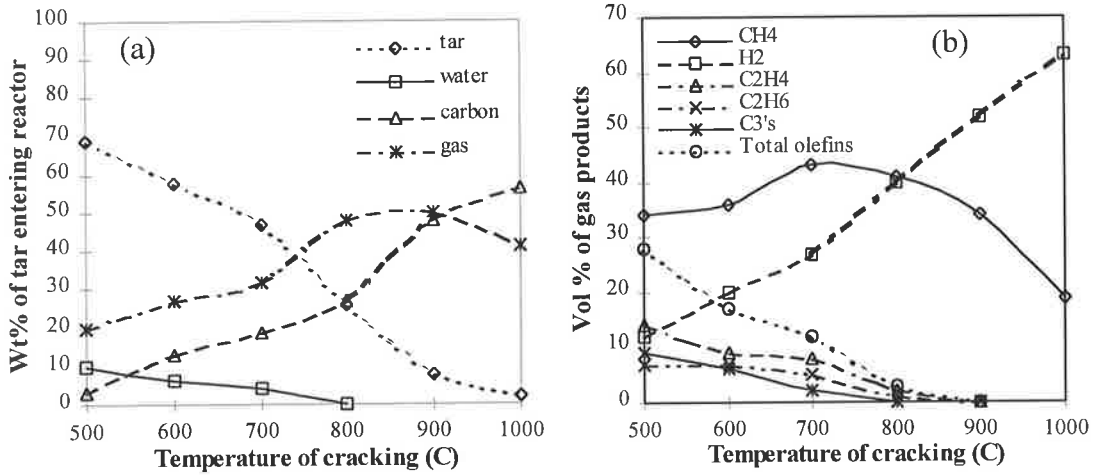

Figure 2.11 (a) Overall yields of products from tar cracking in a static bed (b) Composition of gas products.

Studies by Tyler (1980) found that the bed material had a significant affect upon the yields obtained during pyrolysis of bituminous coals. Upon substitution of the bed material from sand to petroleum coke (specific surface area of 1.6 m^2g^{-1} as compared to 0.01 m^2g^{-1} for sand), the tar yield decreased from 29 to 25 %. However, no change in hydrocarbon gas yields below 600°C occurred, with only a slight decrease in olefin yield above this temperature. In another test utilising activated char as the bed material (surface area 800 m^2g^{-1}), the tar yield was reduced to less than 3% of the coal (daf), with no increase in hydrocarbon gas yields.

The data clearly demonstrates that beds of char, typical of gasification systems, results in a reduction in tar yields which is dependent upon the specific surface area and hence, activity of the char material. The absence of any significant increase in the yields of low molecular weight hydrocarbons, indicates that the reduction in tar yield via polymerisation reactions occurring with char structure and not by gas phase thermal cracking reactions.

2.6.3 PRE-MIXED VOLATILE COMBUSTION

There has been much conjecture as to which phase the volatiles undergo combustion in. Some investigators suggest combustion to occur only in particulate phase, such as Pillai (1976), while others, only in the bubble phase. Prins (1987) and Roberts et al. (1987) used video analysis, where it was observed that flames attached to devolatilising coal particles in the bubble phase were extinguished upon entry into particulate phase. It was deduced from this evidence that the volatiles burn in the bubble phase only. Stubington et al. (1990a) concluded that investigators using the visual techniques failed to detect volatile combustion within the particulate phase as the combustion flame is not visible due to rapid gas-solid heat transfer and large thermal capacity of the bed. This results in only a small temperature difference between the gas and bed particles and hence, no observable flame. To elucidate the location and mechanisms of volatile combustion under fluidised-bed conditions, investigators have studied the ignition and combustion of stoichiometric pre-mixed combustible fuel with air (Hayhurst, 1991; Dennis et al., 1982; Hesketh et al., 1991; van der Vaart, 1985, 1988, 1992; Ogada et al., 1996). Consensus has been that these mixtures do not burn in the bed below a critical temperature, which well exceeds normal ignition temperatures. Below this critical temperature, the mixture explodes violently as bubbles burst and ignite at the bed surface.

Van der Vaart (1985) measured freeboard pressure pulsations during stoichiometric pre-mixed propane combustion and successfully showed characterisation of bubble ignition in the freeboard. As the bed temperature was increased, the intensity of explosions increased to a maximum, owing to the transition from forced to spontaneous ignition of bubbles.

As temperatures increased above the critical temperature, a typical value observed for propane was approximately 830°C, combustion intensity decreased as bubbles ignited progressively lower down in the bed, or until they were igniting just after their formation at the distributor, possibly as a pre-mixed flame jet on every orifice in the distributor. Hayhurst (1991) made a similar observation using a sound level indicator to measure the intensity of noise resulting from the combustion of carbon monoxide and propane.

Hayhurst (1991) observed that the critical temperature decreased with an increase in fluidising velocity and decrease in bed particle size. This was most likely caused by the fact that increasing the amount of excess air increases the bubble fraction in the bed and the likelihood of bubbles coalescing to form larger bubbles at given heights in the bed. The ignition of a bubble depends upon its size, such that larger bubbles ignite at lower temperatures. Dennis et al. (1982) similarly concluded that bubbles of fuel and air had to reach a critical size before their ignition. By considering the bubbles as a well-stirred reactor and assuming bubbles to grow by coalescence, a correlation was derived to calculate the minimum diameter $D_{e,\,min}$ (m) for an igniting bubble as:

$$D_{e,\min} = \frac{9U_{mf}}{2A[M]}\exp\left(\frac{E}{RT}\right) \qquad \text{....2.19}$$

where A is the pre-exponential factor for chain-branching ($dm^3mol^{-1}s^{-1}$) ; $[M]$, the concentration of a general molecule ($moldm^{-3}$); T temperature of the bed (K); E activation energy for a combustible mixture ($Jmol^{-1}$). Typical value for $A[M]$ is 1.8×10^{13} s^{-1}. Dennis et al. (1982) postulated that as bubbles do not ignite until their temperature well exceeded normal ignition temperature of 493°C for a propane/air mixture, the ignition was controlled by a balance between near-isothermal chain branching and radical recombination with surrounding sand particles.

Further evidence to support this hypothesis was the work done by Hayhurst (1991). He added various small quantities of porous alumina particles coated with platinum to the bed of silica sand.

Subsequently the explosive over-bed combustion of propane progressively decreased in intensity upon the addition of more catalyst. Propane began burning in the particulate phase on the surface of the platinum, this being determined visually from the glow of the catalyst pellets. From these observations, it was concluded that the sand particles quench the free radical reactions and therefore particulate phase combustion of volatiles does not occur. However, van der Vaart (1985) found that the critical temperature actually increased with increasing operating velocity. It was argued that ignition was thermally controlled as a result of the decrease in the gas residence time.

The fact that ignition of hydrocarbon gas/air mixtures are only possible at temperatures well in excess of normal ignition temperatures implies that some prohibitive mechanism exists. In a fluidised-bed there are three physical properties which could be responsible for quenching (van der Vaart, 1985):

- Heat transfer from the gas
- Mass transfer from the gas
- The residence time of the gas

For a given exothermic reaction, two competing thermal processes exist. Heat generation due to reaction increasing system temperature, thereby accelerating the reaction as usually approximated by an Arrhenius type expression. Equally, as temperature rises so does the rate of heat loss from the system. At a sufficient temperature, rate of reaction and consequently heat generation surpasses the heat transfer resulting in an explosion. This simplified theory of thermal explosion can be modelled for a spherical system and the critical diameter needed for ignition be derived as follows (van der Vaart, 1985)

$$D_{crit} = \frac{6RT_o^2 h}{CHEA} e^{E/RT_o} \qquad \text{....2.20}$$

where h is the heat transfer coefficient, C concentration of fuel, H the heat of reaction and A the pre-exponential factor.

This equation is of the same form as that derived by Dennis et al. (1982) based on spontaneous chain branching ignition theory. Alternatively, rather than ignition being actively quenched via either heat or mass transfer, the reactants could simply require a certain amount of time to ignite. The induction period corresponds to either a build-up of free radicals or generation of a local hot spot. Jackson et al. (1954) observed ignition delay time for a stoichiometric propane and air mixture at 740°C in the order of 1.5 seconds. As previously highlighted, gas residence times are typically less than half a second, therefore indicating spontaneous bubble ignition within the bed could be difficult.

Stubington et al. (1990a) concluded that the discrepancies in reported critical temperatures amongst the various authors may be explained by the differing operating conditions used. For small bed particles (<500μm), the bubbles would be under the clouded regime (ie. the bubbles are surrounded by a denser cloud region). This cloud inhibits the mixing of gas between the two phases. Whereas in a cloudless bubble, gas circulates straight through the bubble from the bottom to top and continues up through the bed above the bubble. In the clouded bubble regime, restriction in gas circulation culminates in bubble phase gas heating up more slowly and therefore not attaining ignition temperature until the bubble approaches the top of the bed. Increasing the gas velocity results in an associated increase in bubble size and consequently moves the bubble further into the clouded bubble regime (LaNauze, 1985). This explains the observed effect by van der Vaart (1985) of increasing critical temperature with operating velocity. Furthermore, the reported decrease in critical temperature with increasing bed particle size (van der Vaart, 1985; Hayhurst, 1991) is due to faster exchange of gas between phases as the bubble moves towards the cloudless regime. However, essential to the idea of either thermal or radical quenching is the growth of bubble diameter with bed height. The point when the bubble has reached its critical diameter, such that the surface to volume ratio has reduced sufficiently, ignition is then possible. Consequently, higher fluidising velocities result in larger bubbles at a given bed height, and the volume effect (heat generation or radical propagation) will be greater than surface effect (heat transfer or radical termination).

This results in ignition at a lower bed temperature, as observed by Dennis et al. (1982) and Hayhurst (1991). As the bed particle size distribution used by van der Vaart (1985), Dennis et al. (1982) and Hayhurst (1991) in their experiments are all of similar size range, the exact nature of bubble phase combustion ignition remains unclear.

It thus follows that if bubble phase ignition is difficult, will combustion occur in the particulate phase with its unfavourable high solids content. Hesketh et al. (1991) performed experiments in an incipiently fluidised-bed to determine the temperature at which volatiles began to combust within the particulate phase without the complication of bubble phase combustion. It was confirmed that the combustion of pre-mixed methane-air and propane-air mixtures was inhibited below specific critical temperatures. Propane combustion was found to be inhibited below 835°C, while methane below 915°C. The inhibited particulate phase combustion of volatiles was assumed to be caused by free radical quenching on the surface of sand particles within the particulate phase. Stubington et al. (1990a) reviewed the data of Broughton (1975) who observed that the fraction of unburnt fuel leaving the bed decreased with increasing bed size. If combustion did not occur in the particulate phase, then fuel bypassing would be expected to increase owing to larger emulsion phase gas flow, which would produce the exact opposite to that observed by Broughton (1975). Furthermore, the completion of combustion within short bed heights is strong evidence that combustion of pre-mixed gas and air occurs rapidly in the particulate phase at temperatures down to at least 800°C. Van der Vaart (1985) shares this view, in concluding that while flame combustion may not be possible in the emulsion phase, some sort of chemical reaction is occurring there.

Thus, for bed temperatures below the critical temperature, volatiles released within the particulate phase will undergo decomposition reactions and combust only if they pass into a bubble that is above the minimum bubble size. For bubbles below this critical size, combustion can only occur when bubbles burst and ignite at the bed surface. For bed temperatures above the critical temperature, stable combustion in both the particulate and bubble phases occurs.

The most detailed understanding of volatile combustion has been by the collection of works by van der Vaart (1985, 1988, 1992) through the use of an air-cooled suction probe to measure in-bed axial gas profiles during pre-mixed combustion of methane and propane with air. Chemical analysis of the major and minor products at 750 and 850°C for stoichiometric combustion of propane and air is shown in Figure 2.12.

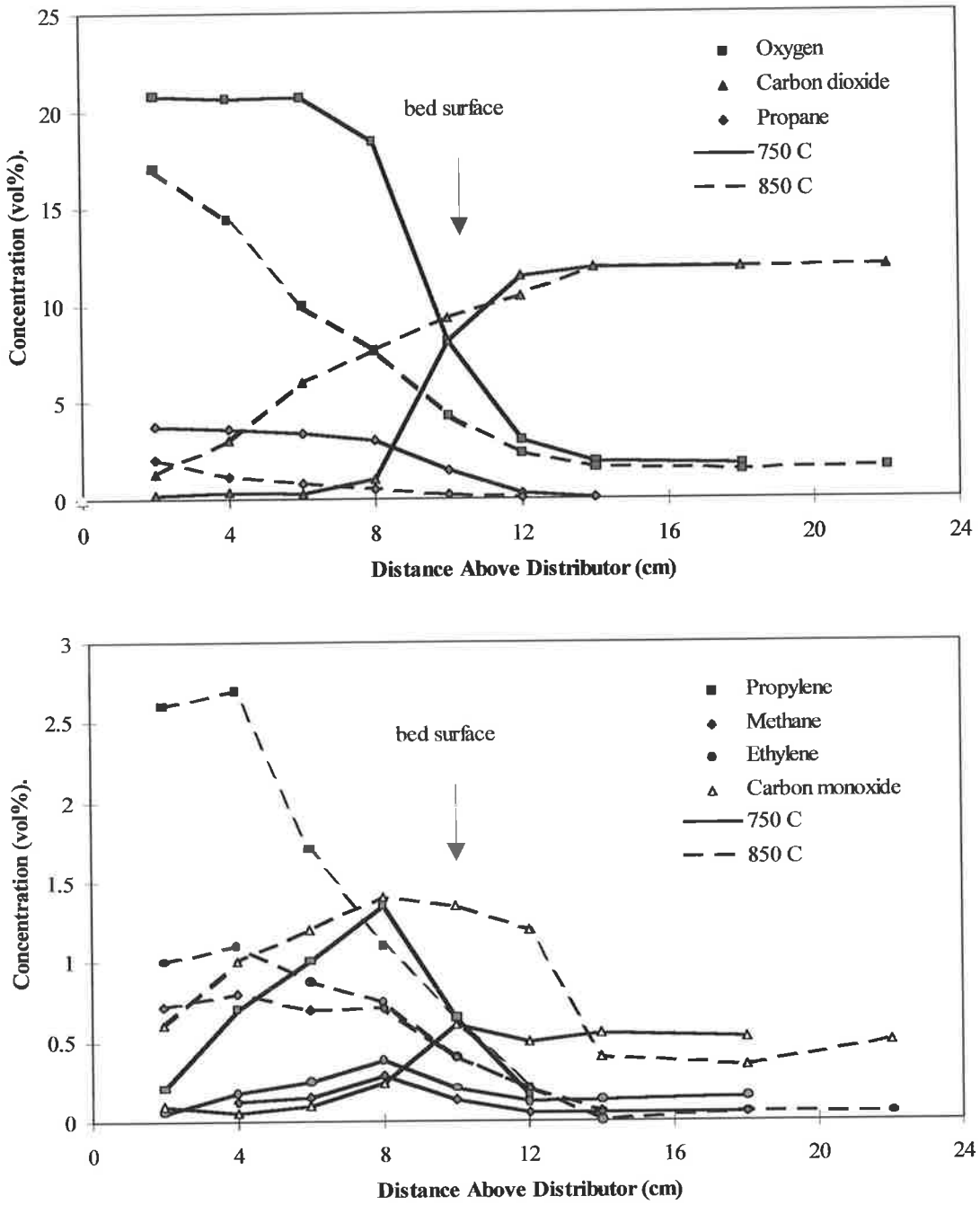

Figure 2.12 Axial concentration profiles of chemical species from in-bed probe measured by gas chromatograph in FBC. (reproduced from van der Vaart (1988))

At a bed temperature of 750°C, very little in-bed conversion occurs. Practically all of the CO_2 produced occurs within 3 cm of the top of the fluidised-bed, with very little oxygen consumed before the bed surface. The sudden conversion of the various species at the bed surface corresponds to the violent explosive nature of combustion at temperatures below the critical bed temperature. The slight decrease in propane yield observed corresponds to the generation of intermediates (methane, ethylene and propylene) caused by thermal cracking (pyrolysis) reactions. Considerably more propylene formed than ethylene or methane, which form in approximately equal amounts, with the maximum conversion for all three primary intermediates occurring at the same bed height. However, this result is somewhat inconsistent with observations made by Doolan et al. (1983), Calkins et al. (1984), Xu et al. (1989) and Hesp et al. (1970). They found ethylene to be the main percussor from thermal cracking reactions. The chemical analysis results of Van der Vaart explain the qualitative observations made by Dennis et al. (1982) and Hayhurst (1991) on the observed flame colour during combustion of intermediates on the divisions of high temperature hydrocarbon oxidation reactions as summarised by Fristrom and Westenberg (1965).

$$C_3H_8 \rightarrow \text{Cracking Products } (C_2H_4, C_2H_2, CH_4) \rightarrow CO \rightarrow CO_2 \qquad ....2.21$$

Upon increasing the bed temperature to 850°C, it is clearly observable from Figure 2.12 that in-bed conversion of volatiles occurs gradually throughout the bed. Nearly all of the propane was consumed before the bed surface by either thermal cracking or combustion reactions. The formation of intermediates are more rapid, with maximum conversion increasing with rising bed temperature and the maxima occurring at the same point for all three intermediates. The peaks of the intermediates are more diffuse than at lower temperatures. Van der Vaart (1985) concluded that the critical temperature does describe the transition from over-bed burning or ignition to in-bed ignition. Rather, the bed temperature at which in-bed conversion via a steady reaction becomes great enough to reduce the fuel concentration at the surface so that ignition is not possible. Furthermore, the reactions occurring in the bed are of the same time scale as the gas residence time indicating the spread in reaction zone due to the very efficient heat transfer environment in the bed.

Thus, the explosive nature of combustion at lower bed temperatures at the bed surface and in the freeboard being only possible due to the significantly reduced heat transfer conditions present there and only if in-bed reaction has not depleted fuel to below the lower flammability limit. To support this case, van der Vaart (1985) added platinum doped alumina particles and calcium carbonate to the bed operating below the critical temperature. Upon introduction, the bed immediately quietened which was associated with the heterogeneous combustion on the surface of the catalyst. The fluidised-bed acted as a perfectly mixed vessel with practically constant concentrations of the various species throughout the bed. Hayhurst (1991) reported similar findings.

By increasing the fluidising velocity and bed particle size, the in-bed production of intermediates decreased. This result was supported by findings for propane pyrolysis experiments, where the residence time of the reactants was the most important factor determining conversion. To compare conversion due to cracking in the presence of oxygen, van der Vaart (1985) conducted a series of tests under a nitrogen atmosphere. Under pyrolysis conditions, the reactor behaved more or less like a perfectly mixed vessel, indicating reactions involved are slow relative to gas mixing in the bed. It was observed in particular that ethylene production was half that under combustion conditions. This difference was attributed in part to the general description of high temperature oxidation as oxygen-catalysed pyrolysis of the hydrocarbon fuel, such as oxidation without chain branching reactions shown below (Hayhurst, 1991):

$$C_3H_8 + O_2 \rightarrow C_3H_7 + HO_2$$
$$C_3H_7 + O_2 \rightarrow C_3H_6 + HO_2 \qquad \text{....2.22}$$

2.6.4 Effect of Volatiles on Char Combustion Rate

Because of the transition of volatile combustion to within the bed as temperature increases, the oxygen distribution and consequently the char combustion reaction rate will be affected.

The volatiles will compete with char for the available oxygen, so the question arises: does the oxygen react preferentially with volatile matter or char in the bed? Hesketh et al. (1991) observed the burn-out times of a batch of char particles in a bed of sand, fluidised by a propane-air mixture by measuring the bed temperature response. The burn-out time of the char was determined from the overall heat balance on the fluidised-bed as follows (Hesketh et al., 1991),

$$\frac{d}{dt}(m_b C_{pb} T_b) = \Delta H_c r_c N_p + hA_h (T_f - T_b) - m_g C_{pg} (T_b - T_g) \qquad \text{....2.23}$$

where left-hand side represents the rate of change of bed heat content. The three terms on the right represent (i) rate of heat production by char, (ii) the rate of heat supply by furnace, (iii) the rate of heat convection by fluidising gas. However, this method may lead to considerable errors as the propane added is assumed to supply a constant additional heat input which does not change with char burn-out. Such an assumption does not seem plausible. If propane increases the char burn-out times, then equally, the char must influence the propane combustion rate and therefore the calculated burn-out times using this method. Alternative measurement techniques include,

(1) observing the extinction of burning particles
(2) measuring the CO_2 output
(3) measuring the particle weight loss

For char burn-out time in the presence of volatiles, the first two methods are inappropriate because propane combustion generates (a) flames and (b) CO_2. Thus, the weight loss method as successfully employed by Andrei et al. (1985) is left. This method used a moveable wire mesh basket, shaped to fit within the fluidised-bed to retrieve char particles. The basket was immersed at the commencement of the experiment in the sand bed and then withdrawn after a selected time interval from the bed and quenched in a stream of nitrogen. Each batch of collected char particles were re-weighed and weight loss for each batch recorded as a function of time.

By using this technique, any influence of propane is mitigated. The only concern with this technique is the possible inaccuracies arising from weight loss measurement of char particles during burn-out due to loss of ash. It has been well documented that as char burn-out progresses an ash layer forms around the coal particle (Wang et al., 1972; Park et al., 1987; Froberg et al., 1978; Andrei et al., 1985; Blackman et al., 1994 and Brunello et al., 1996). In order to minimise the fracturing of the ash layer and consequent errors in mass loss balance, a fine sand size and low excess superficial operating velocity will be necessary. Figure 2.13 shows the results of char burn-out times between 750°C and 950°C in air and an air/2.5 vol% propane mixture (Hesketh et al., 1985). The introduction of propane into the fluidising stream results in an increase in the char batch burn-out time, which increases with increasing temperature. This corresponds to the combustion of propane in the bed, which reduces the local oxygen concentration, as shown in Figure 2.12, and consequently the char combustion rate. Thus, it may not necessarily be beneficial to raise bed temperatures in the presence of volatiles, as this leads to a decrease in char combustion efficiency (Hesketh et al., 1985).

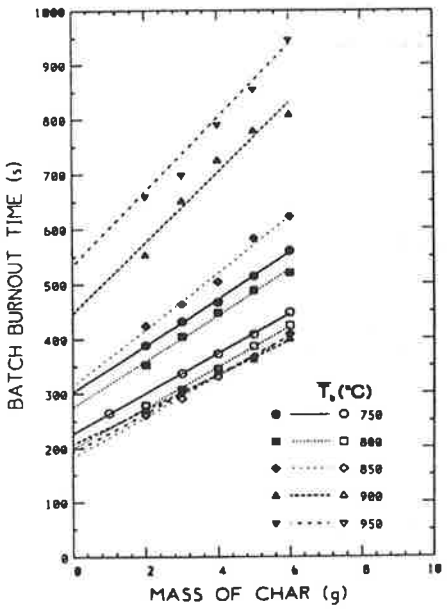

Figure 2.13 Batch burn-out times for char in 0.41 mm diameter sand, $U\text{-}U_{mf} = 0.22$ ms^{-1}. (Solid symbols) Char combustion in air/2.5 vol.% propane, (Open symbols) Char combustion in air. (taken from Hesketh et al., 1991)

2.6.5 NON PRE-MIXED VOLATILE COMBUSTION

Clearly pre-mixed volatile combustion does not occur in a real operating bed. Obviously, volatiles must mix with oxygen supplied from fluidisation gas before combustion can occur. The importance of mixing was demonstrated by Stubington et al (1990a) in a review of literature comparing non pre-mixed (both single and multiple injection) and pre-mixed gas combustion in fluidised-beds. It was found that pre-mixed gas combustion being typically complete within a 50 mm bed depth while bed heights of 1-2 orders of magnitude larger are required to obtain complete combustion for non-premised gas combustion.

Bautista-Margulis et al. (1996) investigated the combustion of 1-3 mm high-volatile coal particles in a calorimetric fluidised-bed combustor. It was found that the fraction of volatiles burnt in the freeboard region for excess air levels ranging from 0 to 40% and bed temperatures of 800, 850 and 900°C to be 0.44-0.20, 0.36-0.09 and 0.3-0.02, respectively. In subsequent model development, the fraction of volatiles transferred into the freeboard was influenced by the mean solid radial dispersion coefficient, D_{sr}, which was treated as an adjustable parameter. Thus concluded, the mixing of volatiles and oxygen in the bed region controls gas-phase combustion. Van der Honing (1991) similarly supports this conclusion.

Accurate modelling of coal combustion must take into account the following factors in relation to volatile combustion (Stubington, 1980):

- The concentration distribution of volatile release, both radially and axially within the bed. This depends on coal particle dispersion in the radial and axial directions and on the coal devolatilisation rate.
- The gas exchange rate between bubbles and the particulate phase. This depends on the bed particle and bubble size. This will define the bubble regime and extent of gas interchange.
- Molecular diffusion within the particulate phase.

2.6.6 Reaction Schemes And Kinetics Of Volatile Combustion

In order to obtain a concise description of the complete combustion process of the volatiles, the mechanisms of each of the volatile components needs to be considered. The extremely complex reaction mechanisms involved along with difficulties in the acquisition of reliable experimental kinetic rate data and the prior lack of concern of volatile combustion have resulted in little information being available. Smoot and Thurgood (1979) have reviewed the literature on hydrocarbon oxidation mechanisms. The oxidation of methane has received the most attention by researchers, with limited work reported on ethane, ethylene, acetylene and propane. Oxidation mechanisms presented to date have had limited comparison to experimental data and thus lack accurate kinetic data for the many involved reactions. Other researchers have tended away from mechanistic studies and have used global reactions, which take the various hydrocarbons to carbon monoxide and other products. An example for this global reaction for heavy hydrocarbon combustion is shown below (Smoot and Thurgood, 1979):

$$C_nH_m + (n/2)O_2 \rightarrow (m/2)H_2 + nCO \qquad ....2.24$$

The rate for long chain and cyclic hydrocarbons was given by:

$$dC_H/dt = -ATp^{0.3}(C_H)^{0.5}(C_o)\exp(-E/RT) \qquad ....2.25$$

where T is the temperature in K, p is the pressure in Pa, C_H and C_o are molar concentrations in kmol m^{-3}, t is time in s, A and E are the Arrhenius parameters and shown below in Table 2.4.

Table 2.4 Arrhenius parameters.

Hydrocarbon	A	E/R
Long-chain	59.8	12.20×10^3
Cyclic	2.07×10^4	9.65×10^3

Presently, modelling volatile combustion either assumes that the volatiles burn instantaneously as they are evolved or the combustion of carbon monoxide, methane or propane can be used as a model volatile, generally employing their global kinetics for oxidation (Shaw et al., 1990). The use of global reactions to account for the oxidation of heavier molecular weight fractions will be undoubtedly warranted, given the difficulty in incorporating a detailed chemical kinetic reaction mechanism such as that of Dagaut et al. (1987). In a detailed study by Shaw et al. (1990) the global kinetics of coal volatile combustion for 14 coals ranging from bituminous to lignite were determined (volatile matter content ranging between 40 to 80%). The reaction rate on a mass basis was treated as a reaction that was r^{th} order in volatile concentration (C_v) and $(n-r)^{th}$ in oxidant concentration (C_{ox}).

$$dC_v/dt = k[\rho^{(n-1)} C_v^{\ r} C_{ox}^{\ (n-r)}] \qquad ....2.26$$

The reaction velocity was determined from the reaction efficiency which was described by the overall energy balance and in terms of the reaction rate, which enabled the construction of Arrhenius plots to determine the global kinetic constants. It was assumed that the reaction orders for fuel and oxidant were both unity. An Arrhenius plot for over 600 experimental values of rate constants from the combustion of volatiles from fourteen coals was constructed. The activation energy values ranged from 5.6 to 18.6 kcal mol^{-1}, with two thirds of the values in the range 11.5 ± 2 kcal mol^{-1}. Thus concluded that the rate of combustion of coal volatiles does not show any dependence on coal rank.

Cho et al. (1995) reported the burning velocities of noncondensible volatiles from four coals representing ranks from sub-bituminous to low volatile bituminous. It was observed that the rates of volatile combustion change during the course of secondary decomposition, and show a significant rank dependence. Pulverised coal samples are pyrolysed in a novel coal flow reactor that independently regulates the extent of secondary decomposition. However, unlike Shaw et al. (1990), the tar and soot are filtered out and noncondensibles collected and stored.

This was seen essential as secondary decomposition of tar drastically alters the composition of the noncondensible combustible mixtures and thus the combustion rates. The fraction of soot collected was used to signify the extent of secondary decomposition. Combustible mixtures were prepared by mixing noncondensibles with oxygen and nitrogen and ignited in a combustion bomb. Laminar burning velocities are determined from transient pressure measurements during flame propagation. The concentration of gas species were quantitatively determined using FTIR and GC spectroscopy. The noncondensibles were segregated into two groups based on the qualitative form of their change during secondary decomposition. The "H_2 group" contains H_2, CO and C_2H_2. These are relatively fast burning species. The "CH_4 group" contains all hydrocarbons except C_2H_2, with all components of this group burning at roughly the same relatively slow rate. As a result of the considerably different combustion rates between the two groups, the measured burning velocities and lower heating values were found to change rapidly with varying extent of secondary decomposition and coal rank. The burning velocities tripled for all coals except for subbituminous Dietz coal, which doubled, as extent of secondary decomposition increases from 50 to 100%.

This increase in burning velocity was approximately proportional to variations in H_2 concentrations. This tendency is consistent with the conversion of oxygen and hydrogen in tar into CO and H_2, and of light hydrocarbons into acetylene. The rank dependence of the laminar burning velocities was directly related to the composition of the primary products evolved during coal devolatilisation, which varies with rank. The increase in burning velocities for higher rank coals are consistent with the evolution of significant proportions of H_2 and tar as primary products. While lower rank coals evolve relatively higher proportions of CO, CO_2, H_2O and noncondensible hydrocarbons, and a lower tar fraction as primary species. Cho et al. (1995) compared reaction rates for the noncondensible volatiles they obtained with that of Shaw et al. (1990) (soot and noncondensibles) along with other reported rates for soot oxidation. The reaction rates from Cho et al. (1995) were between one and two orders of magnitude higher than Shaw et al. (1990) and approximately an order of magnitude faster than the soot oxidation rate.

Apparent activation energies ranged from 83-135 kJ mol^{-1} as compared to the much lower values reported by Shaw et al. (1990) of between 38 and 59 kJ mol^{-1}. The study of Cho et al. (1995) was specifically directed to high temperature pulverised coal flames, where a significant difference in primary products released and extents of secondary decomposition of volatiles are to be expected, thus limiting the contribution of hydrocarbons to the burning velocity. Therefore, the global kinetics determined by Shaw et al. (1990) are deemed more appropriate for use to model the combustion of volatile matter under fluidised-bed conditions. An interesting proposal by Cho et al. (1995) was the possible description of combustion of volatile mixtures using only two pseudo components, hydrogen and carbon monoxide. By simply adding a hydrocarbon species such as methane, this postulation is essentially the same as the simple stoichiometric reaction scheme proposed by Gururajan et al. (1992) to describe the partial decomposition/combustion of volatiles. Gururajan et al. (1992) developed a steady-state isothermal model for a bubbling fluidised-bed coal gasifier. Comparisons of the predicted exit gas compositions from the model with experimental data from three pilot-scale gasifiers were made. The assumption of either complete or partial instantaneous volatile combustion resulted in significant sum-squared errors in the predicted product gas flow rates. By assuming volatiles undergo instantaneous decomposition, a significant reduction in error resulted. Gururajan et al. (1992) thus concluded that volatiles undergo partial combustion/decomposition in the bed. A simplified stoichiometric reaction scheme was derived to estimate the products of partial combustion/ decomposition of coal volatiles according to

$$C_vH_aO_bS_cN_d + \frac{1}{2}\left[v - \frac{1}{8}\left(\frac{a}{2} - c - \frac{3d}{2}\right) - b\right]O_2 \Rightarrow \frac{1}{4}\left(\frac{a}{2} - c - \frac{3d}{2}\right)CH_4 + \frac{1}{2}\left(\frac{a}{2} - c - \frac{3d}{2}\right)H_2 + \left[v - \frac{1}{4}\left(\frac{a}{2} - c - \frac{3d}{2}\right)\right]CO + cH_2S + dNH_3 \quad \text{....2.27}$$

Gururajan et al.'s (1992) model is very much an over simplification of the problem, as it is only a fancy line fitting exercise with published experimental results. A more detailed kinetic reaction scheme would be necessary. However, it does provide an ideal starting point of what major reactions need consideration in gasification modelling.

2.7 FLUIDISED-BED COAL GASIFICATION MODELLING

Various models have been proposed in the literature to predict the performance of fluidised-bed gasification and a comparison of features of these models is summarised in Table 2.5. The meanings of each column title and number in Table 2.5, which represents major features built into these models, are further explained in Table 2.6.

The two-phase theory hydrodynamics model has been most widely used in the modelling of hydrodynamics in fluidised-bed coal gasifiers. In two-phase theory, the bubbling fluidised bed is divided into two discrete phases; namely the bubble phase (or lean phase) and the emulsion phase (or dilute phase). The emulsion phase consists of the solids which are fluidised by that fraction of the feed gas required to achieve minimum fluidisation, that is, this phase is assumed to operate under minimum fluidisation conditions. The gas in excess of that required to achieve the minimum fluidisation (u_o - u_{mf}) is then assumed to pass through the bed as bubbles, thus forming the bubble phase (Davidson and Harrison, 1963). The two-phase theory of fluidisation accounts for bubble formation and growth and in this regard, it can be considered as the next stage in the development to a more complex hydrodynamic representation from simplified CSTR models.

It is generally accepted that the solids are well mixed within the emulsion phase (Yan et. al., 1998), consistent with observations regarding the solids mixing apparent in bubbling fluidised-beds. The gas passing through the bed in the bubble phase has been modelled via a "plug flow" reactor model in all those models considered above. The gas residing in the emulsion phase however has been considered as being either well mixed (Caram and Amundsen, 1979; Weimer and Clough, 1981; Overturf and Reklaitis, 1983; Saffer et. al., 1988; de Souza Santos, 1989; Gururajan et. al., 1992) or in plug flow (Neogi et. al., 1986; Ma et. al., 1988; Ciesieczyk and Gawdzik, 1994; Chatterjee et. al. 1995, Yan et. al., 1998). The suitability of these two assumptions regarding the nature of the emulsion phase gas flow has not been critically examined (ie plug flow vs CSTR assumption).

Table 2.5 A comparison of features of fluidised-bed gasifier models in the literature. (reproduced from Yan, 1999)

Reference	A	B	C	D	E	F	G	H	I	J	K	L	M	N	O	P	Q	R
Weimer and Clough, 1981	4	2	1	yes	2,4	3,5	2,3,6	yes	2,4	3,5	no	yes	yes	no	yes	no	3,4	3
Ma et al., 1988	4	2	2	yes	3,4	5,7	2,4,5	yes	1,3	3,5	yes	no	no	yes	yes	no	2,3	2
de Souza-Santos, 1989	4	2	2	no	3,4	6,7	2,3,6	yes	1,4	4	no	yes	yes	yes	yes	no	3,4	3
Ciesielczyk and Gawdzik, 1994	4	3	2	no	3,4	2,3	1	no	1,3	1	no	no	no	no	yes	no	3	2
Bi et al., 1997	4	2	2	yes	3,4	4,7	1	no	2,4	4	no	no	no	no	yes	no	3,4	2
Saffer et al., 1988	4	2	1	no	2,4	2,3	2,3,5	no	2,4	1	no	no	no	no	no	no	1	2
Gururajan et al., 1992	4	3	1	no	2,4	2,7	2,3,5	no	1,3	1,4	no	no	no	no	no	no	1	2
Neogi et al., 1986	4	1	2	no	2,4	1	1,4	no yes	1,4	2	no	no no	no no	no yes	no no	no	1	2
Purdy et al.,1984	4	3	2	yes	3,4	5,7	2,4,5	no	1,3	2,3,4	yes	yes	no	no	yes	no	2	2
Sundaresan & Amundson, 1979b	1,2,4	2	1	no	2,4	2,3	1	no	2,3	1	no	no	no	no	yes	no	1,2	1
Caram and Amundson, 1979	1,2,4	3	1	no	2,4	2,3	1	yes	1,3,4	2	no	no	no	no	no	no	2	2
Yoshida & Kunii, 1974	2	2	1	no	3,4	3,4	1	no	2,4	2	no	no	no	no	no	no	1	1
Matsui et al., 1987	2	1	1	no	2,4	1	1	no	4	2	no	yes	no	no	yes	no	1	2
Sett & Bhattacharya, 1988	3	1	2	no	2,4	3,6	1	no	2,4	2	no	no	no	no	no	no	4	2
Haggerty & Pulsifer, 1972	3,4	1	2	no	2,4	1	1	no	1,4	2	no	no	no	no	no	no	1	2
Mori et al., 1983	3	1	2	no	2,4	2,3	2,3	no	2,4	1	no	no	no	no	no	no	1	2
Purdy et al., 1981	1	1	1	no	1	2,7	2,3	no	1,3	4	no	no	no	no	no	no	1	2
Pukanic et al., 1978	1	1	1	no	1	2,3	2,3	yes	2	2	no	yes	yes	no	no	no	2	2
Yan and Rudoph, 1995	1	1	1	no	1	4,7	2,3		3	2	no					yes	2	2

Table 2.6 Features of fluidised-bed models.

A. Hydrodynamic Models
1. simplified hydrodynamic model
2. three-phase model
3. bubble assemblage model
4. Two-phase model

B Net flow
1. no
2. defined as the excess gas flow but not incorporated into conservation equations.
3. due to gasification only and incorporated into conservation equations.
4. due to devolatilisation, gasification and combustion reactions and incorporated into conservation equations.

C. Volume fractions of bubble phase in the bed
1. constant with bed height
2. variation with bed height

D. Jet region model
yes or no

E. Flow patterns in the bed
1. Gas and solids are all well mixed.
2. Gas in plug flow in the dilute phase but well-mixed in emulsion phases.
3. Gas in plug flow in both the dilute and emulsion phases.
4. Solid phase is well mixed.

F. Char combustion
1. no
2. Instantaneous
3. CO_2 is sole product
4. diffusion control
5. kinetic control
6 both kinetic and diffusion control
7. CO/CO_2 ratio is an adjustable parameter

G. Coal devolatilisation
1. no
2. instantaneous
3. product composition and yield from empirical correlations
4. product composition and yield from experimental data
5. product feed into gasifier with reactants
6. product uniformly released in the bed
7. reaction kinetics

H. Homogeneous combustion reactions
yes or no

I. Gasification reactions
1. CO_2 gasification is not considered
2. CO_2 gasification considered
3. Johnson kinetics model
1. kinetics from other correlations or experiments

J. Water-gas shift reactions
1. in equilibrium in the emulsion phase
2. in equilibrium in both phases or in the bed
3. non-catalysed kinetics in the bubble phase
4. non-catalysed kinetics in the emulsion phase
5. catalysed kinetics in the emulsion phase

K. Thermodynamic and transport properties of gases are defined as a function of T, P and C.
yes or no

L. Kinetics of formation of H_2S and COS
yes or no

M. Particle shrinking kinetics and particle size distribution
yes or no

N. Entrainment and elutriation
yes or no

O. Heat transfer model
yes or no

P. Heat loss model
yes or no

Q. Temperature
1. isothermal, input temperature
2. isothermal, include overall energy balance
3. non-isothermal, calculate gas temperature
4. non-isothermal, calculate particle temperature

R. Comparison with experimental data
1. no
2. with laboratory or pilot scale gasifier
3. with full scale gasifier

More recently however, it has been suggested that an assumption of plug flow in the emulsion phase gas and well mixed for the emulsion phase solids provides a more realistic representation of the actual behaviour in the bed (Yan, 1999).

From the literature reviewed by Gururajan et al. (1992) and Yan (1999), major shortcomings or assumptions that do not represent actual situations in the fluidised-bed gasifiers were identified. Some of these fundamental deficiencies outlined by Yan (1999) are briefly highlighted. Most critical to the successful modelling of coal gasification has been the treatment thereof for the 'net flow' concept (Column B in Table 2.5). 'Net flow' has been either neglected or treated incorrectly in the models where two-phase theory or three-phase theories are incorporated. The 'net flow' concept is different from the excess gas flow concept defined by the two-phase theory. It refers to the net generation of gas in the emulsion phase due to coal devolatilisation, homogeneous and heterogeneous reactions, and subsequent transfer of this gas to the bubble phase in order to maintain the incipient fluidisation conditions in the emulsion phase. For many fluidised-bed reaction systems, including fluidised-bed combustion of coal, volume change of gas in the bed is usually small and is commonly ignored in fluidised-bed reactor modelling (Yates, 1983). However, the volume change of gas due to reactions in a bubbling fluidised-bed coal gasifier can be significant if low rank coals are used. This has been ignored in the fundamental mass conservation equations in many fluidised-bed coal gasifier models (Column C in Table 2.5). Only a few models (Caram et al., 1979; Gururajan et al., 1992; Ciesielczyk and Gawdzik, 1994) included the net flow term in the conservation equations, but only considered the contribution of gasification reactions which is applicable for char gasification only.

Coal devolatilisation is commonly ignored in modelling (Column G in Table 2.1) (Caram et al. 1979; Sundaresan and Amundson, 1979b; Sett and Bhattacharya, 1988; Saffer et al. 1988; Kunii and Levenspiel, 1991; Gururajan et al. 1992; Ciesielczyk and Gawdzik, 1994 and Bi et al. 1997). The applications of these models are limited to only char and high rank coals. In the case where volatile matter evolution is treated, devolatilisation is assumed instantaneous and perfectly mixed with incoming fluidising gas stream. Furthermore, homogeneous combustion reactions (Column H

in Table 2.5) are often ignored, even for many models including a devolatilisation step. This varies the rates of combustion reactions in the bed because gas concentrations accounted in the model are different from actual behaviour in the bed. In other words, a very important phenomenon occurring in the fluidised-bed is ignored, ie. the competition for oxygen between char and gas in the bed.

Lastly, a majority of models (Column K in Table 2.5) treat gas transport properties as constants and ignores the effects of the operating temperature, pressure and gas concentrations on these properties. The transport properties have been found to have a significant effect on the model predictions (Yan, 1999).

In summary, Yan (1999) stated that model predictions from complex hydrodynamics models (such as three-phase model) do not show any significant improvements over those from the two-phase model, since the model predictions are more sensitive to the reaction kinetics than to hydrodynamics parameters. Most importantly, two features that ought to be included in any advanced model based on the two-phase theory of fluidisation hydrodynamics is the consideration of the 'net flow' concept and non-isothermal characteristics of coal gasification in fluidised-beds.

2.8 GAS COMBUSTION MODELLING IN A FLUIDISED-BED

Various shortcomings of current fluidised-bed gasification system models have been highlighted, in particular the poor treatment of devolatilisation and subsequent volatile combustion. To add further to the already complex task of coal gasification modelling would be the inclusion of the concentration distribution of volatile release, both radially and axially within the bed. This of course requires a description of coal particle dispersion in the radial and axial directions and the use of a detailed finite coal devolatilisation model (Stubington et al., 1990, 1992; van der Honning, 1991). The difficulties of incorporation of such a volatile combustion scheme are well documented (Srinivasan et al., 1998; La Nauze, 1985). It therefore appears useful to consider the behaviour of pre-mixed homogeneous combustion of gas in a fluidised-bed as a substitute sub-model of the more complex problem and provide a useful test for validation of reactor models (Van der Vaart, 1992; Srinivasan et al., 1998). A number of attempts to model pre-mixed gas combustion in fluidised-beds have been reported in literature as summarised in Table 2.7.

Table 2.7 Summary of mathematical models for gas combustion in fluidised-beds.

Reference	A	B	C	Other Comments
Broughton (1975)	I	III	III	Reaction in dense phase only
Pillai (1976)	I	III	I	
Yanata et al. (1975)	III	I	III	
Makhorin et al. (1985)	I	III	I	
van der Vaart et al.(1986)	I	II	I	
van der Vaart (1985)	I	II	II	Reaction in bubble phase only
van der Vaart (1992)	I,II	I	I,II	
Hayhurst et al. (1990)	I	I	III	Reaction in bubble phase only
Hayhurst (1991)	I	III	III	Reaction in bubble phase only
Achara et al. (1985)	I	III	III	Reaction in dense phase only
Srinivasan et al. (1998)	II	III	I	
Jeng et al. (1997)	IV	I	III	Spouted bed

(A) Model type: I, two phase bubbling bed model. II, three phase bubbling bed model. III, porous media (fixed bed). IV, plug flow reactor.

(B) Gas flow pattern: I, plug flow in both bubble and emulsion phase. II, well-mixed in both bubble and emulsion phase. III, plug flow in bubble phase, well-mixed in emulsion phase

(C) Energy balance: I, non-isothermal bubble phase, isothermal emulsion phase. II, non-isothermal bubble and cloud phase, isothermal emulsion phase. III, isothermal bed.

The most advanced studies to date are those of van der Vaart (1992); Jeng et al. (1997) and Srinivasan et al. (1998). Van der Vaart (1992) compared model predictions based on three varying hydrodynamic assumptions in relation to the bubble phase with experimental data for pre-mixed methane combustion. The three model assumptions were:

- two phase theory, constant bubble size
- three phase theory, constant bubble size
- three phase theory, variable bubble size

The model based on the three phase theory with bubble growth most accurately predicts bubble ignition. In particular the added mass transfer resistance introduced by the cloud phase could explain the tailing in methane conversion experimentally measured at higher bed temperatures. Furthermore, the inclusion of a bubble growth correlation reduced ignition times as smaller bubbles rise more slowly in the bed and have a smaller surface to volume ratio, which aids heat transfer. It follows that high temperature oxidation of methane can be satisfactorily explained by thermal ignition theory (van der Vaart 1992). Excellent agreement between experimental results and model predictions for methane concentration profiles. Given that no parameters were adjusted to fit the system and that a kinetic expression was used for the overall (complete) combustion of methane based on an entirely different reactor configuration, is quite remarkable.

However, van der Vaart (1992) assumed constant excess gas velocity in the bed. This may well be valid for the case of an isothermal bubble phase, but not for a non-isothermal bubble assumption as used in van der Vaart's model (Srinivasan et al., 1998). As the bubble temperature increases due to combustion, the corresponding decrease in density results in an increase in superficial gas velocity. The emulsion phase gas temperature is not expected to change appreciably from that of the bed temperature given the excellent heat transfer environment. Therefore, the minimum fluidisation velocity will remain unchanged and the assumption of constant excess gas velocity not valid.

Srinivasan et al. (1998) developed a three-phase dispersion model, which took into account variations in the superficial gas velocity on bubble properties and cross-flow parameters in overall mass balance. Model predictions showed good agreement when compared to experimental data of van der Vaart (1988, 1992) for pre-mixed combustion of propane and methane with air. In an attempt to improve model predictions, various reactions were confined to occur in either emulsion or bubble phases, with the oxidation of ethylene the most sensitive to model predictions. Most importantly, model results were very sensitive to comparatively minor variations in reaction rate parameters. The calculations were most sensitive to variations in the activation energy for propane pyrolysis. A comparison of the sensitivity of model calculations with experimental data for propane combustion to small variances in the activation energy for ethylene oxidation is shown below in Figure 2.14.

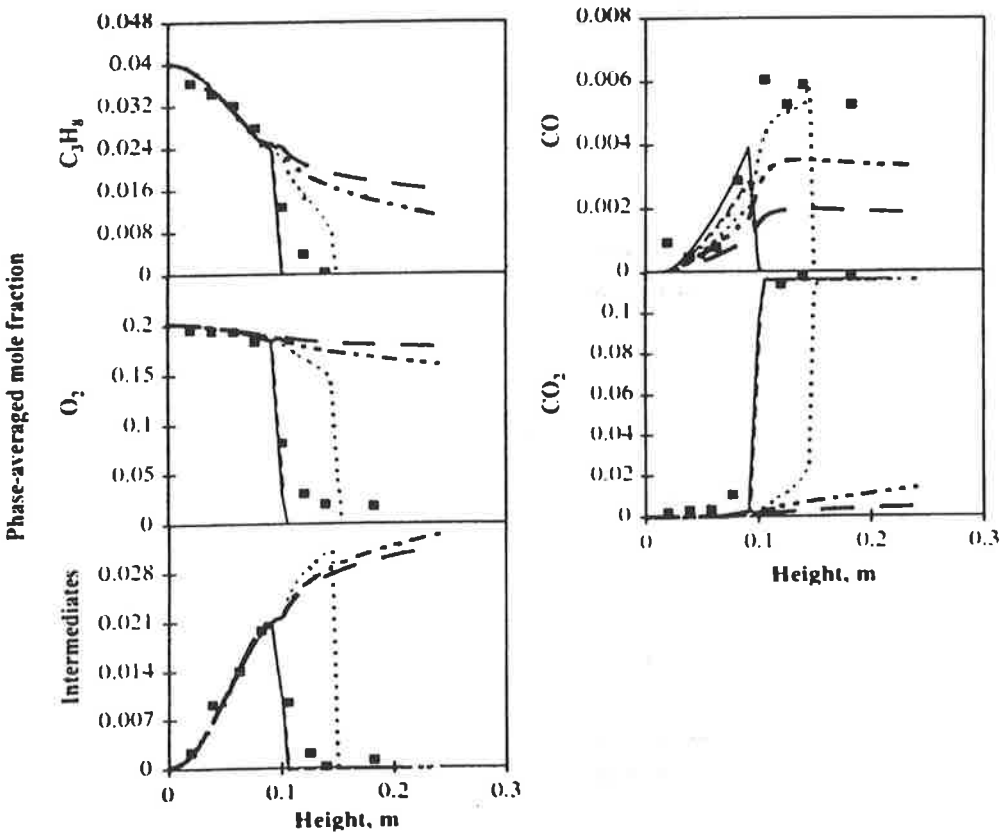

Figure 2.14 Comparison of model calculations with data (■) on propane combustion, T_{bed} = 1023 K. Effect of activation energy of C_2H_4 oxidation (bubble phase only) on model predictions: ——, E = 209 kJmol^{-1}; – – –, E = 211.1 kJ mol^{-1}; · · · ·, 213.6 kJmol^{-1}; – · –, 214.2 kJmol^{-1}, – · · –, 215.3 kjmol^{-1}, — — E = 219.5 kJmol^{-1}.

Jeng et al. (1997) developed a sophisticated kinetic model for propane combustion in a spouted bed using CHEMKIN code with bed hydrodynamics simulated as a plug flow reactor. The comprehensive reaction mechanisms and kinetics for propane oxidation in the gas phase was taken from Dagaut et al. (1987). Furthermore, a comparison of model results was made which included radical quenching mechanisms for HO_2, OH, O, H, to account for the observed heterogeneous effect of bed particles on ignition delay (Hayhurst, 1991; Dennis et al., 1982). The inclusion of radical quenching reactions improved the model predictions over consideration of gas phase mechanisms only, with concentrations including intermediate species (CH_4, C_2H_6, C_2H_4, C_3H_6, CO), found to show good agreement with experimental data in most cases.

The question that remains for fluidised-bed gas combustion modelling, are model predictions more sensitive to the reaction kinetic parameters or to hydrodynamic considerations. From the review of the above three advanced models, which scan the range of possibilities, this is not clear. From the conclusions of Yan (1999) on fluidised-bed gasification modelling, it appears most likely that it is a combination of both. Thus, a two phase model incorporating the 'net flow' concept and a non-isothermal bed, with a reasonable number of simple global reactions to account for gas phase decomposition and partial combustion of propane and its intermediates, appears to occupy the middle ground in this respect.

2.9 CONCLUSIONS FROM LITERATURE REVIEW AND OBJECTIVES OF THE PRESENT STUDY

2.9.1 DEVOLATILISATION TIME

The literature review presented in this chapter has revealed the following points with regard to devolatilisation time of low rank coals:

- The devolatilisation times of large coal particles pertinent to their utilisation in fluidised-bed combustion and gasification have been extensively reported in literature.
- The devolatilisation time was found to be influenced by the bed temperature, gas environment, particle size, moisture content, coal type and operating pressure.
- The devolatilisation time has been characterised by a classic empirical particle diameter power law relation.
- Large discrepancies in reported values for the exponent n, with most data in the range of 0.9 to 1.6.
- Evaluation of the distribution in reported exponent values for n, reveals two major centres for data at 1.0 and 1.5.
- Variability of experimental results attributed to the differences in the type of apparatus employed, definition of devolatilisation time, operating conditions, coal type, batch size and particle fragmentation.
- It has been generally acknowledged that coal devolatilisation is controlled by three main factors, heat transfer to and within the particle, chemical kinetics of pyrolysis and mass transfer of volatile products within the particle.
- For particle sizes below 1.0 mm, chemical kinetics is rate controlling.
- Current theory defines that the devolatilisation time be proportional to the square of the particle diameter, indicative of either heat or mass transfer control.
- Based on a new treatment which compares dimensionless evolution/heat-up time ratio versus a modified Damkohler/Biot number ratio, large particle devolatilisation in fluidised-beds is heat transfer controlled.

- Clearly, it is evident that experimental results, regardless of measurement technique, do not correlate with proposed square law theory.

2.9.2 VOLATILE COMBUSTION

The literature review presented in this chapter has revealed the following points with regard to volatile combustion in fluidised-beds:

- Low-rank coals contain significant amounts of volatile matter, up to 50 wt %. Understanding the subsequent release and combustion of coal volatiles within the bed is of paramount importance to the successful operation of a fluidised-bed combustor or gasifier.
- Volatile evolution and combustion processes occur at rates of one to two orders of magnitudes faster than char combustion which in turn is several orders of magnitude faster than char gasification.
- For laboratory and pilot scale coal gasifiers, carbon conversion is controlled by fast processes of coal devolatilisation and volatile decomposition and combustion.
- Volatile combustion in FBC affects oxygen distribution across bed, char burn-out times, NO_x formation, heat released between freeboard and bed, heat exchange areas, and coal particle feed point spacing.
- It is desirable to achieve high in-bed combustion efficiencies in FBC to maximise heat transfer through the inert emulsion phase to steam tubes.
- The presence of propane leads to an increase in char burn-out times and a subsequent decrease in carbon combustion efficiency.
- The in-bed combustion of volatiles under FBC conditions have been found to be dependent upon the rate of mixing between volatiles and oxygen, bed temperature, height and particle size, number of coal feed entry points, coal feed particle size and fluidisation conditions (operating velocity and geometry).
- Volatile secondary decomposition occurs via two principal reaction pathways; Thermal cracking (pyrolysis) and Repolymerisation (condensation).
- Secondary decomposition of volatile matter primarily focused on thermal cracking of tar products.

- Predominance of low molecular weight C_1-C_3 olefins over alkanes in the product distributions.
- Dominant product of gas phase thermal cracking reactions between 700 and 900°C is ethylene. At higher temperatures, acetylene becomes the major product.
- Addition of char to system alters reaction mechanism away from thermal cracking to repolymerisation reactions.
- A significant number of experimental studies into pre-mixed gas phase combustion under FBC conditions have been reported in the literature to ascertain in which phase(s) volatiles combust.
- Below a critical bed temperature, homogeneous oxidation can only occur in the bubble phase so long as it is above a minimum critical size. Otherwise, combustion will only occur in the freeboard region or at the bed surface as bubbles erupt, characterised by violent explosive combustion. As bed temperature increases, there is a gradual transition to stable conversion throughout the bed, where combustion may occur in both emulsion and bubble phases.
- The critical temperature was found to be influenced by excess fluidising velocity and bed particle size and is a function of molecular weight, ie higher molecular weight species poses a lower critical temperature for their in-bed oxidation.
- The inhibition of oxidation below critical bed temperatures has been postulated to be a result of radical quenching with sand particles or thermally controlled.
- The addition of platinum coated alumina particles or calcium carbonate was found to aid particulate phase oxidation associated with the heterogeneous combustion on the catalyst surface.
- Discrepancies in reported critical temperatures for oxidation of hydrocarbons is a result of the different bed particle sizes used. This influences the bubble regime under which the bed operates, ie clouded or cloudless bubbles.
- Non pre-mixed combustion typically requires 1-2 orders of magnitude larger bed depths in order to achieve complete combustion as compared to pre-mixed combustion.
- There is currently a lack of suitable kinetic expressions for high temperature decomposition and oxidation of coal volatiles.

2.9.3 VOLATILE COMBUSTION MODELLING

The literature review presented in this chapter has revealed the following points with regard to volatile combustion modelling in fluidised-beds:

- Two phase theory most widely used in literature to model bed hydrodynamics during fluidised-bed coal gasification.
- Many fundamental deficiencies exist in current models in the literature, most critically has been the treatment thereof for the 'net flow' concept.
- The 'net flow' refers to the generation of gas in the emulsion phase due to coal devolatilisation, homogeneous and heterogeneous reactions and subsequent transfer of this gas to bubble phase in order to maintain incipient fluidisation state in emulsion phase.
- Incorporation of the volume change in gas flow due to reactions for low-rank coal fluidised-bed gasification is paramount to successful model predictions.
- Modelling of coal devolatilisation process was typically ignored altogether or assumed to occur instantaneously and products fed into the reactor with fluidising stream.
- Modelling of volatile combustion process has either been ignored altogether or assumed to burn instantaneously.
- Vitally important to include volatiles in modelling as the important phenomenon of competition for oxygen between char and volatile combustion is otherwise ignored.
- The difficulties of incorporating a detailed description of coal particle dispersion in both the radial and lateral directions and the use of a finite coal devolatilisation model to account for volatile concentration distribution in the bed is well documented.
- It appears useful to consider the behaviour of pre-mixed volatile combustion of gas in a fluidised-bed as a substitute sub-model of the more complex problem to provide a useful test for validation of reactor models.
- It is not clear whether model predictions are more sensitive to hydrodynamic or kinetic parameter constraints.

2.9.4 LIMITATIONS IN THE CURRENT LITERATURE

Based on the literature review presented in this chapter it has been possible to highlight several areas, which require significant improvement. The most distinctive of these areas for devolatilisation time has been the development of a suitable theory supported by a simple, reliable, quantitative technique to characterise the rate of devolatilisation for low-rank coal particles under a variety of experimental conditions. The inability of theoretical predictions to match experimental data can be attributed to ill informed conclusions based on variable experimental data because of the use of a myriad of experimental definitions and operating conditions. The importance of devolatilisation time in context to volatile dispersion and subsequent combustion modelling have been highlighted. Thus, accurate prediction of devolatilisation time will have ramifications relating to coal particle feed spacing in the bed.

Current modelling of fluidised-bed gasification of coal has either ignored or poorly treated devolatilisation and subsequent combustion of volatiles in the bed. As a substantial amount of the energy released is in the form of volatile matter, with homogeneous decomposition and combustion reaction rates many orders of magnitude greater than heterogeneous oxidation and gasification reactions, it is vital that homogeneous reactions are satisfactorily accounted for in reactor models. The importance of volatile combustion and its impact on char combustion of low-rank coal has received scant attention in the literature. Furthermore, the inaccuracies of the current experimental techniques used in the literature have been highlighted. Thus, there is a further need for experimental verification of the influence of volatile combustion on the char combustion rate, particularly for highly reactive chars typically derived from low-rank coals.

Numerous experimental studies have been conducted in relation to volatile matter combustion under FBC conditions, in particular in-bed gas sampling of pre-mixed hydrocarbon/air mixtures to determine the rate and location of volatile combustion.

While qualitatively it is expected that similar dependencies shall arise for fluidised-bed gasification of low-rank coal, there are distinct differences in relation to the bed environment as compared to FBC conditions. Unlike for FBC, where the principal make-up of the bed is inert sand, the proportion of combustible char in the bed for FBG is an order of magnitude greater than in FBC (25-40 % as compared to 1-3 %, respectively). Furthermore, air is supplied in excess of stoichiometric quantities for FBC, unlike reducing environment in FBG conditions where steam is the principal reagent. The implications for FBG of coal will be:

- The reducing environment in a FBG will lead to significant thermal cracking and the partial combustion of volatile intermediates to CO.
- The high proportion of char inventory within the bed will ensure the complete consumption of oxygen well before the bed surface.

Thus, there is an immediate need for an experimental investigation to quantify the gas phase reactions of volatiles in environments simulating fluidised-bed gasifiers. Knowledge gained will aid in verification of mathematical models and help determine design parameters, such as the requirement for secondary air injection into the freeboard.

2.9.5 Objectives of the Present Study

Based on the literature review presented here, and the limitations of present status of knowledge identified in the previous section, the objectives of the present study are as follows:

- To develop a simple measurement technique for coal devolatilisation time, capable of producing reliable and repeatable data. To test the influence of various operating parameters on the devolatilisation behaviour of coal particles in a fluidised-bed environment.
- To develop a suitable theoretical expression that successfully integrates experimental observations for devolatilisation time of coal particles in a fluidised-bed environment.

- Investigate the influence of coal volatile matter, as simulated by propane, upon the combustion rate of highly reactive low-rank coals. This is to be achieved by using an alternative technique to the literature based on the measurement of the periodic weight loss of a batch of coal particles.
- To perform a detailed chemical analysis of the in-bed axial concentration profiles during pre-mixed propane and air combustion under simulated fluidised-bed gasification environment.
- To develop a suitable mathematical model that can accurately account for gas combustion under fluidised-bed gasification conditions.

CHAPTER 3

EXPERIMENTAL

3.1 INTRODUCTION

As has been mentioned, a practical understanding of coal devolatilisation and subsequent combustion of volatiles is fundamental to the successful development of a good predictive mathematical model to simulate fluidised-bed coal conversion processes. This section outlines a description of the experimental apparatus used and the techniques employed in this study to measure the temperature response of a low-rank coal particle during devolatilisation, char weight loss with increasing burn-out time and the in-bed axial concentration profiles for pre-mixed combustion of propane in a fluidised-bed gasifier. A very significant but largely unreported proportion of time and effort was expended in the development of the experimental system, including engineering design, construction, process instrumentation and control and commissioning of the reactor, gas analysis system including sample probe and sampling manifold and familiarisation with Fourier transform infrared spectroscopy. The experimental results reported here are believed to provide the first comprehensive data on volatile combustion under fluidised-bed gasification conditions. Furthermore, the results provide a new insight into coal devolatilisation process based on a novel experimental technique and definition time to measure the devolatilisation time of a coal particle in a fluidised-bed.

3.2 EXPERIMENTAL APPARATUS

The fluidised-bed reactor used in this study was fabricated in the chemical engineering workshop by staff of the Department of Chemical Engineering, University of Adelaide. Some specifications of the reactor were based on the fluidised-bed combustion reactor developed by Linjewile (1993). The rig consists of four main sub-units including the packed bed steam generator/gas preheater, water cooled plenum chamber, fluidising chamber, gas sampling and temperature measurement system.

Preheater/generator comprise of a 25 mm i.d. by 400 mm long 253 MA stainless steel tube filled with ceramic saddles supported on a stainless steel wire mesh. Gas was fed from the top of the reactor and a water outlet also fitted just above the top of the packing. Water flow rate was regulated by a KDG 1100 water flow meter with a range of 0 to 28 cc min^{-1} at 20°C. The gas flow to the preheater is supplied via gas cylinders, or an air compressor and regulated by three Metric Series tube size 10E, 14E and 24E rotameters. The gas supply pressure was 40 kPa. The outlet temperature of gas/steam mixture was set at 250°C. This was measured by a thermocouple located along the connection pipe between the preheater/generator and the fluidised-bed gasifier. The packed bed preheater/generator was heated by four 450 mm vertically suspended Kanthal type DS silicon carbide bayonet heating elements capable of delivering a maximum of 8 kW. Two of the elements are connected to a dimmerstat 28D-3P variable transformer enabling the input voltage to be regulated between 0% and 100% of the maximum and forms the base heating load. The remaining two elements are connected to a PAC-15 series thyristor and controlled by a Shimaden SR17 PID temperature controller, and provides the additional heating load required to maintain the set-point temperature. The furnace section was surrounded with refractory bricks supported in an angle iron frame.

A unique feature of the fluidised-bed gasifier is the water cooled plenum chamber. The chamber was surrounded by a water-cooled jacket with a K-type thermocouple silver soldered to the underside of the distributor plate to maintain the surface temperature of the plenum chamber and distributor plate at 400°C. This is well below the auto ignition temperature for propane of 450°C. Chemically pure propane gas (99.9999%) supplied by BOC gases from a gas cylinder was regulated through a double needle valve and a KDG 1100 flow meter arrangement. This ensured a constant supply pressure of 20 kPa as measured by a DP 0-30 kPa gauge. Above the feed inlet of the propane a stainless steel wire mesh was inserted in between the bottom flange of the plenum chamber to aid thorough mixing of gas entering the fluidised bed. To ensure even gas distribution over the bed cross-section, CO_2 was fed as a tracer gas through the propane line into an oncoming stream of air.

Gas analysis tests across the distributor plate were subsequently conducted using the water-cooled probe connected to the FT-IR spectrometer. Even mixing of CO_2 with air was observed.

The fluidising chamber comprises a 102 mm i.d. by 600 mm long 253 MA stainless steel tube fitted with a perforated gas distributor plate with 121 holes of 0.4 mm diameter arranged in 8 mm triangular pitch. The bed temperature was measured by a 1.5 mm type K thermocouple located 30 mm above the distributor plate. The pressure drop across the bed was measured by two manometer tapping's located 50 mm and 300 mm above the distributor plate connected to a Dwyer m-400 water manometer. The thermocouple outputs from the entire system were displayed on a Shimaden SD 10 digital readout via a Shimaden KR 10 thermocouple selector unit on the control panel. The fluidising gasifier chamber was similarly enclosed by refractory bricks and electrically heated in the same arrangement as the preheater/generator system. The supply and apparatus pressures were monitored by Blackwood pressure gauges.

An over-bed coal screw feeder and hopper located 400 mm above the distributor plate was used to fed +2.5 - 3.1 mm Yallourn coal char particles. The mechanical screw feeder was fitted with a water-cooled jacket in addition to a nitrogen purge stream introduced into the coal hopper to prevent char combustion and gas backflow, with subsequent condensation of vapour in the feeder. The coal feeder was calibrated based on the controlled rotational speed of the motor driving the feeder, and was recorded manually. The gas exiting from the reactor was passed through a well-insulated cyclone, which removed the elutriated solid particles. After leaving the cyclone the gas stream passed through two water-cooled heat exchangers in series. This resulted in the condensation of steam, which was collected in a condensate receiver and measured using a volumetric cylinder. A side draw of the off-gas could be sampled before passing through a MT-5 Toyo gas meter to measure the volumetric flow rate of the off-gas from the reactor and vented to atmosphere via extraction unit assembly. The bed material for all experimental conditions was quartz sand filled to a static bed height of 10 cm. A schematic of the apparatus is shown in Figure 3.1.

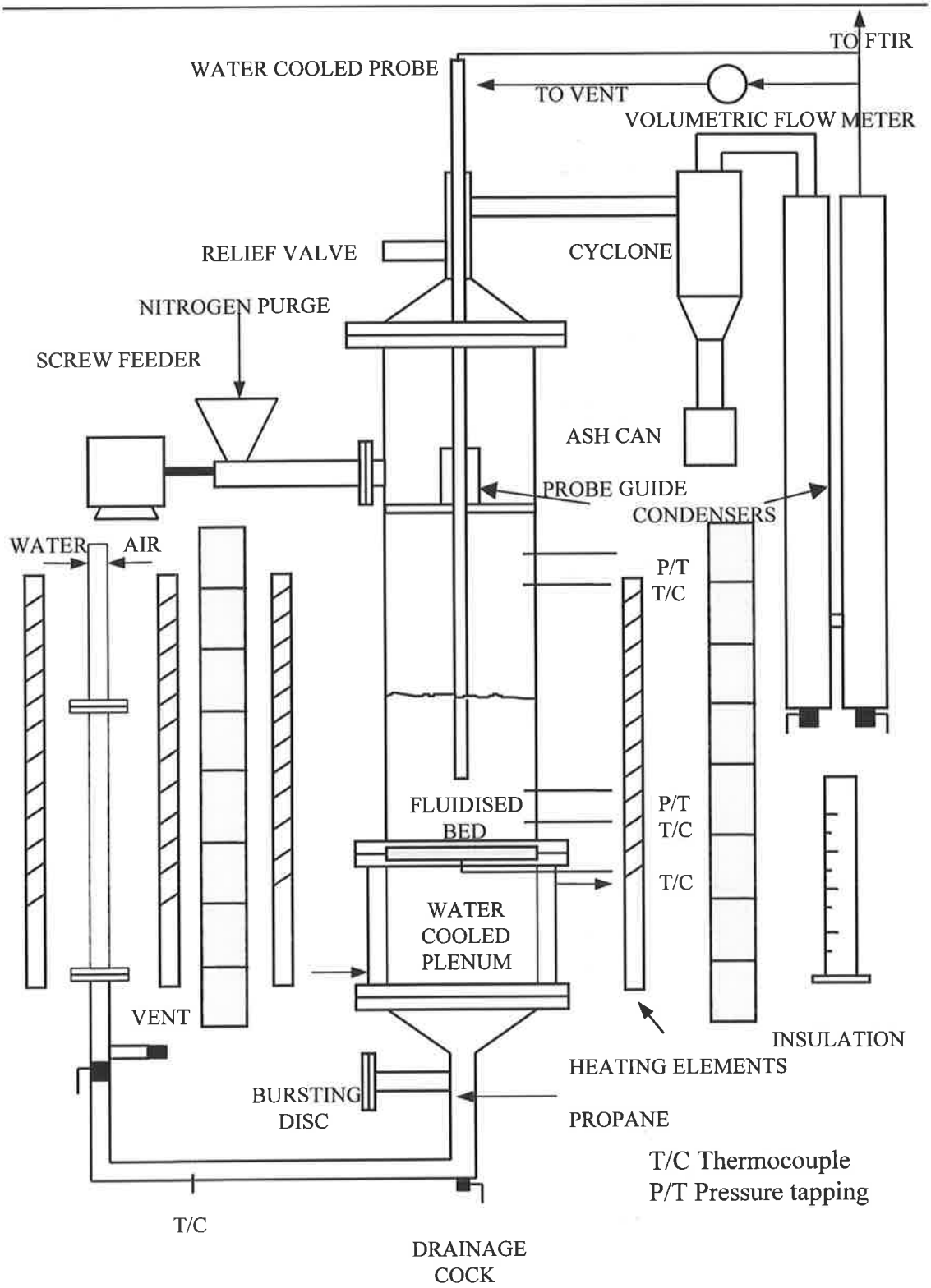

Figure 3.1 A schematic of the experimental apparatus

Continuous gas sampling from various points along the axial direction were taken using a water-cooled stainless steel probe fitted with a stainless steel wire mesh tip. Water vapour is a common source of interference when determining gas-phase compound concentrations using FTIR spectroscopy.

Gas conditioning typically involves cooling, separating and dehumidification of the sampled gas. As the water cooled probe effectively cools the sample gas to room temperature, subsequent conditioning only requires a water trap to separate condensed steam and a tapered drying tube filled with self indicating silica beads to absorb the residual moisture. The gas was drawn through the FTIR gas cell by a BUSCH 150 mbar dry rotary vane vacuum pump located upstream. A constant cell vacuum pressure of -80 kPa is controlled by using a needle valve located upstream from cell. Exhaust gas from pump is then split, with gas metered on-line through a ADC infrared flue-gas analyser for continuous monitoring of carbon monoxide (CO), carbon dioxide (CO_2) and propane (C_3H_8) and remanning gas vented via the extraction unit. Symmetrical diatomic molecules (eg. N_2 and O_2) are not infrared-active and must be analysed using other techniques. For O_2, a MC O_2 analyser (model PMA-10) was used to monitor the concentration. Calibration of these analysers were conducted prior to each experiment by passing through standard gas mixtures to correct for the zero and span of the meter. The ADC infrared analyser was used purely as qualitative guide and allowed for immediate and meaningful interpretation of the profiles and state of gasification in the system. All quantitative gas analysis, except for oxygen, was via the FTIR spectrometer.

Quantitative data was collected by a Perkin-Elmer System 2000 FTIR spectrometer equipped with a liquid cooled mercury-cadmium-telluride (MCT) detector. A Graseby Specac 10 cm gas cell equipped with zinc selenide windows is used to monitor for CO_2, CO, C_3H_8, propylene C_3H_6, ethane C_2H_6, ethylene C_2H_4, acetylene C_2H_2, and methane CH_4. During the present tests, spectra are collected in a continuous mode at a resolution of 4 cm^{-1}, where 25 scans are added to form an average single beam spectrum for each bed sampling point. An absorbance spectrum is produced from the ratio of the average spectrum and a background reference spectrum (100% nitrogen) collected immediately prior to each sample point in the bed. Software facilities are used for automated baseline correction of each of the absorbance spectra files before integration of specific band areas for comparison with calibrated spectra of known concentrations using Quantbasic software. The calibration spectra are generated by passing known concentrations of each gas to be

measured through the cell at the reference cell pressure. All special gas mixtures were prepared by BOC gases and NATA certified. Integration band regions for each gas component are listed in Table 3.1. Figure 3.2 outlines the on-line gas analytical system and Figure 3.3 shows the calibration curves for the various gas components at a vacuum pressure of -80 kPa and at ambient temperature. In all instances, the fitted calibration curve regression coefficient, R^2 was greater than 0.99.

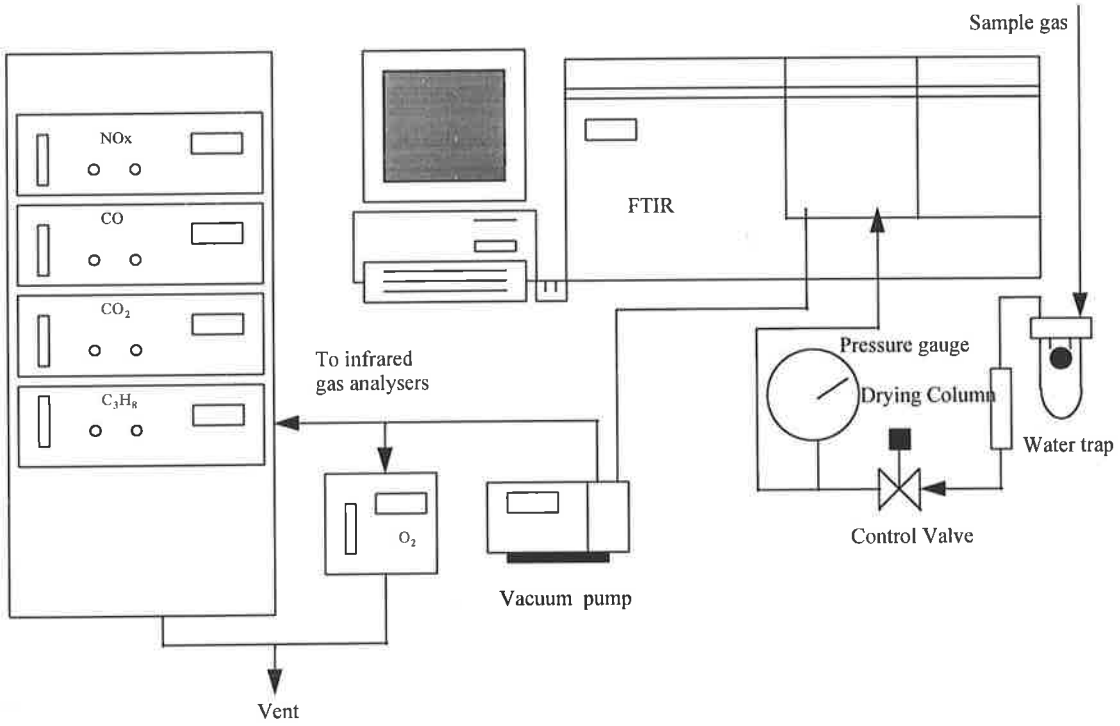

Figure 3.2 A schematic of the gas analysis system

Table 3.1 FTIR integration band regions for sampled gas species.

Component	Band region of integration (wave number, cm^{-1})
Methane	3020-3010
Ethane	2960-2950
Propane	2971-2965
Acetylene	735-725
Ethylene	952-944
Propylene	916-907
Carbon monoxide	2230-2143
Carbon dioxide	2349-2389

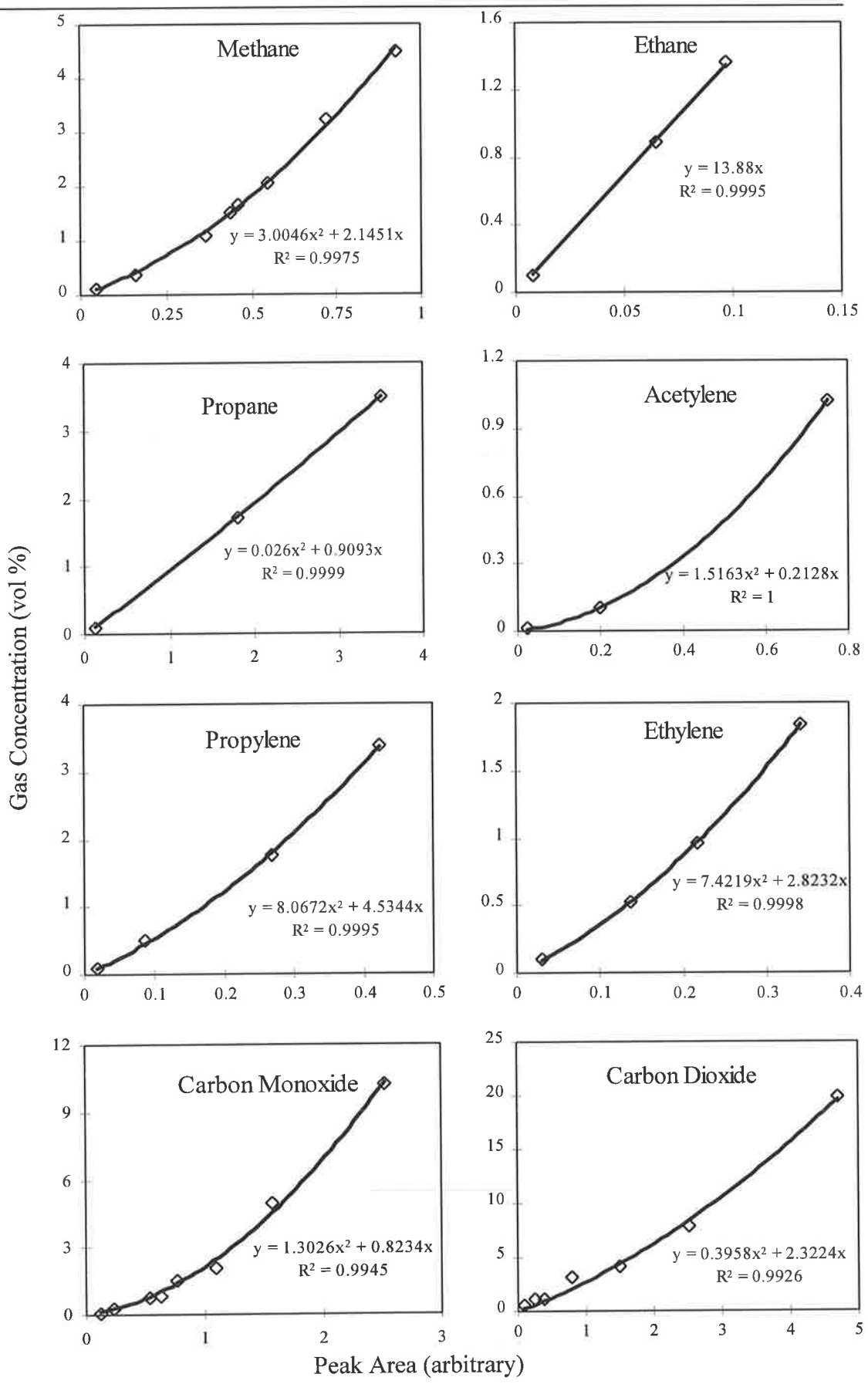

Figure 3.3 Calibration curves for gas species

A schematic diagram of the water-cooled probe used to sample gases from fluidised-bed and to act as a heat shield for the thermocouple during particle temperature measurements is illustrated below in Figure 3.4.

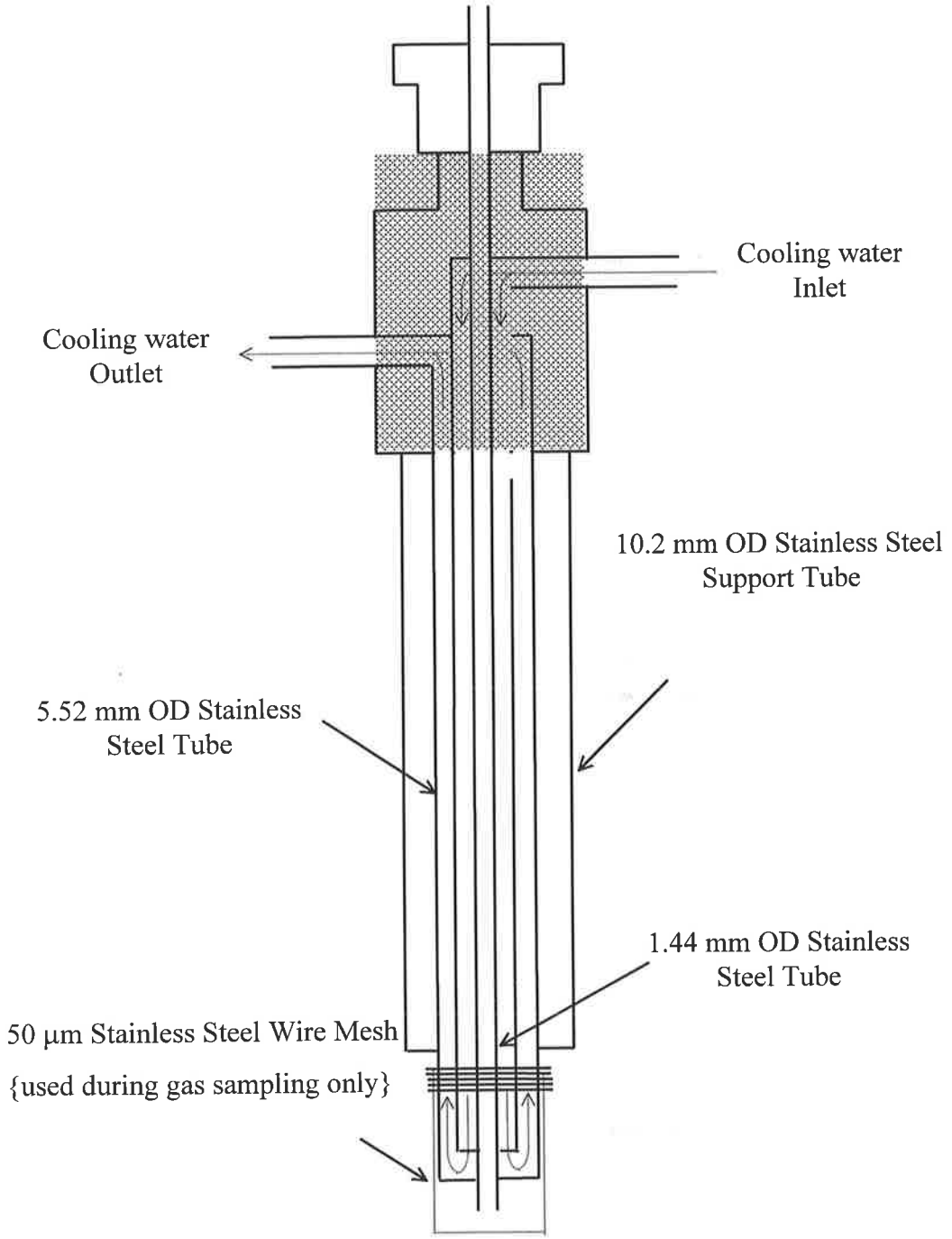

Figure 3.4 A schematic of the water-cooled probe

For particle temperature measurements, the fluidised-bed cover and water-cooled probe guide were removed to allow for easy insertion of the probe. A sufficiently long thermocouple was threaded through the inner tube of the probe and connected to data logging device. To prevent the influx of air into the bed during experimental runs, a nitrogen purge stream of approximately 10 l min^{-1} was introduced via the coal feeder. The temperature measurements obtained in this investigation have been collected via the use of a 1.0 mm K-type Chrome-Alumel thermocouple with a 310 stainless steel sheath. The thermocouple is connected to a Pico TC-08 8 channel thermocouple A/D data logging system interfaced with a standard IBM compatible personal computer.

The signal from the TC-08 input device is analysed by Picolog data logging software. The software has in-built cold junction compensation algorithms as well as algorithms for thermocouple curve normalisation based on the type of thermocouple in use thus enabling temperature measurements to be recorded automatically at pre-determined intervals. Temperature readings were recorded at intervals of 3 s, which enabled the signal filter to be used. The signal filter determines the relative amount of electrical noise and adjusts the thermocouple signal automatically. For each coal particle size interval, the experiment was repeated three times and an arithmetical average temperature profile calculated.

Similarly for particle weight loss measurements, the fluidised-bed cover and water-cooled probe guide were removed to allow for easy insertion of mesh basket. For the duration of the experiments, oxygen concentration of the diluted air stream was maintained at 10% v/v. The oxygen concentration of the fluidising gas stream was checked with an oxygen analyser by sampling the gas in the bed using the water cooled probe. As the measurement technique relies on the difference between the initial and final weights of the particle, the ash content of the coal must be preserved. As char burn-out progresses, a thin ash layer forms around the particle. In order to minimise the fracturing of this ash layer and consequent error in mass loss balance, a fine sand size was employed and the bed excess superficial operating velocity was kept to twice the minimum fluidisation velocity.

The technique of Andrei et al. (1985) was used to measure the time resolved burn-out history. An 850 μm mesh basket was inserted into the fluidised bed and sand was allowed to percolate through. From a batch of pre-sieved and dried +3.175 -3.35 mm Loy Yang coal particles, seven coal particles were taken and weighed. The particles were dropped into the bed and a stop-watch started. At predetermined time intervals after the completion of devolatilisation (extinction of volatile flame), the basket was removed and placed into a quenching chamber. Nitrogen gas acted as the quenching medium. After a sufficient time the basket was carefully withdrawn and char particles retrieved and reweighed and weight loss determined. Summaries of main operating parameters during particle temperature, char weight loss and volatile combustion experiments are outlined in Tables 3.2, 3.3 and 3.4.

Table 3.2 Operating parameters for particle temperature experiments.

Bed Temperature	°C	750, 850, 950
Sand particle size	μm	180-350
Sand density	kg m^{-3}	2600
Minimum fluidisation velocity, u_{mf}	m s^{-1}	0.035
Operating pressure	kPa	101.3
Static bed height	mm	100
Superficial operating velocity	m s^{-1}	0.10
Gas feed temperature	°C	250
Steam feed rate	kg hr^{-1}	0.23
Air/Nitrogen feed rate	l min^{-1} (STP)	12

Table 3.3 Operating parameters for weight loss experiments.

Bed Temperature	°C	700, 800, 900
Sand particle size	μm	180-250
Sand density	kg m^{-3}	2600
Minimum fluidisation velocity, u_{mf}	m s^{-1}	0.027
Superficial operating velocity	m s^{-1}	0.06
Operating pressure	kPa	101.3
Static bed height	mm	100
Coal particle size	mm	+3.175 -3.35
Gas feed temperature	°C	250
Propane feed rate	dm^3 min^{-1} (STP)	0.3
Air/Nitrogen feed rate	dm^3 min^{-1} (STP)	10

Table 3.4 Operating parameters for volatile combustion experiments.

Bed Temperature	°C	750, 850, 950
Sand particle size	μm	350-500
Sand density	kg m^{-3}	2600
Minimum fluidisation velocity, u_{mf}	m s^{-1}	0.063
Operating pressure	kPa	101.3
Static bed height	mm	100
Superficial operating velocity	m s^{-1}	0.25
Gas feed temperature	°C	250
Char particle size	mm	+2.5 -3.1
Steam feed rate	kg hr^{-1}	0.6-0.7
Char feed rate	kg hr^{-1}	0.28-3.0
Air feed rate	dm^3 min^{-1} STP)	25-30
Propane feed rate	dm^3 min^{-1} (STP)	0.8-1.0
O_2/coal	kg kg^{-1} daf	1.1
H_2O/coal	kg kg^{-1} daf	2.0
O_2/H_2O	kg kg^{-1}	0.9
O_2/C_3H_8 molar ratio		4.4

It should be noted that the relative feed rates of propane to char was based on the assumption of a low-rank coal with a volatile matter content of 40 wt% daf. Subsequent flow rates of air and steam are based on typical feed ratios reported in the literature for fluidised-bed gasification of low-rank coals (Neogi et al. 1986; Goyal et al. 1990). Furthermore, the sand size was changed to allow for direct comparison with the data of van der Vaat (1985) under FBC conditions, where a 350-500 μm sand size range was used. The bed particle size is known to influence the combustion behaviour of volatile matter (van der Varrt, 1985; Srinivasan et al., 1998). The choice of propane as a practical volatile substitute was based on its thermochemical and combustion properties resembling more those of complex fuels (coal volatile matter) than light hydrocarbons like methane and ethane (Dagaut et al. 1987). This is supported by the work of Mullins (1953), who observed that the ignition delay time for propane was approximately the same as compared to other C_4-C_{11} aliphatic hydrocarbons and aromatic hydrocarbons. Furthermore, propane has been consistently used in the literature as a synthetic volatile under FBC conditions (van der Varrt, 1985; Hayhurst, 1991; Dennis et al., 1982; Hesketh et al., 1991).

3.3 SAMPLE PREPARATION

A South Australian and a Victorian low-rank coal were selected for the current study to observe the effects of particle size, bed temperature and moisture content on the devolatilisation time. A further five coals of varying rank were investigated to observe the effect of coal type on the devolatilisation time. The proximate and ultimate analyses of all seven coals are shown in Table 3.5.

Table 3.5 Proximate and ultimate analyses of coals used in devolatilisation time experiments.

	Proximate Analysis (wt%)				Ultimate Analysis (%daf)				
Coal Name	Moisture (ar)	Ash (db)	VM (db)	FC (db)	C	H	N	S	O (by diff.)
Bowman Coal	52	11.6	49.2	39.2	69.4	4.6	0.5	4.6	20.9
Morwell Coal	55	2.4	48.2	49.4	68.9	4.9	0.53	0.32	25.3
Surat 252	14.4	12.3	45.3	42.4	78.8	6.36	1.04	0.46	13.3
G-Qld 184 Coal	12.0	30.5	28.2	41.3	80.5	5.56	1.81	0.42	11.7
I - Qld 177 Coal	15.0	21.2	26.0	52.8	79.4	4.09	1.27	0.29	14.9
Bowen 249	8.7	11.8	25.4	62.8	86.2	5.14	2.02	0.63	6.0
Bowen 238	6.1	11.6	9.0	79.4	91.7	3.60	1.80	0.8	2.1

Spherical coal particles were produced by using a linear shear to smooth the sides of 8, 10 and 15 mm cubes cut from a large lump of coal. Once prepared the particles were stored in an air tight container to avoid drying taking place. Prior to the temperature measurements, 1 mm holes were drilled to the centre of the coal particles. Dry particles were prepared by drying the wet coal particles produced via the above-mentioned technique. Due to brittleness of the dried coal particles, holes were drilled prior to drying. In addition, as significant particle shrinkage was observed during drying, it was necessary for slightly larger 1.2 mm holes to be drilled to accommodate the 1 mm thermocouple after drying. The coal particles were placed into a temperature controlled oven initially at 40°C for several hours before the temperature was incrementally increased by 20°C to 105°C and allowed to dry overnight to ensure

all moisture was removed. It was found that if particles dry too rapidly, significant cracking or even fragmentation occurs. Finally, coal samples used to investigate the effect of coal moisture on the devolatilisation time were dried for varying lengths of time by the above method. Periodic measurement of individual particle weight loss allowed for determination of moisture content of coal particles. Once again, all coals were stored in an air tight container to avoid absorption of moisture.

Table 3.6 details the proximate and ultimate analyses of Loy Yang coal used in the weight loss experiments. A size fraction of +3.175 -3.35 mm is used in the current study. The proximate and ultimate analyses for Yallourn char prepared by the Australian Char Pty. Ltd. at 800°C used in volatile combustion experiments is also listed in Table 3.6. Further details of char preparation can be sought from Bhattacharya et al. (1998). A size fraction of +2.5 -3.1 mm is used in the current study and is collected and sieved from a sealed plastic lined drum. The char sample was stored in an air tight container to avoid absorption of moisture.

Table 3.6 Proximate and ultimate analyses of Loy Yang coal and Yallourn char.

Proximate Analysis, as received, wt%	Loy Yang coal	Yallourn char
Moisture	10.0	7.1
Volatile matter	45.3	3.6
Fixed carbon	43.4	85.6
Ash	1.3	3.7
Ultimate analysis, % wt (dry basis)		
Carbon	67.4	92.4
Hydrogen	4.9	0.8
Nitrogen	0.6	0.7
Oxygen	25.5	1.9
Sulfur	0.2	0.23
Ash	1.4	4.0

3.4 DEVOLATILISATION TIME MEASUREMENT

Coal particle devolatilisation time has been dealt with extensively in the current literature as reviewed in chapter 2. The variability of the experimental results have been attributable to the differences in the type of apparatus employed, definition of devolatilisation time, operating conditions, coal type, batch size and particle fragmentation (Stubington et al., 1997; van der Honing, 1991; Stubington et al., 1991). Many of these experiments are best described as qualitative in their methods and there is significant discrepancy surrounding the influence of a number of parameters, as well as uncertainty in theoretical postulations. A fundamental aim of this section of work is to develop a simple and reliable technique for measuring the devolatilisation time of large mm-sized coal particles. Four methods have been used to date in the literature to measure the devolatilisation time, these being;

- total volatile weight loss measurements by a thermogravimetric analysis (TGA)
- the time during which a visible flame was observed (flame period/extinction)
- volatile evolution by gas analysis under pyrolysis conditions
- CO_2 gas analysis under combustion conditions

Measuring the weight loss with time of coal by TGA is the most accurate of all the four techniques. However, the particle environment in a TGA is significantly different to that compared in a fluidised-bed. In particular, heating rates are more than a magnitude greater in fluidised-beds and thus, these results are not quantitatively applicable to fluidised-beds (Stubington et al., 1991). Furthermore, weight loss measurements in fluidised-beds are impossible due to differences in buoyancy between phases and vigorous bubbling action of the bed.

Volatile or CO_2 gas analysis has proven to provide the most quantitative method thus far for measuring the devolatilisation time of coal in fluidised-bed. Morris and Keairns (1979) measured the methane evolution profile during pyrolysis of -4.0 + 0.5 mm sub-bituminous coal, while Stubington et al. (1992, 1997) measured the carbon dioxide evolution profile during combustion experiments of -12.0 + 2.0 mm bituminous coals.

However, the down side to these techniques is the requirement for adjustment of the off-gas concentration curves to compensate for time lag and gas dispersion occurring within the fluidised-bed and sampling line. Furthermore, the exact definition of the end-point is ambiguous due to the tailing effect of volatile release. An example of this has been the change in definition times between the work of Stubington et al. (1997) and Stubington et al. (1992) to mirror observations based on flame extinction time experiments. As will be shown and discussed in subsequent section detailing results from current experimental findings, this change in definition time is not necessary.

The most frequently used technique in the literature to measure the devolatilisation time is the flame extinction time. The flame extinction time is defined as the time of particle injection into the bed until the extinction of any visible flame at the bed surface or around the particle. It has been generally observed that the particle floats at the top of the bed surface during devolatilisation and only once char combustion has commenced does the particle sink below the bed surface (Pillai, 1981, 1982; Schluter et al., 1997). From the authors experience it can be difficult to ascertain the exact point of the extinction of the diffusion flame surrounding the particle and the commencement of char combustion at the surface.

In a review of literature by Ross (1996), it was suggested that the uncertainties in reported rates of devolatilisation might well be clarified through particle temperature measurements. Numerous investigators have measured the coal particle centre temperature for particle sizes ranging between 6.4-20 mm in fluidised-beds (Stubington et al., 1984; Tomeczek et al., 1990; Pillai, 1985; Heidenreich, 1999; Zhang et al., 1990; Schulter et al., 1996; Baskakov et al., 1987; Tia et al., 1991; Kilic et al., 1993; Adesanya et al., 1995; Dincer et al., 1996; Linjewile (1993); and Winter et al., 1997). However, for the experiments performed in relation to devolatilisation, it was simply a means to demonstrate the time lag before the centre of the particle reached the bed temperature. Thus of course supporting the view that devolatilisation of a large coal particle is heat transfer controlled (Stubington et al., 1984; Tomeczek et al., 1990; Pillai, 1985; Heidenreich, 1999; Zhang et al., 1990).

Heidenreich (1999) investigated the relative roles of heat transfer and chemical kinetics in controlling the devolatilisation of large particles. A better indication of the controlling regime during devolatilisation could be obtained by considering the ratio between the time required for evolution of volatile matter and the time required for the particle to reach the maximum devolatilisation temperature. For large coal particles undergoing devolatilisation in a fluidised-bed environment, the ratio of the two times was unity, indicating that devolatilisation is heat transfer controlled (refer to Section 2.5.1 and Figure 2.6). Thus, the time required for the centre temperature of a particle to reach the final devolatilisation temperature, or in this instance the bed operating temperature, can be used to define the characteristic devolatilisation time.

Heidenreich (1999) observed that for + 10 -11 mm Bowmans coal particles that the particle temperature profiles for the insertion of a bare thermocouple into the centre of the coal particle, termed "*conventional technique*" during drying/devolatilisation are affected by thermal conduction along the thermocouple sheath toward the junction end. This leads to an overestimation of the actual temperature response. In order to mitigate this effect, shielding the thermocouple sheath from the bed environment significantly reduced the external heat transfer to the thermocouple. The thermocouple was inserted through a water-cooled probe. If the water-cooled probe was pressed against the measured particle, the opposite was observed in that heat was conducted away from the particle to the probe thus influencing the temperature response. However, if a gap was left between the probed and particle surface, the probe was unable to fully alleviate conduction effects along thermocouple sheath to the junction end. Thus, it was found that the presence of "*shielding coal particles*" to act as a thermal barrier and replicate the axial temperature profile of the thermocouple as in the measured particle during devolatilisation significantly improved the result. Based on these findings, Heidenreich (1999) deduced and optimally found that for fluidised-bed conditions, a two shielding particle-one equivalent particle diameter separation between the water-cooled probe and shielding particles gave the best result. This method was to provide a reliable and reproducible technique for quantification of the temperature response of coal particles. The experimental arrangement of the particle temperature measurement is shown in Figure 3.5.

A thin stainless steel wire was wrapped around the particles and secured onto the thermocouple to prevent particles from slipping off. A comparison of modified technique with conventional technique is shown in Figure 3.6 for a dry Bowmans coal particle at 600°C in a fluidised bed (Heidenreich 1999).

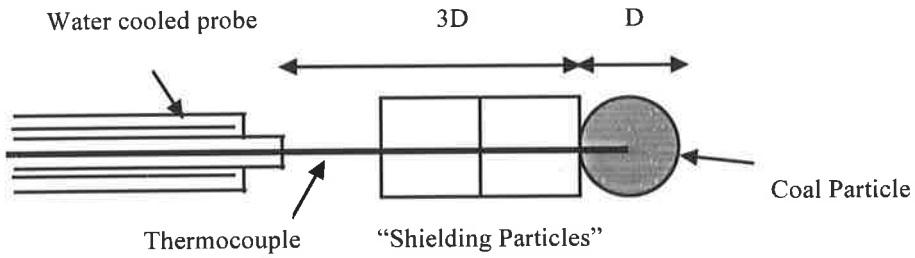

Figure 3.5 Modified three particle, water cooled probe technique for measuring the particle temperature response of coal in a fluidised-bed reactor (Heidenreich, 1999).

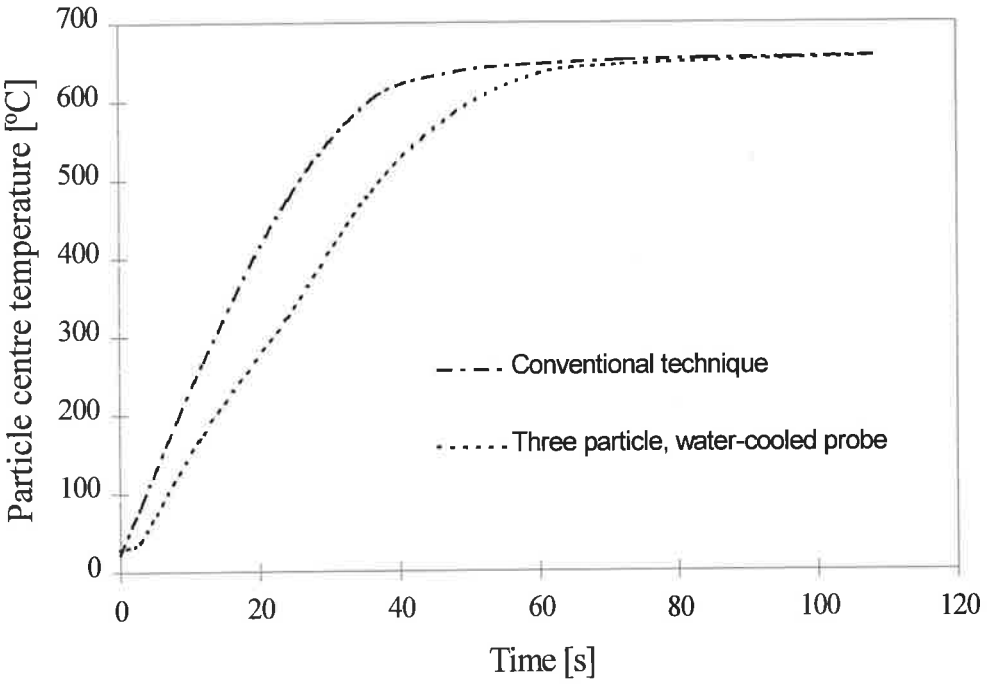

Figure 3.6 Measured temperature response at the centre of + 10.0 -11.0 mm dry Bowmans coal particles in the fluidised-bed Reactor at 600°C. Data obtained using the conventional technique as well as the three particle and water-cooled probe technique (reproduced from Heidenreich, 1999).

Statistical analysis by Heidenreich (1999) showed that the modified technique was statistically different to "*conventional technique*" and repeatable within a 95% confidence interval. To confirm that the modified technique is capable of generating reproducible data, a statistical analysis for raw data of a three repeat run of the particle temperature measurement for 10.5 mm Bowmans coal particles during pyrolysis at 850°C is conducted. The raw measurement data is shown in Figure 3.7. In order to perform a standard statistical test on this data, it would be convenient to describe the data collected from each run with a single value which would be representative of the data. A convenient parameter for this purpose would be the weighted mean heating rate (Megalos, 1998) defined as:

$$\left.\frac{dT}{dt}\right|_{mean} = \frac{\Sigma\left(\frac{dT}{dt}t\right)}{\Sigma t} \qquad \ldots 3.1$$

This technique has been effectively used to investigate reactivity data for various coals from various experimental conditions by Megalos (1998), which is analogous to the situation presented here. Using Equation 3.1, the data presented in Figure 3.7 was analysed and the results presented in Table 3.7.

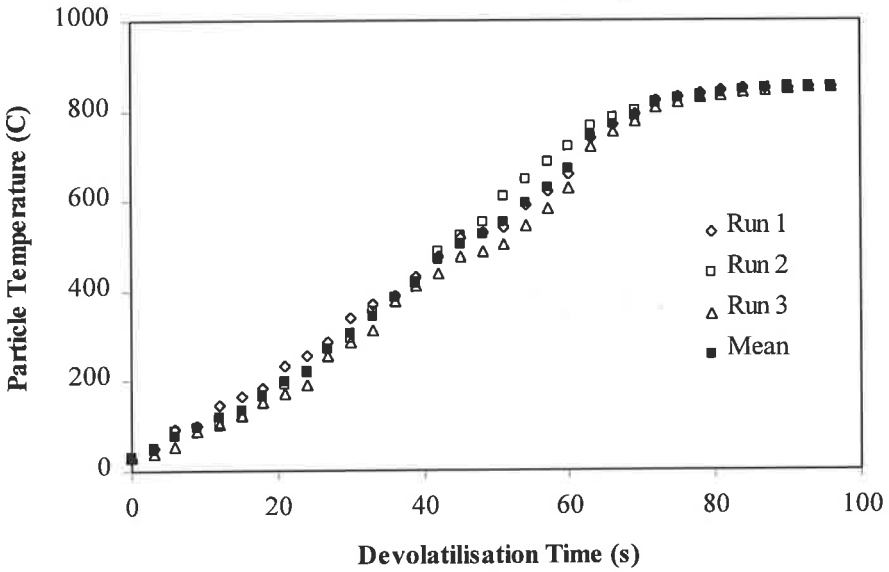

Figure 3.7 The measured temperature response at the centre of 10.5 mm Bowmans coal particles during pyrolysis at 850°C.

Table 3.7 Statistical data based on the temperature data present in Figure 3.7.

Run No.	$\left.\frac{dT}{dt}\right\|_{mean} (K.s^{-1})$	$\overline{\left.\frac{dT}{dt}\right\|_{mean}} (K.s^{-1})$	$\sigma\left(\left.\frac{dT}{dt}\right\|_{mean}\right)$
1	6.849		
2	6.377	6.471	0.3402
3	6.188		

Based on these values a simple z-test based on an average sampling distribution can be carried out. The z-test parameter is defined as (Perry and Green, 1984):

$$z = \frac{\bar{x} - \mu_o}{\sigma / \sqrt{N}} \qquad \ldots.6.2$$

Considering that the sample has three data points, the probability statistic for a 95% confidence interval from the T-distribution tables is $P_{0.025,2} = 4.303$ (Perry and Green, 1984). Thus, 95% of the data are likely to lie between the limits of:

$$-4.303 \leq z = \frac{\bar{x} - \mu_o}{\sigma / \sqrt{N}} \leq 4.303 \qquad \ldots.6.3$$

Given that $\mu_o = 6.471$, $\sigma = 0.3402$ and $N = 3$, then 95% of the data should lie between the limits of 5.626 and 7.317.

Thus using the temperature response technique to measure the devolatilisation time, accordingly the devolatilisation time requires redefinition as the time from particle immersion into the bed until the particle centre temperature equals the bed temperature. It must be noted that in the presence of oxygen, such that char combustion overlays the completion of coal devolatilisation, the particle temperature is observed to continually rise above the bed temperature, unlike when nitrogen is used, where the particle temperature attains the bed temperature. The values reported here are the mean of three runs.

Flame extinction time experiments were also conducted at 850°C in air for comparison with the current method for Bowmans coal. Individual particles were dropped into the bed with the devolatilisation time measured using a stopwatch, from the time particles contact the bed until the extinction of the visible volatiles flame surrounding the particles. The values reported here are the mean of three runs.

3.5 GAS SAMPLING IN FLUIDISED-BEDS

A number of investigations have measured concentration profiles of gas species in fluidised-beds (Broughton, 1975; Pillai, 1976; van der Vaart, 1985, 1988, 1992; van der Vaart and Davidson, 1986; Hayhurst and Tucker, 1990; Hesketh and Davidson, 1991, Kojima et al., 1993; Linjewile, 1993; Schluter, 1994; Ogada and Werther, 1998). Early work by Broughton (1975) and Pillai (1976) into chemical analysis of propane combustion were obtained by using non-cooled probes, in which complete conversion was obtained within a short distance of the distributor. This outcome is not surprising however, as the high surface temperature of the metal probe would facilitate the decomposition and combustion reactions of propane, resulting in the observed high conversion rate. Van der Vaart (1985) saw the evidence of this during freeboard temperature measurements using a suction pyrometer. A metal screen used to prevent entrainment of solids into the pyrometer was found to glow intermittently, this was especially evident at low bed temperatures when significant concentrations of hydrocarbons are liberated into the freeboard. Thus the residual fuel was reacting on the metallic surface of the screen. Therefore, any gas analysis probe must be cooled to prevent this surface oxidation.

Generally it has been the case in the literature, for probes to be cooled either by air or water in a double pipe configuration. No discernible difference in the reported effectiveness of either cooling medium has been reported. Van der Vaart (1985) used air as the cooling medium based solely on minimising the chance of cracking the quartz reactor in case of accidental collision between reactor wall and probe due to difference in probe temperatures if water was used (30°C for water and 180°C for air). For the current experimental study, the gas sample probe was water-cooled, based on

previous successful operation by Linjewile (1993) and Schulter (1994) on measuring the particle surface CO/CO_2 product ratio during char combustion. However, the sintered stainless steel plug used in these previous studies to prevent entrainment of solids into the sample tube was found to provide excessive pressure drop at the required sample flow rates needed to minimise gas residence times and provide minimum flow conditions needed by gas analysers. A 50 μm stainless steel wire mesh tied to the probe inlet with wire replaced the plug as illustrated in Figure 3.4.

3.6 SUMMARY

This chapter has dealt with the apparatus and techniques used in the experimental investigations carried out in this study for results to be reported in Chapters 4, 5 and 6.

A new experimental technique to measure the devolatilisation time has been developed. This technique measures the particle centre temperature, where the devolatilisation time is defined as the time taken for the centre temperature of a coal particle to equal the surrounding bed temperature. The modified temperature response technique of Heidenreich (1999) was used as the basis for particle temperature measurement. This technique makes use of a water-cooled probe to insulate the thermocouple from the surrounding heat transfer environment as well as a number of particles on the thermocouple tip to act as a thermal barrier to heat conduction along the thermocouple sheath. This technique was subsequently used to obtain the following particle temperature data, which will play a critical role in both the development and validation in the prediction of coal devolatilisation time:

- -14.5 +6.5 mm wet Bowmans and Morwell coal particles in a fluidised-bed under pyrolysis, combustion and gasification conditions at 850°C.
- -14.5 +6.5 mm wet Bowmans coal particles in a fluidised-bed at 750°C, 850°C and 950°C
- -14.5 +6.5 mm Bowmans and Morwell coal particles in a fluidised-bed for various coal moisture contents 0 to 50 wt% in combustion conditions at 850°C.
- -17.5 +6.5 mm dry coal particles for seven coals ranging from lignite to anthracite in a fluidised-bed under combustion conditions at 850°C.

An experimental study of the influence of volatile matter combustion, simulated by propane, and its interaction on char combustion reactions in a bubbling fluidised-bed was outlined. The experimental technique of Andrei et al. (1985) was used to measure the time resolved weight loss history by retrieving char particles from the bed by a mesh basket at various time increments after being dropped into the bed.

The specific intentions of this section are to:

- measure and report the effect of temperature on combustion rate of char with and without propane feed
- compare char burn-out times
- apply a simple correlative method, based on rate-controlling process, for correlating rate data.

A new experimental fluidised-bed gasifier was developed which incorporated a unique water-cooled plenum chamber to allow for the investigation of volatile matter combustion, as simulated by propane pre-mixed with air and steam, under gasification conditions with and without char feed. This work is believed to provide the first comprehensive data set on gas profiles on volatile combustion under conditions prevailing in a fluidised-bed gasifier. Such data is essential for the development of a suitable mathematical model for fluidised-bed gasification of coal. The apparatus was subsequently used to obtain in-bed gas concentration profile data for CO, CO_2, C_3H_8, C_3H_6, C_2H_6, C_2H_4, C_2H_2, and CH_4 as determined using FTIR spectroscopy under the following conditions:

- Propane pyrolysis (in a nitrogen/steam fluidised-bed)
- Propane gasification (in a air/steam fluidised-bed)
- Char gasification (in a air/steam fluidised-bed)
- Propane/char gasification (in a air/steam fluidised-bed)

This data forms an excellent basis for comparison with the impending model development.

CHAPTER 4

DEVOLATILISATION TIME

4.1 INTRODUCTION

The use of low-rank coals is greatly dependent upon the behaviour of the volatile matter, which can account for up to 50% of the specific energy for low rank coals. It is well documented that volatile combustion in fluidised-bed combustors has numerous ramifications relating to their design and operation (Stubington et al, 1997). Thus understanding volatile release and their subsequent mixing with oxygen and combustion is of paramount importance. The devolatilisation time and the rate of coal particle mixing within a fluidised-bed will define the concentration distribution of volatiles throughout the bed.

This section presents results obtained on the devolatilisation times by measuring the particle centre temperature history for various particle sizes (6.5-14.5 mm) at different bed temperatures (750, 850, 950°C) and gas environments (simulating pyrolysis, gasification and combustion conditions) for a South Australian and a Victorian low-rank coal in a fluidised-bed. The effects of moisture content (0 to 50 wt%) and coal type (lignite through to anthracite) were also investigated. The devolatilisation time was defined as the time taken from immersion of the particle into bed until the centre temperature of the coal particle equalled bed operating temperature. Results were correlated with classic empirical particle diameter power law relation.

A new theoretical treatment of coal particle devolatilisation time has been established where the devolatilisation time is found to be proportional to the particle size. This theory is contrary to the current square-law dependency assumed by others in the literature and is supported by the current experimental findings. Furthermore, experimental inconsistencies in exponent values for devolatilisation times reported in the literature have been resolved.

4.2 PARTICLE TEMPERATURE DATA

Particle temperature measurements were carried out using the modified particle temperature measurement technique outlined in Section 3.4 using a 102 mm fluidised-bed reactor. Temperature measurements were repeated three times for each coal particle size to ensure the repeatability of the measurements and the arithmetical average temperature profile then calculated. The devolatilisation time was defined as the time from particle immersion into the bed until the particle temperature equalled the bed temperature.

In the presence of oxygen, such that char combustion overlaps the completion of coal devolatilisation, the particle temperature is observed to continually rise above the bed temperature, unlike when nitrogen is used, where the particle temperature attains the bed temperature. The magnitude of the particle burning temperature exceeding the bed temperature is determined by various factors such as the relevant heat and mass transfer rates, carbon type, kinetics of the carbon-oxygen reaction and the CO/CO_2 product ratio local to the char particle (Schluter et al., 1996). The magnitude and factors affecting the excess char particle burning temperature will not be discussed in any further detail as it is outside the scope of the current thesis.

Figures 4.1-4.6 show typical particle temperature profiles measured for various Bowman and Morwell coal particles ranging between 6.5-14.5 mm in pyrolysis, gasification and combustion atmospheres at 850°C. It can be clearly seen as the particle diameter increases, that the time required for the centre temperature of the coal particle to reach the bed temperature increases. Also, as the oxygen concentration increases by changing from nitrogen to air, the particle heating time required reaching the bed temperature decreases. For the larger coal particle sizes of between 10.5-14.5 mm, the evaporation of moisture is observable by the presence of a plateau in the temperature response at 100°C. Figures 4.7-4.8 show typical particle temperature profiles measured for various Bowman coal particles ranging between 6.5-14.5 mm in a combustion atmosphere at 750°C and 950°C, respectively.

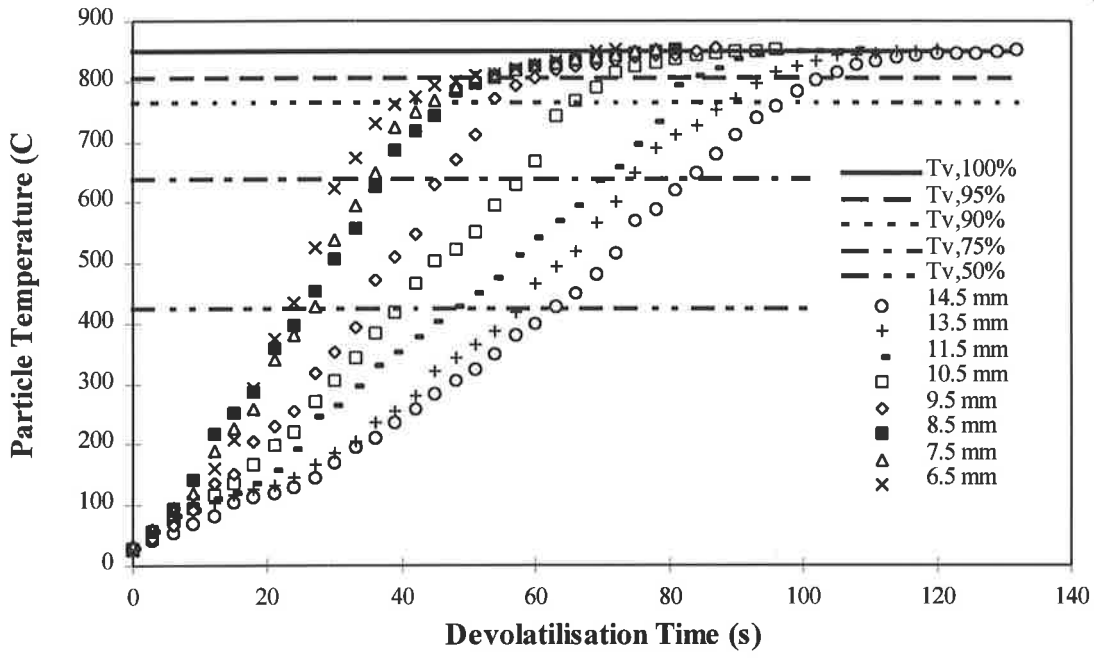

Figure 4.1 Experimental data for the temperature response at the centre of +6.5 -14.5 mm wet Bowman coal particles at 850°C in a nitrogen atmosphere.

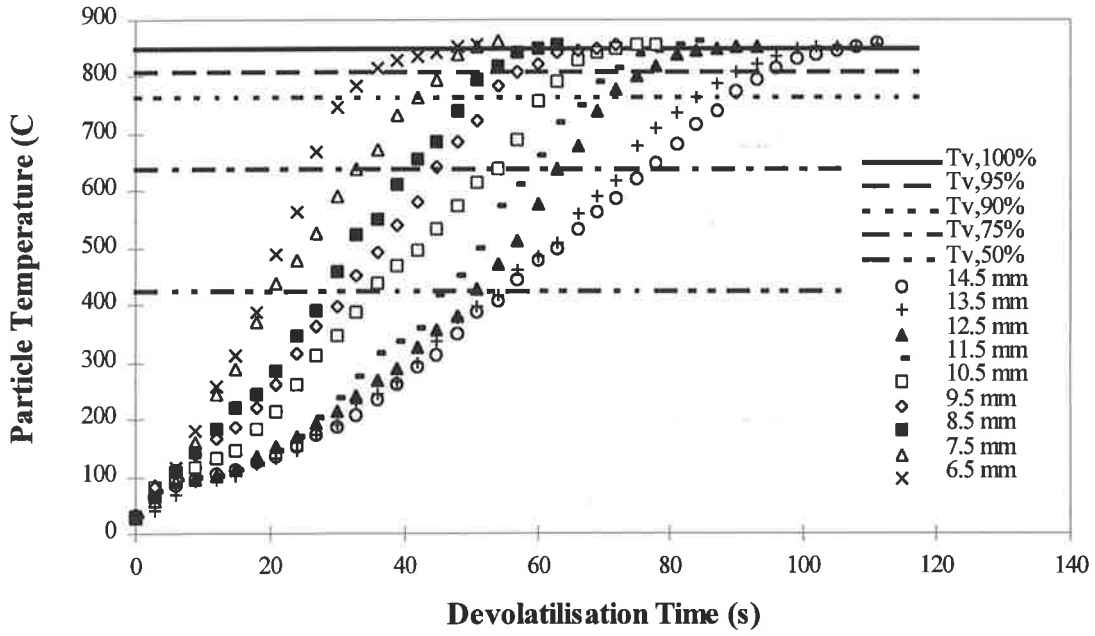

Figure 4.2 Experimental data for the temperature response at the centre of +6.5 -14.5 mm wet Bowman coal particles at 850°C in an air/steam (70/30 vol%) atmosphere.

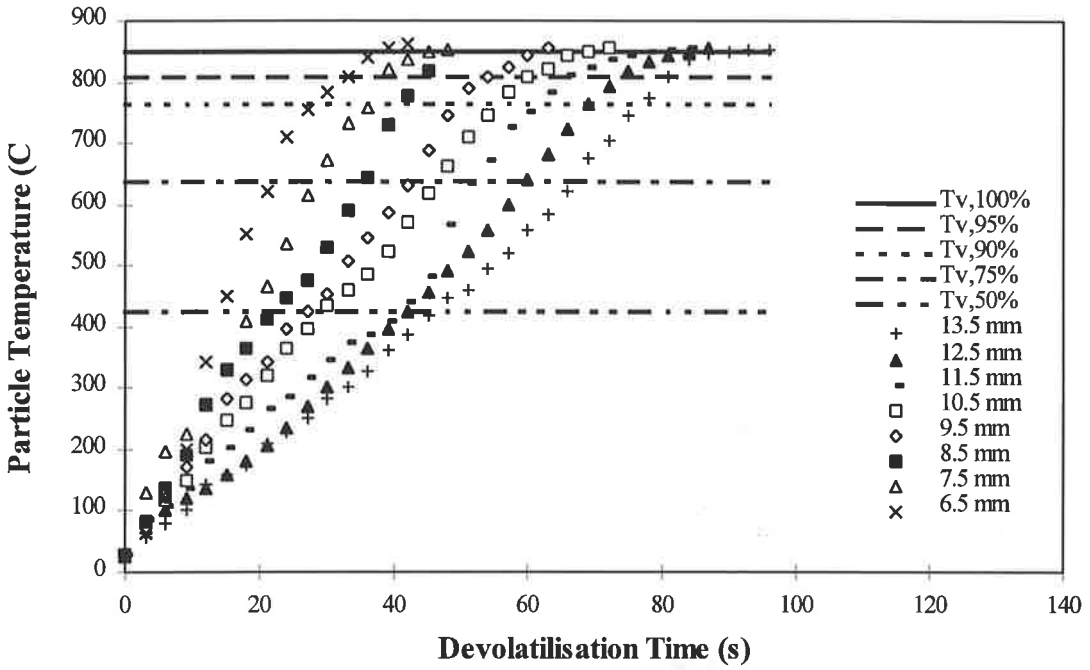

Figure 4.3 Experimental data for the temperature response at the centre of +6.5 -14.5 mm wet Bowman coal particles at 850°C in an air atmosphere.

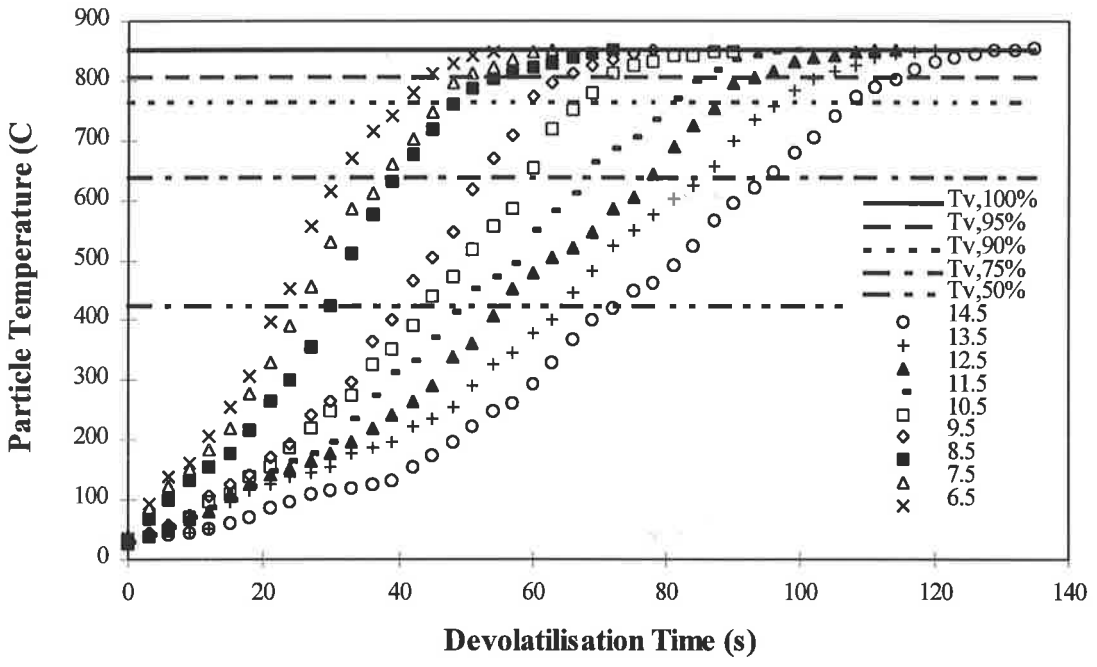

Figure 4.4 Experimental data for the temperature response at the centre of +6.5 -14.5 mm wet Morwell coal particles at 850°C in a nitrogen atmosphere.

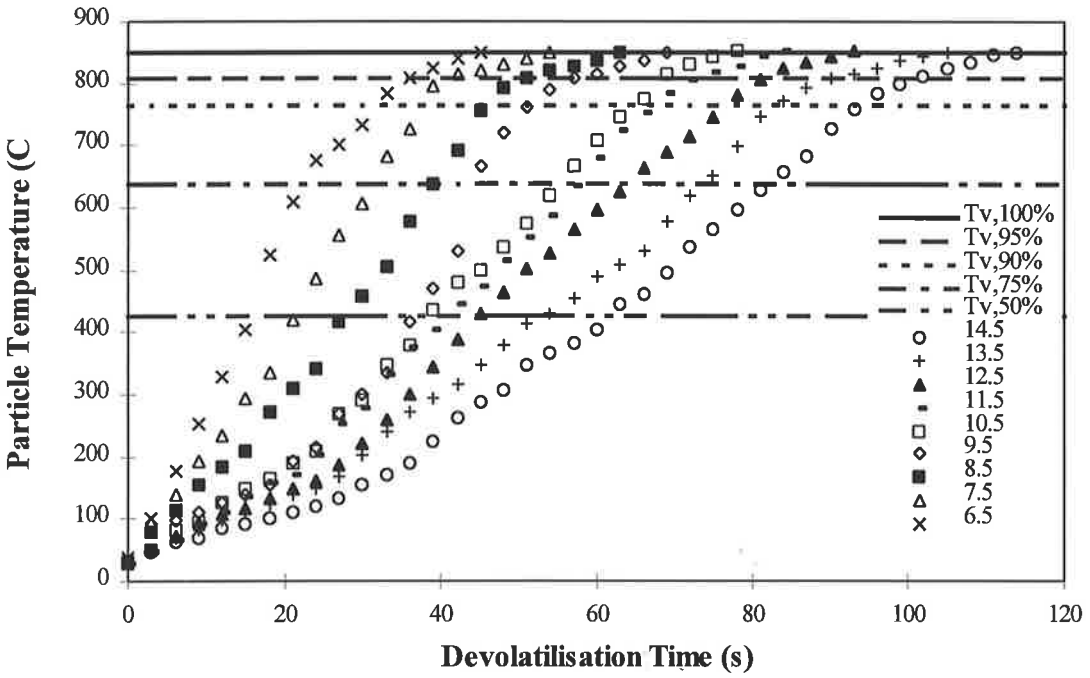

Figure 4.5 Experimental data for the temperature response at the centre of +6.5 -14.5 mm wet Morwell coal particles at 850°C in an air/steam (70/30 vol%) atmosphere.

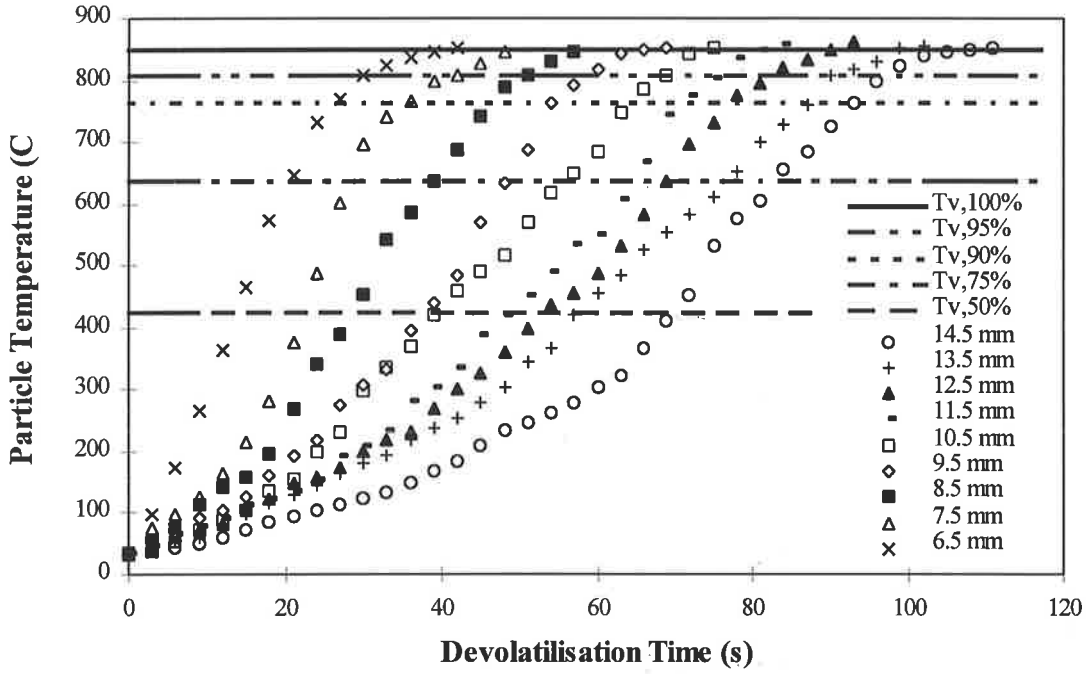

Figure 4.6 Experimental data for the temperature response at the centre of +6.5 -14.5 mm wet Morwell coal particles at 850°C in an air atmosphere.

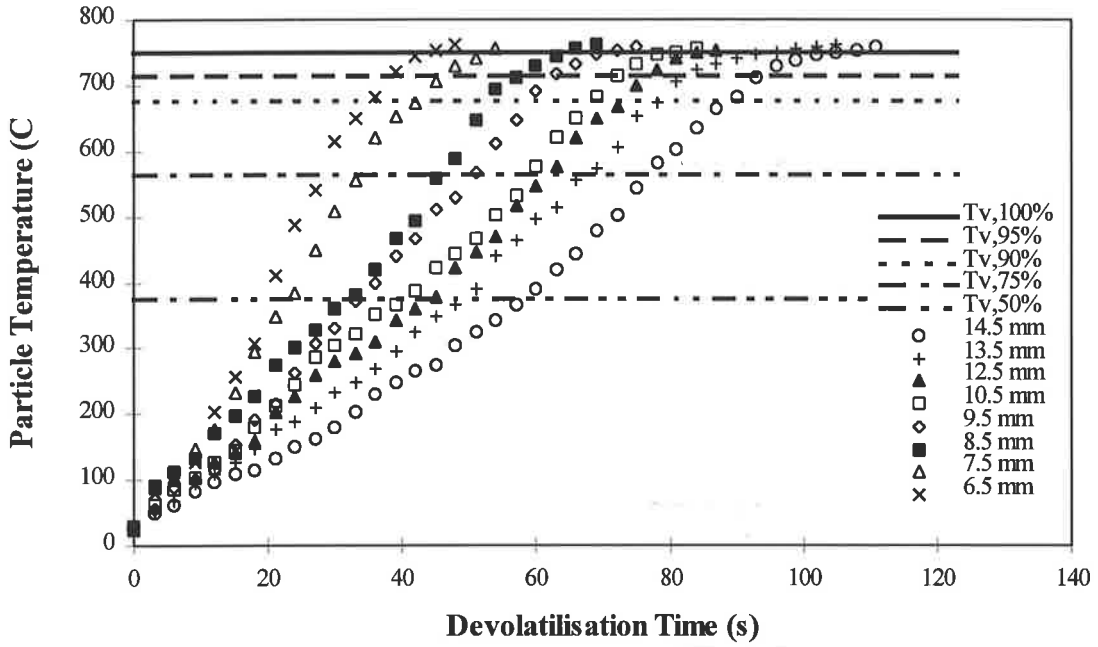

Figure 4.7 Experimental data for the temperature response at the centre of +6.5 -14.5 mm wet Bowman coal particles at 750°C in an air atmosphere.

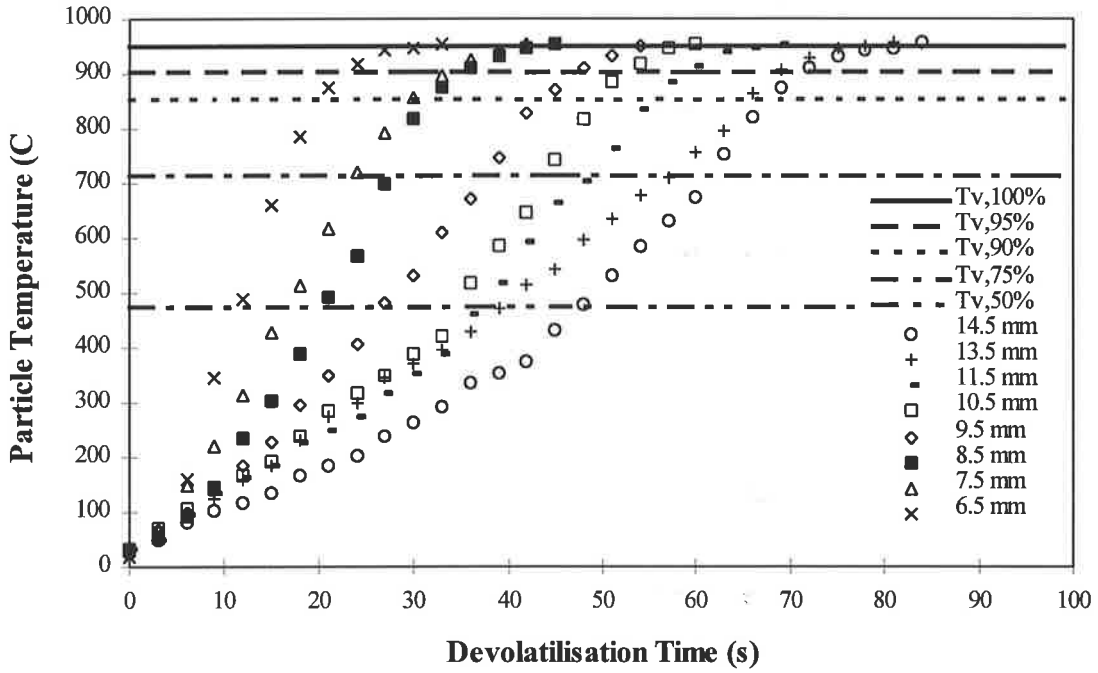

Figure 4.8 Experimental data for the temperature response at the centre of +6.5 -14.5 mm wet Bowman coal particles at 950°C in an air atmosphere.

Including for comparison Figure 4.3 at 850°C, the time required for the centre temperature of the coal particle to reach the bed temperature decreases with increasing bed temperature. This is consistent with experimental data for the temperature response at the centre of -9 + 8 mm and -11 + 10 mm wet Bowman coal particle experiments reported by Heidenreich (1999) at 600°C , 700°C and 800°C in a nitrogen atmosphere in a convective flow tube and fluidised-bed reactor.

Figure 4.9 shows typical particle temperature profiles measured for various coal moisture contents ranging between 0 to 50 wt% for particle sizes ranging between +8.0 -15.0 mm at 850°C in air for Morwell coal. The effect of moisture content upon the particle centre temperature response is observable, signified by a temperature plateau at 100°C for high moisture content samples consistent with the literature. Direct determination of the effect of coal moisture content from the temperature profiles is somewhat ambiguous due to the various particle sizes employed. A clearer trend of the effect of moisture on the devolatilisation time will be given in subsequent section 4.5.

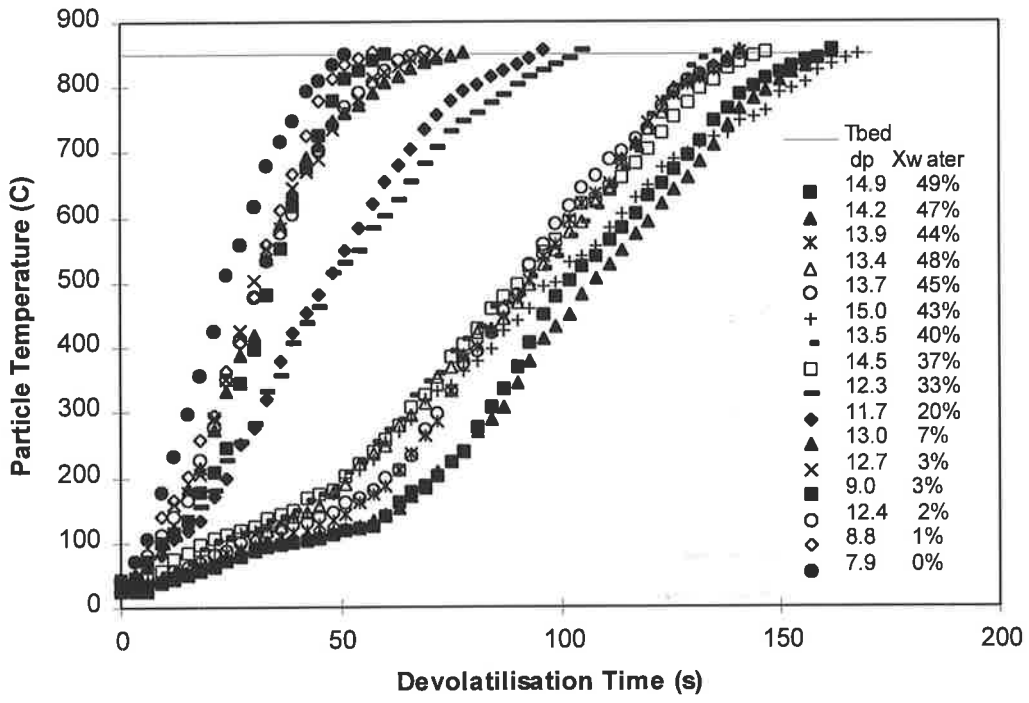

Figure 4.9 Experimental data for the temperature response at the centre of +8.0 -15.0 mm Morwell coal particles at 850°C in a air atmosphere at various coal moisture contents ranging between 0 - 50 %wt.

Figures 4.10-4.16 show typical centre particle temperature profiles measured for seven coals ranging from lignitic to anthracitic in rank of varying particle sizes between +7.0 -17.5 mm at 850°C in an air atmosphere.

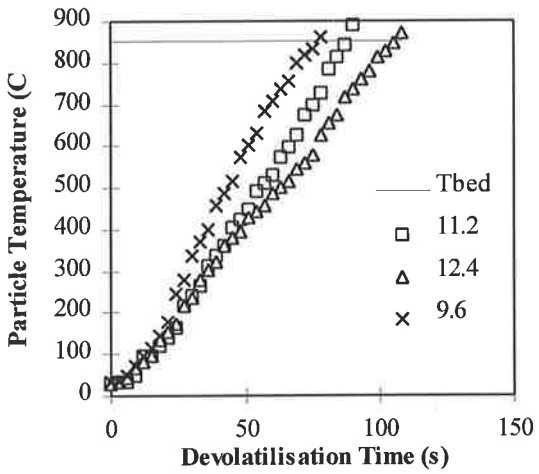

Figure 4.10 Experimental data for the temperature response of dry Qld.-177I coal particles at 850°C in air.

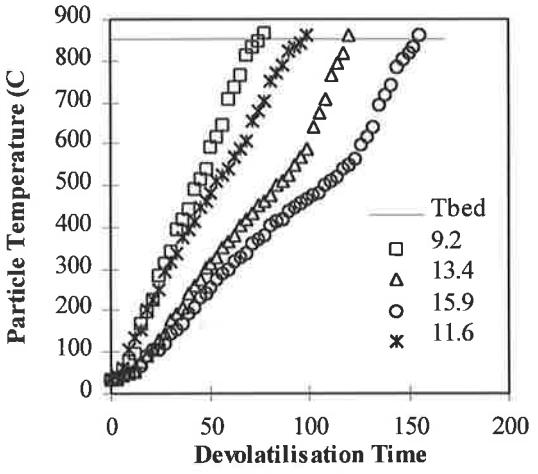

Figure 4.11 Experimental data for the temperature response of dry Surat-252H coal particles at 850°C in air.

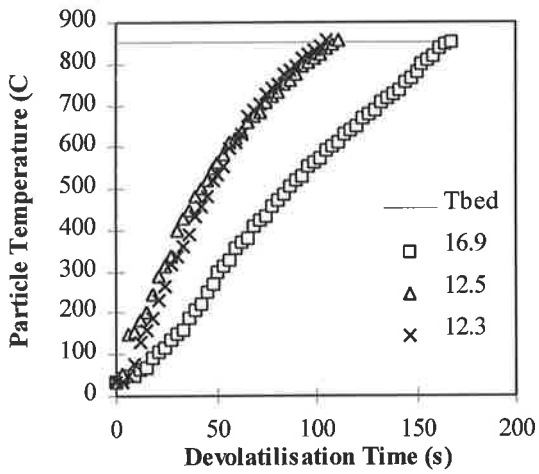

Figure 4.12 Experimental data for the temperature response of dry Bowen-238A coal particles at 850°C in air.

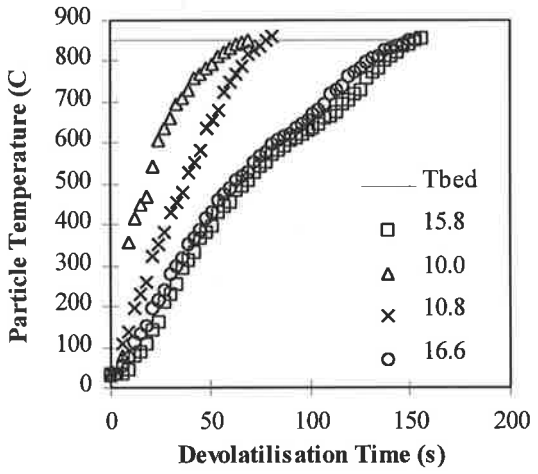

Figure 4.13 Experimental data for the temperature response of dry Qld.-184G coal particles at 850°C in air.

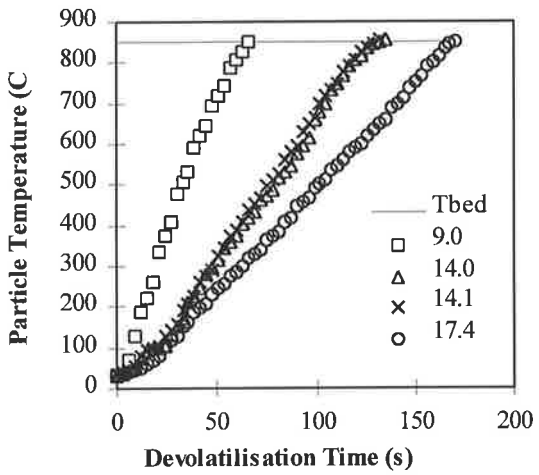

Figure 4.14 Experimental data for the temperature response of dry Bowen-249C coal particles at 850°C in air.

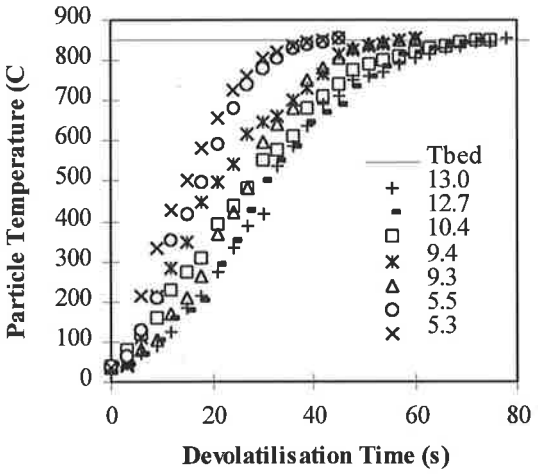

Figure 4.15 Experimental data for the temperature response of dry Morwell coal particles at 850°C in air.

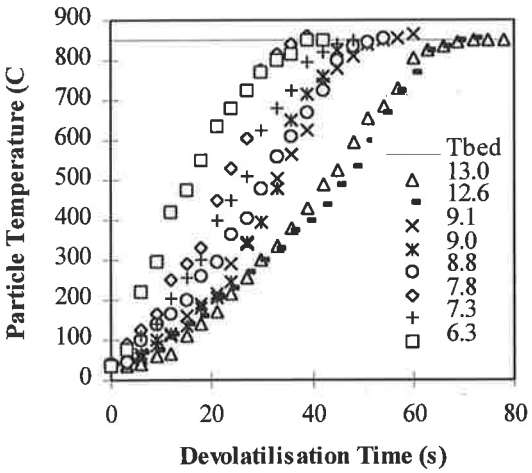

Figure 4.16 Experimental data for the temperature response of dry Bowman coal particles at 850°C in air.

Due to the inherent differences in moisture content of the various coal types, particles from all seven coal types were oven dried. Because of difficulties in producing spherical samples for higher rank coals and the high failure rate due to excessive cracking of low-rank coals (particularly Bowman and Morwell coals), temperature profiles shown in these figures represent individual particle runs. In instances where similar particle sizes happened to be repeated, good agreement is shown which is in accordance with previous temperature profile data for similar particle sizes.

4.3 DEVOLATILISATION TIME RESULTS

From the particle temperature profiles shown in previous section, the characteristic devolatilisation times, t_v, can be ascertained by determining the intersection point of the particle centre temperature with the prescribed final devolatilisation temperature for each coal particle size under the various experimental conditions investigated. Subsequent figures in this section show plots of the devolatilisation time as a function of initial particle diameter. Furthermore, data are correlated based on classic power-law relation used extensively in the literature (Equation 2.1). The associated values for the pre-exponent factor, A, and exponent, n, are summarised on each figure by trend-fitting the data using Microsoft EXCEL.

4.3.1 EFFECT OF GAS ENVIRONMENT

The effect of changing atmosphere on the devolatilisation time for Bowman and Morwell coals are shown in Figures 4.17(a) and 4.17(b), respectively. It is clearly observable that as the oxygen concentration is reduced, the devolatilisation time increases. The devolatilisation times for Bowman and Morwell coal particles in a nitrogen atmosphere were found to be 38% and 24% longer than in air, respectively. These results are in agreement to those reported by Panagakis (1995), Lufei et. al. (1993) and Stubington et. al. (1991), all reported increases in the devolatilisation time of 35%, 45% and 19%, respectively. The devolatilisation times for Bowman and Morwell coal particles in a gasification atmosphere (O_2 - 15 vol%) were found to be 10% and 8% longer than in air, respectively. Stubington et al. (1992) reported that devolatilisation times were found to be longer in nitrogen diluted air stream at an oxygen concentration of 10 vol% but did not stipulate to what magnitude. The resultant decrease in devolatilisation time with changing atmosphere, especially from nitrogen to air, is attributed to the formation of a laminar diffusional volatile flame around the coal particle. This increases the particle heating rate, and therefore decreasing the devolatilisation time (Agarwal et al., 1987). A similar effect of varying oxygen concentration on the rate of char combustion under external diffusion control supports this view (Schluter et al., 1997).

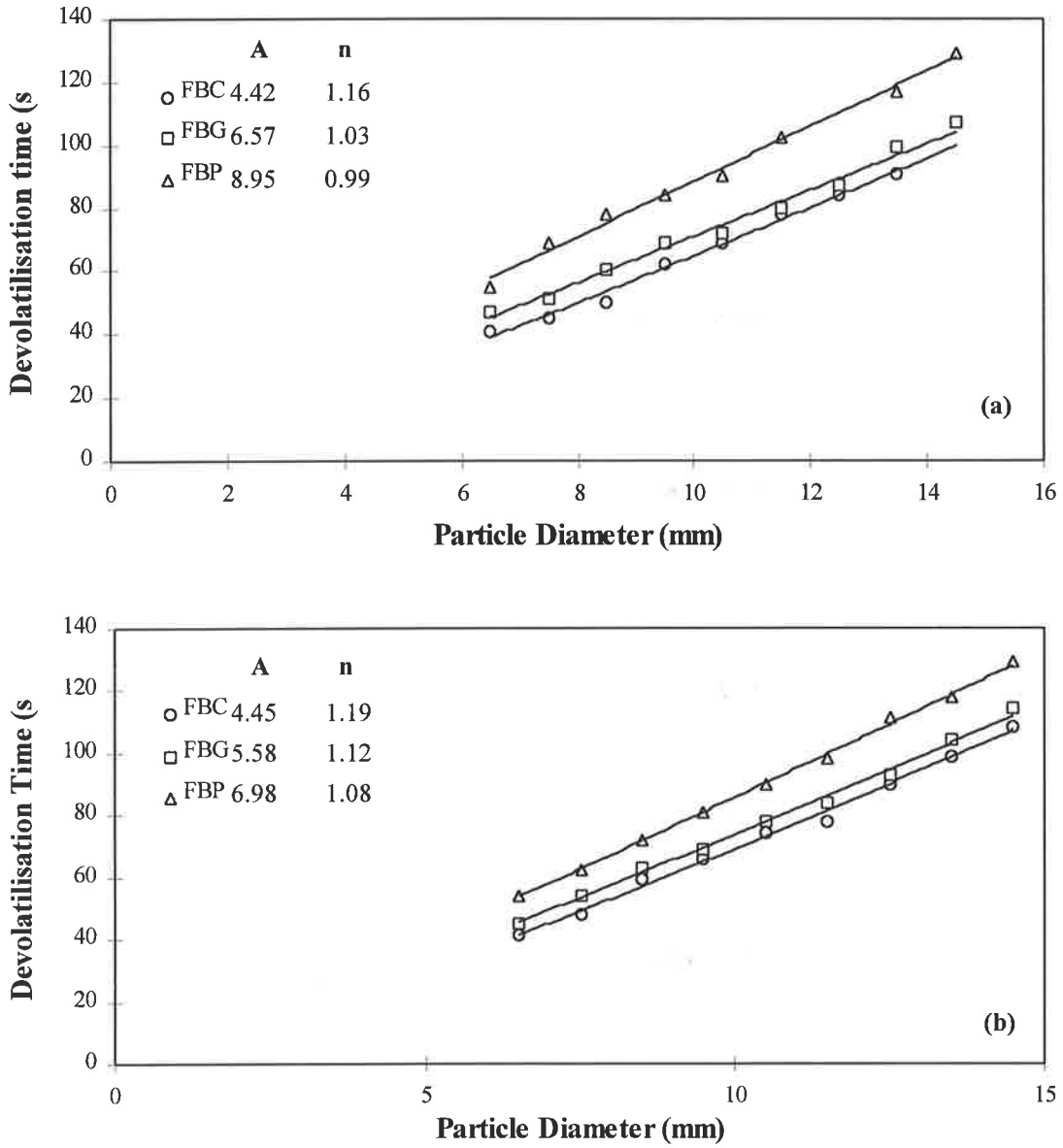

Figure 4.17 Comparison of devolatilisation time in differing gas environments for (a) Bowmans and (b) Morwell coal particles fluidised in, air (O_2 - 21 vol%) (O), air/steam 70/30 vol% (O_2 - 15 vol%) (□), nitrogen (O_2 - 0 vol%) (Δ).

However, Lufei et al. (1993) reported that the devolatilisation time did not change significantly until the oxygen concentration fell below 3 vol%. Halder and Saha (1993) reported similar findings. These results seem somewhat doubtful and inconsistent. Simply, as the oxygen concentration is reduced, incomplete or partial combustion of volatiles would progressively occur. The resultant heat generation due to the exothermic combustion reactions would decrease.

Therefore, a progressive reduction in the heat transfer to the particle occurs and the subsequent increase in total devolatilisation time explained. Qualitative evidence to support this view was observed experimentally. During experiments conducted under gasification conditions, the volatile flame produced soot indicating partial combustion, unlike the diffusional flame formed under combustion conditions during devolatilisation. Furthermore, Schulter et al. (1997) observed during flame extinction time experiments, that the height and luminosity of the volatile flame decreased with decreasing oxygen concentration.

A unique feature of the temperature response technique for measuring the devolatilisation time is the ability to ascertain arbitrary intermediate completion times and further attempt to elucidate the controlling mechanism behind the devolatilisation process. An indicative plot of the times taken for particle temperatures to reach 50, 75, 90, 95 and 100% of the final bed temperature as a function of particle size for Bowman coal in air at 850°C is shown in Figure 4.18.

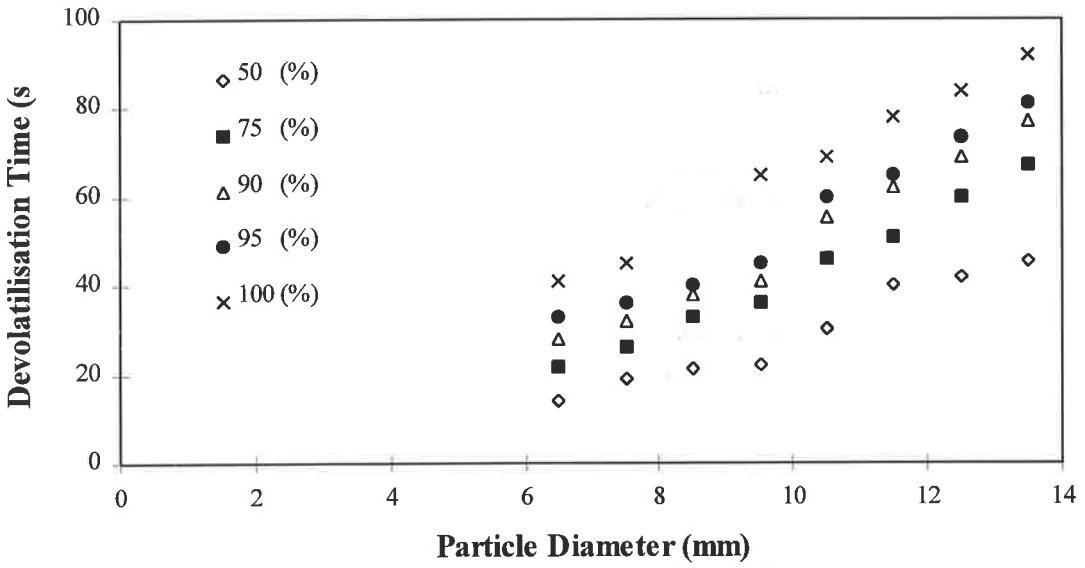

Figure 4.18 Comparison of centre temperature response profile at various completion percentages of the final bed temperature for the devolatilisation of Bowmans coal in air at 850°C

Consequentially, the exponent n is determined for each data set and summarised in Table 4.1 for both Bowman and Morwell coals. The subsequent exponent values are plotted as a function of percent completion of devolatilisation for particle temperatures at 50, 75, 90, 95 and 100% of the final bed temperature, for all three gas environments for Bowman and Morwell coals as illustrated in Figure 4.19.

Table 4.1. Devolatilisation time correlation parameters for Bowman and Morwell coals at various completion percentages of the final bed temperature in varying gas environments.

Coal and Gas Environment	Percent completion	Pre-exponential factor A	Exponent n
Bowman (nitrogen)	50	0.62	1.66
	75	1.11	1.57
	90	1.74	1.45
	95	2.56	1.32
	100	4.73	1.14
Bowman (air/steam)	50	1.15	1.47
	75	2.15	1.35
	90	3.48	1.21
	95	4.04	1.18
	100	6.57	1.03
Bowman (air)	50	1.91	1.30
	75	2.52	1.31
	90	4.10	1.18
	95	5.76	1.07
	100	8.96	0.99
Morwell (nitrogen)	50	0.65	1.76
	75	0.88	1.73
	90	1.71	1.52
	95	2.43	1.40
	100	4.45	1.19
Morwell (air/steam)	50	0.77	1.64
	75	1.33	1.55
	90	2.57	1.34
	95	3.28	1.27
	100	5.59	1.12
Morwell (air)	50	1.30	1.49
	75	2.05	1.43
	90	3.70	1.25
	95	4.20	1.22
	100	6.98	1.09

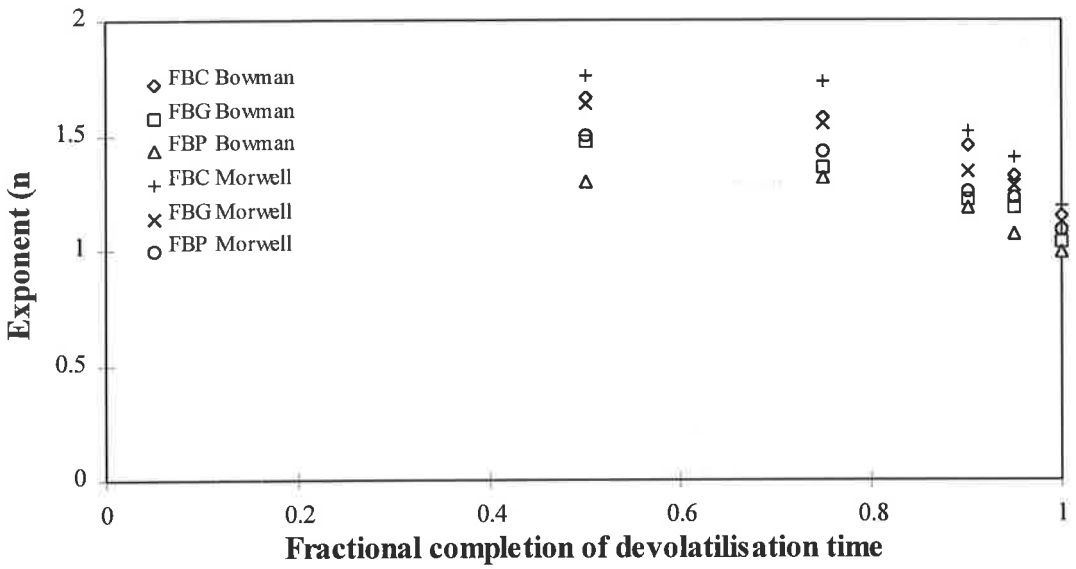

Figure 4.19 Effect of gas environment on the exponent *n* as determined by Equation 2.1, at various fractional completions of the total devolatilisation time during the devolatilisation of Bowman and Morwell coals at 850°C.

Table 4.1 and Figure 4.19 clearly demonstrate that the exponent *n* increases in magnitude as the percent completion of devolatilisation decreases. Thus it appears that the mechanism controlling the devolatilisation process varies with particle temperature/volatile evolution history. At low particle temperatures heat transfer is rate controlling, while at higher particle temperatures approaching that of the bed temperature, chemical kinetics play an increasing role. This is consistent with the fact that devolatilisation at the lower temperatures of between 200 to 400°C, is associated with the cleavage of weak carboxyl, hydroxyl and aliphatic bonds. While temperatures greater than 650°C involve the decomposition of strong heterocyclic components and condensation of aromatic structures (van Heek and Hodek, 1994). Furthermore, the rate of increase and final value of the exponent *n* increase with oxygen concentration. This further confirms that the formation of a laminar diffusional flame front around the particle surface increases heat transfer to the coal particle. Thus resulting in a reduction in the total devolatilisation time and supports the conclusion that large coal particle devolatilisation in a fluidised-bed environment is heat transfer controlled.

4.3.2 Effect of Bed Temperature

Figure 4.20 compares the devolatilisation times and correlation parameters for Bowmans coal at 750, 850 and 950°C in air. The coal devolatilisation time and correlation parameter A were found to decrease as the bed temperature increases which is in general agreement with reported literature. The pre-exponential parameter was found to exhibit the following proportionality relationship

$$A \propto 1/T^{3.0} \qquad \text{....4.1}$$

Pillai (1991) observed a similar result and reported an exponent value of 3.8. Lufei et al. (1993) reported exponent ranges from 1.20 to 2.19 for lignite and bituminous coals. As concluded by Pillai (1991), radiative heat transfer may well be an important mechanism controlling the rate of heat transfer and hence the volatile evolution rate. This conclusion is supported by coal devolatilisation modelling work conducted by Heidenreich (1999), where it was observed that radiative heat transfer can account for up to 75% of the total heat transfer to the particle surface.

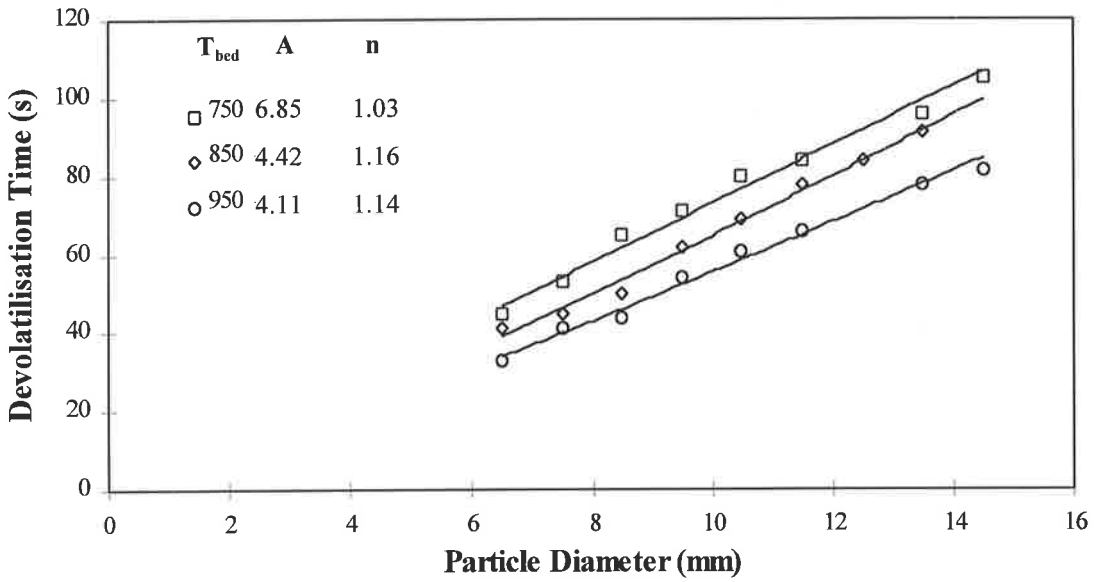

Figure 4.20 Comparison of devolatilisation times at 750°C, 850°C and 950°C for Bowmans coal particles fluidised in air.

Once again plots of the times taken for particle temperatures to reach 50, 75, 90, 95 and 100% of the final bed temperature as a function of particle size for the three bed temperatures were conducted. Results of devolatilisation correlation parameters for bed temperatures at 750°C and 950°C in air are summarised in Table 4.2. (Refer to Table 4.1 for correlation parameters at 850°C).

Table 4.2. Devolatilisation time correlation parameters for Bowman coal at various completion percentages of the final bed temperatures at 750°C and 950°C in air.

Coal and Bed Temperature	Percent completion	Pre-exponential factor A	Exponent n
Bowman (750°C)	50	1.68	1.33
	75	3.05	1.22
	90	4.74	1.11
	95	5.39	1.08
	100	6.86	1.03
Bowman (950°C)	50	0.53	1.70
	75	0.95	1.58
	90	1.50	1.46
	95	2.24	1.32
	100	4.02	1.14

The subsequent exponent values are plotted as a function of percent completion of devolatilisation for particle temperatures at 50, 75, 90, 95 and 100% of the final bed temperature, at all three bed temperature for Bowman coal as illustrated in Figure 4.21. This figure once again demonstrates that the exponent n increases in magnitude as the percent completion of devolatilisation decreases for all three bed temperatures. Obviously, it is appreciated that the reaction rates and amounts of volatile matter released will be different at different temperatures. Nevertheless, it was anticipated in keeping with previous results of the influence of oxygen concentration on the rate of devolatilisation, that the data for the higher bed temperature of 950°C to exhibit exponent values greater than those at 850°C, in particular, at the lower completion times of 50 and 75%. Whether this observation is simply experimental deviation or in fact that a maximal asymptotic particle heating rate may be present (dominated by internal rather than external heat transfer control) is not clear. Heidenreich (1999) conducted a sensitivity analysis on the influence of thermophysical and heat transfer parameters on devolatilisation model predictions.

It was observed that a 25% reduction in the convective heat transfer coefficient results in an average absolute reduction in the temperature response and the fraction of volatile matter evolved by less than 2 and 5 %, respectively. Furthermore, the deviation in model predictions in this case were significantly lower than for similar changes in coal thermophysical parameters. This was supported by taking into consideration the overall heat transfer coefficient between the surroundings and the centre of the particle (Heidenreich, 1999). Based on a similar reduction of 25% in the external heat transfer coefficient, the overall heat transfer coefficient decreased from 50.4 $Wm^{-2}K^{-1}$ to 49.2 $Wm^{-2}K^{-1}$ at 600°C. Thus, it was concluded that particle heating process is internal heat transfer controlled under fluidised-bed operating conditions. However, the model developed by Heidenreich (1999) does not incorporate the effect of energy feed-back due to volatile combustion at the particle surface. Similarly, using the Biot number to characterise the relative importance of internal or external heat transfer control during coal devolatilisation modelling may not be strictly valid (Prins et al. 1989; Agarwal et al. 1984(a)). As reviewed in Section 2.5.1, the Biot number compares the relative magnitude of external surface convection and internal conduction resistances to heat transfer.

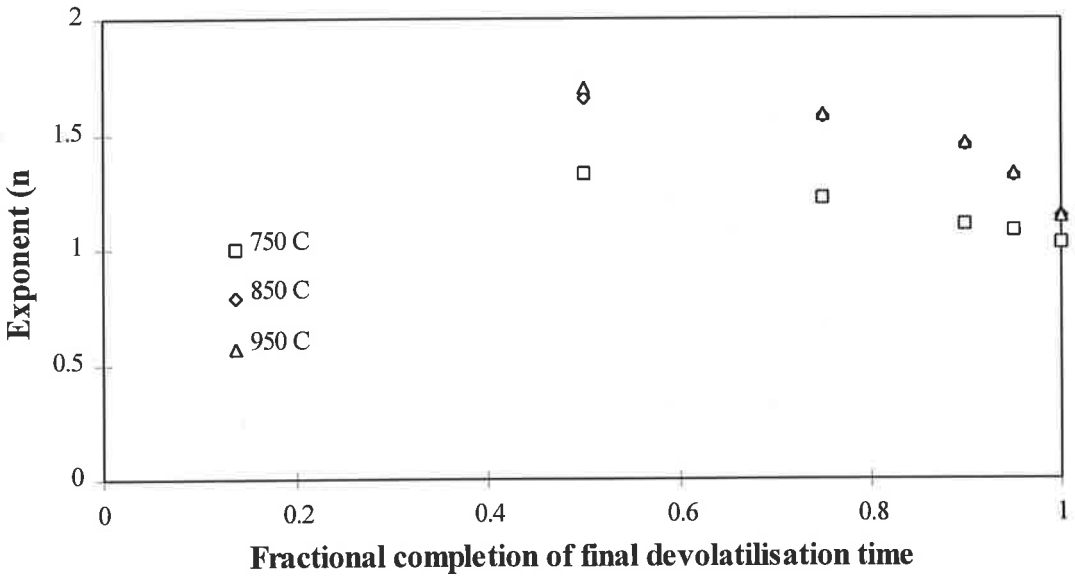

Figure 4.21 Effect of bed temperature on exponent *n* at various fractional completions of the total devolatilisation time during the devolatilisation of Bowman coal in air.

However, the formation of a diffusion flame front around the particle surface would alter the mode of external heat transfer to conductive and radiative heat transfer from flame front. This of course is not explicitly taken into consideration when calculating the Biot number unless implicitly accounted for by estimating an effective convective heat transfer coefficient similar to Equation 2.12. Clearly, if internal heat transfer controls the particle heating rate as suggested in the literature, then corresponding reductions of up to 38% with changes in gas environment on the total devolatilisation time observed during the current measurements would not result. It can be concluded that atmospheric fluidised-bed devolatilisation of large coal particles is heat transfer controlled, with the relative dominance of either internal or external heat transfer dependent on operating conditions. An Arrhenius correlation of the effect of temperature on parameter A is shown in Figure 4.22. Qualitative comparison with the reported data of Stubington et al. (1991) based on the 90% weight loss definition of devolatilisation time conducted in a thermogravimetric analyser in air is also shown. Obviously, direct comparison of the result is impossible given the significantly differing particle heating environments between a TGA and fluidised-bed.

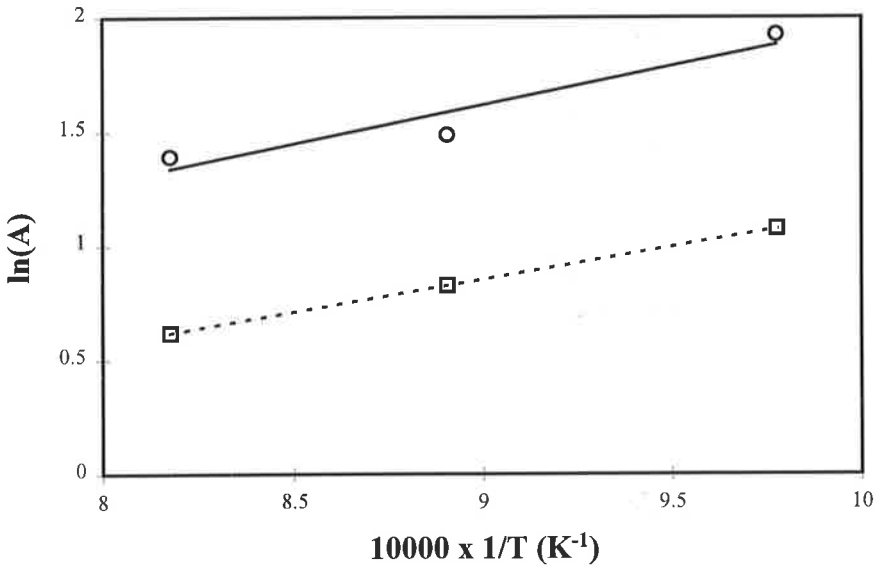

Figure 4.22 Effect of temperature on correlation parameter A in air. current work Bowman coal (○), Stubington et al. (1991) using 90% weight loss definition of devolatilisation time (□).

The current experimental values of A were correlated by the following equation

$$A = 0.237 \exp\left[\frac{3396}{T}\right] \quad \text{....4.2}$$

This corresponds to activation energy of only 28.2 $kJmol^{-1}$ and compares favourably to that found by Lufei et al. (1993) of 18.6 $kJmol^{-1}$. As stipulated by Lufei et al. (1993), this is a very small activation energy on chemical kinetic scales, which once again supports that the rate control mechanism for large coal particle devolatilisation in fluidised-beds being heat transfer controlled.

4.3.3 Comparison with Literature Data

Figure 4.23 shows a comparison of devolatilisation times for various measurement techniques used in fluidised beds at 850°C under pyrolysis and combustion conditions. Good agreement of current flame extinction time data with similar data reported by Stubington et al. (1992, 1997) and Zhang et al. (1990) is obtained. Both data of Stubington et al. (1992, 1997) for the CO_2 gas profile measurement technique have been plotted, differences being the treatment of endpoint definition of devolatilisation time. The more recent definition of Stubington et al. (1997) yields profile characteristics very similar to the flame extinction time. This change in endpoint definition between their successive literature publications was objective, based on the paradigm that the flame extinction time is a true representative measurement technique. As will be discussed briefly, this may well be considered incorrect and the former definition believed to better represent true volatile evolution time. A reasonable agreement for volatile evolution data of Stubington et al. (1984) and the old endpoint definition for CO_2 gas profile (Stubington et al., 1992) with the current temperature response method in nitrogen and air respectively is observed, given differences in coal types used. This supports theoretical conclusions of Heidenreich (1999) outlined in section 2.5.1, which formed the basis for validation of the current temperature response method, where the volatile evolution rate would be limited by the particle heating time for large coal particle devolatilisation in a fluidised-bed.

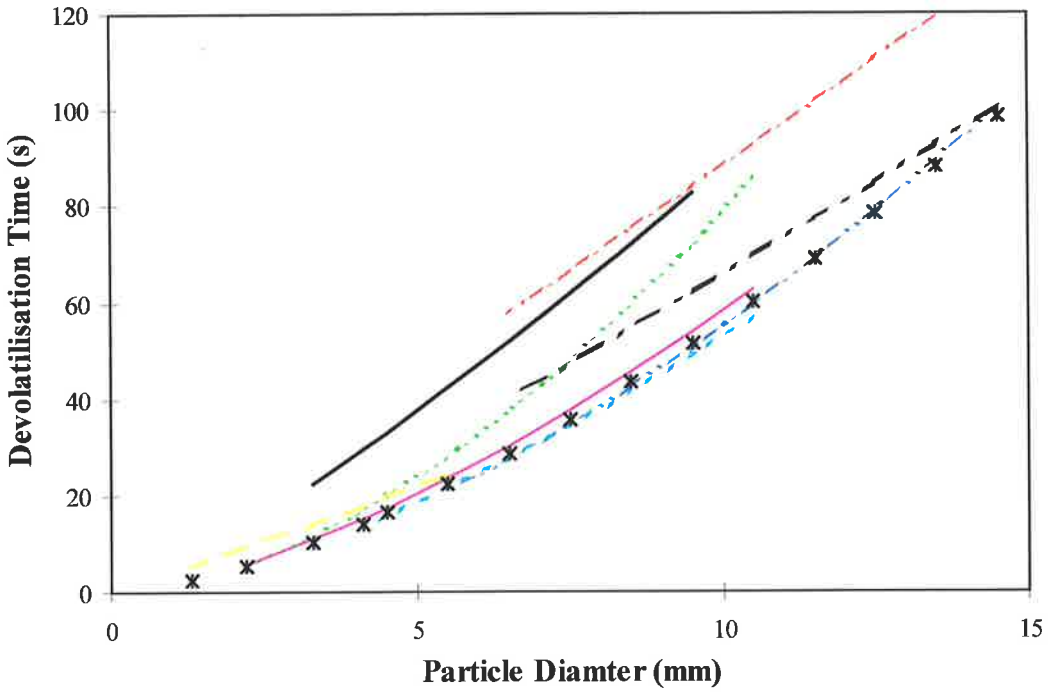

Figure 4.23 Comparison of devolatilisation times from various measurement techniques in fluidised-beds at 850°C. (note: data of Morris and Keairns (1979) collected at 872°C).

Table 4.3 Legend reference and devolatilisation time correlation parameters for the literature data shown in Figure 4.23.

Symbol	Method and reference	A	n	Atmosphere
-·-·-	Temperature response (present data)	8.96	0.99	N_2
— - —	Temperature response (present data)	4.43	1.16	Air
*	Flame extiction time (present data)	1.65	1.52	Air
———	Flame extiction time (Stubington et al., 1997)	1.84	1.50	Air
-·-·-	Flame extinction time (Zhang et al., 1990)	1.35	1.61	Air
.....	CO2 profile (Stubington et al., 1992)	1.48	1.72	Air
- - -	CO2 profile (Stubington et al., 1997)	1.67	1.50	Air
— —	Volatiles evolution (Morris and Keairns, 1979)	4.146	1.03	N_2
———	Volatiles evolution (Stubington et al., 1984)	5.18	1.23	N_2

As highlighted in the literature review (Section 2.5.1) and the previous section, the variability in observed devolatilisation time power law correlation parameters, in particular the exponent *n*, can be attributed to the difficulty in determining the exact completion point of devolatilisation.

None more so than those techniques that quantify the devolatilisation time by recording the exiting concentration of volatiles or carbon dioxide with time. An example of the carbon dioxide evolution profile reproduced from Stubington et al. (1997) showing change in devolatilisation endpoint definition time with previous work (Stubington et al., 1992) is shown in Figure 4.24.

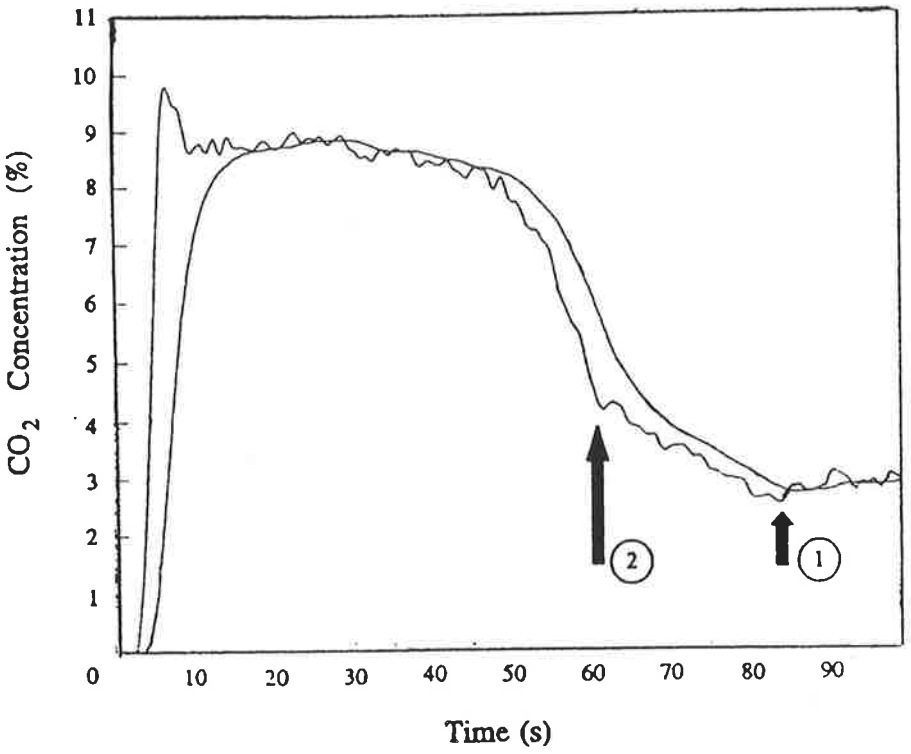

Figure 4.24 CO_2 evolution profiles (smooth curve; logged data, bumpy curve; corrected for lag and gas dispersion) for a 9.97 mm diameter Blair Athol coal particle, showing change in devolatilisation endpoint definition from Stubington et al. (1992), ①, and Stubington et al. (1997), ②.

The most favoured technique in the literature for determination of the devolatilisation time is the so called flame extinction time (FET). Comparison of the exponent values from various sources in the literature were shown in Figure 2.4 and Table 4.3. Figure 2.4, shows that experimental data reported in the literature can be segregated into two distinct bands, with peaks at values of 1.0 and 1.5. The second band centralised about an exponent value of 1.5 can be attributed to data collected using the FET technique, aided by reference to Table 4.3.

Flame extinction time experiments were conducted for both Bowman and Morwell coals in air at 850°C and compared with the temperature response technique at 95 and 100% completion of centre particle temperatures of the final bed temperature in Figure 4.25 (a) and (b), respectively. The FET results for Bowman coal particle sizes between 1 and 6 mm was taken from the data of Schluter et. al. (1997).

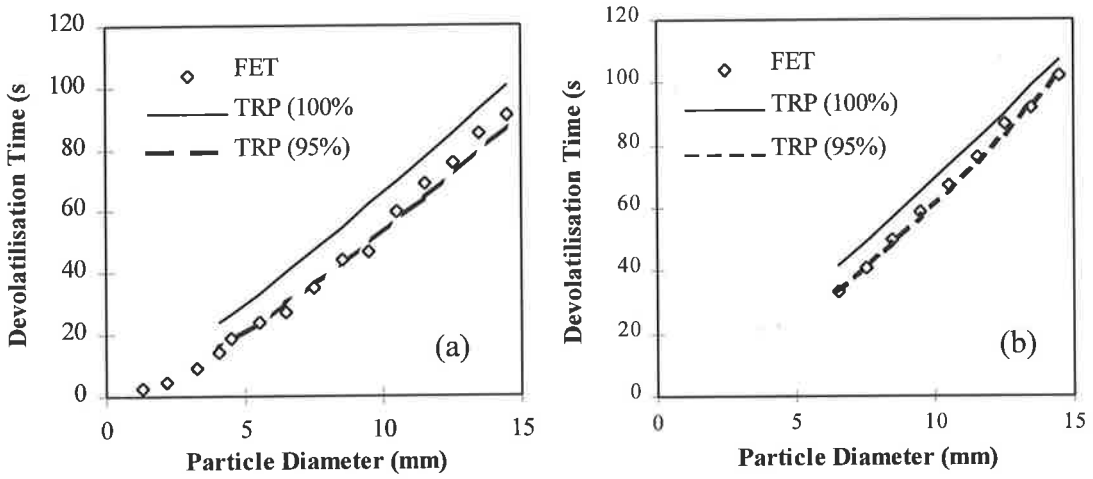

Figure 4.25 Comparison of flame extinction time with temperature response technique at 95 and 100% completion of centre particle temperature of the final bed temperature for (a) Bowman and (b) Morwell coal particles in air at 850°C.

The FET data compare favourably to the 95% definition time for the temperature response profile (TRP). This clearly demonstrates the importance of the selection of the devolatilisation endpoint definition. Comparing temperature response profiles for Bowman and Morwell coal particles at 850°C in air (shown in Figures 4.3 and 4.6), with the CO_2 profile shown in Figure 4.24 reveals an interesting characteristic. Near the completion of devolatilisation, a significant tailing effect is observed. This has been extensively reported in the literature during measurements of devolatilisation volatile product yields, in particular by Morris and Keairns (1979) when defining 95% devolatilisation times from methane evolution profiles. In the case for the TRP method, a significant period of time elapses for the particle centre temperature to be raised within the final 50°C of the bed temperature, approximately 20 seconds for a 10.5 mm diameter particle. A similar time period can be observed in the CO_2 profile of Stubington et al. (1997) highlighted between points, ① and ②, in Figure 4.24.

This decline in the particle heating rate near the completion of devolatilisation for Bowman and Morwell coals occurs consistently for all experimental conditions, as displayed in section 4.2. This reduction in the devolatilisation rate can therefore help explain the difference in experimental results based on the FET method. Nearing the completion of devolatilisation, there is an insufficient volatile flux at the particle surface to support a distinct visible volatile diffusional flame. This period is most likely characterised by simultaneous oxidation of char and volatile matter at the particle surface. Hence, the shortened devolatilisation times and observed difference in the exponent parameter for FET method.

4.3.4 Effect of Coal Type

The most contentious variable amongst investigators is the influence of coal type on the devolatilisation time. As Table 2.2 in the literature review section highlights, Urkan et al.(1994), Eatough et al. (1996) and Pillai (1981) found that devolatilisation times were dependent upon coal type while Stubington et al. (1991, 1992) did not find any correlation. The effect of coal type for seven coals ranging from lignite to anthracite in rank was investigated for various particle sizes as shown in Figure 4.26.

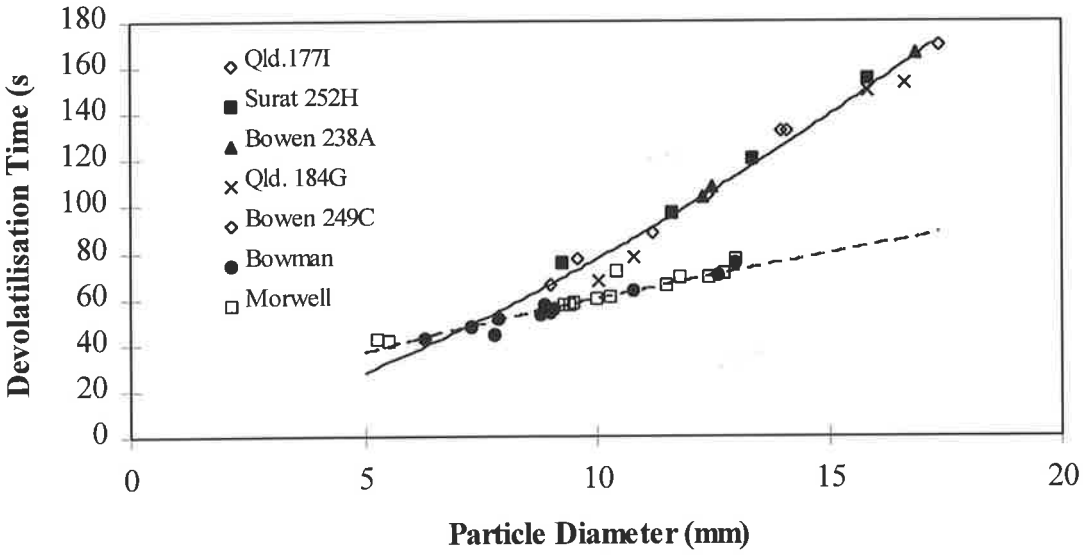

Figure 4.26 Effect of coal type on the devolatilisation time for various particle sizes at 850°C in air.

There is a pronounced difference in the devolatilisation times between low-rank Bowman and Morwell coals (lignite) and the higher rank coals (bituminous-anthracite). Peeler (1999) found a similar result during weight-loss experiments conducted for various coal types. Results of devolatilisation correlation parameters are summarised in Table 4.4. The higher rank coals exhibit an exponent value that is characteristic of the second band centralised about exponent value of 1.5 in Figure 2.4. Thus the scatter of data around this region can be attributed to the influence of coal type along with experimental definition of the devolatilisation endpoint, as discussed in previous section.

Table 4.4 Devolatilisation time correlation parameters for effect of coal type at 850°C in air.

Coal Rank	Pre-exponential factor A	Exponent n
	2.67	1.46
High ——		
Low - - - - -	12.12	0.73

However, this distinction between lignite and other higher ranked coals is in general at odds with the influence of coal type reported by others, where the devolatilisation time increases with increasing rank (Urkan et al., 1994; Eatough et al., 1996; Pillai, 1981). Urkan et al.(1994) best presented this behaviour by plotting the flame extinction time of 5 mm coal particles of various rank against the volatile matter to fixed carbon ratio (VM/FC) to characterise the influence of coal type on the devolatilisation time. This is illustrated in Figure 2.7 of the literature review. Urkan et al. (1994) postulated that the increase in flame extinction times with coal rank is a consequence of increased times for the centre temperature of a coal particle to reach the temperature at which devolatilisation is complete. This is clearly not the case. Observing the temperature profiles for the effect of coal type shown in Figures 4.10-4.16, there is a distinction in the profile nature between the lignite and higher rank coals, but no disparity amongst the higher-rank coals. Generally, the higher rank coals exhibit a linear temperature profile throughout the devolatilisation process unlike the low-rank Bowman and Morwell coals. A comparison of centre temperature response profiles at various completion percentages of the final bed temperature for

the devolatilisation of all seven coals in air at 850°C is shown in Figure 4.27. The exponent value n is determined for both the low-rank coals (Bowman and Morwell) and high-rank coals (Qld.-184G, Qld.-177I, Bowen 249, Bowen 238, Surat 252). The subsequent exponent values are plotted as a function of percent completion of devolatilisation for particle temperatures at 50, 75, 90, 95 and 100% of the final bed temperature as illustrated in Figure 4.28.

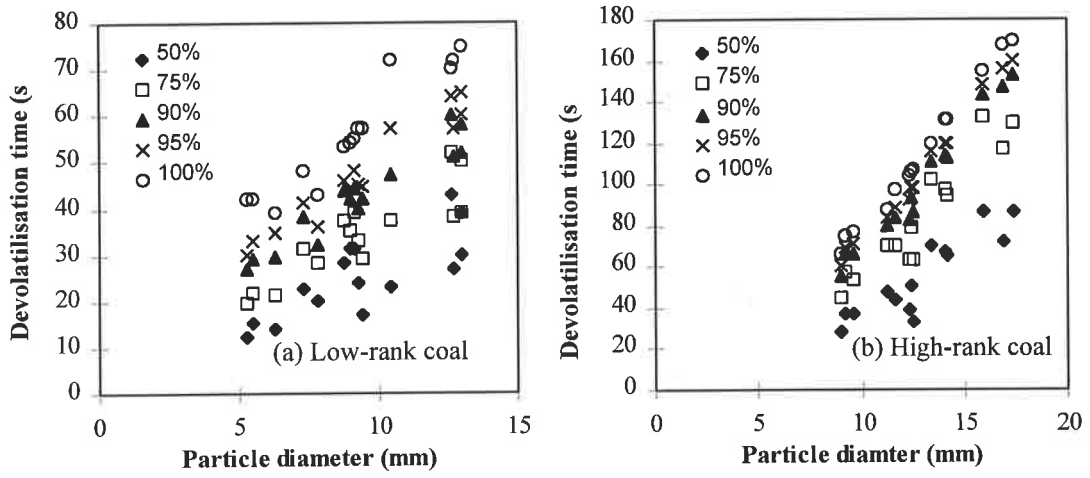

Figure 4.27 Comparison of centre temperature response profile at various completion percentages of the final bed temperature for the devolatilisation) in air at 850°C of (a) low-rank Bowman and Morwell coals; (b) high-rank coals (Qld.-184G, Qld.-177I, Bowen 249, Bowen 238, Surat 252.

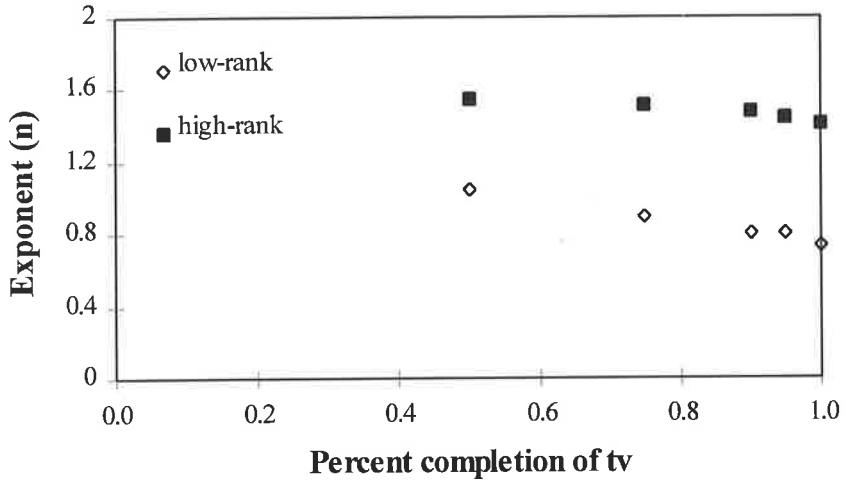

Figure 4.28 Effect of coal type on the exponent n at various fractional completions of the total devolatilisation time at 850°C in air.

The result presented in Figure 4.28 highlights two points. Firstly the relative independence of the exponent parameter n with the degree of completion, in particular for the high-rank coals. This is not surprising in view of particle temperature profiles. Secondly, for the low-rank coals, the exponent values are much lower than corresponding data for wet Bowman and Morwell coals under similar operating conditions. This suggests that the nature of the trend for the exponent parameter n at earlier stages of devolatilisation shown in Figures 4.19 and 4.21 be influenced by the evaporation of moisture.

4.3.5 Effect of Coal Moisture Content

The effect of coal moisture content as compared to the ratio of devolatilisation times for oven dried and moist coals is shown in Figure 4.29, along with data of Urkan et al. (1994). As evident from this figure, there is a good agreement with data of Urkan et al. (1994). As the moisture content increases, the effect is more pronounced, as would be expected as more water must be evaporated from the coal particle suppressing the particle heating rate.

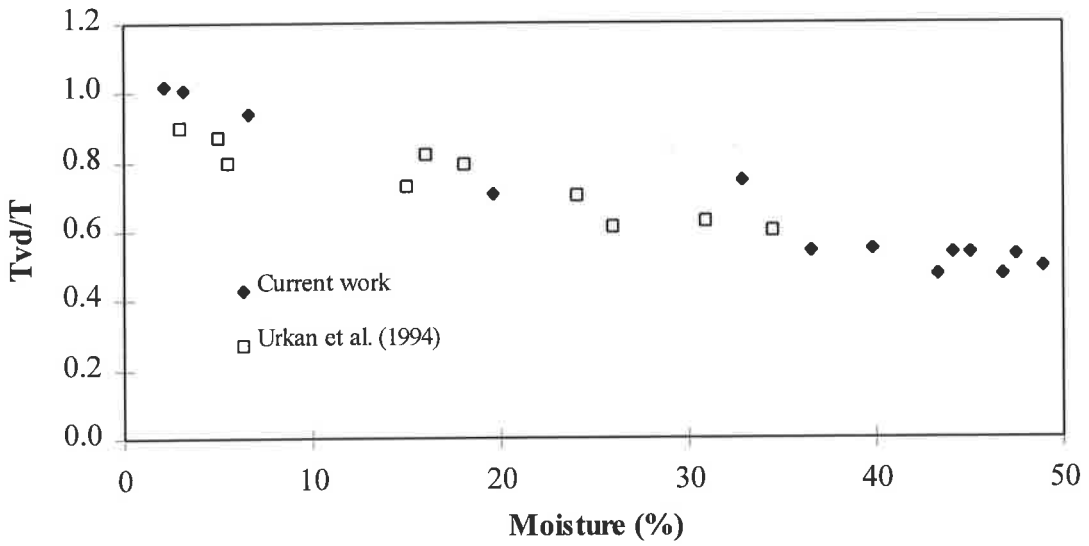

Figure 4.29 Effect of moisture content on the ratio of devolatilisation time for dried and moist coals at a bed temperature of 850°C in air.

The evaporation of moisture can be considered essentially as a heat transfer related mechanism. This explains why at lower temperatures (or early completion times) the exponent n in Figures 4.19 and 4.21 appears to approach the theoretical square law dependence associated with heat transfer control. While at higher temperatures, it steadily decreases as chemical kinetics play an increasing role. This is clearly demonstrated in Figure 4.30, which compares the exponent n at various completion times for dry and wet Bowman and Morwell coal particles at 850°C in air. Comparing this figure with Figure 2.8 of the measured temperature response for a 10 mm wet and bone dry Bowman coal particle in a fluidised-bed at 750°C and 850°C, the influence of coal moisture and its evaporation on the exponent n is not surprising.

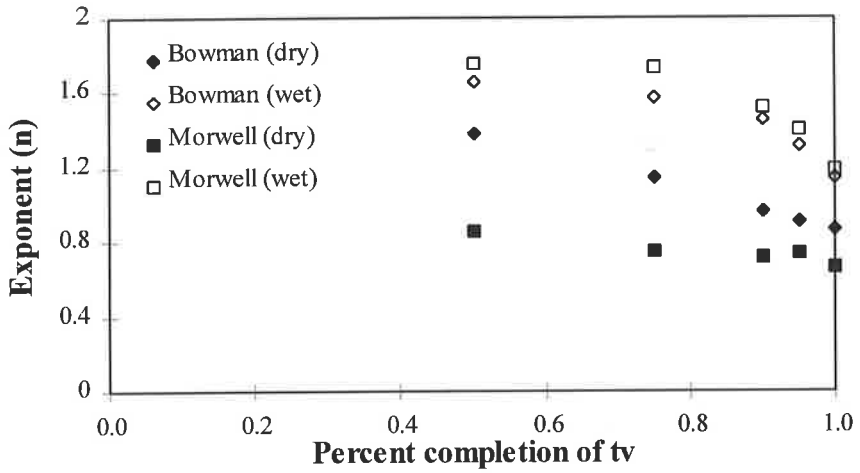

Figure 4.30 Comparison of the exponent n at various fractional completions of the total devolatilisation time for devolatilisation of dry and wet Bowman and Morwell coal particles in air at 850°C.

4.4 THEORETICAL CONSIDERATIONS

As highlighted in section 2.5.1 of the literature review, the current theoretical hypotheses define that the devolatilisation time of large coal particles in fluidised-beds is proportional to the square of the particle diameter. However, experimental literature data does not support this theory. Based on devolatilisation modelling conducted by Heidenreich (1999), a new theoretical treatment to distinguish between

heat transfer and chemical-kinetically controlled regimes during devolatilisation has been developed as outlined in section 2.5.1. However the key question relating to whether the devolatilisation time of large coal particles under heat transfer control should be proportional to the square of the particle size remains. A close inspection of the dimensionless time versus the dimensionless Biot/Modified Damkohler number ratio reveals that the necessary coefficients for time dependency of devolatilisation upon the contributions of internal/external heat transfer, chemical kinetic limitations and particle size are neatly represented. Figure 4.31 illustrates a plot of the dimensionless time, t_{95}/T_{95} versus the negative natural log of (Da'/Bi) number ratio.

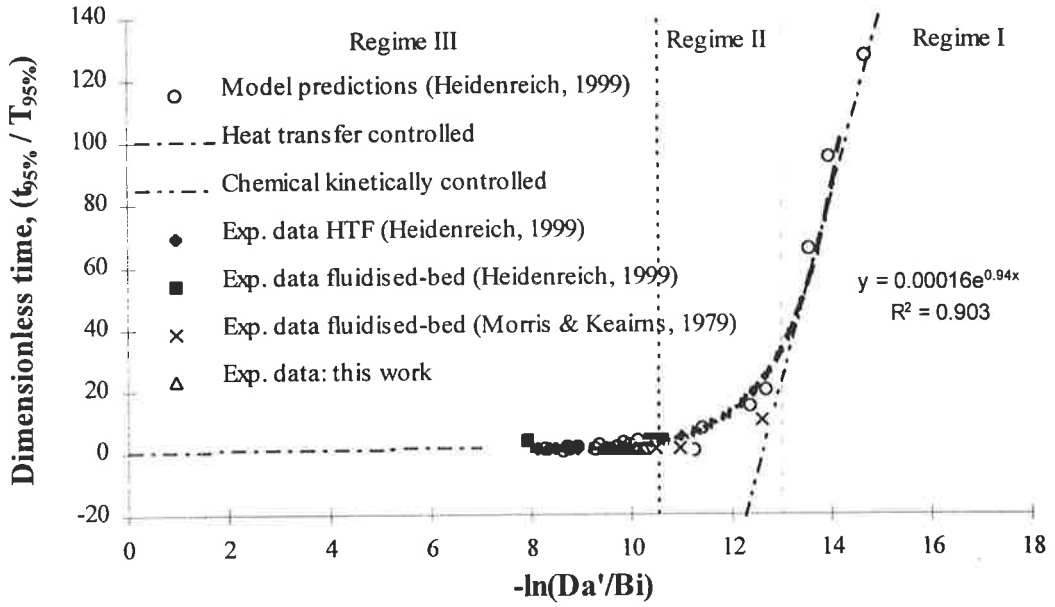

Figure 4.31 Plot of experimental data and model predictions for dimensionless evolution/heating time ratio, t_{95}/T_{95} versus the natural log of Modified Damkholer to Biot number ratio, -ln(Da′/Bi). HTF denotes Horizontal tube furnace; convective flow reactor. Current work denotes temperature data for Bowman coal in nitrogen at 850°C.

Fitting a trend line to model and experimental data, the ratio of dimensionless time, t_{95} / T_{95} can be correlated to -ln(Da′/Bi) ratio as follows;

$$\frac{t_{95}}{T_{95}} = 0.00016e^{-\ln\left(\frac{Dd}{Bi}\right)^{0.94}} \qquad \text{....4.3}$$

Substituting expression for modified Damkohler/Biot number ratio (Equation 2.11) and rearranging yields

$$T_{95} = \left[6250\, t_{95} \left(\frac{r' \rho_0 C_p}{h_o} \right)^{0.94} \right] d_p^{0.94} \qquad \text{....4.4}$$

or

$$t_{95} = T_{95}\, 0.00016 \left(\frac{h_o}{r' \rho_0 C_p d_p} \right)^{0.94} \qquad \text{....4.5}$$

Which is analogous to classic empirical power-law relation Equation 2.1 for $n = 0.94$ reported in the literature. Hence, a new theoretical definition of the power-law relation has been derived which is consistent with the literature findings of devolatilisation time being directly proportional to the particle size. Furthermore, it is now possible to quantitatively define the pre-exponent parameter A of the empirical power-law correlation and verify the observed influences of operating parameters such as bed temperature and gas environment on the devolatilisation time. As shown in sections 4.3.1 and 4.3.2, the pre-exponent parameter A is found to decrease with increasing oxygen concentration and bed temperature.

Theoretically, these experimental observations are satisfactorily accounted for by Equation 4.4. The effective heat transfer coefficient h_o, would be enhanced by the combustion of volatiles at the particle surface and the increased contribution by radiative heat transfer with increasing bed temperature. Thus, the pre-exponent parameter A would decrease as observed experimentally. Furthermore, it was observed that the pre-exponential constant A was proportional to the inverse of T^3 (Section 4.3.2). Relating the fact that in Equation 4.4, A is proportional to inverse of the overall heat transfer coefficient, $A \propto 1/h_0$ and the overall heat transfer coefficient accounts for both convective and radiative heat transfer, as defined in Equation 2.12. This indicates radiative heat transfer is the dominating mechanism ($h_{rad} \propto T^4$) and controls the rate of heat transfer and hence the volatile evolution rates for large particles in a fluidised-bed. Furthermore, literature reports no influence of superficial operating velocity on the devolatilisation time.

Thus, convective heat transfer is not the dominating mechanism for heat transfer at high temperatures in a fluidised-bed and in fact h_o is a weak function of d_p and rather, a strong function of temperature. It is appreciated that the modified reaction rate r', will also alter with changes to experimental conditions, (in particular operating temperature) but as large particle devolatilisation is heat transfer controlled, it is of less significance.

In order to ascertain the validity of the expression over the entire range, a test for chemical kinetic control is conducted, where t_{95} should be independent of particle size (Agarwal et al. 1984(a)). From Equation 4.5, an expression for the heating time, T_{95} is required. Heisler (1947) derived analytical solutions to the transient particle heat balance with convective boundary assuming constant thermal diffusivity. The dimensionless centre temperature $\frac{T_{95\%} - T_0}{T_\infty - T_0}$ was plotted as a function of the Fourier number ($4\alpha t/d^2$) for various Biot numbers. Thus, obtaining a value for the Fouier number for a particular particle Biot number hence:

$$Fo = 4\alpha t/d^2$$
$$\rightarrow t \propto d^2 \qquad \ldots.4.6$$

The time taken for the centre temperature to reach 95% of the final temperature $T_{95} \propto d_p^2$. Assuming the treatment of Prins et al. (1989) and Agarwal et al. (1984a), for low Reynolds number corresponding to stagnant oxidising conditions, Nusselt number being approximately equal to 2 for all particle diameters $\rightarrow h \approx d^{-1}$). Thus substituting relevant proportional variables into Equation 4.5 yields:

$$t_{95} = d_p^{\,2}\, 0.00016 \left(\frac{\frac{1}{d_p}}{r' \rho_0 C_p d_p} \right)^{0.94} \qquad \ldots.4.7$$

Taking that the exponent as being approximately unity, as 0.94 is experimentally determined $n \rightarrow 1$

$$t_{95} \propto 0.00016/(r'C_p\rho_o) \qquad \ldots.4.8$$

The evolution time is dependent on the chemical reaction rate r', ie chemical kinetic control and t_{95} is not dependent on the particle size as observed in the literature. Care must be taken in the validity of this result at hand, as it should not be taken outside the limit of the assumption of stagnant oxidising conditions where Nusselt number is approximately equal to two.

4.5 SUMMARY

The devolatilisation times of seven coals were determined by measuring the centre temperature responses for single particles held stationary in a bench scale atmospheric fluidised-bed reactor. The devolatilisation time was defined as the time taken from particle immersion into the bed until the centre temperature of the coal particle equalled the bed temperature. Bed temperature, oxygen concentration, particle size, moisture content and coal rank were found to influence the devolatilisation time.
The results were correlated with the classic empirical particle diameter power law relation where it was observed that the devolatilisation time was directly proportional to the particle diameter. This is contrary to current theory based on heat transfer control, which defines a square law relationship.

In comparing the current technique with the flame extinction time and CO_2 profile measurements, discrepancies in the reported exponent parameter values n, from correlation with devolatilisation time power law relation have been resolved. The affect of coal type and coal moisture on the variation of reported exponent parameter values has been highlighted.

A new theoretical treatment to distinguish between heat transfer and chemical-kinetically controlled regimes of coal devolatilisation based on the ratio between the 95% evolution time, t_{95} and the time required for 95% heating of the particle centre, T_{95}, versus the modified Damkholer number to Biot number ratio, has been used to derive an analogous equation to that of the empirical power-law correlation, being directly proportional to the particle diameter (exponent, n, equal to 0.94). It is now possible to quantitatively define the correlation parameter A, and explain experimental observations relating to the influence of bed temperature and gas atmosphere upon the devolatilisation time. The observed effects of these variables are consistent with that of heat transfer to and within the particle as the rate controlling step for large particle devolatilisation in fluidised-beds.

CHAPTER 5

INFLUENCE OF VOLATILES ON THE COMBUSTION RATE OF CHAR

5.1 INTRODUCTION

This chapter reports an experimental study of the combustion of volatile matter, simulated by propane, and its interaction with char combustion reactions in a bubbling fluidised-bed. As highlighted in Chapter 2, numerous studies have been reported on coal devolatilisation, char combustion and volatile combustion in a fluidised-bed. The rate of char combustion depends on the bed temperature, oxygen concentration, particle diameter, inorganic species and char structural properties such as pore size distribution and internal surface area (Andrei et al., 1985; La Nauze, 1985).

Of significant importance has been the realisation that the in-bed combustion of premixed synthetic volatiles does not take place below the *so-called* critical bed temperatures. There is gradual transition from violent over-bed to stable in-bed combustion with increasing bed temperature. Experimental results have quantitatively shown that little oxygen is consumed in the bed at temperatures below 750°C for propane. As the bed temperature rises the oxygen concentration in the bed decreases as a result of gradual conversion of volatile matter throughout the bed, leading to a significant reduction in the oxygen concentration. Thus, the char particle will be in competition with the volatile matter for the available oxygen.

While the drive to increase in-bed volatile combustion may in fact lead to a dichotomy for fluidised-bed combustion of coal, in that higher bed temperatures led to a decrease in carbon combustion efficiency, this outcome will be ideal for gasification. By reducing the extent of char combustion in favour of volatile combustion, more char is available to undergo gasification and thus, increase the extent of char gasification conversion (Gururajan et al. (1992). Hesketh et al. (1991) has been the only study reported to have examined the effect of volatiles on the rate of char combustion.

The specific intentions of this chapter are to: (1) measure and report the effect of temperature on combustion rate of char with and without propane feed for a Victorian low-rank coal at atmospheric pressure; (2) compare char burn-out times; (3) apply a simple correlative method, based on rate-controlling process, for correlating rate data.

The weight loss and burn-out times for a batch of seven coal particles in the size fraction +3.35 -3.175 mm were examined at temperatures of 700°C, 800°C and 900°C. A bed of silica sand (+250-180μm) was fluidised either by a pre-mixed nitrogen diluted 10% v/v oxygen stream or a nitrogen diluted 10% v/v oxygen, 3% v/v propane mixture. Char particles were retrieved at various time increments after the completion of devolatilisation, by the means of a movable gauze basket and quenched in a nitrogen stream as conducted by Andrei et al. (1985). As the measurement technique relies on the difference between the initial and final weights of the particle, the ash content of the coal must be preserved. As char burn-out progresses, a thin ash layer forms around the particle. In order to minimise the fracturing of this ash layer and consequent error in mass loss balance, a fine sand size was employed and the bed excess superficial operating velocity was kept to twice the minimum fluidisation velocity. Details of experimental system have been given in Chapter 3. The choice of propane as a practical volatile substitute was based on its thermochemical and combustion properties resembling more those of complex fuels (coal volatile matter) than light hydrocarbons like methane and ethane (Dagaut et al. 1987). This is supported by the work of Mullins (1953), who observed that the ignition delay time for propane was approximately the same as compared to other C_4-C_{11} aliphatic hydrocarbons and aromatic hydrocarbons. Furthermore, in the study by Hesketh et al. (1991) propane was used as a synthetic coal volatile to examine its effect on the rate of char combustion. Thus, in accordance with literature propane will be similarly used to simulate the presence of volatile matter.

5.2 CHAR COMBUSTION CORRELATIONS

Many models of varying complexity have been developed to describe the process of char combustion in fluidised-bed combustors (Ross et al., 1981; Blackman et al. 1994; Borghi et al. 1985 and La Nause et al., 1983). Available data for coal particle sizes

greater than 1 mm suggest that the combustion rate at high temperatures in air at atmospheric pressure to be diffusion controlled (Essenhigh, 1981; Ross et al., 1981). While for particles below 1 mm in size, the combustion rate was mainly influenced by chemical kinetics. The simple diffusion control equation for oxidation of a char particle in laminar flow was used to compare with experimental data and is given by Equation 5.1, where symbols are defined under Nomenclature.

$$dm_p / dt = k_c A_p (C_{ob} - C_{os}) M_p S \qquad ....5.1$$

Following the treatment proposed by Blackman et al. (1994), at low flow rates, assuming concentration of oxygen at the surface of the char particle, C_{os} to be zero, upon integrating, the classical diffusion controlled oxidation rate for a shrinking particle is obtained, as shown in Equation 5.2;

$$d_{po}^2 - d_p^2 = (8 D_o C_{ob} M_p S / \rho_p) t = C_1 t \qquad ...5.2$$

By rearranging Equation 5.2, it can be expressed in terms of particle mass as;

$$m_p^{2/3} = m_{po}^{2/3} - C_2 t \qquad ....5.3$$

Thus a plot of $m_p^{2/3}$ versus t should produce a straight line (Blackman et. al., 1994). It has also been reported that during char combustion experiments by Andrei et al., (1985); Blackman et al., (1994) and Wang et al. (1972), an ash layer surrounding the particles formed. Thus, as char burnout proceeds, the formation of an ash layer may influence the diffusion of oxygen to the char surface and hence, char burning rates to some degree. Assuming constant particle size and a linear concentration gradient across the ash layer, with concentration of oxygen at the particle surface assumed to be zero, $C_{os} = 0$, integration of Equation 5.1 gives (Blackman et. al., 1994):

$$d_p = d_{po} - (8 D_{oa} C_{ob} M_p S / \rho_p)^{1/2} t^{1/2} = C_3 t^{1/2} \qquad ....5.4$$

Which in terms of mass can be expressed as,

$$m_p^{1/3} = m_{po}^{1/3} - C_4 t^{1/2} \qquad ....5.5$$

Thus, under this condition, a plot of $m_p^{1/3}$ versus $t^{1/2}$ should produce a straight line.

5.3 COMBUSTION PHENOMENOLOGY

Upon the introduction of coal particles onto the surface of the fluidised-bed, the particles drifted towards the wall due to the motion of the bed. The coal particles are seen to float on the bed surface, buoyed by the evolution of volatiles during devolatilisation. The formation of a laminar diffusion flame was observed in close proximity to the particle, the extent of the flame formation dependent on bed temperature, as similarly observed by Schluter et al. (1997) and Andrei et al. (1985). The height of the flame was seen to be considerably taller at higher temperatures, which is consistent with the more rapid devolatilisation of coal with bed temperature reported in Chapter 4. During the course of devolatilisation the coal particles did not glow but were observed to appear black against the bright red background of the bed, presumably as a consequence of endothermic pyrolysis reactions (Andrei et al. 1985). As volatile evolution decreased, the laminar flame decreased in size until a thin, spherical diffusion flame enveloped an ever glowing particle. The char particles would sink into the bed and appear periodically at the bed surface as brightly glowing specks. With increasing char burnout, the formation of an ash layer surrounding the char particle could be seen.

The combustion of pre-mixed propane and air in the bed behaved qualitatively the same as previously reported by others under FBC conditions (Hayhurst, 1991; Dennis et al., 1982; Hesketh et al., 1991; van der Vaart, 1985, 1988, 1992; Ogada et al., 1996). At the lower bed temperatures of 700°C and 800°C, propane combustion was characterised by violent over-bed combustion, as bubbles of propane exploded at or above the bed surface. The higher freeboard temperatures associated with this unstable explosive combustion could be seen in the form of sand particles that were blown into the freeboard, which glowed with a greater intensity against the red background of the bed. Upon heating the bed to the highest temperature of 900°C, combustion noise ceased, this was associated with the transition to stable in-bed combustion of propane. This is consistent with reported critical temperatures for in-bed combustion of propane at 835°C under FBC conditions reported in the literature (Hesketh et al., 1991; van der Vaart, 1985).

5.4 EFFECT OF PROPANE ON CHAR COMBUSTION RATE

Figure 5.1 shows the results of time-resolved weight loss measurements for Loy Yang coal at 700°C, 800°C and 900°C, respectively, in a stream of 10% v/v oxygen and 10% v/v oxygen and 3% v/v propane mixture. It can be seen from the plots of weight loss versus time that the introduction of propane into the fluidising stream results in a decrease in the combustion rate of char, particularly discernible at the highest bed temperature of 900°C.

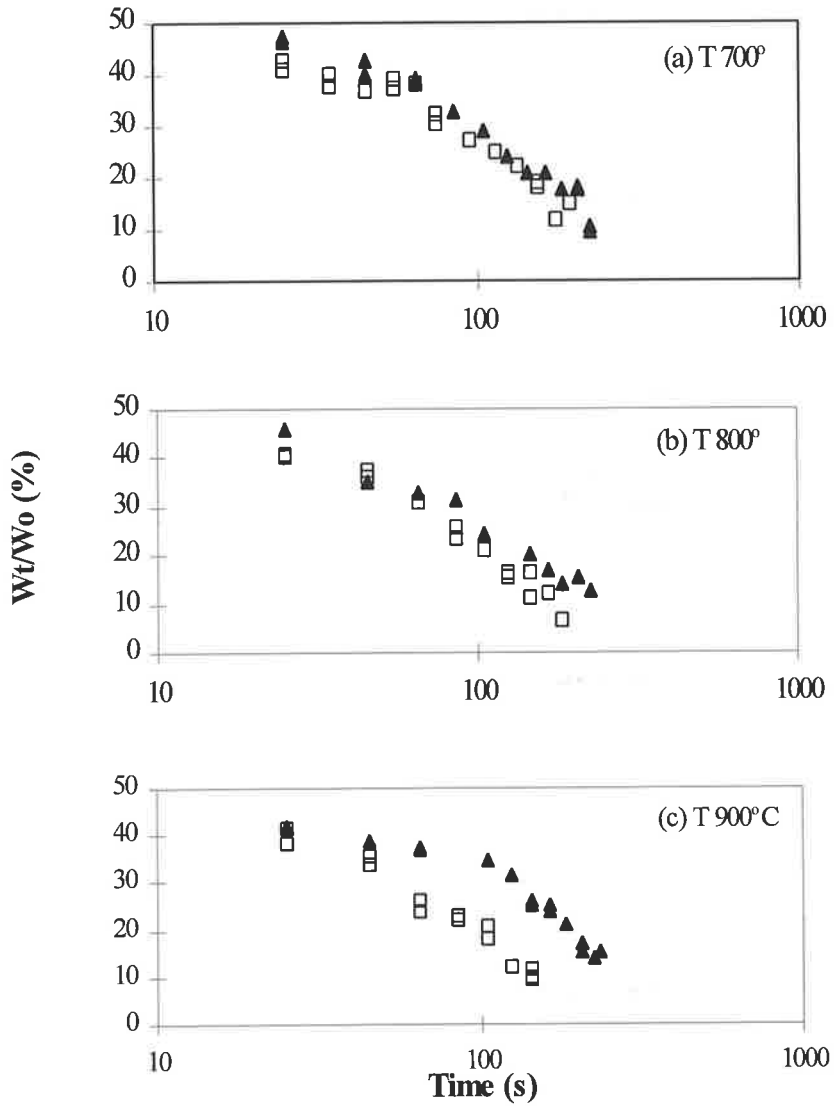

Figure 5.1 Weight remaining Wt/Wo (%) versus time (s) at bed temperatures of 700°C, 800°C and 900°C for a batch of +3.35 -3.175 mm Loy Yang coal particles in a fluidised bed. Combustion in 10% v/v oxygen, 3 % v/v propane (▲), Combustion in 10% v/v oxygen (□).

This result is consistent with the fact that in-bed combustion of propane increases with bed temperature and thus consumes an increasing fraction of oxygen in the fluidising gas. The effect of bed temperature on char combustion rates can be seen more clearly by considering single particle burn-out times obtained by the intercept of each weight loss plot. Figure 5.2 shows a comparison of the single particle burn-out time of char particles as a function of bed temperature with and without propane against the data of Hesketh et al. (1991). There is a good agreement between this work and Hesketh et al. (1991). The burnout times for char particles under a propane/air mixture are 18, 39 and 88% longer, than under an air mixture at the corresponding bed temperatures. Hesketh et al. (1991) reported increases in char burnout times of between two to three times at the highest bed temperature investigated of 950°C. It can be seen that the difference between the burnout times increases substantially above 800°C. This is consistent with the reported critical bed temperature for in-bed combustion of propane of 835°C (Hesketh et al., 1991; van der Vaart, 1985). Above this critical temperature, considerable proportions of the propane and intermediate species burn in the bed. Thus, the char particle is competing with the volatile matter for the available oxygen. Consequently, the drive to increase in-bed volatile combustion to reduce over-bed burning that results in high freeboard temperatures and subsequent formation of pollutant NO_x species results in a dichotomy for FBC. While in-bed volatile combustion efficiency increases with higher bed temperatures, char combustion rates and subsequently carbon combustion efficiency will decrease. However, this outcome for FBG of coal is ideal, as more char is available to undergo gasification reactions.

The extended burn-out times at the higher bed temperatures of 800°C and 900°C were expected, the difference at the lower bed temperature was not, as propane is known to burn in the splash zone and freeboard (Hesketh et al., 1991; van der Vaart, 1985, 1988). A similar result has been reported by Hesketh et al. (1991). Hesketh et al. (1991) concluded that the char particles spend a proportion of their time at the bed surface, as witnessed during the course of char burn-out experiments by the periodic observation of glowing char specks. Thus at the lower bed temperature of 700°C, propane combustion at the bed surface results in a dramatic reduction in local oxygen concentration.

This can be seen by referring to in-bed chemical analysis of propane combustion under FBC conditions shown in Figure 2.12 in Chapter 2, as reproduced from van der Vaart (1988). The oxygen concentration plummets from over 18 vol% to less than 4 vol% in the space of 4 cm. Thus anytime spent by the char particle at this location will lead to a significant decrease in combustion rate and therefore an increase in burn-out times.

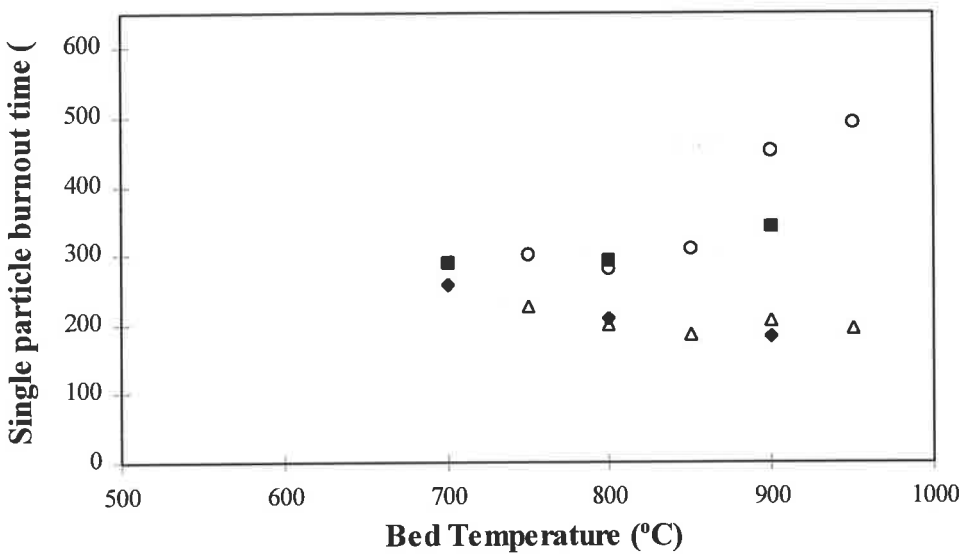

Figure 5.2 Comparison of the single particle burnout times versus bed temperature for a batch of + 3.35 - 3.175 mm Loy Yang coal particles in a fluidised bed with the data of Hesketh et al. (1991). Combustion in 10% v/v oxygen (◆), Combustion in 10% v/v oxygen, 3 % v/v propane (■), Combustion in air (Hesketh et al., 1991) (Δ), Combustion in air, 2.5 % v/v propane (Hesketh et al., 1991) (O).

Referring to the combustion of char in air only, the burn-out times decrease as bed temperature rises, suggesting the influence of chemical reaction kinetics on the combustion rate. However, the data for char combustion at 900°C compares well with that of Hesketh et al. (1991), where the oxidation rate above 850°C is insensitive to temperature, indicating a change to diffusion controlled combustion. It is expected that for highly reactive coals, typical of low-rank coals such as Loy Yang, that char combustion would be diffusion controlled at high temperatures.

Figure 5.3 compares the time-dependence of mass loss for the data based on the shrinking-core diffusion theory as derived by Blackman et al. (1994) where a plot of char mass remaining$^{2/3}$ versus time should be linear. The straight lines in this figure and in the following figure to be presented, are linear least-square regression fits, for which the statistical correlation coefficients are displayed on each figure. As can be seen from this figure, the experimental data show a linear form for the correlative method based on the shrinking-core particle diffusion model.

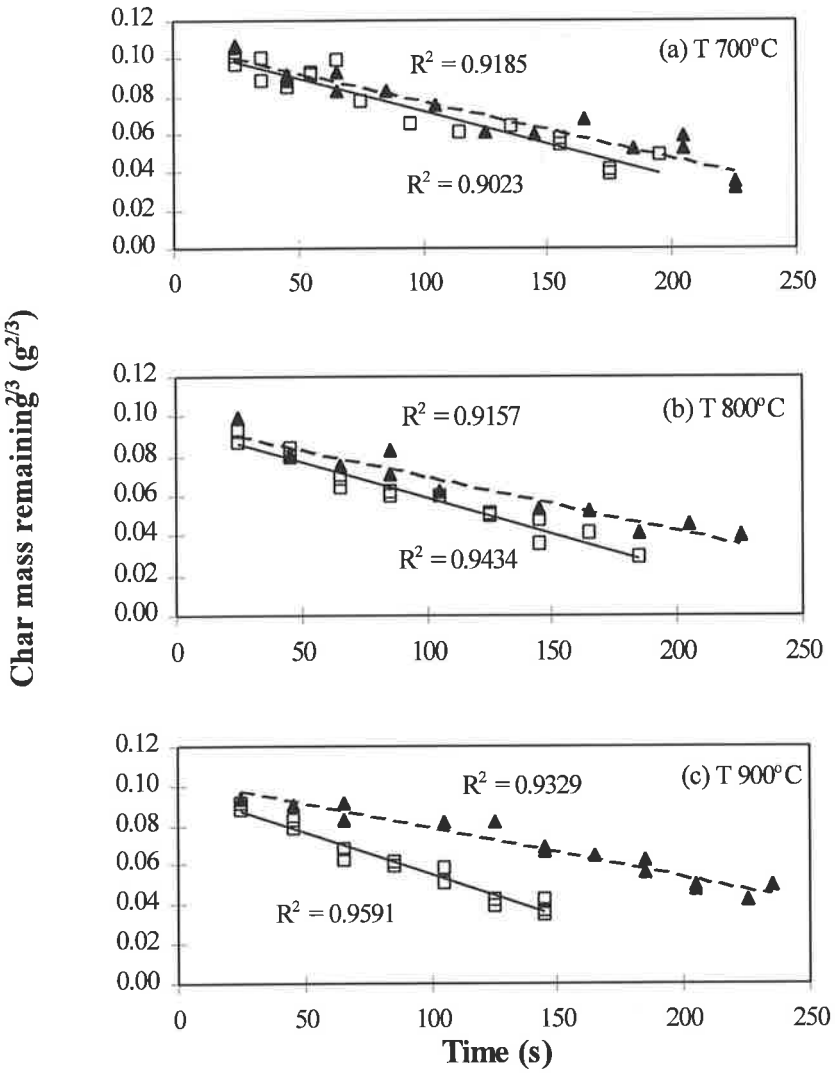

Figure 5.3 (Char mass remaining)$^{2/3}$ versus time at bed temperatures of 700°C, 800°C and 900°C for a batch of +3.35 -3.175 mm Loy Yang coal particles in a fluidised bed. Combustion in 10% v/v oxygen, 3 % v/v propane (▲), Combustion in 10% v/v oxygen (□).

It is observed that the linearity of the plots, as defined by the R^2 values, is in every case >0.90 and improves with increasing temperature. The better fit of the data with increasing temperature certainly suggests diffusion limitations and that at the lowest bed temperature of 700°C, the rate of combustion may indeed be influenced by chemical kinetics. This assertion is supported by the work of Brunello et al. (1996).

It was observed upon retrieval and quenching of char particles that an ash layer forms around the char particles. Similar results for the formation of an ash layer during char burn-out have been reported by Wang et al., (1972); Park et al., (1987); Froberg et al. (1978); Andrei et al. (1985); Blackman et al. (1994) and Brunello et al. (1996). The presence of an ash layer could increase diffusion resistance and lower the transition temperatures to diffusion controlled combustion and increase the char burn-out time. There appears to be some conjecture in the literature to whether the ash layer may influence the char burning rate. Wang et al., (1972); Park et al., (1987); Froberg et al. (1978) and Blackman et al. (1994) reported an influence, while Andrei et al. (1985) and Brunello et al. (1996) otherwise. The observed difference in these findings most likely caused by the difference in experimental apparatus used. Andrei et al. (1985) and Brunello et al. (1996) investigated burn-out times using a fluidised-bed in contrast to the simple devices such as a muffle furnace or heated ceramic tube by Wang et al., (1972); Park et al., (1987); Froberg et al. (1978) and Blackman et al. (1994). The relative placid environment of these reactor systems is in direct contrast to the highly agitated state of a fluidised-bed. Thus, the ash layer thickness in a fluidising environment will most likely be less as compared to these other simple reactor systems as a result of the erosion effects of the sand bed material. Thus, the impact that the ash layer has on any additional diffusion limitations under a fluidising environment may well be inconsequential.

In order to determine whether this ash layer surrounding the burning core influenced the combustion rate, a modified diffusion controlled equation for a thin ash layer, as given in Equation 5.4 derived by Blackman et al. (1994), was used to evaluate the experimental data. Figure 5.4 compares the time-dependence of mass loss for the data as a plot of (char mass remaining)$^{1/3}$ versus (time)$^{1/2}$, which should produce a linear fit according to Equation 5.5.

The lower regression values for the ash layer control assumption upon the combustion rate indicates that the ash layer does not impose any additional diffusion resistance on char burning rates, which is in agreement with Andrei et al. (1985) and Brunello et al. (1996). In order to ascertain from a statistical viewpoint, whether or not the data presented in Figures 5.3 and 5.4 differ, a standard t-test based on the residual coefficients for the plots will be conducted.

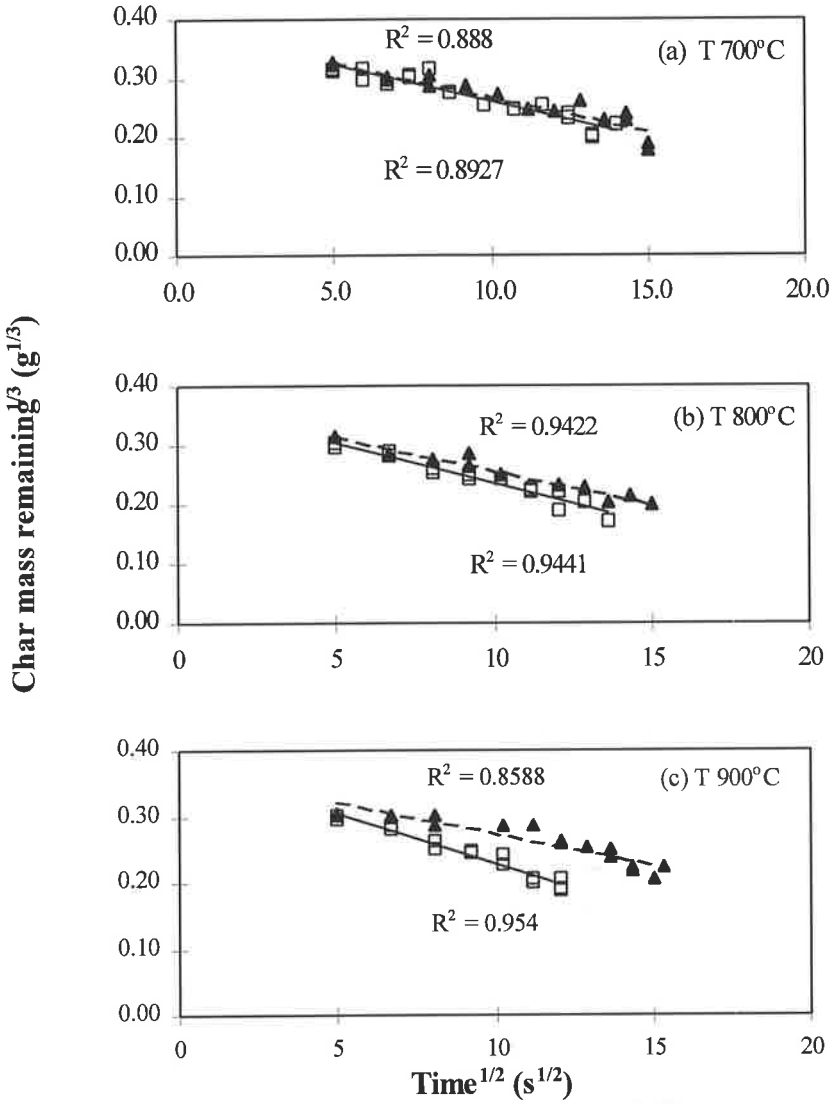

Figure 5.4 (Char mass remaining)$^{1/3}$ versus (time)$^{1/2}$ at bed temperatures of 700°C, 800°C and 900°C for a batch of +3.35 -3.175 mm Loy Yang coal particles in a fluidised bed. Combustion in 10% v/v oxygen, 3 % v/v propane (▲), Combustion in 10% v/v oxygen (□).

Table 5.1 Statistical data based on the char mass remaining data present in Figures 5.3 and 5.4.

Run No.	Shrinking-core Particle Diffusion			Ash Layer Diffusion Control		
	R^2	$\bar{x}_1$	s_1	R^2	$\bar{x}_2$	s_2
1	0.8588			0.9329		
2	0.8927			0.9157		
3	0.9422	0.9133	0.06113	0.9185	0.92865	0.03261
4	0.9441			0.9023		
5	0.888			0.9434		
6	0.954			0.9591		

The t-test parameter is defined as (Perry and Green, 1984):

$$t = \frac{\bar{x} - \mu_o}{\sigma / \sqrt{N}} \qquad \ldots.5.6$$

The null hypothesis would be defined by:

$$H_o: \mu_1 = \mu_2 \text{ with } H_1: \mu_1 \neq \mu_2 \qquad \ldots.5.7$$

Where $\bar{x}_1$ is the population mean based on the standard analysis, and $\bar{x}_2$ is the proposed population mean which is that of the ash diffusion control limitation. For this application, it was assumed that $\sigma_1^2 = \sigma_2^2$ as the variation in the experimental techniques are identical. With $\alpha = 0.05$ and 10 degrees of freedom, the critical values of t are ± 2.228. Accept H_o if $-2.228 \leq$ sample $t \leq 2.228$. Otherwise reject H_o and accept H_1. For the sample the pooled variance estimate is given by ($5\ df_1 = 5\ df_2$):

$$s_p = \sqrt{\frac{0.06113^2 + 0.03261^2}{2}} = 0.04899 \qquad \ldots.5.8$$

The sample t statistic:

$$\text{Sample t} = \frac{(0.9133 - 0.92865)}{0.04899\sqrt{1/6 + 1/6}} = -0.5426 \qquad \ldots.5.9$$

Since the sample value of t falls within the acceptance region, accept H_o that the mean values are equal. Thus, the ash layer does not impose any additional resistance to diffusion.

5.5 SUMMARY

The influence of the combustion of a synthetic volatile (propane) simulating the presence of volatiles emitted by devolatilising coal particles upon the combustion rate of Loy Yang coal was investigated. A comparison of the single particle burn-out time of char particles as a function of bed temperature showed good agreement with the data of Hesketh et al. (1991). It was found that the char burnout times increased substantially from 13 to 88% as the bed operating temperature was raised from 700°C to 900°C, respectively, upon the introduction of 3% v/v propane into a nitrogen diluted, 10 % v/v oxygen air fluidising stream. The increasing difference in the burnout times with increasing bed temperature is associated with the transition of over-bed to in-bed combustion of propane. At the highest bed temperature of 900°C, the rate of char combustion is diffusion controlled while the influence of kinetics is evident at the lower bed temperatures. The ash layer formed during char burn-out does not impose any additional resistance on the char combustion rate as similarly observed by others in the literature (Andrei et. al., 1985 and Brunello et al., 1996).

CHAPTER 6

PRE-MIXED COMBUSTION OF PROPANE IN FBG

6.1 INTRODUCTION

Numerous experimental studies have been conducted to investigate the combustion of volatiles under bubbling fluidised-bed combustion (FBC) conditions. The influence of volatile combustion on oxygen distribution within the bed and subsequent increase in char burn-out times have been well documented (Hesketh et al., 1991; Ross et al. 1999). However, such data in relation to the combustion of volatiles under gasification conditions is currently lacking in the literature and is essential to the development of a suitable mathematical model for fluidised-bed gasification of low-rank coal. This chapter reports the results of an experimental study into the combustion of volatile matter, simulated by propane, and its interaction with char gasification reactions in a bubbling fluidised-bed coal gasifier. The choice of propane as the practical volatile substitute was based upon its thermochemical and combustion properties resembling more those of complex fuels (coal volatile matter) than light hydrocarbons like methane and ethane (Dagaut et al. 1987). Experiments were performed under conditions prevailing for propane pyrolysis (in a nitrogen/steam fluidised-bed), propane gasification (in an air/steam fluidised-bed), char gasification only (in an air/steam fluidised-bed without propane) and in propane/char gasification (in an air/steam fluidised-bed). Propane was introduced into a water-cooled plenum chamber and was pre-mixed with air and steam before injection into a 102 mm diameter stainless steel fluidised-bed. An over bed coal screw feeder was used to feed +2.5 -3.1 mm Yallourn coal char particles. In bed axial gas samples were measured at three bed temperatures of 750, 850 and 950°C using a stainless steel water-cooled gas sample probe. Gas concentrations for CO_2, CO, C_3H_8, C_3H_6, C_2H_6, C_2H_4, C_2H_2, and CH_4 were determined by using FTIR spectroscopy. Details of experimental system have been given in Chapter 3. The experimental results reported here are believed to provide the first set of comprehensive data on volatile combustion under conditions prevailing in a fluidised-bed gasifier.

6.2 EXPERIMENTAL RESULTS

6.2.1 PROPANE PYROLYSIS

It has been well documented that the initial stages of hydrocarbon oxidation is the thermal cracking of parent fuel molecule to lower molecular weight hydrocarbons (Dagaut et al. 1987; Jess, 1996; Fristrom and Westenberg, 1965). As this study is primarily concerned with homogeneous decomposition and combustion of volatiles under gasification conditions, detailed analysis of propane pyrolysis solely under inert conditions will not be conducted here. Further details on the effect of various operating parameters on the thermal decomposition of propane under nitrogen conditions can be sought from van der Vaart (1985). The only experiment conducted based on a technical consideration was to compare propane decomposition under inert and reducing environments.

Figure 6.1 illustrates the in-bed concentration profiles of propane and intermediates produced at 750°C during the thermal pyrolysis of propane under nitrogen and nitrogen/steam conditions. Also included for comparison in Figure 6.1 is the data of van der Vaart for propane pyrolysis at 800°C in a bed of 250-425 μm quartz sand. No discernible difference within experimental deviation is observed between the two gas environments. Jess (1996) similarly reported that steam had little to no influence on reaction rates of primary products during thermal conversion of aromatic hydrocarbons. There is progressive decomposition of propane with distance from the distributor, with the co-current formation of lower molecular weight hydrocarbon species. However, and rather interestingly, van der Vaart (1985) observed that his system behaved as a perfectly mixed vessel. Accordingly, it was concluded that the decomposition reactions involved are slow relative to the gas mixing in the bed, with the residence time of the reactants to be the most important factor determining conversion. This observed uniformity of concentration is somewhat perplexing in comparison with the current work and thermal cracking data reported by Calkins et al. (1984), Doolan et al. (1983) and Hesp et al. (1970). As propane is expected to be ideally mixed with nitrogen, mixing limitations would only exist between bed phases.

As sampling technique measures both phases essentially indiscriminately, conclusions in this regard can not be made. While it is appreciated that gas residence times are relatively fast in fluidised-bed processes, in the order of approximately 0.5s necessitated by high fluidising velocities, to suggest reaction rates are of this time scale is dubious to say the least. If this were the case, then undoubtedly little conversion of propane would occur at all within the bed. Given van der Vaart's own reported work for propane conversion under combustion conditions, were yields of cracking products increased with bed height, it offers little credence to the observations and conclusions made by van der Vaart (1985) under pyrolysis conditions. As to how and what possible influences could have resulted in such observations is not evident.

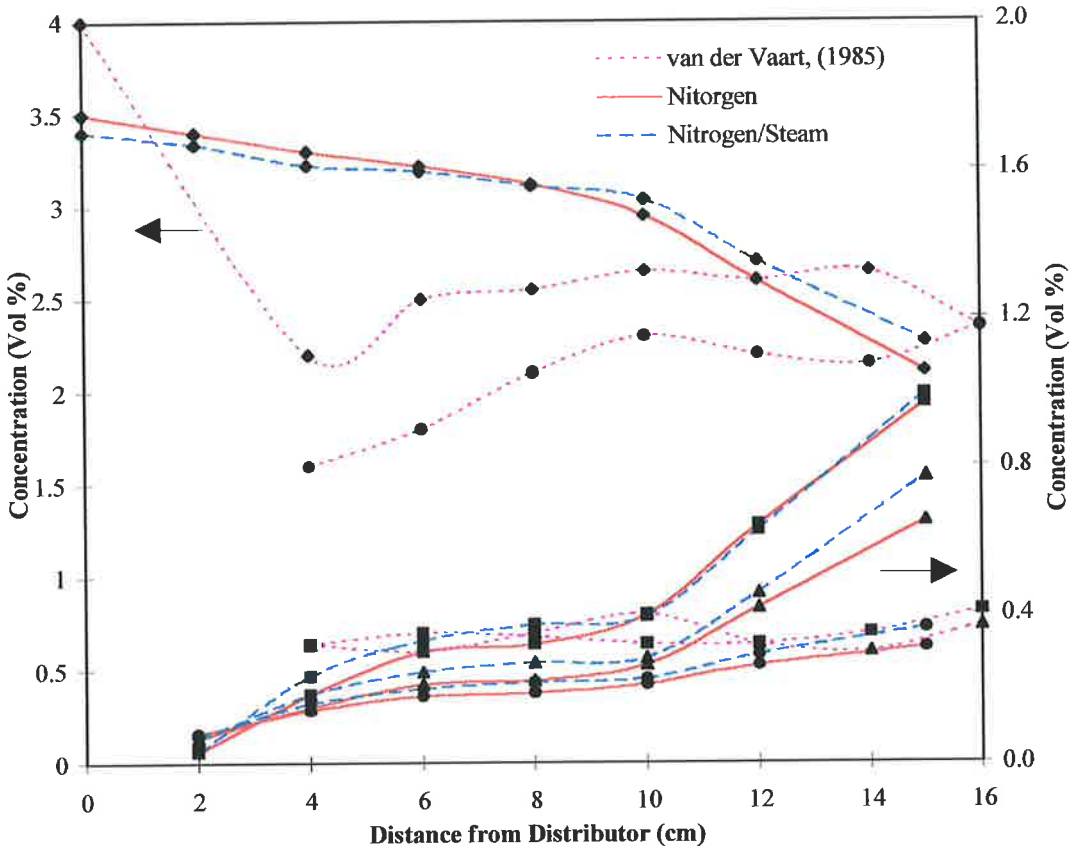

Figure 6.1 Comparison of in-bed axial gas concentration profiles during propane pyrolysis at 750°C under nitrogen and nitrogen/steam conditions for C_3H_8 (◆), C_2H_4 (▲), C_3H_6 (●), CH_4 (■). For comparison, the data of van der Vaart (1985) for propane pyrolysis at a bed temperature of 800°C; sand size 250-425 μm; bed height 14 cm and excess fluidising velocity of 25 cms^{-1} is also included.

Figure 6.2 illustrates the in-bed concentration profiles of propane and intermediates produced during thermal pyrolysis of propane for three bed temperatures of 750, 850 and 950°C under a nitrogen/steam environment. As clearly shown in Figure 6.2, there is progressive decomposition of propane with distance from the distributor, which increases significantly with increasing bed temperature. The major products formed of similar amounts are ethylene and methane intermediates for all three bed temperatures. Van der Vaart (1985) made a similar observation for proportional methane and ethylene yields during pyrolysis of propane at 800°C. However, van der Vaart (1985) observed that the major intermediate product formed was propylene unlike the current work. As to why such a disparity exists between the two results is not known. As reviewed in Section 2.6.2, an investigation into the secondary decomposition reactions of volatile matter using a two stage system, Calkins et al. (1984) found that the dominant product for the gas phase secondary cracking reactions of coal tar was ethylene, with a maximum yield occurring at 950°C. The maximum propylene yield occurred at 800°C, at one quarter of the maximum ethylene yield. Calkins et al. (1984) also observed that at temperatures above 800°C, a substantial proportion of the hydrocarbon gas cracks to produce acetylene. A similar trend at the higher bed temperatures of 850 and 950°C in the formation of acetylene is observed in the current study. Similar observations were made by Doolan et al. (1983) during the pyrolysis of n-octane. In all cases presented in this study, a negligible amount of ethane is detected and no further reference shall be made. This observation is also consistent with that of van der Vaart (1985, 1988). It was also observed during operation that significant quantities of carbonaceous residue (soot) could be seen lining the wall of the secondary glass condenser and dissolved in collected condensate. Hesp et al. (1970) reported that over 50% of the tar entering their cracking reactor at 1000°C resulted in the formation or deposition of carbon or soot. While the significantly longer gas residence times and the packing of the reactor with coke undoubtedly influenced the high conversions observed by Hesp et al. (1970), it does highlight an important reaction pathway for propane decomposition. It is pertinent to note in particular for fuel gas production, that the formation of soot and possible survival of higher hydrocarbons is to be avoided, as this leads to gas turbine damage (Jess, 1996).

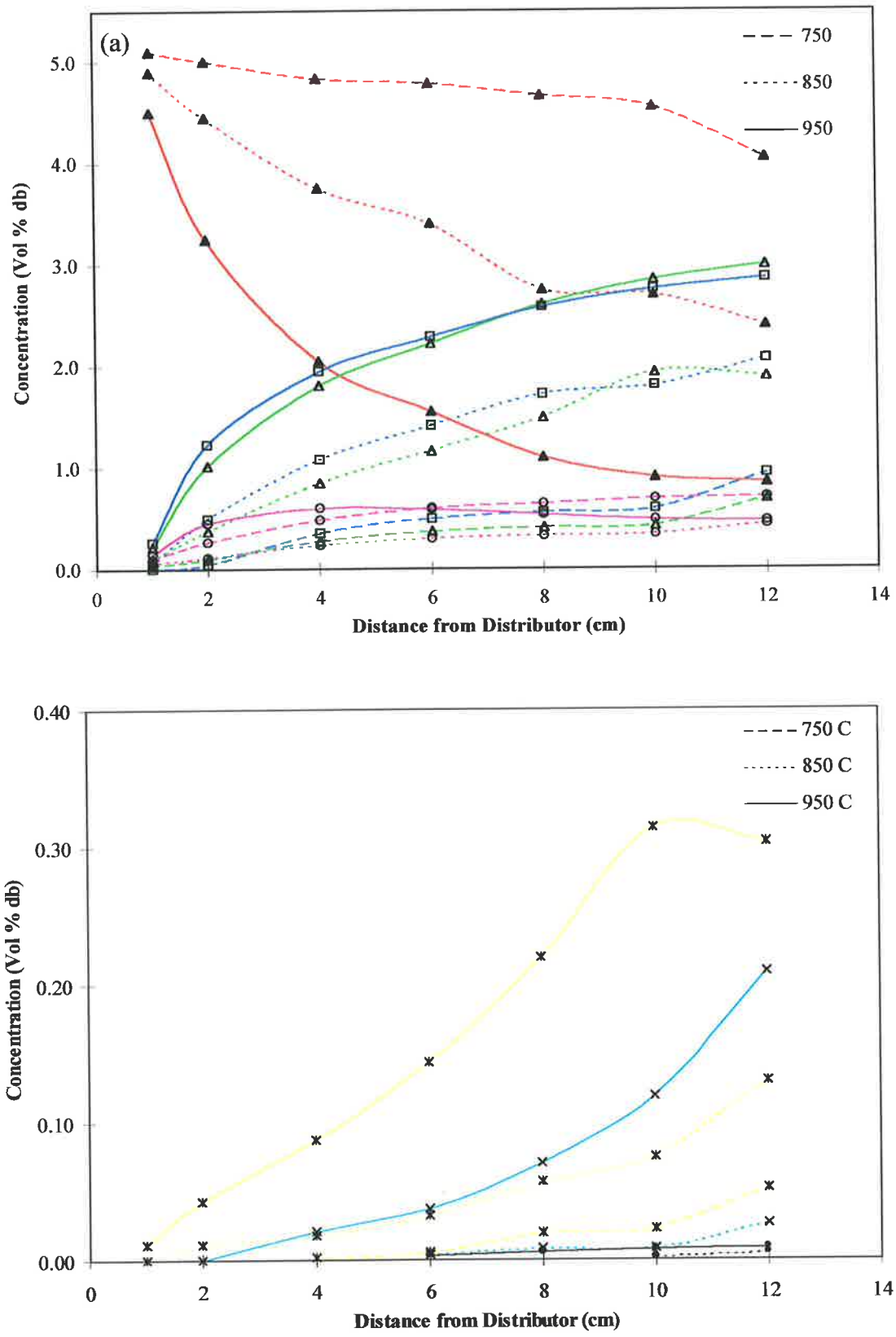

Figure 6.2 In-bed axial gas concentration profiles during propane pyrolysis at 750, 850 and 950°C (a) C_3H_8 (▲), CH_4 (□), C_2H_4 (Δ), C_3H_6 (O) (major species); (b) C_2H_2 (×), CO (*), CO_2 (●) (minor species).

At the higher bed temperatures of 850 and 950°C, the formation of carbon oxides are evident. Carbon monoxide is produced in greater quantities and formed earlier than carbon dioxide. Thus, a series of reaction scheme is apparent, consistent with experimental findings of Jess (1996).

- Primary cracking reactions lead to the formation of lower C-chain hydrocarbons.
- Condensation reactions result in the formation of soot and condensable products.
- Carbon monoxide formation occurs by consecutive reaction of soot and hydrocarbons with steam.
- Consecutive reaction of carbon monoxide with steam to produce carbon dioxide and hydrogen (ie. water-gas shift reaction).

6.2.2 PROPANE GASIFICATION

Figures 6.3 (a) and 6.3 (b) show the effect of bed temperature on the in-bed concentration profiles during the combustion of propane in an air/steam environment. These results show a very good agreement to those of Hesketh et al. (1991) and van der Vaart (1985, 1988) for propane combustion under FBC conditions. At the lower bed temperature of 750°C, what little propane that converts before the bed surface cracks to form hydrocarbon intermediates. This is consistent with observations for pyrolysis conditions and findings reported in the literature (Hesketh et al., 1991; van der Vaart, 1985, 1988). As observed by van der Vaart (1985, 1988), the maximum concentration of intermediates occurs at the same position in the bed for a given temperature. Again, methane and ethylene are the major products with propylene and acetylene (at the higher bed temperatures) being the minor products. These results are consistent to that found by Hesketh et al. (1991), however, disagrees yet again with van der Vaart (1985, 1988) who found propylene to be the major intermediate product formed. The rapid conversion of oxygen and formation of carbon dioxide at the bed surface is consistent with reported violent explosive nature of gas combustion at low bed temperatures under FBC conditions (Hesketh et al., 1991; Hayhurst et al., 1991; van der Vaart, 1985, 1988, 1992, Dennis et al., 1982; Schluter et al. 1997).

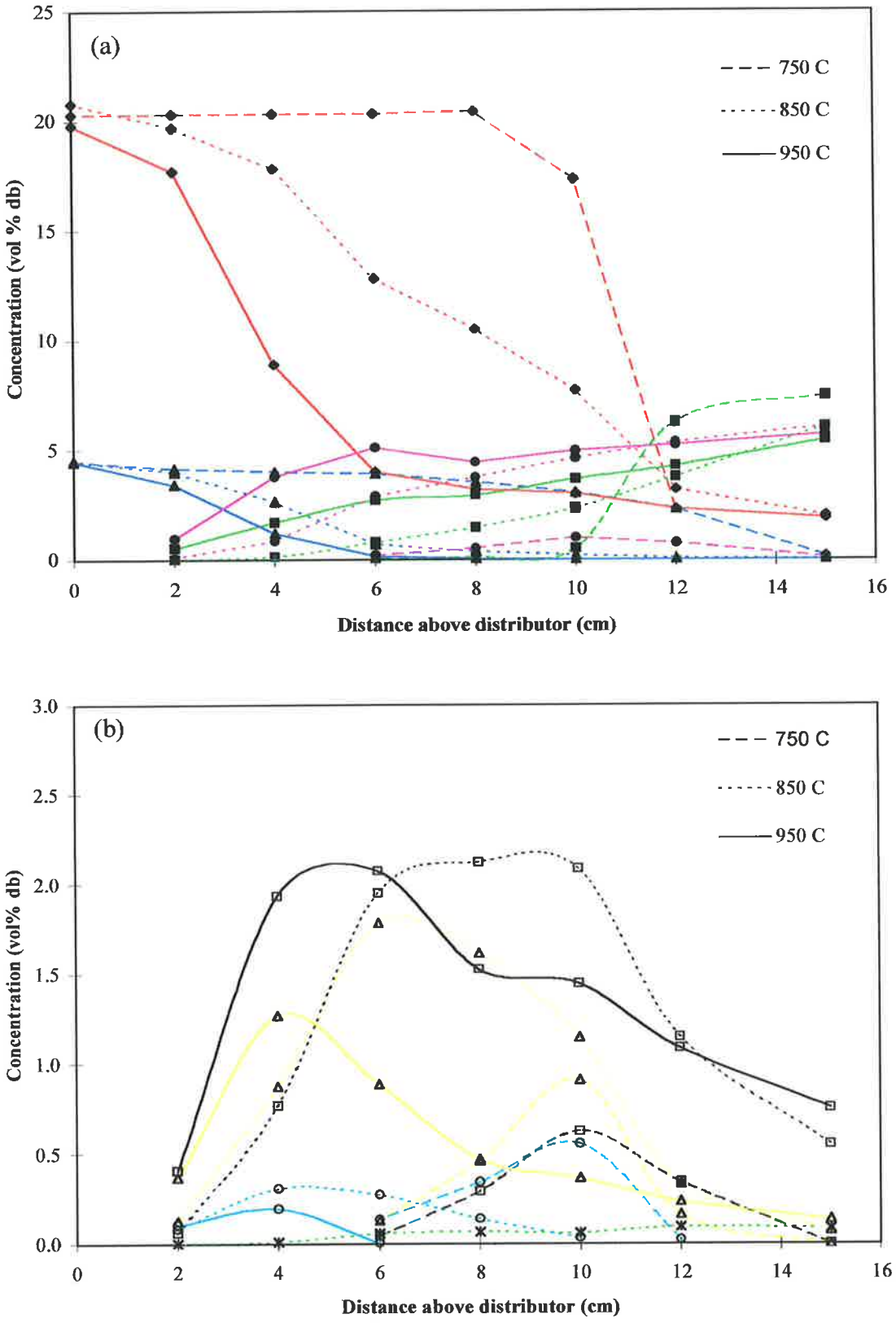

Figure 6.3. In-bed axial gas concentration profiles during propane gasification at 750, 850 and 950°C. (a) O_2 (◆), C_3H_8 (▲), CO (●), CO_2 (■), (major species) (b) CH_4 (□), C_2H_4 (Δ), C_3H_6 (O), C_2H_2 (×) (minor species).

As the bed temperature increases successively to 850 and 950°C, increasing gradual conversion to carbon oxides over entire bed height is observed, with carbon monoxide surviving well into the freeboard. This is consistent with bed operation above the so-called critical temperature reported in the literature (Hesketh et al., 1991; Hayhurst et al., 1991; van der Vaart, 1985, 1988, 1992, Dennis et al., 1982; Schluter et al. 1997). Van der Vaart (1985, 1988) and Hesketh et al. (1991) found relatively similar concentrations of carbon oxides leaving the bed surface, where carbon dioxide is the major product. The difference simply explained by the differing equivalence ratio used. A sub-stoichiometric propane/air mixture was used in the present study, consistent with a gasifying atmosphere, as compared to stoichiometric quantities for FBC conditions (van der Vaart, 1985, 1988; Hesketh et al., 1991). It is also evident that with increasing bed temperature, the formation of intermediates and carbon oxides is more rapid, with their peaks more diffuse and lower in the bed. Van der Vaart (1985) made a similar observation. This result is also consistent with experimental data for propane pyrolysis shown in Figure 6.2, where intermediates form lower down in the bed with increasing bed temperature. These results further confirm that high temperature hydrocarbon oxidation proceeds in a series reaction network as summarised by Fristrom and Westenberg (1965) (van der Vaart, 1985, 1988).

6.2.3 CHAR GASIFICATION

Figure 6.4 shows the in-bed axial concentration profiles during the gasification of Yallourn coal char. For all three bed temperatures, there is rapid consumption of oxygen within the bed, with all oxygen consumed well before bed surface. The increased oxygen consumption with temperature from 750 to 850°C is consistent with the combustion rate moving from a combined chemical kinetic/mass transfer controlled regime to external diffusion controlled combustion (Schluter et al. 1996, Ross et al., 1999). Above this temperature, combustion rates do not show any significant variation with temperature as char combustion depends on the mass transfer of oxygen to the surface of particles. This is observable in Figure 6.4 as signified by the similar trends for the oxygen profile at 850 and 950°C.

As the bed temperature increases from 750°C through 850°C to 950°C, there is a significant change in carbon monoxide concentration relative to carbon dioxide. The likely principal contributing reactions to influence these yield changes are of course char gasification and combustion reactions along with the water-gas shift reaction.

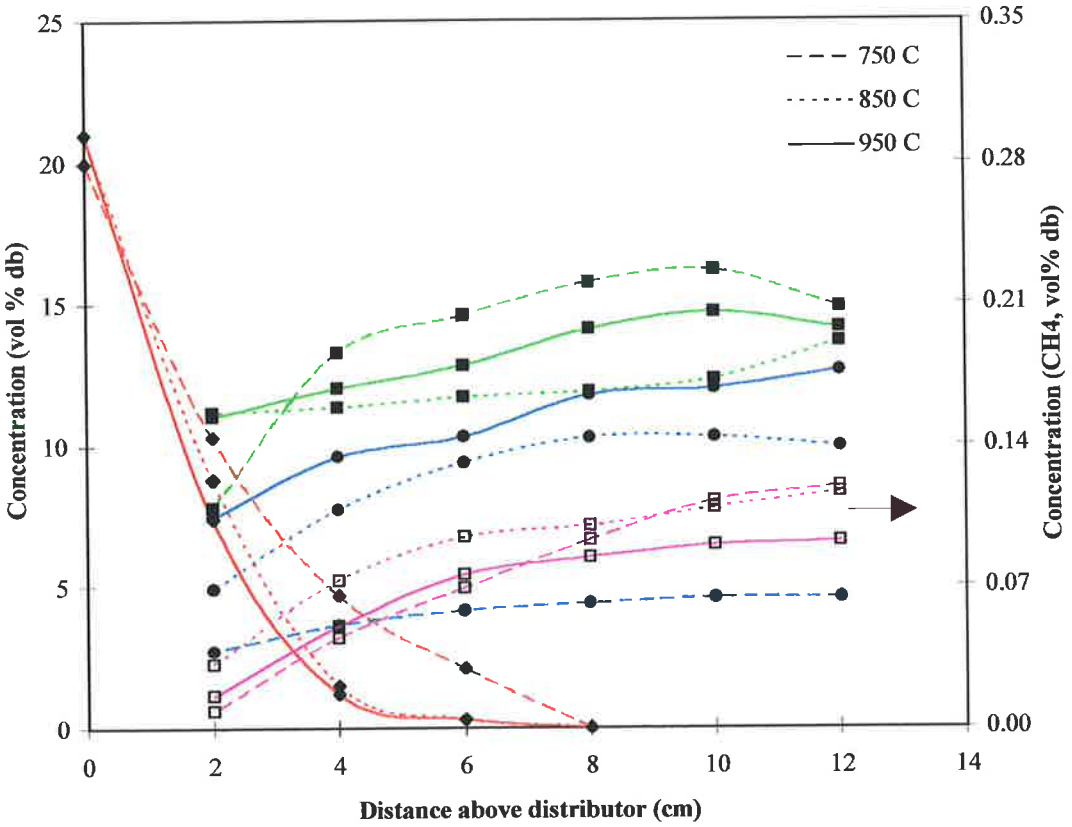

Figure 6.4 In-bed axial gas concentration profiles during char gasification at 750, 850 and 950°C for O_2 (◆), CO (●), CO_2 (■),CH_4 (□).

It is common knowledge that char combustion reaction rates are many orders of magnitude greater than char gasification reactions. Thus, it would be logical to expect that carbon conversion be dominated by char combustion reactions near the distributor plate. This is clearly demonstrated from the initial rapid consumption of oxygen within the bed. Kojima et al. (1993) and Matsukata et al. (1993) during on-line gas sample analysis of char gasification products have reported similar findings. As previously stated, combustion rates are not expected to change to any significant extent with temperature above 850°C.

Hence the change in composition in carbon oxide concentrations, is not a result of any significant changes in carbon conversion due to combustion reactions. Fluidised-bed gasification modelling work conducted by Yan et al. (1998b, 1999) supports this conclusion. It is well recognised that the combustion product distribution coefficient, ϕ, in the char partial combustion reaction (Equation 6.1) depends on many factors including particle temperature and size, coal rank, oxygen concentration and mineral impurities (Arthur, 1950; La Nauze et al. 1982; Ross et al. 1981; Schluter et al 1995,1996).

$$C + \phi O_2 \Rightarrow 2(1-\phi)CO + (2\phi-1)CO_2 \qquad ....6.1$$

Schluter et al. (1996, 1995) observed for combustion of a lignite char in an incipiently fluidised-bed combustor, that the CO/CO_2 product ratio increased with temperature and was expressed in Arrhenius form as,

$$CO/CO_2 = 52.6\exp(-3891/T) \qquad ....6.2$$

To date, no experimental data for the combustion product distribution coefficient under gasification environment exists in the literature. From modelling simulations, Yan et al. (1998) concluded values for the parameter ϕ lie in the range of between 0.75 to 0.85 if and only if homogeneous combustion reactions are included. Kojima et al. (1993) calculated a parameter value of 0.7 based on curve fitting the data of Matsukata et al. (1993) which agrees well with conclusions of Yan et al. (1998). Kojima et al. (1993) reported that carbon monoxide predominantly forms over carbon dioxide at higher bed temperatures in the combustion region. Furthermore, Kojima et al. (1993) reported at operating temperatures of 1173 and 1273 K, carbon dioxide profiles in the combustion zone were similar.

A similar observation is seen in the current work for carbon dioxide concentrations at 1123 and 1223 K in the combustion zone of the bed region. Unfortunately, it is somewhat more difficult to ascertain the relative contribution of char gasification and water-gas shift reactions to product yields without hydrogen concentration profiles. It is well known that steam gasification reactions are endothermic. Thus, thermodynamically higher temperatures favour these reactions.

As such, only a comparison with predicted concentration profiles reported by Yan et al. (1998b) could be used to help clarify the relative contribution of char gasification reactions. Recent modelling by Yan et al. (1998b) showed that many previous modelling studies that compared the predicted carbon conversion due to devolatilisation, char combustion and gasification, were significantly influenced by the non inclusion of homogeneous combustion reactions, which compete for available oxygen in the modelling reaction scheme. A very active zone exists near the distributor where both char combustion and homogeneous gas combustion dominate all reaction processes. This reaction zone decreases rapidly upon moving further above the distributor, where the combustion rate is limited by oxygen transfer from the bubble to emulsion phase. Correspondingly, carbon dioxide concentration rises initially very rapidly but then tapers off, with water-gas shift reaction being the main source of formation. Above this zone, the model predicts a rapid initial formation of carbon monoxide and hydrogen due to char gasification reactions, followed by a much slower rate with further increase in bed height. Gas compositions become invariant in the upper bed region, indicating gas phase reactions are approaching equilibrium. This is observed experimentally, where there is a relatively slow increase in concentration for carbon oxide profiles in the upper half of the bed region. Methane production via hydrogen gasification of char is very similar for all three bed temperatures although very small in quantity. This is consistent with experimental data and model predictions reported in the literature for air/steam gasification of coal (Yan et al., 1998b; Neogi et al. 1986; Goyal et al. 1990).

6.2.4 PROPANE/CHAR GASIFICATION

Figures 6.5 (a) and 6.5 (b) illustrate the in-bed axial concentration profiles for a fluidised-bed coal gasifier as simulated by introduction of a synthetic volatile, propane, during the gasification of Yallourn coal char. For the lowest bed temperature studied, 750°C, the oxygen and carbon oxide concentration profiles are very similar to those in Figure 6.4 for char gasification only. This indicates the dominance of char combustion reactions over gasification reactions and negligible propane oxidation, which is consistent with observations for propane gasification in Figure 6.3 (a).

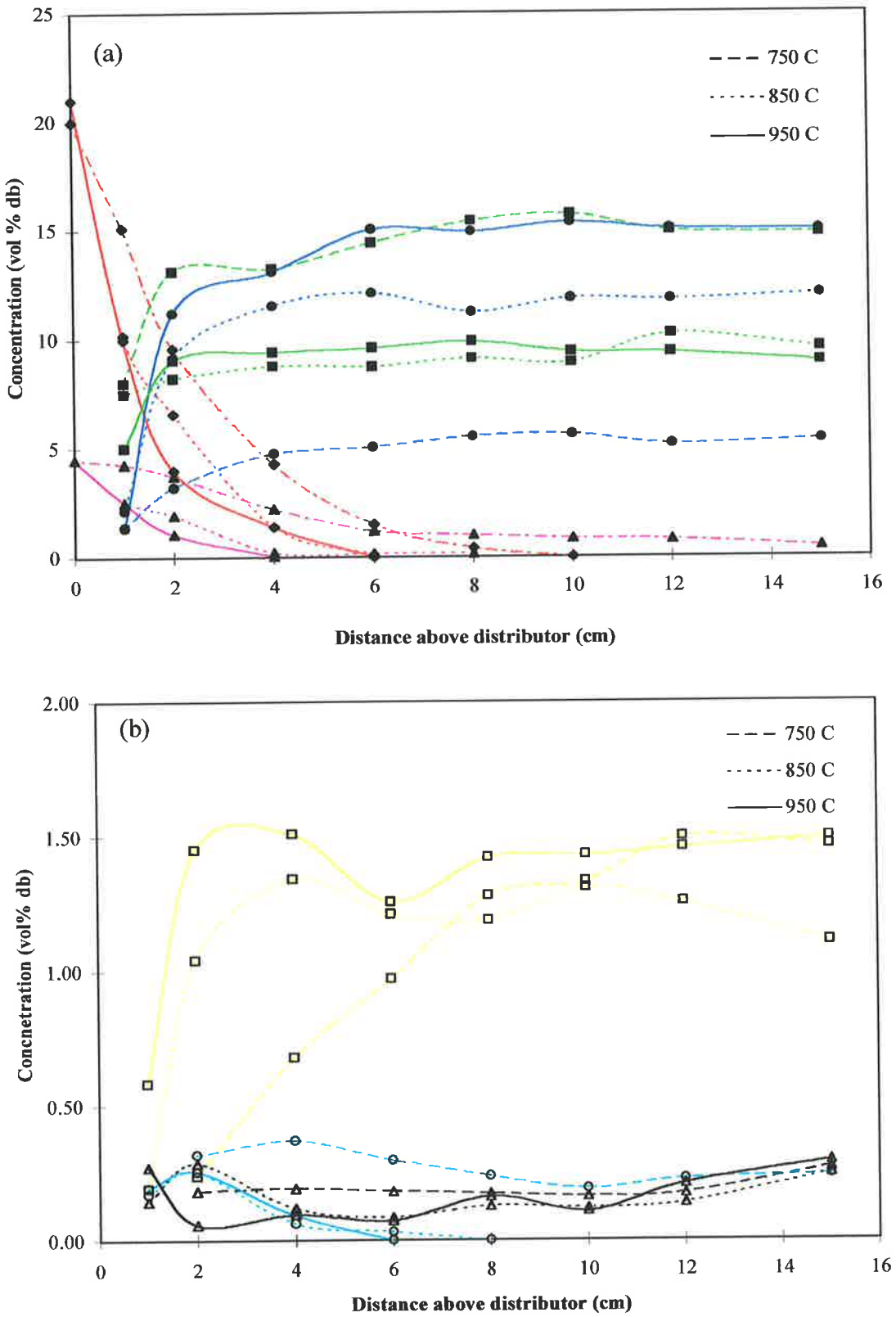

Figure 6.5 In-bed axial gas concentration profiles during propane/char gasification at 750, 850 and 950°C. (a) O_2 (◆), C_3H_8 (▲), CO (●), CO_2 (■), (major species) (b) CH_4 (□), C_2H_4 (Δ), C_3H_6 (O) (minor species).

However, propane decomposition with char feed appears to occur at a faster rate with no apparent concurrent increase in intermediate yields, when compared to a bed filled with sand only. Hesp et al. (1970) and Tyler (1980) observed a significant effect of bed material upon the yield of tar fractions during pyrolysis and thermal cracking experiments. They similarly observed minimal changes to the yields of light hydrocarbon gases. Interestingly, the apparent combination of the methane yield from propane pyrolysis and gasification experiments appears to yield less than for the propane/char gasification experiment. This is consistent with findings reported by Hesp et al. (1970), who found methane to predominate yield upon introduction of a low ash coke. However, such a conclusion is rudimentary. Although the data does indicate that introduction of char material may well act to provide active sites for the secondary decomposition via condensation reactions occurring within the pore structure and not via homogeneous thermal cracking reactions. Further research into this area is required.

The oxygen consumption rates at 850 and 950°C are more rapid than for corresponding case during the sole gasification of char. Obviously, this indicates that the fast homogeneous oxidation reactions of propane and intermediate precursors are competing for available oxygen with char. The resultant influence upon carbon monoxide concentration can be seen in the form of higher concentrations early in the bed and slightly higher overall concentrations exiting the bed as compared to char gasification profiles. In addition, for corresponding temperatures of 850 and 950°C, carbon monoxide concentrations are higher than carbon dioxide concentrations. This indicates that the rapid homogeneous partial oxidation of hydrocarbons depletes the oxygen concentration sufficiently that complete combustion to carbon dioxide is limited. In terms of coal gasification, this outcome is ideal. Furthermore, the amount of propane and other intermediates leaving the bed are not as high as expected due to the apparent enhancement of secondary decomposition reactions with the localised char environment of the bed. Minimisation of such constituents from gas make up is seen to be very beneficial (Jess, 1996).

6.3 SUMMARY

The axial gas concentration profiles in a laboratory scale fluidised-bed gasifier at three bed temperatures of 750, 850 and 950°C have been reported. Four experimental conditions were evaluated for each temperature, these being propane pyrolysis (nitrogen/steam), propane gasification, char gasification and propane/char gasification (all under air/steam environment). For all conditions, propane conversion whether via thermal cracking or oxidation reactions, increased with increasing bed height and temperature. For the lowest bed temperature of 750°C under propane gasification conditions, propane conversion is characterised by a sudden explosive reaction at the bed surface, consistent with the literature results under FBC conditions. As the bed temperature increases successively to 850 and 950°C, propane conversion occurs increasingly throughout the bed to carbon monoxide and carbon dioxide. Introduction of a char feed to simulate gasification environment results in the rapid consumption of oxygen by both heterogeneous and homogeneous reactions. At the lower bed temperature of 750°C, char combustion dominates over gasification reactions. As the bed temperature increases, gasification reactions play an increasing role. The associated carbon monoxide concentration increases, with final yield being correspondingly higher when compared to the sole gasification of char. Thus indicating the contribution of partial volatile combustion to carbon monoxide yields. The char bed enhanced secondary decomposition reactions of the volatiles, as previously observed in the literature.

CHAPTER 7

FBG MODEL DEVELOPMENT

7.1 INTRODUCTION

The literature review present in Chapter 2, along with the detailed chemical analysis of pre-mixed propane combustion under gasification conditions detailed in Chapter 6, have laid the foundation for the development of a comprehensive numerical model of gas combustion under fluidised-bed coal gasification conditions. The literature review has revealed that little emphasis has been placed on the incorporation of homogeneous gas reactions into the reaction scheme of fluidised-bed coal gasifier models. The importance of homogeneous reactions on model predictions has been highlighted by Yan et al. (1998, 1998b, 1999). Of particular importance being the competition with char for available oxygen and the resulting influence on the balance between gasification and combustion reactions on carbon conversion (Yan et al., 1998, 1988b). Simulation results have shown that about 26-41% of feed oxygen is consumed by homogeneous combustion reactions, the percentage of which increases with decreasing coal rank and increasing operating temperature (Yan et al., 1999b).

Furthermore, a fundamental deficiency of many models reported in the literature has been either the incorrect treatment or neglect of the 'net flow' concept (Yan et al., 1998b). The net flow concept is different from the excess gas flow concept defined by two-phase theory of fluidisation. It refers to the net generation of the number of moles of gas in the emulsion phase due to coal devolatilisation, homogeneous and heterogeneous reactions. In contrast, excess gas flow is purely a hydrodynamic concept that deals with the total gas flow, in excess of what is required to maintain minimum fluidisation state in emulsion phase that flows through the bubble phase (Yan et al., 1998b). The net flow contribution has been found to be significant, in the range of 71-87% relative to the feed gas rate. Such volume generation significantly alters fluidisation conditions in the bed and thus will alter reaction rates, mass transfer properties and ultimately predicted product gas compositions (Yan et al., 1998b).

The incorporation of both the net flow concept and a homogeneous combustion reaction scheme in an isothermal model developed by Yan et al. (1998b), lead to significant improvements in model predictions for pilot and commercial scale reactors. Particularly, the behaviour of homogeneous reactions on carbon conversion. However, the homogeneous combustion of gas in a fluidised-bed presents a dramatically different characteristic (van der Vaart, 1992). As has been highlighted in the literature review, the in-bed combustion of pre-mixed hydrocarbon mixtures does not take place below critical bed temperatures. It has been postulated that this is a result of either thermal inhibition or radical quenching reactions preventing ignition. Either way, the bubble phase presents a more favourable reaction volume for homogeneous combustion of various hydrocarbons than the emulsion phase, due to the high volume to surface area ratio and the small volumetric fraction of particles present there (van der Vaart, 1992). While homogeneous combustion has been found to occur in the emulsion phase, the principal flow of gas is through the bubble phase, which has been shown to account for up to 88% of the total product gas flow (Yan et al., 1999c). Thus, the non-isothermal behaviour of the bed resulting from homogeneous combustion reactions must be taken into account through the inclusion of an energy balance for the bubble phase (Srinivasan et al., 1998; van der Vaart, 1992). Therefore, the more recent model developed by Yan et al. (1999c), which extends previous isothermal model developments to consider the non-isothermal behaviour of gases and heat transfer mechanism in the fluidised-bed will be used as the basis for current model development.

Formulation of the fluidised-bed gasifier model has been described in detail elsewhere by Yan et al. (1998b, 1999, 1999b, 1999c), only the basic elements regarding bed hydrodynamics, mass transfer and heat transfer of the model framework are outlined for clarity. General model assumptions and reaction schemes are outlined, with specific changes in relation to pre-mixed propane combustion in an allothermal reactor from the basic non-isothermal model developed by Yan et al. (1999) highlighted. Transport and thermodynamic properties for propane and intermediate species not covered by Yan et al. (1999) are also given.

7.2 MODEL ASSUMPTIONS

A schematic diagram of a bubbling fluidised-bed char gasifier with pre-mixed propane-steam-air mixture in consideration is shown in Figure 7.1. Char is continuously fed into the reactor and reacts with oxygen and steam to produce synthetic fuel gases composed primarily of hydrogen and carbon monoxide and small amounts of methane. Chemically pure propane is used to simulate coal volatile matter that would be released during coal devolatilisation. Homogeneous gas decomposition and combustion reactions for propane and intermediates are included in reaction scheme. The gasifier operates at atmospheric pressure with an operating temperature between 1020-1220 K.

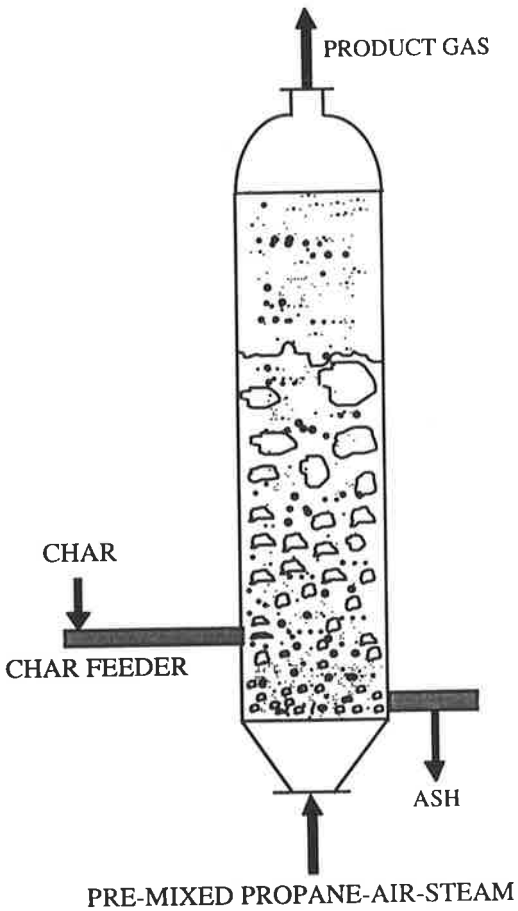

Figure 7.1 A schematic of a bubbling fluidised-bed char gasifier with pre-mixed propane-air-steam feed.

The model formulation is based on the assumptions detailed as follows.

1. The hydrodynamic behaviour of the fluidised-bed is described by the two-phase theory of fluidisation, that is, the emulsion phase is incipiently fluidised and all excess gases flow through the bed as bubbles (Davidson and Harrison, 1963).
2. The effect of the jetting region and its incorporation in to the hydrodynamic representation of the bed was not included.
3. The solid temperature is at steady state and uniform throughout the bed and is obtained by an overall energy balance around the bed.
4. The fluidised-bed consists of a dilute phase and an emulsion phase that can be further divided into an interstitial gas phase and a solid phase. All gases in both the bubble and emulsion phases are assumed to be in plug flow. The gas phase is free of solids, and solids are well mixed within the emulsion phase.
5. The fluidised-bed is one dimensional, with variations occurring only in the vertical direction.
6. The fluidisation state in the bed is maintained in the bubbling mode. The bubble size in the bed is a variable with respect to the bed height. Bubbles are uniform in size at any cross section of the bed but grow by coalescence with other bubbles and addition of the net flow gas as they rise through the bed (Yan et al. 1998b).
7. Mass transfer between particles and emulsion phase gas and between bubble and emulsion phases, are due to both molecular diffusion (driven by concentration differences) and convection (excess gas flow from the emulsion phase to the bubble phase).
8. Coal particles are spherical with a uniform size.
9. Ash particle size and density were assumed to be the same as inert bed media of silica sand used in experiments reported in Chapter 5. Particles are assumed to be spherical with a uniform size. However, ash catalytic properties on water-gas reaction in the emulsion phase were retained except if reaction is assumed to be in equilibrium where there is no catalytic effect.
10. The water-gas shift reaction in both the bubble and emulsion phases may be modelled by assuming the reaction in equilibrium or integrating a rate equation.

7.3 BED HYDRODYNAMICS

A schematic diagram of the two-phase representation of the model is given in Figure 7.2. The emulsion phase minimum fluidisation gas velocity (u_{mf}) is estimated by the correlation developed by Johnson (1979). The emulsion phase voidage and velocity are assumed to be constant. The bubble assemblage model developed by Mori and Wen (1975) is used to account for the growth and coalescence of bubbles above the distributor. According to two phase theory of fluidisation, the bubble size is essential for determining the heat and mass transfer between the two phases and thus the reaction rates in the fluidised-bed. Denis et al. (1982) has observed the importance of bubble size on the combustion rate of propane. The correlation developed by Batu et al. (1978) is used to determine the volume fraction occupied by bubbles, while correlations for bubble rising velocity and bed void fraction taken from Davidson and Harrison (1963) and Kunii and Levenspiel (1991) respectively. The interfacial mass transfer and heat transfer coefficients between the bubble and emulsion phase are estimated using the correlations developed by Sit et al. (1981) and (Kunii and Levenspiel, 1991) respectively. While the mass transfer and heat transfer coefficients between the emulsion gas and particles in fluidised-beds are estimated by the correlations from La Nauze and Jung (1982) and Ranz and Marshall (1952), respectively.

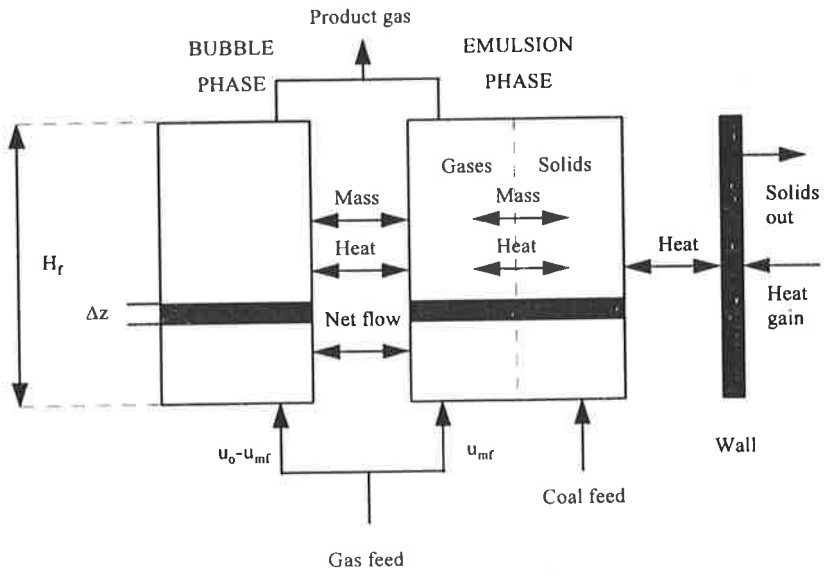

Figure 7.2 A schematic representation of the two-phase theory for a fluidised-bed.

7.4 REACTION SCHEME AND KINETICS

7.4.1 INTRODUCTION

As discussed in the Chapter 2, modelling gas combustion in a fluidised-bed has proven to be a very difficult task. This is compounded by the lack of specific data on high temperature oxidation of hydrocarbons present in the literature and the limited validation with experimental data, with certainly none in the application to a fluidised-bed (van der Vaart (1985). Modelling thus far has used both complex chemical kinetic mechanisms such as that proposed by Dagaut et al. (1987) by (Jeng et al., 1997) or the use of global reactions, such as that proposed by Kozlov (1959) and Hautman et al. (1981) by van der Vaart, (1992) and Srinivasan et al., (1998), respectively.

In keeping with model development of Yan et al. (1999c) and the opportunity provided by current experiments for comparison of a number of intermediates, the general reaction scheme of high temperature hydrocarbon oxidation proposed by van der Vaart (1985) will be used. Details of the overall reaction scheme will be shown, with discussion principally related to homogenous combustion reactions. Further details on the kinetic models used for heterogeneous reaction should be sought from Yan et al. (1998b, 1999)

7.4.2 REACTION SCHEME

It is assumed that the following chemical reactions take place in the gasifier:

Heterogeneous reactions in the emulsion phase:

(1) $C+\phi O_2 \rightarrow 2(1-\phi)CO + (2\phi-1)CO_2$

(2) $C + H_2O \leftrightarrow H_2 + CO$

(3) $C + 2\ H_2 \leftrightarrow CH_4$

(4) $C + 1/2\ H_2O + 1/2\ H_2 \leftrightarrow 1/2\ CO + 1/2\ CH_4$

(5) $C+CO_2 \rightarrow 2CO$

Homogeneous reactions in both bubble and emulsion phase:

(6) $CO + H_2O \leftrightarrow H_2 + CO_2$

(7) $H_2 + 1/2O_2 \rightarrow H_2O$

(8) $CO + 1/2O_2 \rightarrow CO_2$

(9) $CH_4 + 3/2O_2 \rightarrow CO + 2H_2O$

(10) $C_3H_8 \rightarrow C_3H_6 + H_2$

(11) $C_3H_8 \rightarrow C_2H_4 + CH_4$

(12) $C_3H_6 + 3O_2 \rightarrow 3CO + 3H_2O$

(13) $C_2H_4 + 2O_2 \rightarrow 2CO + 2H_2O$

In the above reactions, Reactions (1)-(5), (7)-(13) can result in a change of gas volume in the bed. Reactions (7)-(13) taking place in the bubble phase can only lead to volume change in this phase and do not contribute to net flow. For Reaction (6), two separate rate equations are used for the water-gas shift reaction in the bubble and emulsion phases, due to the catalytic effect of ash in the emulsion phase (Yan et al., 1998b). The model provides options of assuming reaction equilibrium or integrating a rate equation for the shift reaction in both the bubble and emulsion phases.

7.4.3 HETEROGENEOUS REACTIONS

The application of Reaction (1) to the oxygen lean conditions in the gasifier is uncertain, as no published data on the CO/CO_2 product ratio of char combustion is available in the literature under gasification conditions. Therefore the parameter, ϕ, in Reaction (1) is treated as an adjustable parameter, with the rate of Reaction (1) assumed to be under diffusion control and determined from the correlation proposed by LaNause and Jung (1982). The Johnson (1979) kinetic model is used to calculate rates of the gasification Reactions (2) to (4). It should be noted that Reactions (2) to (4) strictly speaking are not reversible, however they were assumed so by Johnson (1979) to account for the complex reacting environment involving the steam-hydrogen-methane reaction (Yan et al., 1998b). The carbon dioxide gasification rate was determined by the expression proposed by Ye et al. (1996).

7.4.4 HOMOGENEOUS REACTIONS

Rates of homogeneous combustion Reactions (7), (8) are calculated by correlations suggested by Haslam (1923), which were derived by considering simultaneous combustion of hydrogen and carbon monoxide. It has often been assumed that when calculating synthesis gas compositions during gasification processes, the water-gas shift reaction is in equilibrium and rate expressions do not have to be considered. However, this assumption is not always valid as has been shown by Yan et al. (1998b), where the incorporation of the water-gas shift reaction kinetics into the gasification model was necessary for good agreement with the experiment results. Modelling the shift reaction as either in equilibrium or driven by kinetics occurs with about an equal frequency of appearance in the literature (Yan et al., 1999). The model provides options of assuming reaction equilibrium or integrating a rate equation for the shift reaction in both the bubble and emulsion phases. Values of the equilibrium constants for the water-gas shift reaction is obtained by correlating the data given by Lowry (1963). The non-catalysed water-gas shift reaction rate is determined by the correlation developed by Karim and Mohindra (1974). While rate equations derived by Wen and Tseng (1979) which consider the catalytic effects of ash on Reaction (6) is used in the model.

7.4.4.1 Volatiles Combustion

Little emphasis has been placed on the incorporation of homogeneous gas reactions into the reaction scheme of fluidised-bed coal gasifier models. The importance of homogeneous reactions on model predictions has been highlighted by Yan et al. (1998, 1998b, 1999). However, even the work of Yan et al. (1998, 1998b, 1999) is a quasi representation of volatile release and combustion in a true gasifier. In these cases, devolatilisation was treated as being instantaneous and perfectly mixed with incoming fluidising gas stream. Furthermore, only CH_4, CO and H_2 homogeneous combustion reactions were considered. In order to represent the more complex decomposition and combustion behaviour of coal volatiles, propane was used to simulate coal volatile matter released during devolatilisation.

The choice of propane as a practical volatile substitute was based on its thermochemical and combustion properties resembling more those of complex fuels (coal volatile matter) than light hydrocarbons like methane and ethane (Dagaut et al. 1987). This is supported by the work of Mullins (1953), who observed that the ignition delay time for propane was approximately the same as compared to other C_4-C_{11} aliphatic hydrocarbons and aromatic hydrocarbons.

Unfortunately, very little is known about the relative kinetics of propane reactions for high temperatures and certainly none pertaining to fluidised-beds. In keeping with the general hierarchical scheme of high temperature hydrocarbon sequence by Fristrom and Westenberg (1965), Reactions (9) to (13) for propane decomposition and intermediates combustion were used, based on the proposed scheme by van der Vaart (1985). The choice of this scheme over that of Hautman et al. (1981) used by Srinivasan et al. (1998) was based on two reasons: (a) the possibility to account for more of the intermediates measured; and (b) the better agreement to experimental data shown by van der Vaart (1985). The kinetic parameters are shown in Table 7.1 (van der Vaart, 1985).

Table 7.1 Kinetic parameters for propane and intermediates (van der Vaart, 1985).

Reaction	Frequency Factor mol s^{-1}	Activation Energy KJ mol^{-1}
$CH_4 + 3/2O_2 \rightarrow CO + 2H_2O$	1.0×10^{12}	169.5
$C_3H_8 \rightarrow C_3H_6 + H_2$	1.0×10^{12}	171.6
$C_3H_8 \rightarrow C_2H_4 + CH_4$	1.0×10^{12}	175.8
$C_3H_6 + 3O_2 \rightarrow 3CO + 3H_2O$	1.0×10^{12}	173.3
$C_2H_4 + 2O_2 \rightarrow 2CO + 2H_2O$	1.0×10^{12}	173.3

The rate expressions used for Reactions (9) to (13) are then,

(9) $-d[CH_4]/dt = 1.0\times10^{12}[CH_4]\exp[-169500/RT]$

(10) $-d[C_3H_8]/dt = 1.0\times10^{12}[C_3H_8]\exp[-171600/RT]$

(11) $-d[C_3H_8]/dt = 1.0\times10^{12}[C_3H_8]\exp[-175800/RT]$

(12) $-d[C_2H_4]/dt = 1.0\times10^{12}[C_2H_4][O_2]\exp[-173300/RT]$

(13) $-d[C_3H_6]/dt = 1.0\times10^{12}[C_3H_6][O_2]\exp[-173300/RT]$

The kinetics used to describe the reaction scheme proposed by van der Vaart (1985) was a gross approximation. The activation energies were estimated based on reported data for overall propane combustion given by Bruno et al. (1983) and Longwell and Weiss (1955) obtained in a stirred tank reactor. The pre-exponential factor was assumed constant for all of the reactions at 1.0×10^{12} $mol^{-1}s^{-1}$. The Arrhenius-type reaction rate expressions were assumed as having either first or second order dependence on reactant concentrations depending on the number of different species involved. These simple expressions were used for both the bubble and emulsion phases, assuming any differences between the phases would arise from physical variations in the environment rather than chemical effects.

7.5 MASS BALANCE

The formulations of the mass balance for the fluidised-bed gasifier model has been described in detail elsewhere (Yan et al., 1998b, 1999). The mole balance for the reactor will be divided into two main parts, the gas and solids phase, as defined by the overall mass balance shown by equation 7.1.

$$F_{coal\ feed} + \left(\sum f_i\right)_{gas\ feed} = F_{char\ out} + \left(\sum f_i\right)_{gas\ products} \qquad ....7.1$$

7.5.1 BUBBLE PHASE

Conservation of mass in steady state for the control volume (Figure 7.2) in the bubble phase can be written as:

$$\underset{[Convection\ in]}{C_{Bi}\ A\ u_{Bi}|_z} \quad - \underset{[Convection\ out]}{C_{Bi}\ A\ u_B|_{z+\Delta z}} \quad + \underset{[Mass\ transfer\ between\ bubble\ and\ emulsion\ phase]}{k_{BE}\ a_B (C_{Ei} - C_{Bi})\ A\ \Delta z}$$

$$+ \underset{[net\ flow]}{\Delta F_{Eii}\ A\Delta z} + \underset{[Generation]}{\delta A\ \Delta z \sum_j^n \alpha_{ij}\ r_{Bj}} = 0 \qquad ....7.2$$

Dividing by Δz and taking the limit as Δz → 0, the differential mass conservation equation for the dilute phase is derived as:

$$\frac{d\,(C_{Bi}u_B)}{dz} = k_{BE}\,a_B(C_{Ei}-C_{Bi}) + \Delta F_{Ei} + \delta\sum_{j=1}^{n}\alpha_{ij}\,r_{Bj} \qquad \text{....7.3}$$

where $u_0 - u_{mf}(1-\delta) = u_B$

Boundary conditions are:

$$C_{Ei} = C_{Bi} = C_{if} \text{ at inlet when } z = 0 \qquad \text{....7.4}$$

7.5.2 EMULSION GAS PHASE

Conservation of mass in steady state for the control volume (Figure 7.2) in the emulsion phase can be written as:

$$C_{Ei}\,A\,u_{Ei}|_z \;-\; C_{Ei}\,A\,u_E|_{z+\Delta z} \;+\; k_{BE}\,a_B(C_{Bi}-C_{Ei})\,A\,\Delta z +$$

[Convection in] [Convection out] [Mass transfer between bubble and emulsion phase]

$$\Delta F_{Ei}\,A\Delta z + \delta A\,\Delta z\sum_{j}^{n}\alpha_{ij}\,r_{Dj} + \delta A\,\Delta z\left[\sum_{j=1}^{k_s}a_s\alpha_{ij}r_{Esj} + \sum_{j=1}^{k_g}\alpha_{ij}r_{Egj} + \sum_{j=1}^{k_v}\alpha_{ij}r_{Evj}\right] = 0 \qquad \text{....7.5}$$

[net flow] [homogeneous reactions] [Hertergeneous combustion, gasification develotilisation reactions]

Dividing by Δz and taking the limit as Δz → 0, the differential mass conservation equation for the emulsion phase is derived as:

$$\frac{d}{dz}(C_{Ei}u_{mf}(1-\delta)) = k_{BE}a_B(C_{Bi}-C_{Ei}) - \Delta F_{Ei}$$
$$+(1-\delta)\varepsilon_{mf}\sum_{j=1}^{k}\alpha_{ij}r_{Ej} + (1-\delta)(1-\varepsilon_{mf})\left[\sum_{j=1}^{k_s}a_s\alpha_{ij}r_{Esj} + \sum_{j=1}^{k_g}\alpha_{ij}r_{Egj} + \sum_{j=1}^{k_v}\alpha_{ij}r_{Evj}\right] \qquad \text{....7.6}$$

with boundary conditions:

$$C_{Bi} = C_{Ei} = C_{if}, \qquad \text{at } z = 0, \qquad \text{....7.7}$$

Considering the volume change along the axis, the above two governing Equations 7.3 and 7.6 are rewritten as a function of mole flow rate in each phase.

$$\frac{df_{Bi}}{dz} = A\left(k_{BE}\ a_B (C_{Ei} - C_{Bi}) + \Delta F_{Ei} + \delta \sum_{j=1}^{n} \alpha_{ij}\ r_{Bj} \right) \quad \text{....7.8}$$

$$\frac{df_{Ei}}{dz} = A\left(\begin{array}{l} k_{BE} a_B (C_{Bi} - C_{Ei}) - \Delta F_{Ei} + (1-\delta)\varepsilon_{mf} \sum_{j=1}^{k} \alpha_{ij} r_{Ej} \\ +(1-\delta)(1-\varepsilon_{mf}) \left[\sum_{j=1}^{k_s} a_s \alpha_{ij} r_{Esj} + \sum_{j=1}^{k_g} \alpha_{ij} r_{Egj} + \sum_{j=1}^{k_v} \alpha_{ij} r_{Evj} \right] \end{array} \right) \quad \text{....6.9}$$

7.5.3 NET FLOW GAS

Summation of bubble and emulsion phase mole balance for all gaseous species in Equations 7.8 and 7.9, the mass transfer and net flow terms are eliminated and accordingly yields:

$$\frac{d}{dz}\left(\sum_{i=1}^{N} f_{Bi} + \sum_{i=1}^{N} f_{Ei} \right) = \frac{d}{dz}(f_T) = A \sum_{i=1}^{N} \left(\delta \sum_{j=1}^{n} \alpha_{ij}\ r_{Bj} \right) + A(1-\delta) \sum_{i=1}^{N} \left(\varepsilon_{mf} \sum_{j=1}^{k} \alpha_{ij} r_{Ej} + (1-\varepsilon_{mf}) \left[\sum_{j=1}^{k_s} a_s \alpha_{ij} r_{Esj} + \sum_{j=1}^{k_g} \alpha_{ij} r_{Egj} + \sum_{j=1}^{k_v} \alpha_{ij} r_{Evj} \right] \right) \quad \text{....7.10}$$

where f_T total mole flow of species *i* of gases (mol s^{-1})

The LHS of Equation 7.10 indicates the change of the total mole flow of all gas species in each control volume along the bed height. The first term on the RHS represents the change in the number of moles of gaseous species in the dilute phase. This term does not contribute to the net flow, because it only occurs in the dilute phase, resulting in a gas volume change there. The second term refers to the generation of gas in the number of moles in the emulsion phase due to the heterogeneous combustion and gasification reactions and the devolatilisation reactions, ie. the net flow term. Introducing a symbol, ΔF_E, to represent this net flow term, the equation for calculating the total net flow of gaseous species is arrived:

$$\Delta F_E = \frac{d}{A_E dz}\left(\sum_{ii=1}^{N_E} f_{Ei}\right) = \sum_{i=1}^{N_E}\left(\begin{array}{l}(1-\delta)\varepsilon_{mf}\sum_{j=1}^{N_E}\alpha_{ij}r_{Ej} + (1-\delta)(1-\varepsilon_{mf})\times \\ \left[\sum_{j=1}^{N_s} a_s\alpha_{ij}r_{Ecj} + \sum_{j=1}^{N_g}\alpha_{ij}r_{Egj} + \sum_{j=1}^{N_v}\alpha_{ij}r_{Evj}\right]\end{array}\right) \quad ....7.11$$

The contribution of each individual species to the net flow is

$$\Delta F_{Ei} = \Delta F_E Y_{Ei} = \Delta F_E C_{Ei} \Big/ \sum_{i=1}^{N_E} C_{Ei} \quad ....7.12$$

Combining Equations 7.11 and 7.12, the equation for calculating the net flow of i^{th} gas species is obtained:

$$\Delta F_{Ei} = \frac{C_{Ei}}{\sum_{i=1}^{N} C_{Ei}} \sum_{i=1}^{N_E}\left[(1-\delta)\left(\begin{array}{l}\varepsilon_{mf}\sum_{j=1}^{N_E}\alpha_{ij}r_{Ej} + \\ (1-\varepsilon_{mf})\left[\sum_{j=1}^{N_c} a_s\alpha_{ij}r_{Ecj} + \sum_{j=1}^{N_g}\alpha_{ij}r_{Egj} + \sum_{j=1}^{N_v}\alpha_{ij}r_{Evj}\right]\end{array}\right)\right] \quad ....7.13$$

Equation 7.13 can be substituted into the mass conservation Equations 7.3 and 7.6 to close the mass balance of gas species in each control volume. Equation 7.13 shows that the net flow is not only due to gasification reactions, but also homogeneous reactions in the interstitial gas, volatiles released from coal and the heterogeneous combustion reactions in the emulsion phase. Thus, the net flow of i^{th} gas species in each control volume can be solved from Equation 7.13, while variations of the total gas molar flow generated in each control volume along the bed height can be calculated from Equation 7.10. Recognising the total molar rate, $f_T = u_0 A C_T$, Equation 7.10 can then be rearranged as:

$$\frac{du_0}{dz} = \frac{1}{AC_T}\sum_{i=1}^{N}\left(\sum_{i=1}^{N_D} f_{Bi} + \sum_{i=1}^{N_E} f_{Ei}\right) \quad ....7.14$$

where C_T is total molar concentration (mol m^{-3}).

Variations of the superficial velocities with an increase in the bed height can be determined by Equation 7.14. Thus, the excess gas flow defined by the two-phase theory can be expressed by:

$$\frac{du_{ex}}{dz} = \frac{du_0}{dz} - \frac{du_{mf}}{dz} \quad or \quad u_{ex} = u_0 - u_{mf} \qquad 7.15$$

The net flow and the excess gas flow are defined in Equations 7.13 and 7.15, respectively. The net flow is a function of reaction rates in the emulsion phase. The excess gas flow is a function of the net flow and increases with increasing bed height as a consequence of contribution of the net flow to the bubble phase along the bed height as illustrated in Figure 7.2.

7.6 ENERGY BALANCE

7.6.1 BUBBLE PHASE

Conservation of energy in steady state for the control volume (Figure 7.3) in the bubble phase can be written as:

$$\left\{\begin{matrix}Heat\ in\\ by\\ convection\end{matrix}\right\} - \left\{\begin{matrix}Heat\ out\\ by\\ Convection\end{matrix}\right\} + \left\{\begin{matrix}Heat\ in\ by\\ interface\\ heat\ transfer\end{matrix}\right\} + \left\{\begin{matrix}Heat\ in\ by\\ net\ flow\\ heat\ transfer\end{matrix}\right\} + \left\{\begin{matrix}Heat\\ generated\\ by\ reaction\end{matrix}\right\} = 0$$

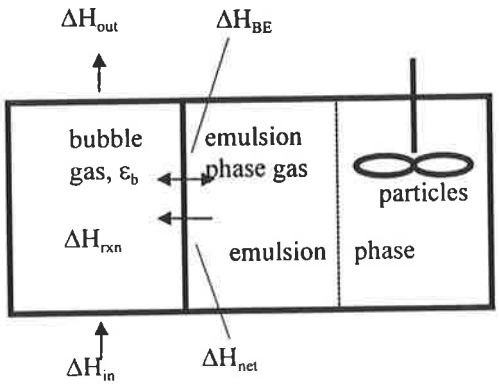

Figure 7.3 Energy balance for the bubble phase in a control volume.

The differential energy conservation equation for the bubble phase is derived as:

$$\frac{dT_B}{dz} = \frac{A\left\{\varepsilon_B h_{BE}\ (T_E - T_B) - \varepsilon_B \sum_{j=1}^{n} \Delta H^0_{Bj}\, r_{Bj} + \sum_{i=1}^{N} \Delta F_{Ei} \overline{C}_{pi} (T_E - T_R)\right\} - \left\{\sum_{i=1}^{N} \Delta H_{Bi} \frac{d f_{Bi}}{dz}\right\}}{\sum_{i=1}^{N} f_{Bi}(z)\left[\overline{C}_{pi} + (T_B - T_R)\frac{d(\overline{C}_{pi})}{dT_B}\right]} \quad \text{....7.16}$$

with boundary condition: $T_B = T_f$, at $z = 0$

Equation 7.16 is the governing conservation equation to predict the temperature of the bubble phase. This equation is the same as the one derived by Ma (1988) except an extra term considering the sensible heat due to the net flow.

7.6.2 EMULSION GAS PHASE

Conservation of energy in steady state for the control volume in the emulsion phase can be written as:

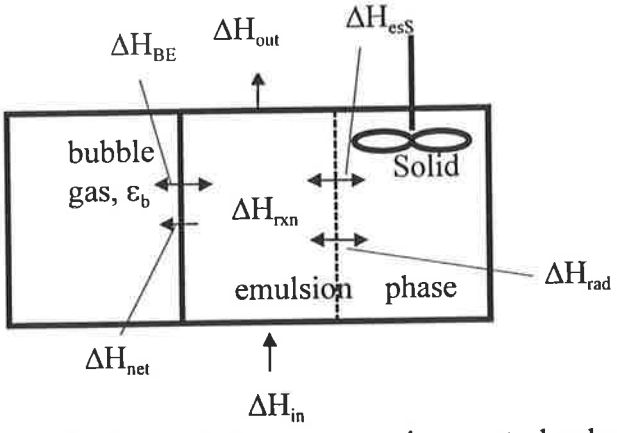

Figure 7.4 Energy balance for the emulsion phase gas in a control volume.

$$\left\{\begin{matrix}Heat\ in\\ by\\ convection\end{matrix}\right\} - \left\{\begin{matrix}Heat\ out\\ by\\ Convection\end{matrix}\right\} + \left\{\begin{matrix}Heat\ in\ by\\ int\,erface\\ heat\ transfer\end{matrix}\right\} + \left\{\begin{matrix}Heat\ in\ by\\ solids-gas\\ heat\ transfer\end{matrix}\right\} + \left\{\begin{matrix}Heat\ in\ by\\ radiation\\ heat\ transfer\end{matrix}\right\}$$
$$- \left\{\begin{matrix}Heat\ out\\ by\\ net\ flow\end{matrix}\right\} + \left\{\begin{matrix}Heat\ from\\ hom\,ogeneous\\ combustion\end{matrix}\right\} = 0$$

The differential energy conservation equation for the emulsion phase gas can be derived as:

$$\frac{dT_E}{dz} = \frac{term1 + term2 + term3 - term4 - term5 - \left\{\sum_{i=1}^{N} \overline{C}_{pi}(T_E - T_R)\frac{df_{Ei}}{dz}\right\}}{\sum_{i=1}^{N} f_{Ei}(z)\left[\overline{C}_{pi} + (T_E - T_R)\frac{d(\overline{C}_{pi})}{dT_E}\right]} \quad ....7.17$$

where

Term 1: Interface heat transfer: $A\,\varepsilon_B\,h_{BE}\,(T_B - T_E)$

Term 2: Heat transfer between gas and solids: $A(1-\varepsilon_B)(1-\varepsilon_{mf})\left\{(\alpha_s\,h_p(T_s - T_E)\right\}$

Term 3: Heat transfer by radiation $A(1-\varepsilon_B)(1-\varepsilon_{mf})\left\{\alpha_s e_E \sigma\left[(T_s)^4 - (T_E)^4\right]\right\}$

Term 4: Sensible heat carried by the net flow $A\,\Delta F_E \Delta H_E$

Term 5: Heat of reactions at 298 K, $A\,\varepsilon_{mf}(1-\varepsilon_B)\sum_{j=1}^{n}\Delta H_{Ej}^{0}\,r_{Ej}$

Equation 7.17 is also the same as the one derived by Ma et al. (1988) except for an extra term (term 4) which considers the sensible heat from emulsion phase to bubble phase due to the net flow.

7.6.3 SOLID PHASE

Since solids in the fluidised-bed gasifier are assumed to be perfectly mixed temperature of solids at steady state is uniform in the bed and is obtained by an energy balance for solid phase. The conservation of energy in steady state for the solid phase can be written as:

$$\left\{\begin{matrix}Heat\ in\\ by\ feed\ coal\\ particles\end{matrix}\right\} - \left\{\begin{matrix}Heat\ out\\ by\ discharged\\ particles\end{matrix}\right\} + \left\{\begin{matrix}Heat\ in\ by\\ gas-solids\\ heat\ transfer\end{matrix}\right\} + \left\{\begin{matrix}Heat\ in\\ by\ radiation\\ heat\ transfer\end{matrix}\right\}$$
$$- \left\{\begin{matrix}Reaction\ heat\\ of\ coal\\ devolatilisation\end{matrix}\right\} - \left\{\begin{matrix}Reaction\\ heat\ of\ coal\\ gasification\end{matrix}\right\} + \left\{\begin{matrix}Reaction\\ heat\ of\ coal\\ combustion\end{matrix}\right\} = 0$$

$$\sum_{j=1}^{k} f_{si,f} H_{si,f} - \sum_{j=1}^{k} f_{si,o} H_{si,o} + V_s\left\{\begin{bmatrix} h_p a_s (T_E - T_s) + a_s e_p \sigma (T_E^4 - T_s^4) + \\ \sum_{j=1}^{k_s} a_s \alpha_{ij} r_{Ecj}(\Delta H_{Ecj}) - \sum_{j=1}^{k_g} \alpha_{ij} r_{Egj}(\Delta H_{Egj}) \\ -\sum_{j=1}^{k_v} \alpha_{ij} r_{Evj}(\Delta H_{Evj}) \end{bmatrix}\right\} = 0 \quad ....7.18$$

However, Equation 7.18 is not easily solved since the heat of reaction of coal devolatilisation is not known.

7.6.4 Overall Energy Balance

The overall energy balance for a fluidised-bed is:

$$\begin{Bmatrix} Enthalpy \\ out\ by\ gases \end{Bmatrix} + \begin{Bmatrix} Enthalpy \\ out\ by\ solids \end{Bmatrix} + \begin{Bmatrix} Enthaly\ out \\ by\ heat\ loss \end{Bmatrix} = \begin{Bmatrix} Enthalpy \\ in\ by\ gases \end{Bmatrix} + \begin{Bmatrix} Enthalpy \\ in\ by\ coal \end{Bmatrix}$$

$$\sum_{i=1}^{n} f_{gi,o} H_{gi,o} + \sum_{j=1}^{k} f_{si,o} H_{si,o} + Q = \sum_{i=1}^{n} f_{gi,f} H_{gi,f} + \sum_{j=1}^{k} f_{si,f} H_{si,f} \qquad \text{....7.19}$$

The RHS of Equation 7.19 refers to the total feed energy entering the bed, where the first and second terms represent the energy carried by feed gaseous reactants and coal, respectively. The LHS of Equation 7.19 deals with total energy leaving the bed, where the first and second terms represent the energy carried by gas and solid products leaving the bed, respectively. The third term Q is the net heat loss from the fluidised-bed to surroundings, including heat loss from the fluidised-bed to the environment and radiant heat loss to the freeboard. The value of Q is a function of the fluidised-bed and ambient temperatures, types and structures of the reactor insulation, and the reactor dimensions. The heat parameter Q, is treated as an adjustable parameter and defined as a fraction of the total feed energy in the model.

However, for the current model simulation, net heat input to the fluidised-bed is assumed as experimental apparatus is operated allothermally ie, heat is supplied to the bed via electrical heating elements. Therefore, amount of fuel added to bed, in this case char is less than that if the bed was operated autothermally. If no such modification was made to model simulation, difficulty in obtaining convergence for non-isothermal model resulted. Typical values of Q as a percentage above the total feed energy entering the bed being in the range of 120 to 130%.

The deferential Equations 7.16 and 7.17 are the governing conservation equations, which predict the temperatures of the bubble and emulsion phases with respect to the bed height. These two equations are the same as the one derived by Ma et al. (1988) besides an extra term considering the sensible heat due to the net flow. However, Equation 7.18 for solid phase energy balance is not easily solved since heat of reaction of coal devolatilisation is not known in the literature. The overall energy balance around the bed is given by Equation 7.19. For the non-isothermal model, the differential Equations 7.16 and 7.7 for temperatures of the gases, and Equation 7.18 for the solid temperature need to be solved simultaneously.

7.7 TRANSPORT AND THERMODYNAMIC PROPERTIES

As mentioned in Section 2.7 of Chapter 2, a majority of models treat gas transport properties as constant values and ignore the effects of the operating temperature, pressure and gas concentration on these properties. This can have a significant effect on the model predictions Yan et al. (1999). The equations and correlations for calculating these properties as a function of operating temperature, pressure and gas concentration are reported for propane, ethylene and propylene. For further details of gas transport coefficients for other gas species refer to Yan et al. (1999).

7.7.1 GAS VISCOSITY

The polynomial equations for calculated pure component viscosities are based on the method of Chung et al. (1984), as with coefficients listed in Table 7.2.

$$\mu = 40.785 \frac{F_c (MT)^{1/2}}{V_c^{2/3} \Omega_v} \qquad \text{....7.20}$$

Viscosities of gas mixtures were estimated by Wilke's method (Wilke, 1950)

$$\mu_m = \sum_{i=1}^{N} \frac{y_i \mu_i}{\sum y_i \lambda_{ij}} \qquad \text{....7.21}$$

where

$$\lambda_{ij} = \frac{\left(1+(\mu_i/\mu_j)^{0.5}(M_{gj}/M_{gj})^{0.5}\right)^2}{[8(1+M_{gj}/M_{gj})]^{0.5}} \quad \text{....7.22}$$

$$\lambda_{iji} = \frac{(\mu_j M_{gj})}{\mu_i M_{gj}}\lambda_{iij} \quad \text{....7.23}$$

Table 7.2 The polynomial coefficients for calculating pure component viscosities and required critical properties based on the method of Chung et al. (1984), (μ=a+bT+cT^2+dT^3, μP).

	μ_r	F_c	Ω_v	ω	V_c	*a*	*b*	*c×10^4*	*d×10^8*
C_3H_8	0	0.958	1.01	0.153	203	49.23	0.1848	0	0
C_3H_6	0.204	0.96	1.01	0.144	181	52.75	0.1955	0	0
C_2H_4	0	0.975	0.95	0.089	130.4	5.838	0.3697	-1.298	2.72

	MW gmol^{-1}	T_b K	T_c K	P_c bar	Z_c	μ_{pi} debye
C_3H_8	44.09	231.1	369.8	42.5	0.281	0
C_3H_6	42.08	225.5	364.9	46	0.274	0.4
C_2H_4	28.05	169.3	282.4	50.4	0.28	0

7.7.2 Gas Diffusivity

Binary gas mixture diffusivity is calculated by the method of Brokaw (1969).

$$D_{ij} = 1.858*10^{-7}T^{1.5}\frac{(0.001(M_{gi}+M_{gJ})/(M_{gi}M_{gj}))^{0.5}}{p\sigma_{ij}^2\Omega_D} \quad \text{....7.24}$$

where

$$\sigma_{ij} = (\sigma_i\sigma_j)^{0.5} \quad \text{....7.25}$$

$$\sigma_i = \left(\frac{1..585V_{bi}}{1+1.3\delta_i^2}\right)^{1/3} \quad \text{....7.26}$$

$$\delta_i = 1.94 \times 10^3 \mu_{pi}^2 \quad \text{....7.27}$$

$$\delta_{ij} = (\delta_i \delta_j)^{0.5}$$

$$\Omega_D = \frac{1.06036}{T^{*0.1561}} + \frac{0.193}{\exp(0.47635T^*)} + \frac{1.03587}{\exp(1.52996T^*)} + \frac{1.76474}{\exp(3.89411T^*)} + \frac{0.19\delta_{ij}^2}{T^*} \quad 7.28$$

$$T^* = \frac{kT}{\varepsilon_{ij}} \quad \text{....7.29}$$

$$\frac{\varepsilon_{ij}}{k} = 1.18(1 + 1.3\delta_i^2)T_{bi} \quad \text{....7.30}$$

$$\frac{\varepsilon_{ij}}{k} = \left(\frac{\varepsilon_i}{k}\frac{\varepsilon_j}{k}\right)^{0.5} \quad \text{....7.31}$$

Assumptions of ideality and similar molecular weights are included in the method, although the polarities of gases are considered by inclusion of dipole moment.

Diffusivity of a multicomponent system is determined by the method recommended by Bird et al. (1960). The equation used is

$$\frac{1}{D_{mi}C} = \frac{\sum[(D_{ij}C)^{-1}(y_j n_i - y_i n_j)]}{n_i - y_i \sum n_j} \quad \text{....7.32}$$

7.7.3 Gas Mean Heat Capacity

The polynomial equations for calculating gas specific heat capacity as a function of temperature were taken from Reid et al (1988). The mean heat capacity of species *i* between T_0 and T is given by;

$$\overline{C}_{pi} = \frac{\int_{T_R}^{T} C_{pi} dT}{T - T_R} = \frac{a_i(T - T_R) + \frac{b_i}{2}(T^2 - T_R^2) + \frac{c_i}{3}(T^3 - T_R^3) + \frac{d_i}{4}(T^4 - T_R^4)}{T - T_R} \quad \text{....7.33}$$

where the coefficients of a, b, c and d are given in Table 7.3.

The heat capacity of a gas mixture is calculated as the molar weighted average of pure component heat capacities:

$$C_{pg} = \sum_{i-1}^{N} y_i C_{pi} \quad \text{....7.34}$$

The enthalpy change of ith component of gases from 298.15 K to T(K) is

$$\Delta \overline{H}_{gi} = \overline{C}_{pi}(T - T_R) \quad \text{....7.35}$$

The enthalpy of each species is given by

$$H_{gi} = H^0_{gi}(T_R) + \overline{H}_{gi} \quad \text{....7.36}$$

Table 7.3 Polynomial coefficients for calculating gas specific heat capacity ($y=a+bT+cT^2+dT^3$, J $mol^{-1}K^{-1}$)

	ΔH_f^0 J $g^{-1}mol^{-1}$	a_I	b_i	$c_i x10^4$	$d_i x10^8$
C_3H_8	-1.04×10^5	-4.224	0.3063	-1.59	3.22
C_3H_6	2.04×10^5	3.71	0.2345	-1.16	2.21
C_2H_4	5.23×10^4	3.806	0.1556	-0.835	1.76

7.7.4 Gas Thermal Conductivity

The polynomial equations for calculating pure component conductivity as a function of temperature were taken from Reid et al (1988).

Table 7.4 Polynomial correlation coefficients for calculating gas thermal conductivity ($k=a+bT+cT^2+dT^3$, W $m^{-1}K^{-1}$)

	a	*b*	*c*	*d*
C_3H_8	1.86×10^{-3}	-4.70×10^{-6}	2.18×10^{-7}	-8.41×10^{-11}
C_3H_6	-7.58×10^{-3}	6.10×10^{-5}	9.97×10^{-8}	-3.84×10^{-11}
C_2H_4	-3.17×10^{-2}	2.20×10^{-4}	-1.92×10^{-7}	1.66×10^{-10}

7.7.5 MEAN SPECIFIC HEAT CAPACITY OF COAL COMPONENTS

The mean specific heats of coal component with a reference temperature of 60°F were correlated by (IGT Coal Conversion Technical Data Book, 1978).

$$\bar{c}_f = 0.696 + 1.69x10^{-3}T - 1.17x10^{-6}T^2 + 3.2x10^{-10}T^3 \quad ....7.37$$

$$\bar{c}_{v1} = 1.68 + 1.69x10^{-3}T \quad ....7.38$$

$$\bar{c}_{v2} = 2..99 + 1.27x10^{-3}T \quad ....7.39$$

$$\bar{c}_a = 0.767 + 2.93x10^{-4}T \quad ....7.40$$

For the purpose of using a simple reference temperature, the above four equations were transformed according to:

$$c_{ps,k} = \frac{\bar{c}_k(T)(T-15.6) - \bar{c}_k(25)(25-15.6)}{T-25} \quad ....7.41$$

where c_{psk} is mean specific heat capacity of component k with a reference temperature 25°C ($Jkg^{-1}K^{-1}$). The calculated mean specific heat capacities were fitted to a linear equation as follows

$$\bar{c}_{ps,k} = a_k + b_k F_k(T) \quad ....7.42$$

Table 7.5 List of the coefficients for the correlation to calculate the heat capacity of coal products (IGT Coal Conversion Technical Data Book, 1978).

Component	$a_k \times 10^{-3}$	b_k	$F_k(T)$	*range (K)*
fixed carbon	-0.853	347.0	ln(T-273)	473-1366
primary volatile*	1.70	1.69	T-273	473-1366
secondary volatile*	3.00	1.27	T-273	473-1366
ash	0.77	0.293	T-273	473-1366

* Secondary volatile is volatile matter up to 10% by mass of the d.a.f. coal and primary volatile is volatile matter in excess of the secondary volatile.

7.8 NUMERICAL SOLUTION SCHEME

The solution algorithm of the model is briefly described as follows:

1. Initial values of the solid temperature T_s (outer loop) in the bed and total carbon conversion, X_c (inner loop) are assumed to be constant throughout the bed according to the assumption that the solids are perfectly mixed. Gas phase temperatures are calculated by governing Equations 6.1 and 6.2 in the non-isothermal simulations.
2. Ten gas species CO, CO_2, CH_4, H_2, H_2O, N_2, O_2, C_2H_4, C_3H_6 and C_3H_8 are considered in the reaction system. The stepwise calculation for solving a system of 20 differential equations for gas species, and for bubble and emulsion phase temperatures, respectively, starts from the bottom of the bed, at $z = 0$, where temperature and flow rates of feed gases are given.
3. The flow rates and temperatures calculated in the previous step are taken as inlet values to the current increment. Outlet values of these variables are assumed, and conditions in the increment are taken to be uniform at a point midway between the inlet and outlet values.
4. Quantities calculated include the minimum fluidisation velocity, superficial velocity, bubble diameter and rising velocity, volume fraction of bubbles, net flow, excess gas flow, rates of mass and heat transfer, rates of reactions and temperatures of emulsion and bubble phases. Mass and energy balances are then solved to obtain new outlet flow rates and temperatures for that control volume.
5. Convergence for a control volume is declared if the difference between successively determined values of each of the 20 variables is less than 0.5%. If convergence is not attained, new estimates of the variables are generated by the Predictor-Corrector method. Then, the newly determined product rates and temperatures are used in the kinelтic rate expressions to calculate new reaction rates, and convergence is again checked. The bubble and emulsion phase gas flow rates and temperatures are determined iteratively on the boundaries of each control volume until the surface of the bed is reached.

6. The fractional carbon conversion is calculated from the carbon flow rates in the coal feed, and both in the gases and in the solid materials leaving the reactor. The result is compared with the previously assumed value. If the estimate of carbon conversion fails to agree within 0.5%, a new estimate of X_c is again generated using the Wegstein method and the calculation steps 1 to 5 are repeated, until the convergence criteria (inner loop) are satisfied.
7. Following convergence of the solution for the total carbon conversion (inner loop) has been obtained at the estimated solid temperature. The new solid temperature is estimated in terms of the total energy leaving the bed. If the calculated value of the total energy leaving the bed, which is a function of the bed temperature, exceeds 0.5% of the total energy entering the bed, a new estimate of T_s is generated using the Wegstein method until the convergence criteria (outer loop) for the solid temperature are satisfied.

7.9 SIMULATION

The main model inputs in simulations are:

1. Char, propane, air and steam feed rates; and gas feed temperature.
2. The water-gas shift reaction type (either kinetic or equilibrium) in both phases.
3. Three standard adjustable parameters are normally incorporated into the gasifier model of Yan (1998). These are (i) the distribution coefficient, ϕ, for combustion products CO/CO_2 in the char partial combustion reaction; (ii) the coal gasification reactivity, f_0, a parameter defined in Johnson's gasification kinetics model and (iii) the heat parameter Q, defined in Equation 7.19.

For current model simulations only the heat parameter was altered. This parameter has by far the greatest influence over model predictions, as it is critical to the overall energy balance of the bed determining the operating temperature of the system through Equation 7.19 and hence, reaction rates and product concentration profiles. Yan (1999d) observed that for gasification model simulations that incorporate homogeneous combustion reactions, if the product distribution coefficient cannot be determined experimentally, a value of the parameter ϕ could be chosen arbitrarily between 0.75 and 0.85 in simulations with a negligible effect on the predictions of the fluidised-bed gasifier model. A summary of the bed operating conditions for the fluidised-bed gasifier is listed in Table 7.6. Input data for model simulation of the gasification of Yallourn coal char is summarised in Table 7.7 and similarly for propane/char gasification in Table 7.8.

Table 7.6 Operating conditions for gasifier model simulation runs.

Items	Units	Values
Operating pressure	atm	1.08
Char particle size	m	2.675×10^{-3}
Bed particle size	m	425×10^{-6}
Char density	kg m^{-3}	1070
Bed density	kg m^{-3}	2600
Orifice hole diameter	m	0.0004
Orifice number	-	140
Reactor diameter	m	0.102
Static bed height	m	0.10

Table 7.7 Model input parameters for fluidised-bed gasification of Yallourn char.

Parameter	Operating temperature (°C)		
	750	850	950
Char feed rate ($kghr^{-1}$)	0.29	0.29	0.29
Propane feed rate ($lmin^{-1}$)	0	0	0
Air feed rate ($lmin^{-1}$)	27.0	27.0	27.0
Steam feed rate ($kghr^{-1}$)	0.66	0.66	0.66
Gas feed temperature (°C)	250	250	250
W-G shift rxn: emulsion phase	kinetic	kinetic	kinetic
W-G shift rxn: bubble phase	kinetic	kinetic	kinetic
ϕ	0.8	0.8	0.8
f_o	1.0	1.0	1.0
Q (× total energy input)	1.36	1.32	1.26

Table 7.8 Input data for the base model simulations of fluidised-bed co-gasification of propane and Yallourn char.

Parameter	Operating temperature (°C)		
	750	850	950
Char feed rate ($kghr^{-1}$)	0.29	0.29	0.29
Propane feed rate ($lmin^{-1}$)	1.19	1.19	1.19
Air feed rate ($lmin^{-1}$)	27.0	27.0	27.0
Steam feed rate ($kghr^{-1}$)	0.60	0.60	0.60
Gas feed temperature (°C)	250	250	250
W-G shift rxn emulsion	kinetics	kinetics	kinetics
W-G shift rxn bubble	kinetics	kinetics	kinetics
k_o RXN (9) (10) (11)#	1×10^{10}	1×10^{10}	1×10^{10}
k_o RXN (12) (13)##	1×10^{11}	1×10^{11}	1×10^{11}
ϕ	0.8	0.8	0.8
f_o	1.0	1.0	1.0
Q (× total energy input)	1.30	1.23	1.14

Propane decomposition and methane combustion reactions
Ethylene and Propylene combustion reactions

7.9.1 HEAT PARAMETER

As can be observed from Tables 7.7 and 7.8, the heat parameter Q, decreases with increasing bed temperature and corresponding char gasification values greater than for co-gasification of propane and char. The decrease in the heat parameter with temperature for propane/char gasification is principally associated with the increase in heat released as a result of increasing homogeneous combustion within the bed. While for under char gasification conditions, the decrease in the heat parameter with temperature is associated with the increase in carbon conversion. The smaller difference between the heat parameter inputs between 750°C and 950°C under char gasification conditions results from the limited contribution by homogeneous combustion reactions, particularly in the bubble phase, to the overall energy balance.

CHAPTER 8

FBG MODEL RESULTS

8.1 INTRODUCTION

The experimental work detailed in Chapter 6 provides reference data on the in-bed axial gas concentration profiles for decomposition and combustion of a simulated volatile matter (propane) under conditions prevailing in a fluidised-bed gasifier. The importance of volatile matter combustion and its influence on carbon conversion was reviewed in Chapter 2. Little consideration has been given to devolatilisation and the subsequent homogeneous combustion of coal volatiles in system models developed to date for fluidised-bed gasification. Chapter 7 described the development of a non-isothermal fluidised-bed gasification model with a particular emphasis on gas combustion of pre-mixed propane. The importance of including a non-isothermal bubble phase in the prediction of in-bed concentration profiles in fluidised-bed combustion modelling of hydrocarbon gases has been well documented (van der Vaart, 1985, 1992; Srinivasan et al. 1998). The aims of this chapter are to:

1. Compare model predictions on the variation of O_2, CO, CO_2, C_3H_8, C_3H_6 and C_2H_4 concentrations with the bed height against experimental data detailed in Chapter 6, at bed temperatures of 750°C, 850°C and 950°C, for char and propane/char gasification.
2. Gain insight into individual reactions occurring within each phase of the bed, which is otherwise impossible to differentiate for current experimental technique.
3. Conduct a parametric study to investigate the influence of design parameters: excess operating velocity and bed particle size on propane combustion behaviour in a FBG.

The main motivation in this chapter, however, is to illustrate the interaction between heterogeneous and homogeneous combustion reactions in a fluidised-bed gasifier and show that by increasing the in-bed combustion efficiency of volatile matter, more char is available to undergo conversion by gasification reactions.

8.2 CHAR GASIFICATION

A comparison of model results (lines) with experimental data (symbols) of in-bed concentration profiles for CO, CO_2, O_2 and CH_4 during the fluidised-bed gasification of Yallourn char at 750°C, 850°C and 950°C is shown in Figures 8.1, 8.2 and 8.3, respectively. The model predictions for char gasification generally show average agreement with experimental data, improving with increasing bed temperature. The principal difference between the model predictions and experimental data is that for the O_2 profile, which obviously impacts upon the CO and CO_2 yields. Model consistently under predicts the O_2 consumption rate, with a significant proportion of the O_2 by-passing the bed unreacted via the bubble phase. An indication of this by-passing via the bubble phase is shown in Figures 8.4 and 8.8 (b), for the predicted bubble phase temperature and mole fraction profiles at 850°C, respectively. The disparity between model predictions and experimental data is due to the assumption of a constant value of 0.8 for the distribution coefficient, ϕ, for combustion products CO/CO_2 in the char partial combustion reaction scheme.

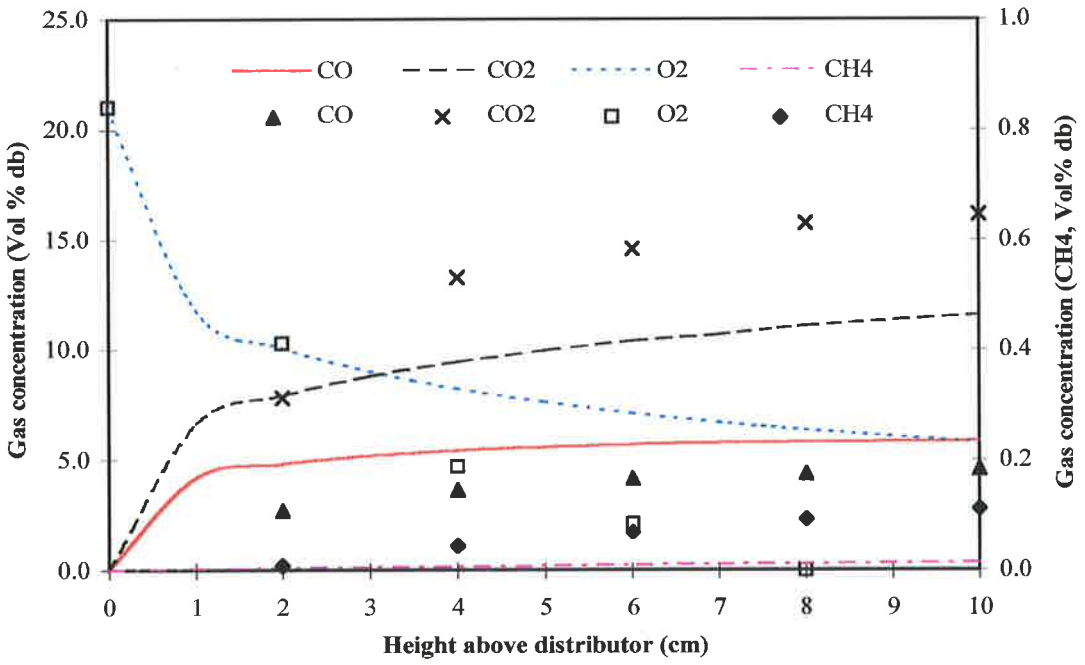

Figure 8.1 Comparison of model predictions (lines) with experimental data (symbols) for gasification of Yallourn char at 750°C.

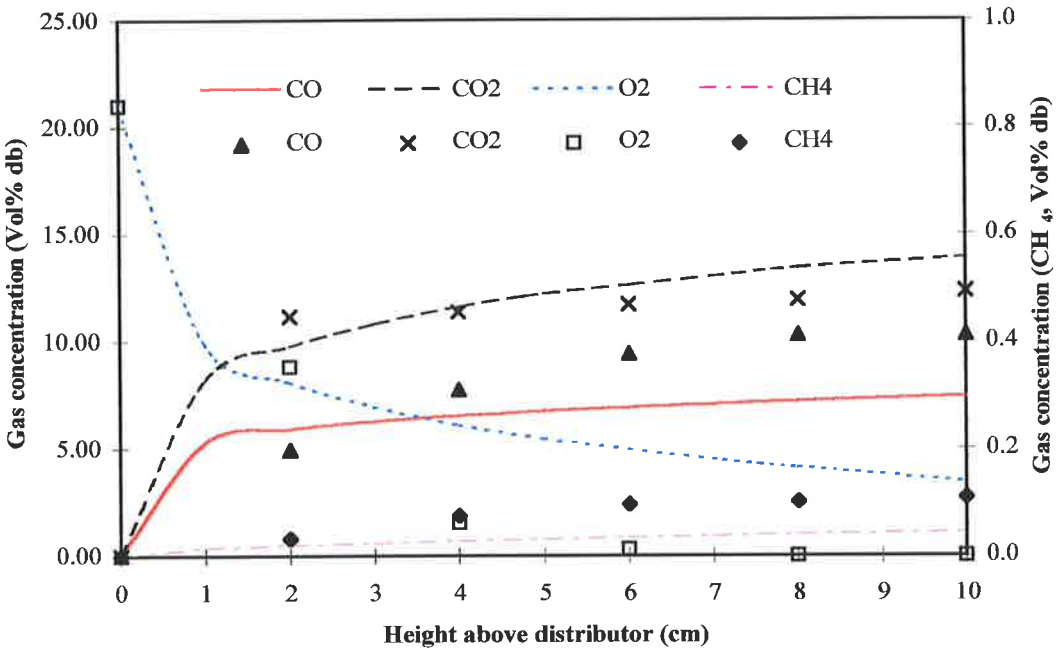

Figure 8.2 Comparison of model predictions (lines) with experimental data (symbols) for gasification of Yallourn char at 850°C.

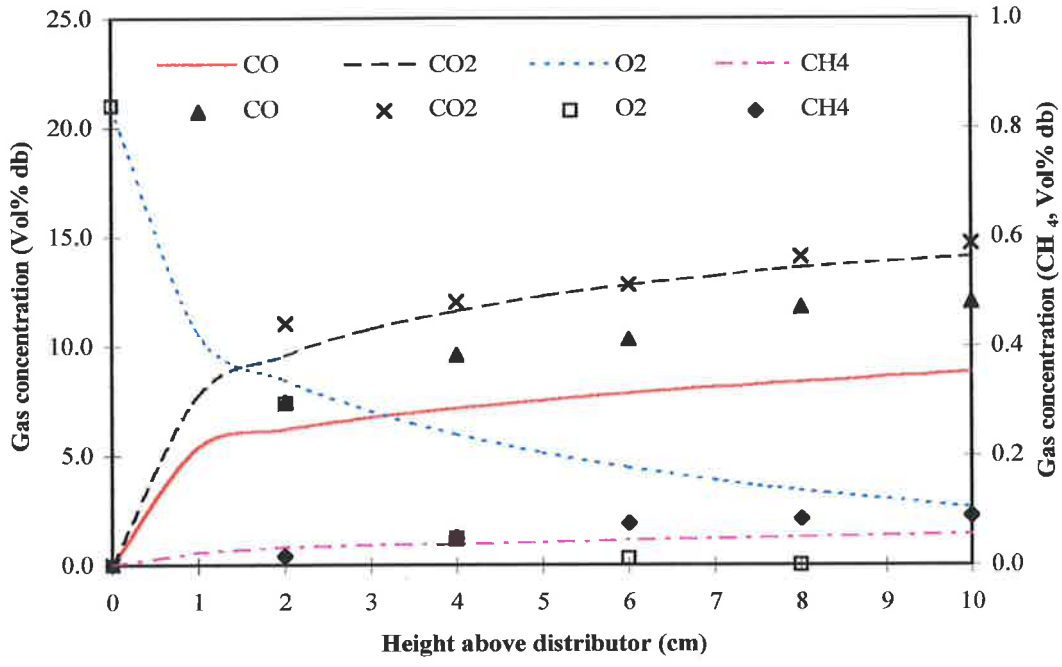

Figure 8.3 Comparison of model predictions (lines) with experimental data (symbols) for gasification of Yallourn char at 950°C.

In modelling fluidised-bed gasification, one of the uncertainties is how to determine the values of the product distribution coefficient ($0.5 \leq \phi \leq 1.0$).

$$C + \phi O_2 \Rightarrow 2(1-\phi)CO + (2\phi-1)CO_2$$

When ϕ equals unity, or 0.5, CO_2 or CO is the sole combustion product, respectively. The value for ϕ depends on many factors including particle temperature and size, coal rank, reactivity, O_2 concentration, and nature of mineral impurities in the coal (Schluter et al. 1996). This leads to uncertainties in the modelling of fluidised-bed gasification because the heat of reaction generated when CO_2 is the sole product is 1.8 times more than for the sole generation of CO. Apart from of course the gas product composition itself being different, a significant effect on the overall energy balance around the fluidised-bed will occur. This stems from the fact that the rates and thus the heat required by the endothermic char gasification reactions increase exponentially with increasing temperature. However, the heat generated from char combustion being diffusion controlled, is less sensitive to the temperature and mainly depends on the value for ϕ. The CO/CO_2 ratio, ϕ, was set at a constant value of 0.8 for all the model conditions presented in this thesis. This assumption was based on the work of Yan et al. (1998), where ϕ could be chosen between 0.75 and 0.85 for simulations incorporating homogeneous combustion. However, for simulations without homogeneous combustion, ϕ varies significantly with operating conditions, particularly with the bed temperature (Yan et al., 1998). Kulasekran et al. (1999) reported during parametric studies for a FBC model, that the CO/CO_2 ratio exerted a strong influence on the heterogeneous and homogeneous combustion dynamics.

Taking Figure 8.1 as an example, the model gives an outlet O_2 concentration of approximately 5%, while the experimental data has approached zero. Equally though, but in the opposite sense, the CO_2 concentration experimentally determined is approximately 5% higher than the model predictions. By increasing the CO/CO_2 ratio to unity, so that for every one mole of O_2 consumed, one mole of CO_2 is produced, the difference between the model predictions and experimental data would decrease. This in fact is consistent with the literature data published by Schluter et al. (1996) on

reported CO/CO_2 product distribution coefficients for a lignite, where CO_2 formation is favoured at lower temperatures. However stating this, it should be noted that it is not the intention of this section to be simply a curve fitting exercise for ϕ. The interest is in the gas-phase reactions and to show that by promoting in-bed combustion of volatiles, carbon conversion via gasification will increase. Thus, in order to ascertain the relative influence of volatiles on the gasification of char, given the uncertainties involved in the determination of ϕ and the conclusions of Yan et al. (1998), a value of 0.8 is to be utilised as the basis for the model simulations. Obviously, this will negatively impact upon the accuracy of the model under char gasification conditions. In order to confirm this point, ϕ was increased to 0.9, subsequently resulting in an improvement in the model predictions for O_2, CO_2 and CO for data collected at a bed temperature of 750°C, as shown in Figure 8.4,

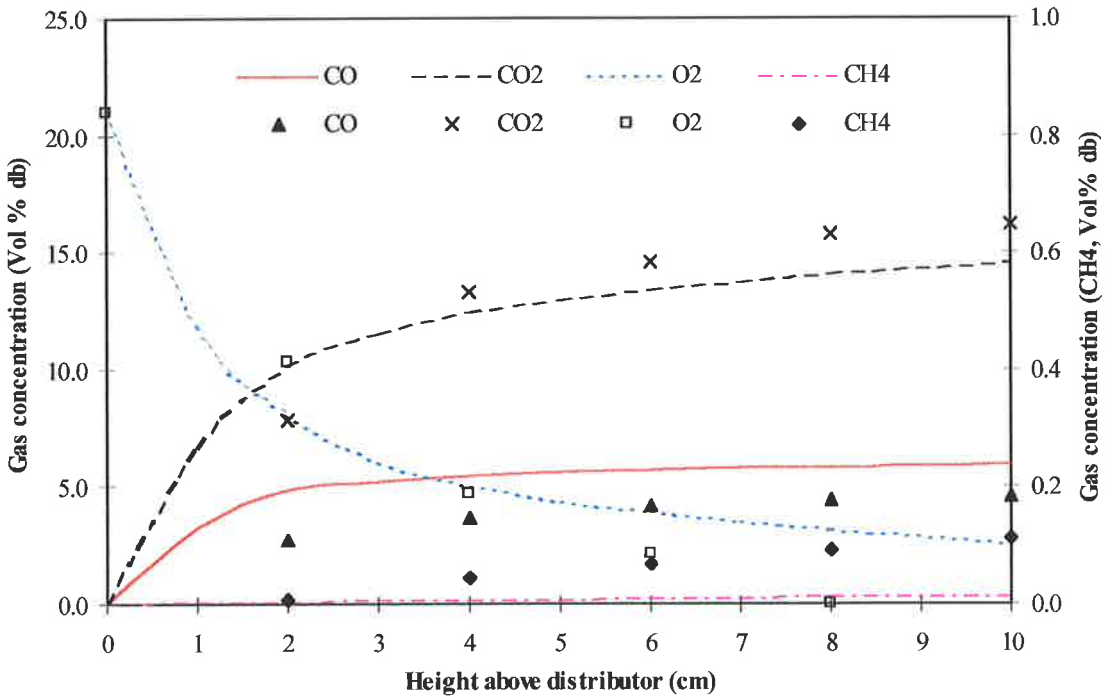

Figure 8.4 Comparison of model predictions (lines) with experimental data (symbols) for gasification of Yallourn char at 750°C with product distribution coefficient ϕ increased to 0.9.

Figure 8.5 shows the predicted temperature profiles for the solids, bubble and emulsion phase gas at 850°C during the gasification of Yallourn char. There is a relatively slow rise in the bubble gas temperature, with the bubbles leaving the bed significantly below the solids temperature. This large temperature difference is from the limited contribution of homogeneous combustion reactions in the bubble phase, resultant of

the fact that char is gasified in the system, where little to no volatile matter is released and the amount of CO and H_2 produced via gasification is very small, particularly at the lowest bed temperature. The primary heat source raising the bubble gas temperature is initially by the sensible heat carried by the net flow gas generated in the emulsion phase due to char combustion reactions and the inter-phase heat transfer between bubble and emulsion phase. As the concentration of CO, H_2, CH_4 and gas temperature in the bubble increase, homogeneous combustion plays an increasing role. However, as the bed depth is very shallow (0.10 m), the gas residence times are correspondingly very short and the predicted bubble phase temperature remains less than the solid temperature.

The extremely rapid increase in the emulsion phase gas to solids temperature after feed gas enters the bed occurs for two reasons. Firstly, the volume of emulsion phase gas typically accounts for only 10 to 15% of the total gas volume in the bed. Thus, the gas is easily heated up to the solids temperature by heat released by homogeneous and heterogeneous reactions in the emulsion phase. Secondly, higher heat transfer rates are encountered in the emulsion phase, principally from thermal radiation by the hot solids.

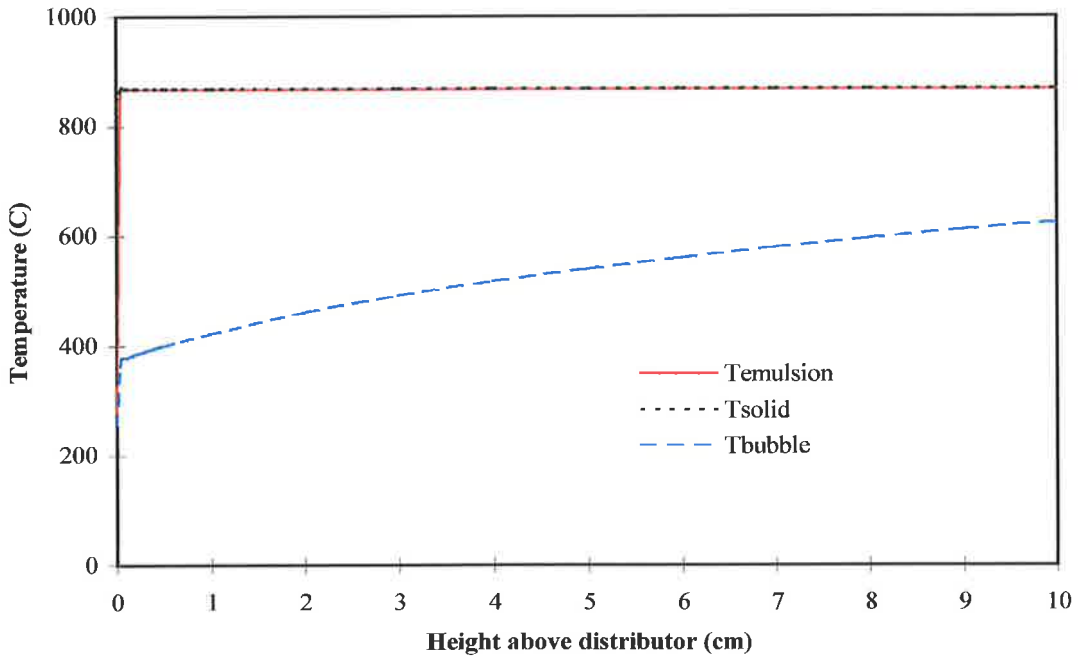

Figure 8.5 Model predictions of the bed temperature profile for solid, emulsion gas and bubble gas phases at 850°C, during the gasification of Yallourn char.

This trend for the bubble phase temperature is consistent for all three bed temperatures as shown in Figure 8.6. The difference between the final bubble temperature (at the bed surface) and solid temperature does decrease with increasing temperature. A clear explanation of this observation can be directed from Table 8.1, for the fraction of the oxygen consumed by char combustion over homogeneous combustion of CO, H_2 and CH_4 and the predicted carbon conversions due to combustion and gasification.

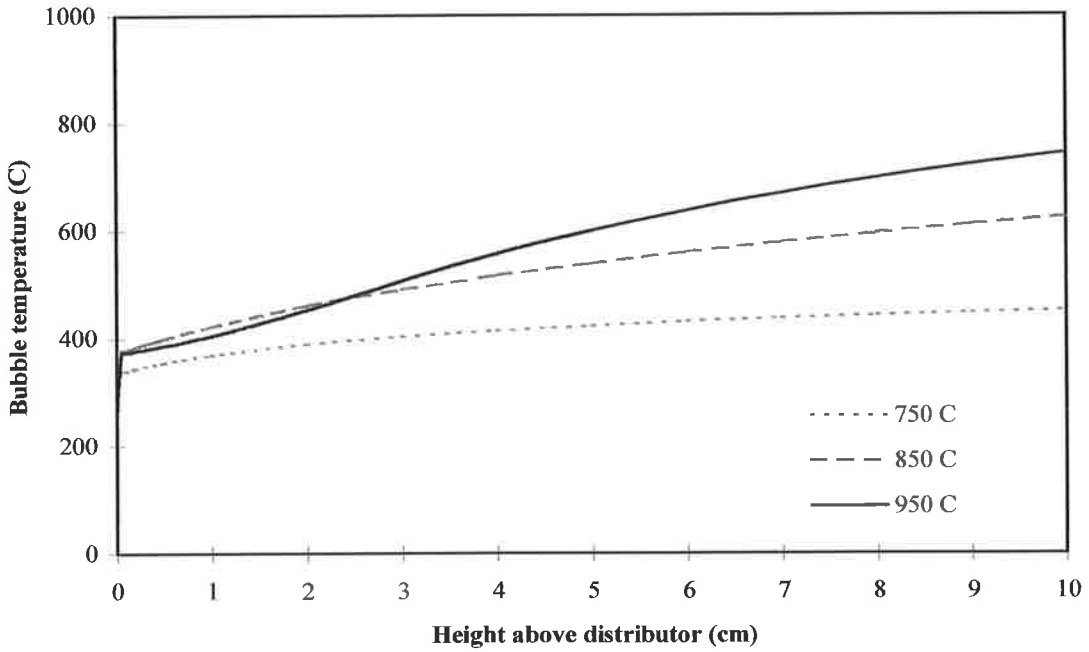

Figure 8.6 Comparison of model predictions for the bubble phase gas temperature at 750°C, 850°C and 950°C during the gasification of Yallourn char.

Table 8.1 A summary of model output parameters for gasification of Yallourn char.

Parameter		750 C	850 C	950 C
O_2 consumption by char combustion / Total O_2 consumption rate	%	99.3	89.9	78.4
Total carbon conversion	%	65.9	87.3	93.0
Carbon conversion due to gasification reactions	%	1.7	27.3	33.7
Carbon conversion due to combustion reactions	%	64.2	60.0	59.3
Excess gas expansion due to 'Net flow'	%	4.5	7.1	8.4

As Table 8.1 summarises, at the lowest bed temperature of 750°C, oxygen consumption and char conversion is dominated by char combustion reactions. As the temperature rises, the fraction of oxygen consumed via homogeneous reactions steadily increases to 21.6 % of the total oxygen consumed in the bed. Figure 8.7 clearly demonstrates this, which shows a normalised plot for the predicted oxygen consumption rates between heterogeneous and homogeneous combustion reactions over the total oxygen consumed as a function of the bed height for all three bed operating temperatures. This is consistent with the findings of Chapter 5, where char burn-out times increase with temperature in the presence of volatiles and in keeping with Chapter 6 and literature findings of favoured in-bed combustion of synthetic volatiles such as propane, methane and carbon monoxide with increasing bed temperature (Hayhurst, 1991; Dennis et al., 1982; Hesketh et al., 1991; van der Vaart, 1985, 1988, 1992). The percentage of oxygen consumed in the homogeneous combustion reactions must equally depend on the amount of combustible gases (volatiles and gasification products) available near the distributor in the bed. In the case of char gasification, volatile matter content is negligible. Thus, the contribution of combustible gases depends on gasification products as the primary source.

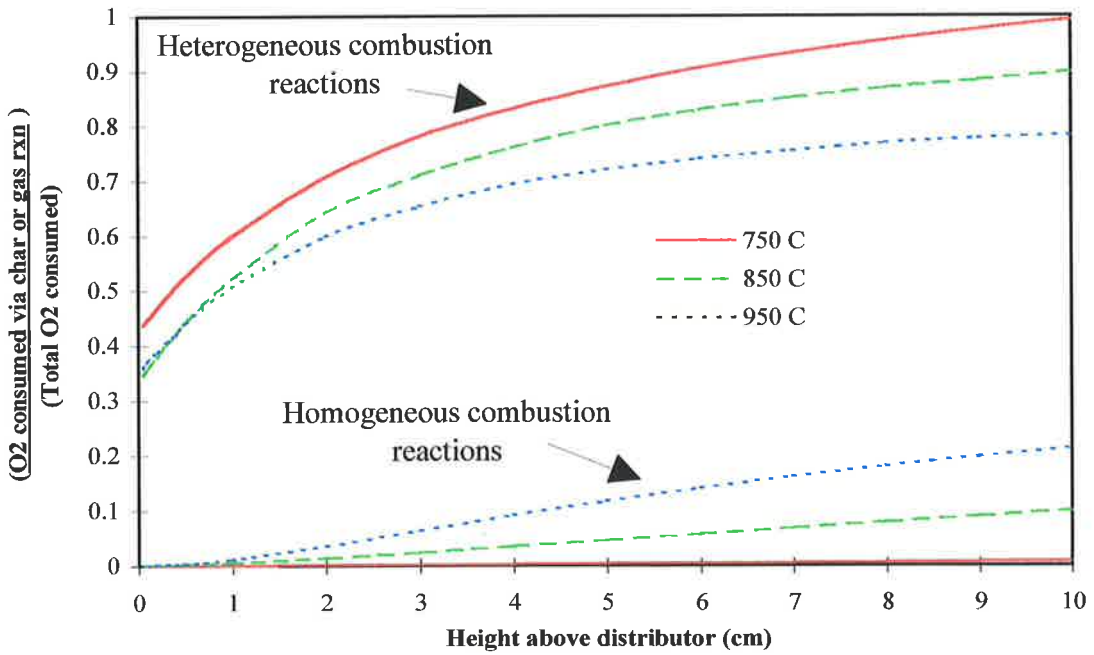

Figure 8.7 Normalised plots for the predicted reaction rates of oxygen in heterogeneous and homogeneous combustion over the total oxygen consumed as a function of bed height at 750°C, 850°C and 950°C during gasification of Yallourn char.

As higher temperatures favour endothermic char gasification reactions, subsequently, concentrations of CO, H_2 and CH_4 will be greater, and homogeneous combustion occurs to a greater extent, increasing the competition between char and volatiles for available oxygen.

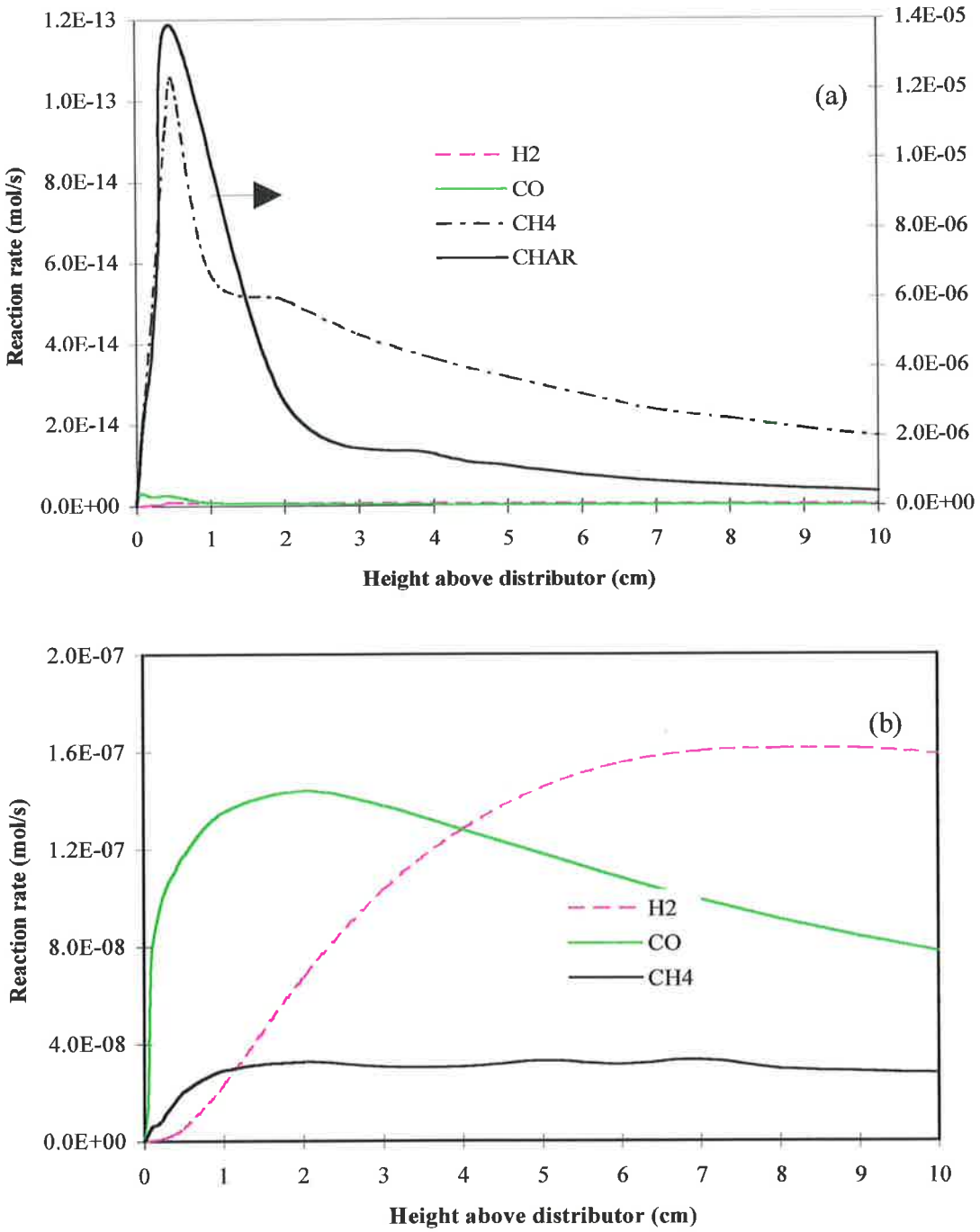

Figure 8.8 Rates of combustion reactions predicted at 850°C for gasification of Yallourn char in (a) the emulsion phase and (b) the bubble phase.

Figure 8.8 presents the profiles of homogeneous and heterogeneous combustion reactions rates expressed in terms of the cross-sectional molar flow rates (mol s^{-1}) for individual species as a function of the bed height in (a) the emulsion phase and (b) the bubble phase. From Figure 8.8(a), combustion of char is initially very fast due to the high availability of O_2 at the inlet of the distributor. At greater bed heights, combustion of char decreases steeply due to: 1) Limited oxygen transfer from both the bubble phase to the emulsion phase and the emulsion phase gas to the solid surface. 2) The competition for O_2 between heterogeneous and homogeneous combustion in the emulsion phase. Consequently, total conversions for homogeneous combustion reactions are considerably higher in the bubble phase than in the emulsion phase. CO and H_2 dominate the homogeneous combustion reactions as shown in Figure 8.7(b), with limited contribution by CH_4 as formation rate is very small due to kinetic limitations. These results are consistent with model predictions of Yan et al. (1998b) for a commercial Wrinkler gasifier based on experimental data of Newman (1948).

Figure 8.9 shows the predicted concentration profiles of the species in the emulsion and bubble phases, otherwise discernible with current experimental arrangement. The oxygen concentration in the emulsion phase falls rapidly from consumption by char combustion reactions. The concentrations of CO and H_2 in both phases increase rapidly in the region near the distributor because of high rates of gasification and combustion in the case for CO. After the initial rise, the CO concentration in the emulsion phase levels off, with CO converted by the water-gas shift reaction. Accordingly, an increase in H_2 concentration in the emulsion phase is evident. The CO concentration difference between the bubble and emulsion phases decreases slowly. The CO formation rate changes very little in the emulsion phase and homogeneous bubble phase combustion of CO gradually decreases from a maximum early in the bed due to the water-gas shift reaction. Concentration of H_2 rises steadily in both phases, rising faster in the emulsion phase due to the higher homogeneous combustion rates in the bubble phase, which continuously increase with bed height (Figure 8.8(b)). Initially the concentration of CO_2 in the emulsion phase increases rapidly due to char combustion. Following the depletion of O_2, the CO_2 concentration rises at a very mild rate due to formation via the water-gas shift reaction. The CO_2 concentration in the emulsion phase is higher than that in the bubble phase, as limited by interphase mass transfer and the zero contribution

from homogeneous combustion reactions as a consequence of the partial combustion reaction scheme. Concentration of steam in both phases initially drop rapidly due to dilution by the formation of CO_2 and CO from char combustion reactions. For the emulsion phase, gasification reactions also consume steam and results in further dilution by the generation of H_2. In both cases, the contribution of CH_4 is negligible.

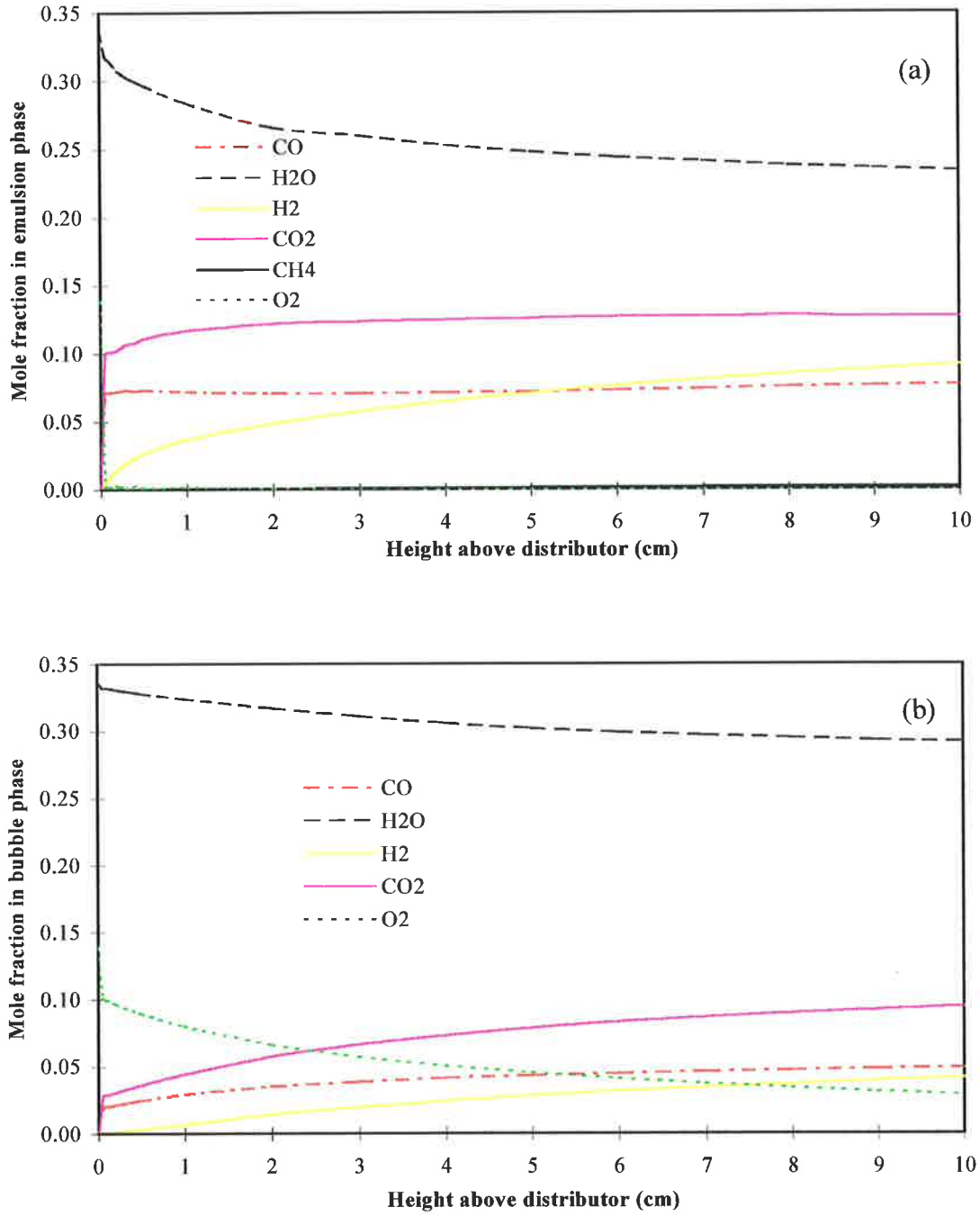

Figure 8.9 Model predictions of bed concentration profiles at 850°C during the gasification of Yallourn char in (a) the emulsion phase and, (b) the bubble phase.

8.3 KINETIC PARAMETER SENSITIVITY ANALYSIS

Modelling gas combustion in a fluidised-bed has proven to be a very difficult task. This is compounded by the lack of specific data on high temperature oxidation of hydrocarbons present in the literature and certainly none pertaining to fluidised-beds. In keeping with the general hierarchal scheme of high temperature hydrocarbon oxidation proposed by Fristrom and Westenberg (1965), Reactions (9) to (13) for propane decomposition and intermediates combustion were used, based on the proposed scheme of van der Vaart (1985). The choice of this scheme over that of Hautman et al. (1981) used by Srinivasan et al. (1998) was based on two reasons: (a) the possibility to account for more of the intermediates measured; and (b) the better agreement to experimental data shown by van der Vaart (1985). The kinetic rate parameters of van der Vaart (1985) for propane combustion as described in Chapter 7, either resulted in an extremely poor fit to the data or caused convergence problems in the energy balance during model simulations.

The kinetics used to describe the reaction scheme as proposed by van der Vaart (1985), were a gross approximation. Van der Vaart (1985) stated in his conclusions that improvements in his own rate constants could be made. "The frequency factors for the unimolecular decomposition of propane, for example, should be reduced since the values refer to second order reactions only." As discussed previously in Chapter 7, the choice of values for the frequency factors and activation energies were based on other experimental findings but are not themselves experimentally determined values. They are essentially best guessed values. The activation energies were estimated based on reported data for overall propane combustion given by Bruno et al. (1983) and Longwell and Weiss (1955) obtained in a stirred tank reactor. The pre-exponential factor was assumed constant for all of the reactions at 1.0×10^{12} $mol^{-1}s^{-1}$. The Arrhenius-type reaction rate expressions were assumed as having either first or second order dependence on reactant concentrations depending on the number of different species involved. These simple expressions were used for both the bubble and emulsion phases, assuming any differences between the phases would arise from physical variations in the environment rather than chemical effects.

The convergence problems for the model are principally associated with the two propane decomposition reactions, with the kinetic parameters and therefore reaction rates simply too fast. Srinivasan et al. (1998) similarly reported the very sensitive nature of model predictions for gas combustion in a fluidised-bed to minor changes in kinetic parameters. Thus, a sensitivity analysis on the kinetic parameters for these reactions is necessary, using the values of van der Vaart (1985) as a reference, with the frequency factor as the chosen variable rather than the activation energy. Ultimately, a best-fit kinetic parameter solution for model simulations to experimental data collected in Chapter 6 is determined. While technically a curve fitting exercise, it will be used to evaluate the model sensitivity to variations of each of the reactions. Is the model more sensitive to decomposition or combustion reactions? Are more reactions required? Essentially a set of kinetic expressions, albeit a gross approximation for propane combustion in a FBG will be determined. Accordingly, the model will then be evaluated under the remaining conditions outlined in the thesis.

A comparison of model prediction for five sets of calculations on the influence of the frequency factor with experimental data collected at 850°C during the co-gasification of propane and char is shown in Figure 8.10. Table 8.2 lists a summary of the kinetic parameters for Reactions (9) to (13) for each *case 1* to *5*, along with the calculated sum-squared error. It should be noted that no model predictions were possible based on a combined frequency factor of 1.0×10^{12} for all Reactions (9) to (13), due to convergence failure of the energy balance. The best fit values for the various estimates of the frequency factors for all gas species are determined by minimising the sum of squared deviations between predicted and measured values. Table 8.2 lists the total sum-squared error for all species and the major species comprised of CO, CO_2, O_2, and C3H8. The sum-squared error is calculated by (Yan et al., 1999b);

$$i = \sum_{j=1}^{N}\left(\frac{x_{ij}^{m} - x_{ij}^{p}}{x_{ij}^{m}}\right)^{2} \qquad \text{....8.1}$$

where x^{m}_{ij} is measured variable of component i for the condition of the jth experiment, x^{p}_{ij} is predicted variable for the condition of the jth experiment and N is the total number of data points.

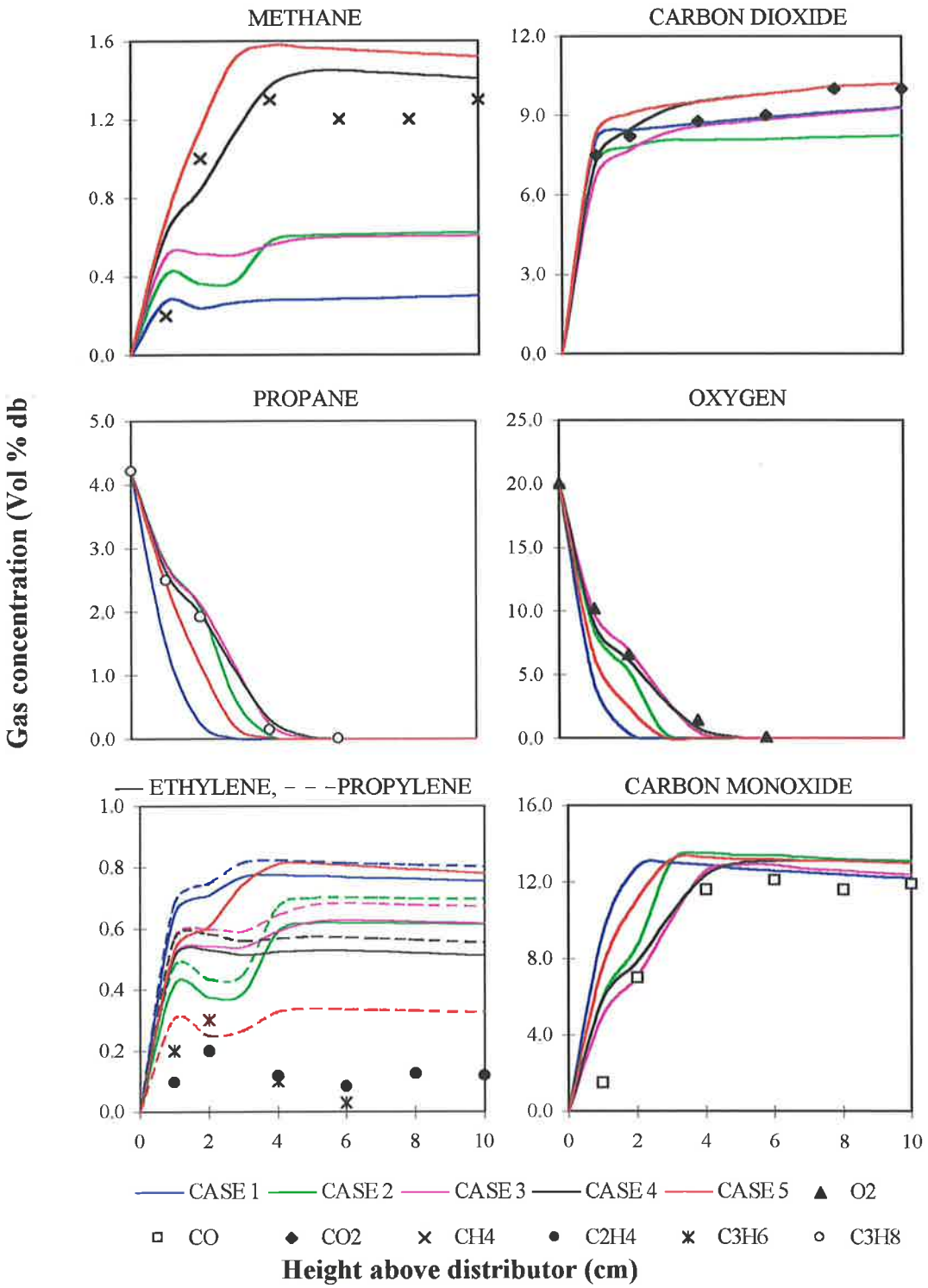

Figure 8.10 Comparison of model predictions (lines) for the influence of the frequency factor with experimental data (symbols) at 850°C for the co-gasification of propane and char. *Case 1*: C_3H_8, CH_4, 1.0×10^{12}, C_2H_4, C_3H_6, 1.0×10^{11}; *Case 2*: C_3H_8, 1.0×10^{10}, CH_4, C_2H_4, C_3H_6, 1.0×10^{12}; *Case 3*: C_3H_8, 1.0×10^{10}, CH_4, C_2H_4, C_3H_6, 1.0×10^{11}; *Case 4*: C_3H_8, CH_4, 1.0×10^{10}, C_2H_4, C_3H_6, 1.0×10^{11}; *Case 5*: C_3H_8, CH_4,1.0×10^{10},C_2H_4, 1.0×10^{11}, C_3H_6, 1.0×10^{12}.

Table 8.2 A summary of the frequency factors used for Reactions (9) to (13) and sum-squared errors for each case highlighted in Figure 8.10.

Reaction	(9)	(10)	(11)	(12)	(13)	Σ error	Σ error
Description	CH_4 combustion	C_3H_8 pyrolysis	C_3H_8 pyrolysis	C_3H6 combustion	C_2H_4 combustion	All species	Major species
Case 1	1.0×10^{12}	1.0×10^{12}	1.0×10^{12}	1.0×10^{11}	1.0×10^{11}	284.0	34.0
Case 2	1.0×10^{12}	1.0×10^{10}	1.0×10^{10}	1.0×10^{12}	1.0×10^{12}	147.8	12.5
Case 3	1.0×10^{11}	1.0×10^{10}	1.0×10^{10}	1.0×10^{11}	1.0×10^{11}	153.2	7.9
Case 4	1.0×10^{10}	1.0×10^{10}	1.0×10^{10}	1.0×10^{11}	1.0×10^{11}	116.2	10.7
Case 5	1.0×10^{10}	1.0×10^{10}	1.0×10^{10}	1.0×10^{12}	1.0×10^{11}	215.7	21.1

As shown in Figure 8.10, significant variations in the model results occur with variations in the frequency factor for individual reactions. Referring to Table 8.2, the frequency factor has been reduced by up to two orders of magnitude from 1.0×10^{12} to 1.0×10^{10} mol s^{-1}. *Case 1* is the closest representation to the conditions used by van der Vaart (1985) that convergence was attainable. The model predictions are most sensitive to propane pyrolysis reactions, which was similarly observed by Srinivasan et al. (1998) in modelling propane combustion under fluidised-bed combustion conditions. However, this result is not surprising given that all other hydrocarbon intermediates depend on these reactions as their sources for formation. Thus, any change to the rates of these two reactions will significantly vary the concentrations of CH_4, C_2H_4 and C_3H_6, which under the current reaction scheme partially combust to CO and thus affect O_2 and CO concentrations. The exothermic combustion reactions of course in turn release energy, which raises the bubble temperature. This speeds up the whole process and results in either very poor agreement with experimental data or the energy balance failing to converge due to combustion run away. The propane concentration deviates most significantly from the experimental data when compared to all other cases for k_o taken to be 1.0×10^{10} mol s^{-1}. The resulting higher concentrations of C_2H_4 and C_3H_6 from the rapid pyrolysis of C_3H_8 consequently increases the partial combustion reaction rates in the bubble phase and affects CO and O_2 concentrations. Accordingly, the sum-squared error is very large.

For *case 2*, a substantial reduction in the sum-squared error occurs by reducing the reaction rate for propane pyrolysis, with all species showing improvement as compared with experimental data. In an effort to reduce the concentration of C_3H_6 and C_2H_2 to attain better agreement with experimental data, the frequency factor for these two species was increased to 1.0×10^{12} mol s^{-1}. Initially this improves agreement however, after the first 4 cm the concentration of C_3H_6 and C_2H_2 rises concurrent with depletion in the O_2 concentration. Referring to Figure 8.11 on the predicted bubble temperature profiles, by increasing the combustion rates of C_3H_6 and C_2H_2, the bubble temperature rises very quickly from the heat released by these exothermic reactions. Consequently increasing the pyrolysis rate of C_3H_8, more C_3H_6 and C_2H_2 was produced and this was associated by a decline in the available O_2. Thus generation outstrips consumption and the concentration spikes at approximately the 4 cm point in the bed.

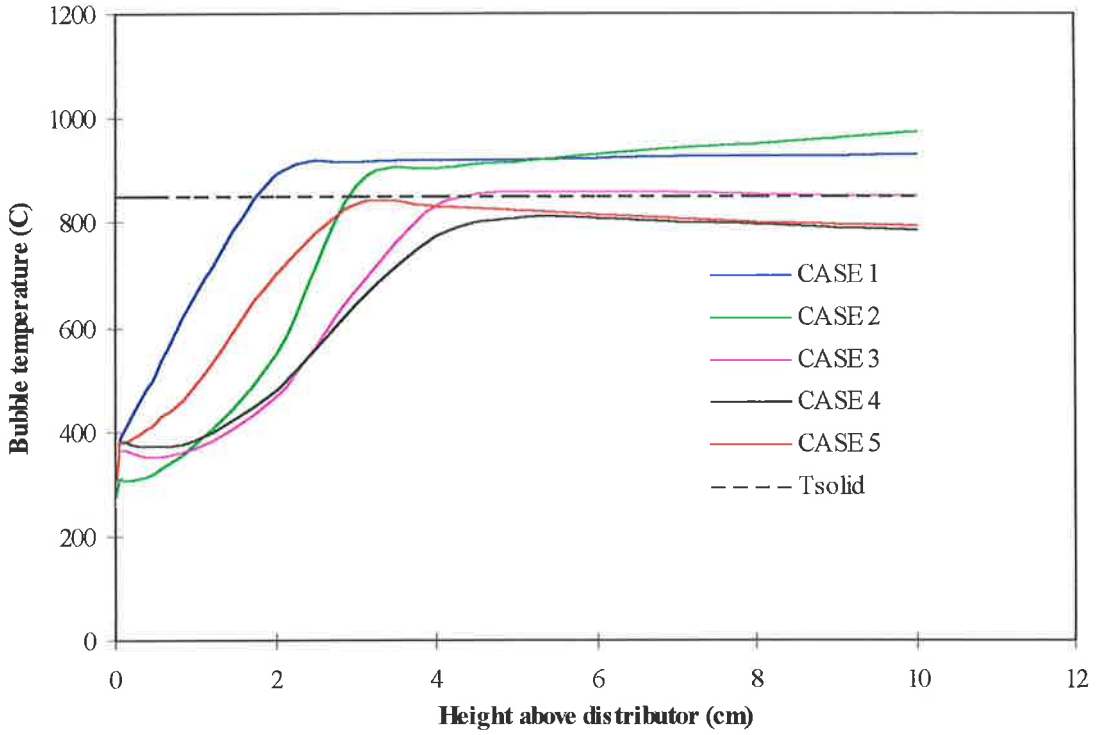

Figure 8.11 Predicted bubble temperature profiles at 850°C for the co-gasification of propane and char.

In an effort to improve the predictions with respect to methane yields, the frequency factor was successively reduced in *case 3* and *case 4*. As can be seen from Figure 8.10 and Table 8.2, this results in the best agreement between model predictions and

experimental data. *Case 3* gives the smallest sum-squared error for the major species while in *case 4* the smallest total species sum-squared error. In an effort to improve the predictions for the intermediate species, an increase in C_3H_6 frequency factor was tested in *case 5*. However, this leads to the previous scenario described for *case 2*, where the bubble temperature rises rapidly and increases the propane pyrolysis reactions. Based on the smallest total sum-squared error, *case 4* was used as the basis for model predictions. While very good agreement was attained between model predictions and experimental data, the incorporation of a pyrolysis reaction scheme for C_3H_6 and C_2H_2 intermediates, as indicated below, would undoubtedly improve model predictions. The influence of secondary decomposition on the combustion rates of coal volatiles has been reported by Cho et al. (1995).

$$C_3H_6 \rightarrow C_2H_2 + CH_4$$
$$C_2H_4 \rightarrow C_2H_2 + H_2$$

Ultimately, this sensitivity analysis has highlighted two important points with regard to volatile matter combustion. Firstly, the extremely sensitive nature of model predictions to the kinetic parameters chosen for homogeneous combustion reactions. Therefore, kinetic data collected under other experimental conditions will not necessarily apply to a fluidised-bed. Secondly, successful modelling of gas combustion in a fluidised-bed requires accurate treatment of homogeneous secondary decomposition reactions, post volatile matter evolution during devolatilisation.

8.4 CO-GASIFICATION OF PROPANE AND CHAR

A comparison of model results (lines) to experimental data (symbols) of in-bed concentration profiles for C_3H_8, CO, CO_2, O_2, C_3H_6, C_2H_4 and CH_4 during the fluidised-bed co-gasification of propane (simulated volatile matter) and Yallourn char at 750°C, 850°C and 950°C is shown in Figures 8.12, 8.13 and 8.14, respectively. The model predictions shown in these figures are the best-fit kinetic parameter representation to the experimental data of Chapter 6 as determined in section 8.3.

The model predictions in Figure 8.12 for 750°C show poor agreement with experimental data, particularly for the carbon oxide species. However, in Figures 8.13 and 8.14 agreement with experimental data at 850°C and 950°C is very good. In the case for the lowest bed temperature of 750°C, the model profiles for the carbon oxides are observed opposite to that experimentally, with CO concentration above CO_2. While C_3H_8 and O_2 concentrations deviate particularly in the first third of the bed, with consumption over predicted. This discrepancy between the model predictions and experimental data is a direct result of homogeneous combustion reactions being calculated to occur within the bed by the model. Consequently, the increase in CO concentration above CO_2, is consistent with the partial homogeneous combustion reaction scheme utilised in the model. This is clearly demonstrated in Figure 8.14, for the predicted oxygen consumption rates via heterogeneous and homogeneous combustion reactions. It has been conclusively shown experimentally by both the current data and elsewhere in the literature (Hayhurst, 1991; Dennis et al., 1982; Hesketh et al., 1991; van der Vaart, 1985, 1988, 1992) that the combustion of propane does not occur to any appreciable extent within the bed at temperatures below the critical bed temperature of 830°C . As discussed in Chapter 6, at 750°C the system behaves in a similar way as during the sole gasification of char, where char partial combustion reactions dominate the carbon conversion. Thus, the disagreement between experimental data and model results at the lowest bed temperature of 750°C can be related to the kinetic parameters used in the current model simulations for the combustion and decomposition reactions of the hydrocarbons.

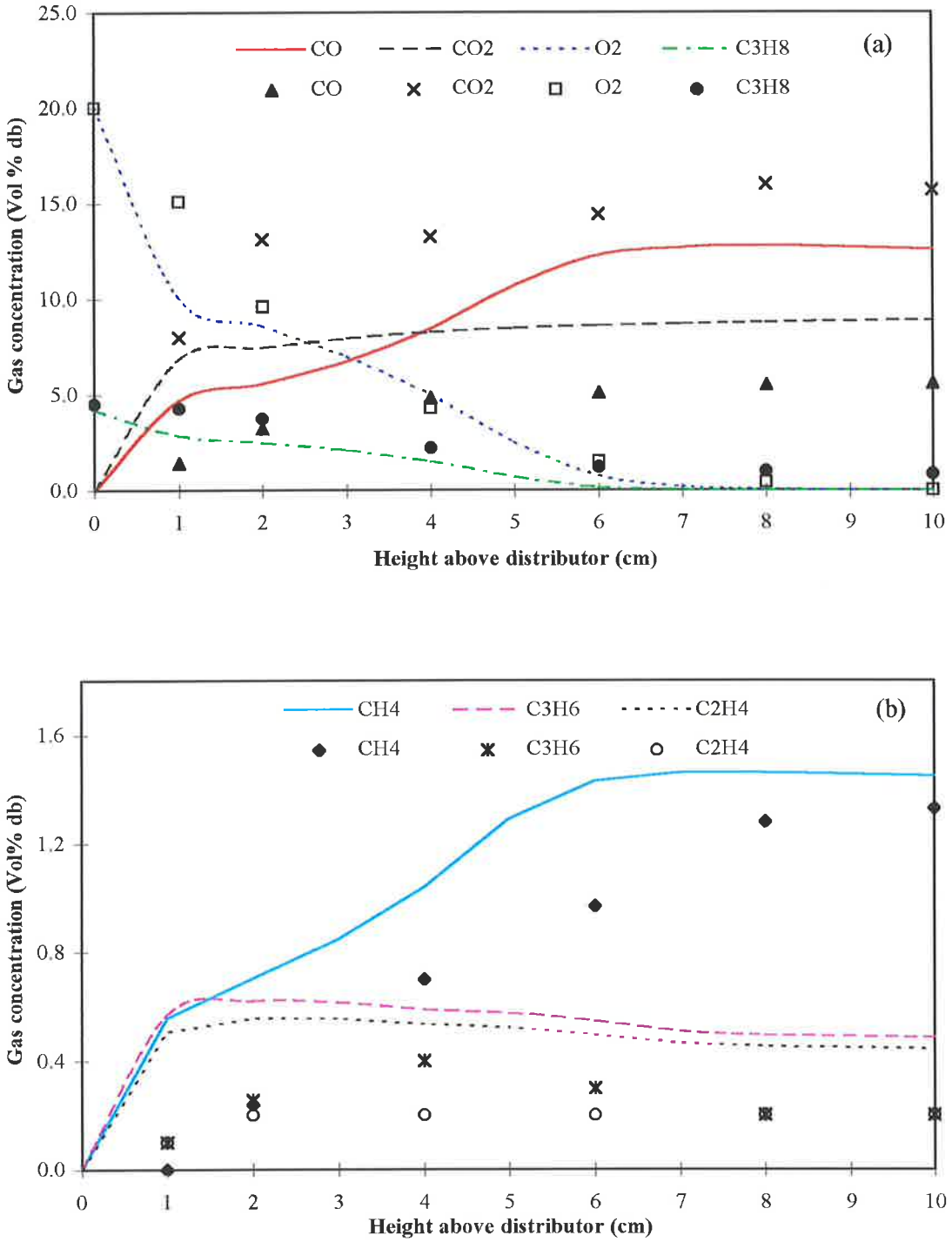

Figure 8.12 Comparison of model predictions (lines) with experimental data (symbols) for co-gasification of propane and char at 750°C; (a) major species, (b) minor species.

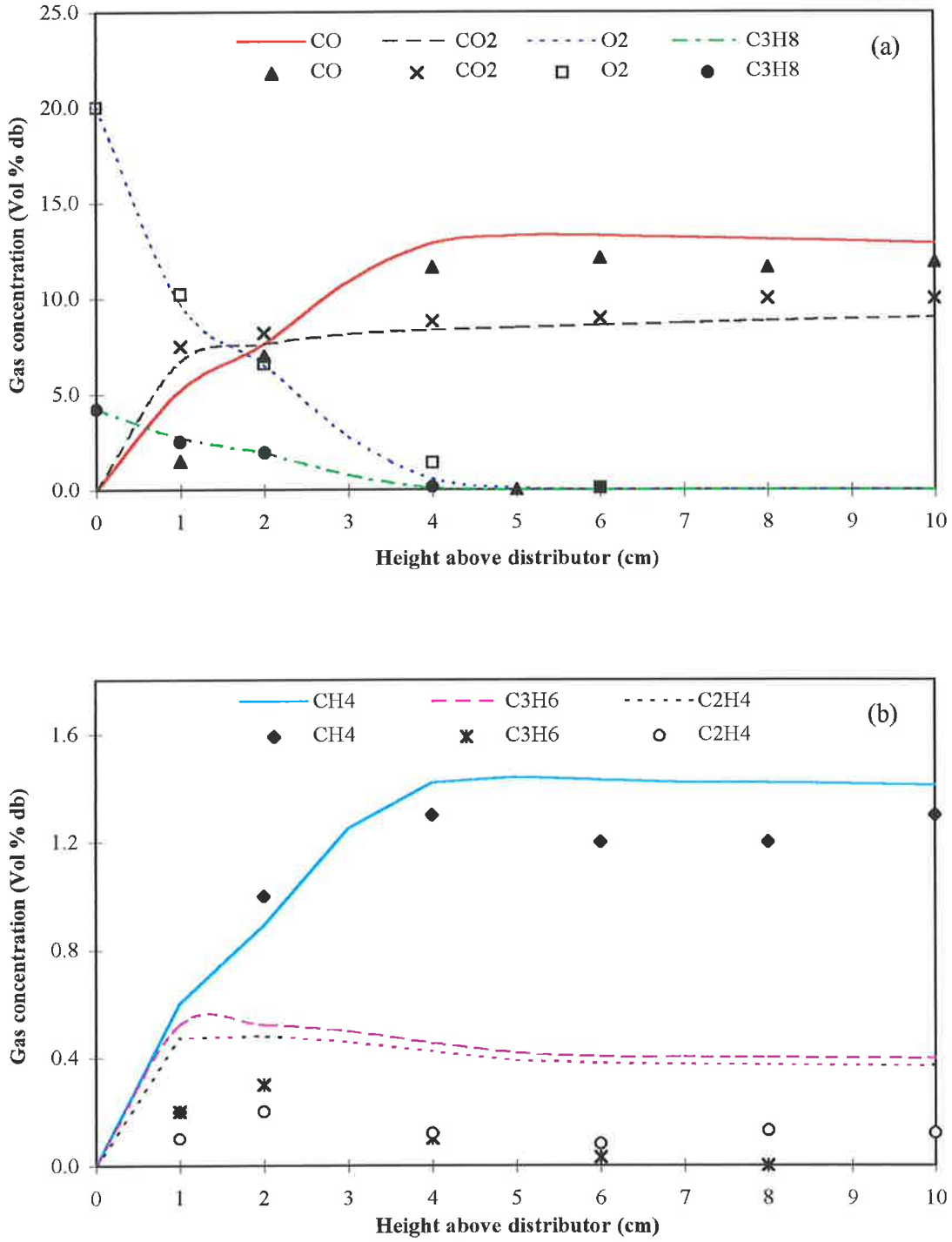

Figure 8.13 Comparison of model predictions (lines) with experimental data (symbols) for co-gasification of propane and char at 850°C; (a) major species, (b) minor species.

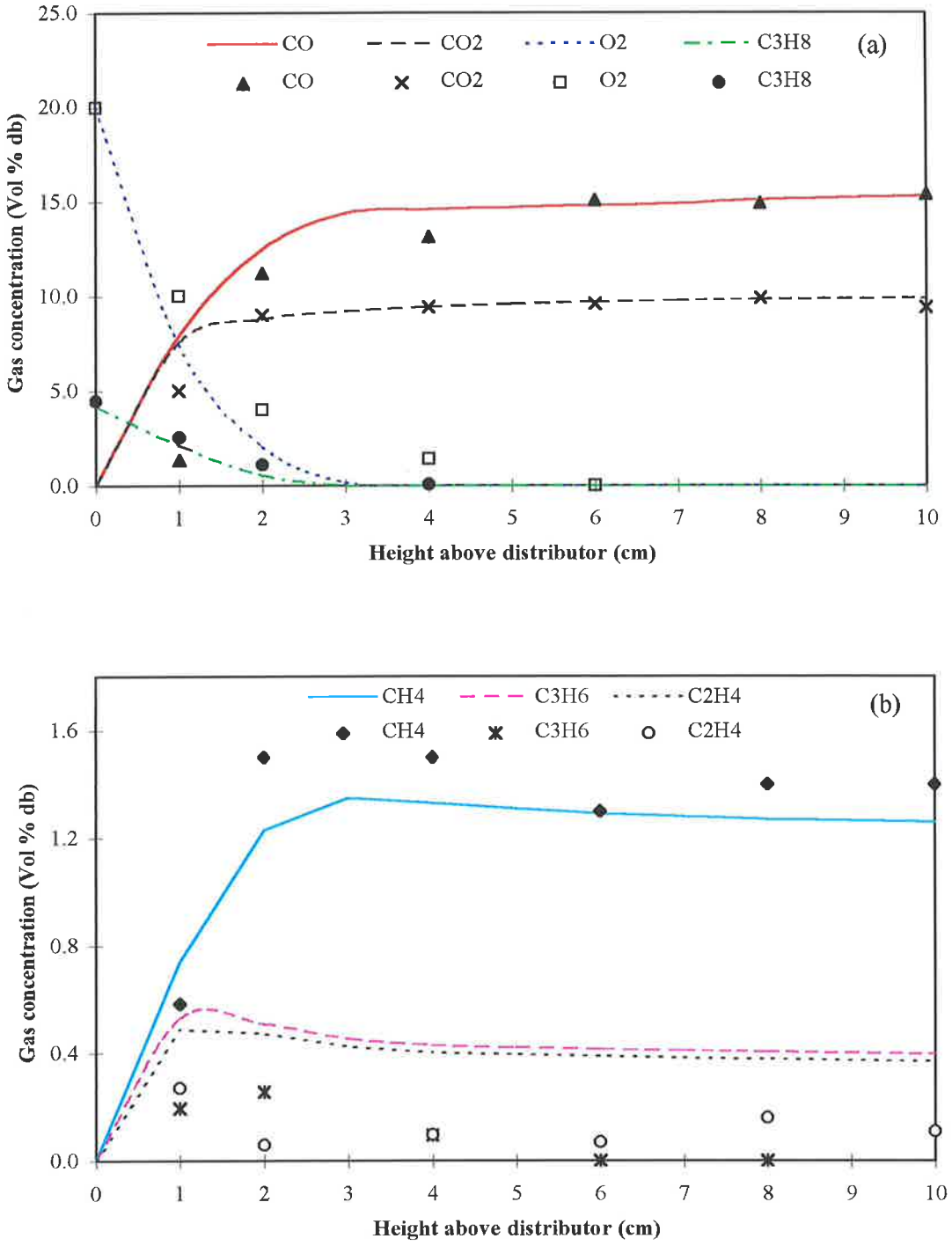

Figure 8.14 Comparison of model predictions (lines) with experimental data (symbols) for co-gasification of propane and char at 950°C; (a) major species, (b) minor species.

However, instant dismissal of the kinetic parameters as being incorrect at these low operating temperatures is not justifiable either, given the unique environment a fluidised-bed represents over traditional gas combustion burners used to acquire kinetic data. The incorporation of radical quenching steps to balance the reaction rates caused by the inhibitive effect of the bed material into the gas phase kinetic mechanism was successfully utilised in a model developed by Jeng et al. (1997). This may be a necessary progression from the simple global scheme utilised here and by others (van der Vaart, 1985, 1992; Srinivasan et al., 1998) for an accurate treatment of gas combustion in a fluidised-bed. While a significant disparity between experimental data and model results exists at temperatures below the critical temperature for in-bed combustion of propane, for FBG further complication of the model reaction scheme is not warranted. Firstly, commercial operation of gasifiers at such low temperatures is not practicable and secondly, excellent agreement of the model data at higher bed temperatures has been shown here.

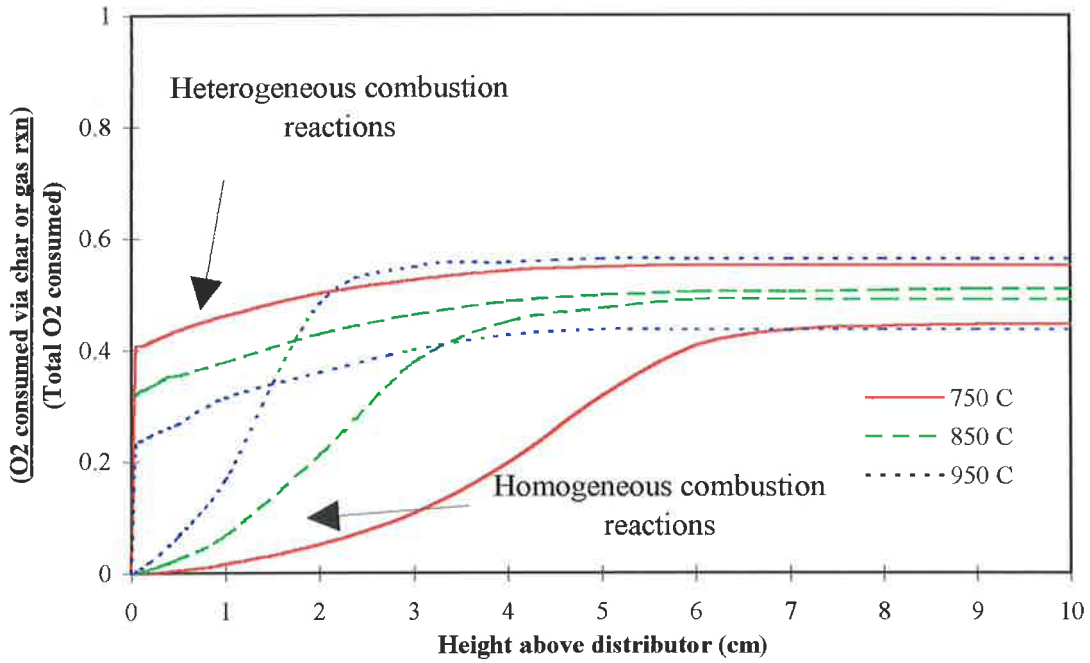

Figure 8.15 Normalised plots for the predicted reaction rates of oxygen in heterogeneous and homogeneous combustion over the total oxygen consumed as a function of the bed height at 750°C, 850°C and 950°C during co-gasification of propane and char.

As shown in Figure 8.15 and summarised in Table 8.3, the amount of O_2 consumed by char combustion reactions are considerably lower than during the sole gasification of char. In addition, due to the initial presence of volatiles and the relatively fast nature of homogeneous combustion reactions, O_2 is completely consumed before the bed surface. The competition of homogeneous combustion for oxygen with char, as experimentally demonstrated in Chapter 5, is reflected in lower overall carbon conversion via combustion reactions for all three bed temperatures. Furthermore, the amount of excess gas expansion due to "net flow" has typically doubled over that for the sole gasification of char. This increase is principally attributed to the change in the number of moles of gas involved in the homogeneous reactions. At the lowest bed temperature of 750°C, the total carbon conversion is still however dominated by char combustion reactions, with gasification reactions accounting for only 1.7 % of the total carbon conversion. The same conversion percentage was predicted for the sole gasification of char. As the temperature rises, the fraction of oxygen consumed via homogeneous reactions steadily increases to 56.4 % of the total oxygen consumed. Most importantly, the amount of carbon to undergo conversion due to gasification has increased in the presence of in-bed combustion of propane and intermediates. This definitive result now validates the qualitative assessment by Gururajan et al. (1992) on the merits of promoting in-bed combustion of volatile matter in a fluidised-bed gasifier.

Table 8.3 A summary of model output parameters for co-gasification of propane and char.

Parameter		750 C	850 C	950 C
$\frac{O_2 \text{ consumption by char combustion}}{\text{Total } O_2 \text{ consumption rate}}$	%	55.2	50.9	43.6
Total carbon conversion	%	52.5	80.9	87.0
Carbon conversion due to gasification reactions	%	1.7	32.4	52.9
Carbon conversion due to combustion reactions	%	50.8	48.5	34.1
Excess gas expansion due to 'Net flow'	%	10.3	14.2	16.5

The predictions of the model for hydrocarbon intermediates produced from cracking of propane shows mixed agreement with data. For C_2H_4 and C_3H_6, the model consistently over predicts experimental observations. However, little improvement can be made in this regard as previously discussed in sensitivity analysis of model kinetic parameters in section 8.3. For CH_4, the model predictions are exceptionally good, with the transitional move of the peak in concentration to a lower position in the bed with increasing temperature well characterised by the model.

Figure 8.16 shows a comparison of model results for the mole fractions of all species in both the bubble and emulsion phases at 850°C. The emulsion phase behaves as anticipated, with O_2 rapidly consumed via char partial combustion reactions to form carbon oxides. The initial slight decrease in the steam mole fraction is attributed to the increase in the number of moles in the emulsion phase gas from heterogeneous partial combustion reactions and not from gasification reactions. This change manifests itself in the dilution of the steam mole fraction as emulsion phase flow is hydrodynamically capped and excess gas must pass into bubble phase via the net flow contribution. The increase in steam mole fraction for the greater portion of the bed is due to the release of water from homogeneous combustion reactions of the hydrocarbons. Propane is completely pyrolysed within the first 0.5 cm of the bed to form intermediates, which reach peak concentration at this same bed height. Above this bed height, intermediates combust at relatively slow rates, limited by the mass transfer of oxygen between bubble and emulsion phases. This is clearly demonstrated in Figure 8.16 on the combustion/decomposition reaction rates of the species with the bed height for both phases. Some initial hydrocarbon oxidation is calculated to occur by the model near the distributor and quickly diminishes with depletion of oxygen due to char combustion reactions. For the bubble phase, the initial rapid change in O_2, CO and CO_2 concentrations is principally due to the net flow and mass transfer between the phases associated with heterogeneous combustion. Propane decomposition and subsequent combustion of intermediates take place further down in the bed as compared with emulsion phase. The peak conversion occurring at approximately 2.5 cm from the distributor plate, as indicated by Figure 8.17.

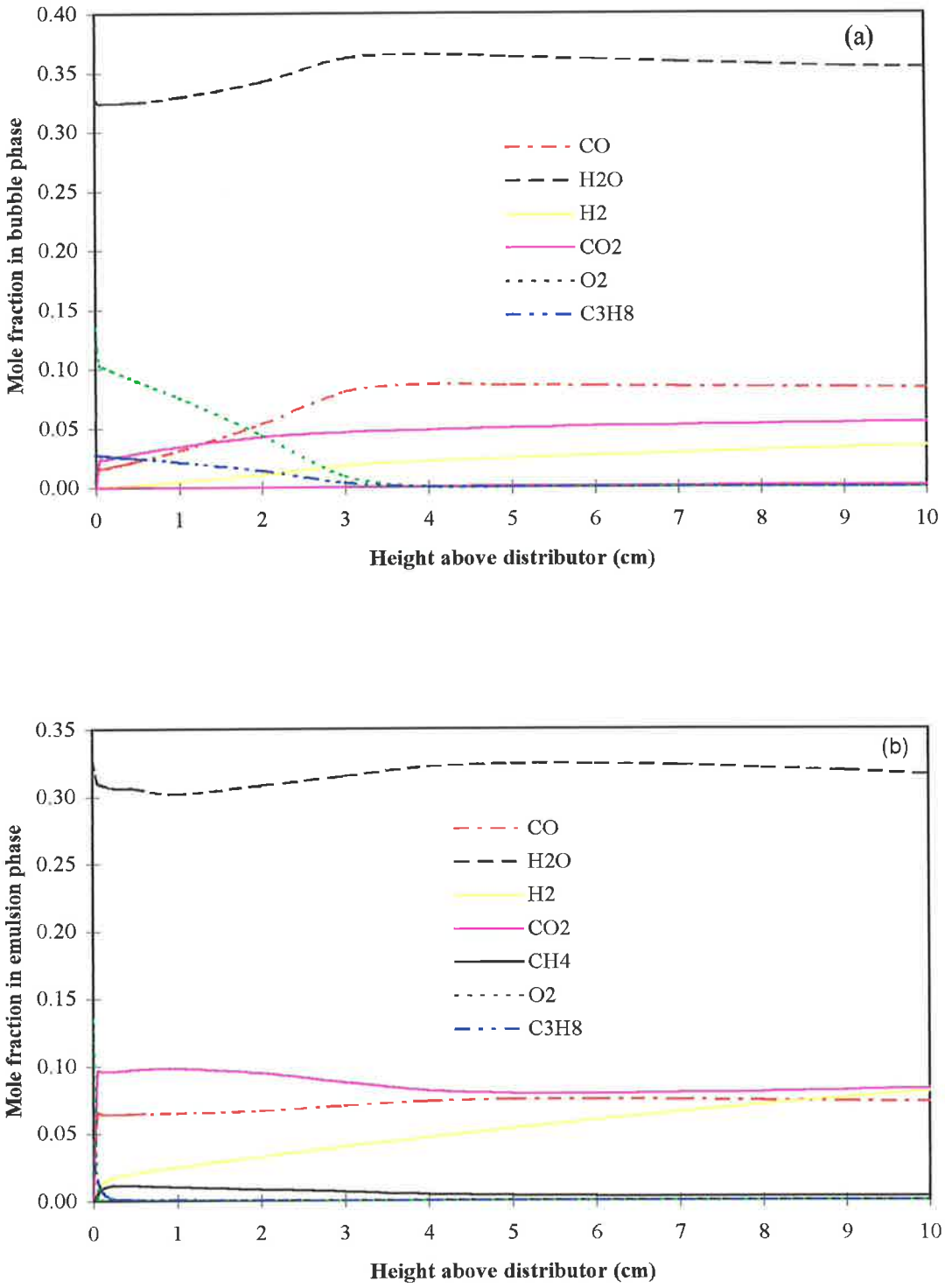

Figure 8.16 Model predictions of in-bed mole fractions of various gas species present during propane/char gasification at 850°C; (a) bubble phase, (b) emulsion phase.

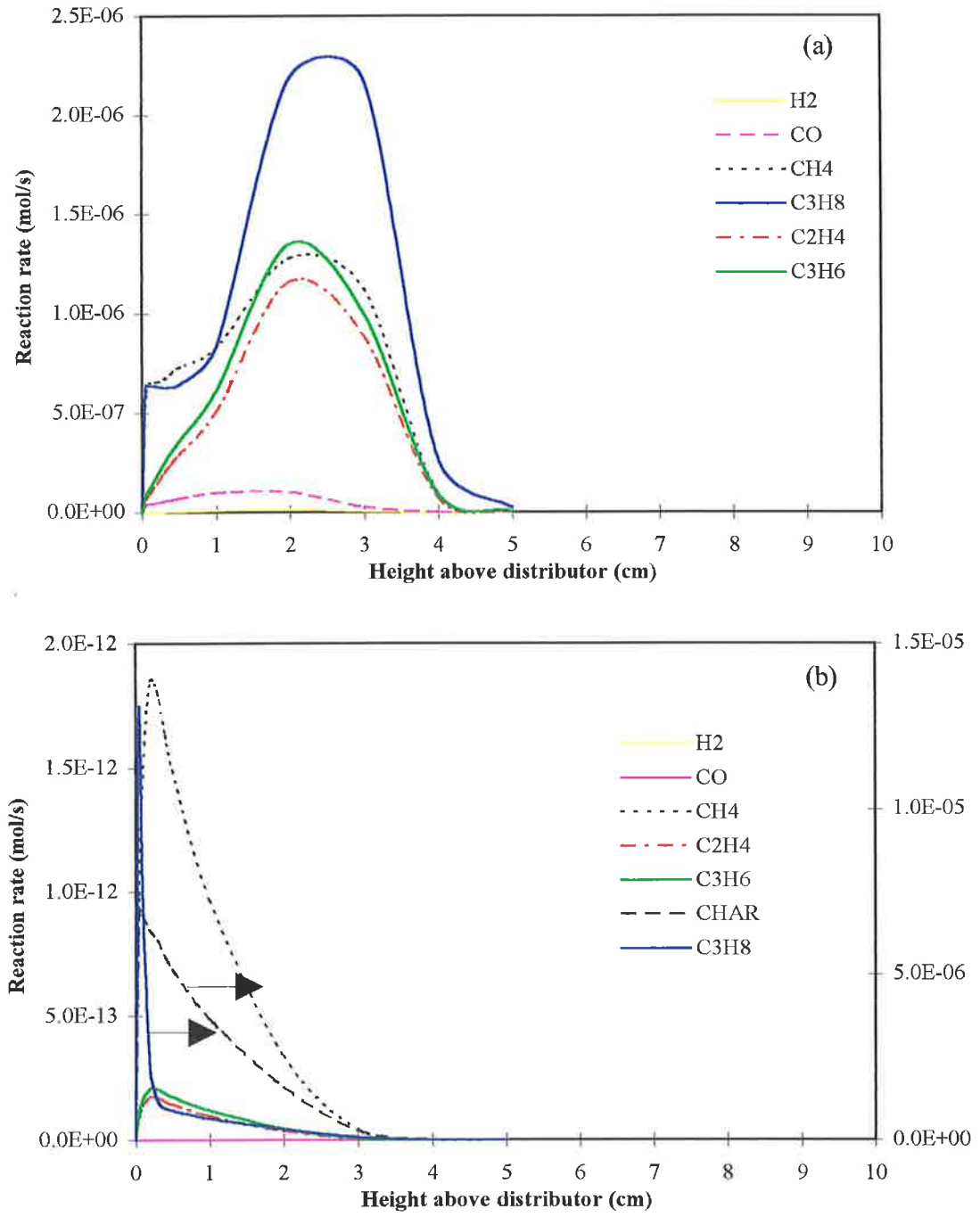

Figure 8.17 Model predictions of in-bed combustion/decomposition reaction rate profiles during propane/char gasification at 850°C; (a) bubble phase, (b) emulsion phase.

Correspondingly, this results in a peak in the bubble phase temperature, which exceeds the solid temperature and represents the location where homogeneous combustion rates are at their maximum.

This is illustrated in Figure 8.18, for the effect of increasing bed operating temperature on the predicted in-bed bubble temperature profile. Above this point, the bubble phase temperature levels off as combustion dies out due to depletion of oxygen. For the highest bed temperature of 950°C, the bubble phase temperature above the combustion region decreases, principally because of the water-gas shift reaction. Interestingly, the bubble exit temperatures at the bed surface for all three bed operating temperatures are very similar. Thus, for the bed operating at 750°C and 850°C, the bubble temperature is in excess of the bed by approximately 100°C and 50°C, respectively. The difference in the temperatures between the two phases at 750°C and 850°C can be explained by the role of the water-gas shift reaction and a simple mass and energy balance for the bubble phase.

As the water-gas shift reaction is endothermic, increasing the bed temperature will increase the reaction rate and consequently suppressing the rise in gas phase temperature. In addition, since the excess fluidisation velocity is constant and the contribution of net flow gas with temperature being relatively small (refer to Table 8.3), the bubble mass flux through the bed can be assumed as essentially identical. The overall conversion in the bubble phase by the bed surface can be taken to be very similar for all three bed operating temperatures (assumption valid for model predictions only). Assuming heat and mass transfer rates are relatively unchanged, an equivalent amount of heat will be released in the bubble phase to raise the same mass of gas. This results in a relatively similar final bubble temperature although the bed operating temperatures vary by 200°C. The small differences in final bubble temperatures with decreasing bed operating temperature is principally attributed to the decreasing contribution of homogeneous combustion reactions occurring at the lower bed temperatures as indicated by Figure 8.15 and Table 8.3. Ultimately, it is clear that as the bed temperature increases, ignition of propane moves closer to the distributor, consistent with model predictions of Srinivasan et al. (1998) and van der Vaart (1985). However, unlike the two previous studies, no sharp spikes in the bubble phase temperature exceeding the solid temperature by more than 1000 K were predicted to occur. Such substantial temperature jumps in the bubble phase does not appear to be a realistic representation of the bubble temperature profile, or consistent with chemical analysis of concentration profiles in the bed.

Experimental verification of such trends is an extremely difficult task and no such data has been reported in the literature. This is primarily due to: 1) the ability to differentiate between the phases; 2) measurement of the bubble temperature requires a rapid response time of the same order as the bubble residence time passing the thermocouple and 3) to isolate radiative heat transfer from bed solids to thermocouple tip. The use of a shielding screen on a suction pyrometer has been observed to catalyse hydrocarbon oxidation reactions on the metal surface, thus affecting measured temperature response (van der Vaart, 1985). However, it would appear that the operating temperature profiles predicted by the current model would represent the true situation in a fluidised-bed gasifier. The temperature of feed gas is usually lower than the bed temperature and will experience a time lag associated with this heating up period in the lower part of the bed. This phenomenon was observed in trial tests of Australia's first circulating fluidised-bed combustion pilot plant (Yan et al. 1998). The development of a pyrometer able to effectively measure the bubble temperature in a fluidised-bed would be a very beneficial step forward in providing further fundamental data required for model validation.

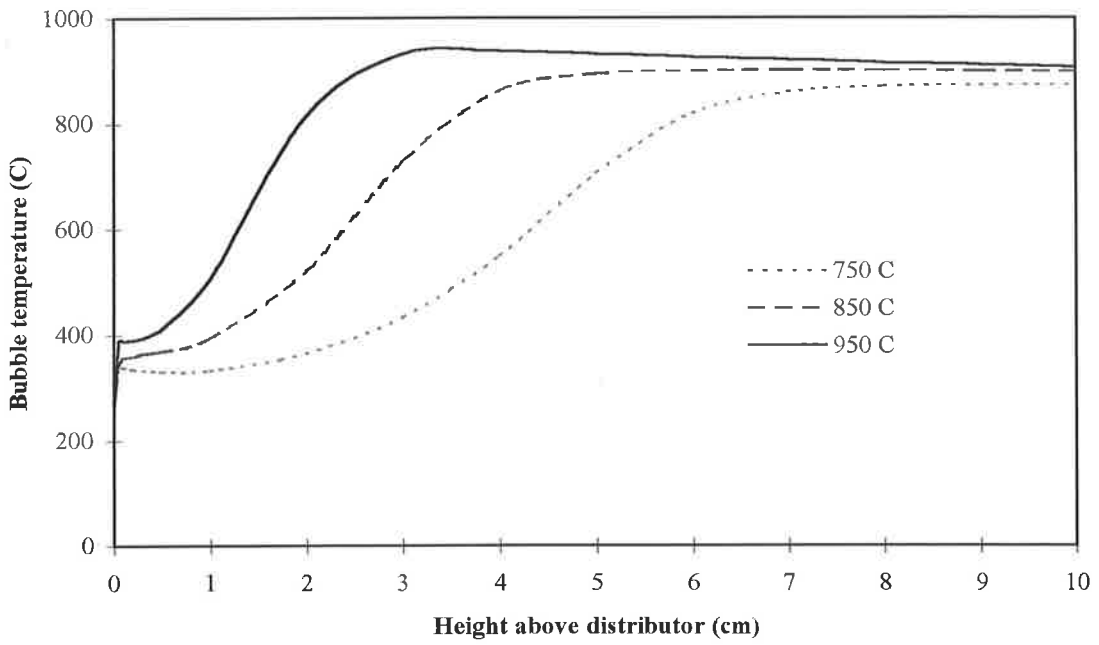

Figure 8.18 Comparison of predicted bubble temperature profile for the operating temperatures of 750°C, 850°C and 950°C during the co-gasification of propane and char at a constant excess fluidising velocity of 25 cm s^{-1}, u_{mf} = 6 cm s^{-1}.

8.5 INFLUENCE OF DESIGN PARAMETERS

Based on the successful comparison of model predictions with experimental data in the previous section, a parametric study to investigate the influence of design parameters: excess operating velocity and bed particle size on propane combustion behaviour in a fluidised-bed gasifier can be conducted in confidence. Figure 8.19 shows a comparison of model predictions for two different mean bed particle sizes of 425 μm (solid line) (u_{mf}, 6 cm s^{-1}) and 775 μm (dash line) (u_{mf}, 25 cm s^{-1}) at 850°C during the co-gasification of propane and char at a constant excess fluidising velocity of 25 cm s^{-1}. These results indicate increased in-bed reaction occurring following a reduction in the mean bed particle size, accompanying an increase in bubble temperature as shown in a comparison of the predicted bubble temperature profiles in Figure 8.20.

The influence of bed particle size on in-bed combustion efficiency of volatiles was observed experimentally and predicted in a model by van der Vaart (1985) for propane combustion in a FBC. However, Srinivasan et al. (1998) observed the opposite with in-bed combustion favoured by increasing particle size for their model predictions. For the conditions they considered, ($u-u_{mf}$ = 25 cms^{-1}, T_{bed} 850°C), there appeared to be a critical particle size (≈ 260 μm), below which the ignition can only occur in the freeboard. Both van der Vaart, (1985) and Srinivasan et al. (1998) explained their observations based on differences in mass and heat transfer rates between the phases. Undoubtedly this is the case however, the apparent contradicting result may not be as it appears "prima facie". One of the critical factors in modelling gas-phase combustion bed hydrodynamics is the heat transfer coefficient between the bubble and dense phases. Interestingly, both van der Vaart (1985) and Srinivasan et al. (1998) modelled using the results of Toei et al. (1972), where it was found that the volume fraction of solids falling through a bubble dominants contribution to the total heat transfer. Both noted that the solids content was an order of magnitude greater than the value recommended by Toei et al. (1972) for an isolated bubble. As the particle size increases, there is a corresponding decrease in bubble-dense phase heat transfer coefficient (Srinivasan et al., 1998). The difference in the results is attributed to the differing inlet gas temperature used by Srinivasan et al. (1998) as compared to

the present model and that by van der Vaart (1985). In the present case, the inlet gas temperature was maintained at 250°C, as compared to the parametric investigation by Srinivasan et al. (1998) where inlet gas temperature equalled the bed temperature. The resultant outcome of this is that in the model by Srinivasan et al. (1998) there is no delay time necessary for the bubble temperature to rise, hence combustion reactions initiate essentially instantaneously. For the small particulate system, the higher heat transfer rate will help dissipate the heat generated from the combustion reactions and thus limit the rise in bubble temperature and in turn conversion. While for increasing bed particle size, the decrease in heat transfer coefficient means the bubble temperature rise is higher and thus increases reaction rates and overall conversion. However, when the gas inlet temperature is below the bed temperature, the smaller particulate system will help heat the bubble gas at a greater rate and hence initiate combustion closer to the distributor as compared to a bed filled with large particles.

Furthermore, van der Vaart (1985) approximated the exchange between emulsion phase and bubble/cloud phase as $0.5\ u_{mf}\ \pi R^2$, where the value of 0.5 is purely empirical. Obviously, as the bed size increases, u_{mf} increases resulting in higher mass transfer rates. For the general reaction scheme used by van der Vaart (1985), as used in the current model, the reactions are of order greater than or equal to 1, so that the higher the concentration of reactants, the higher conversion will be. Thus, the smaller the influence of the emulsion phase on the bubble phase, the faster the reaction rate in the bubble there will be (van der Vaart, 1985). This of course corresponds to a more rapid rise in bubble temperature as observed in Figure 8.20. In the current model the "net flow" term is incorporated into the 2-phase theory of fluidisation. The "net flow" term considers the additional mass transfer from the emulsion phase to the bubble phase due to the net generation of moles of gas from devolatilisation, combustion and gasification reactions as dense phase gas flow is hydrodynamically capped at u_{mf}. A direct comparison of experimental data is difficult and ambiguous due to the following dichotomy. For a constant excess velocity of 25 cm s^{-1} (bubble gas residence time being equal) differing fluidisation states (superficial velocities) with changing particle size occurs.

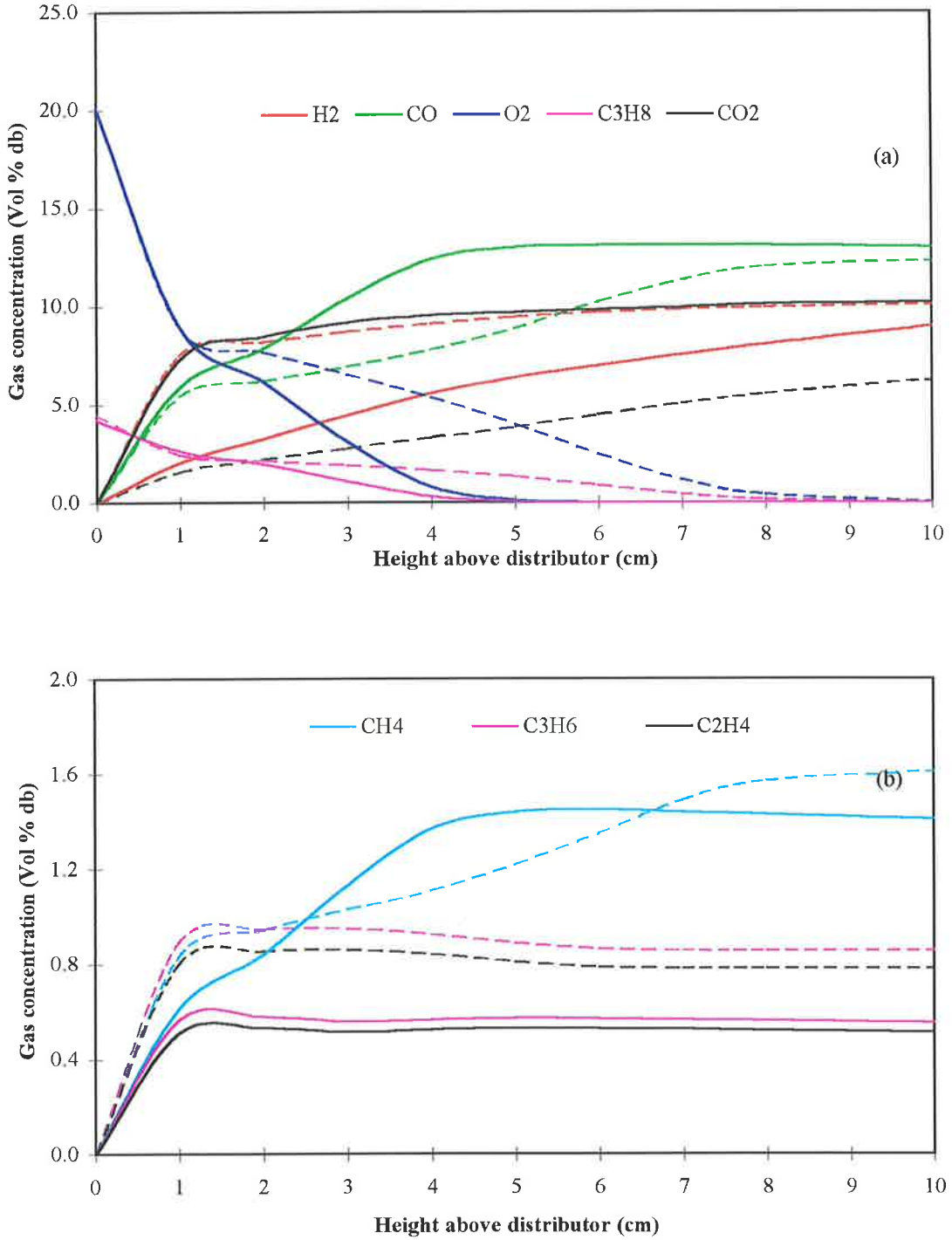

Figure 8.19 Comparison of model predictions of species profiles for two different mean bed particle sizes of 425 μm (solid line) (u_{mf} = 6 cm s^{-1}) and 775 μm (dash line) (u_{mf} = 25 cm s^{-1}) at 850°C during the co-gasification of propane and char at a constant excess fluidising velocity of 25 cm s^{-1}; (a) major species, (b) minor species.

For the large particle size, (u_{mf} = 25 cm s^{-1}, u_o = 50 cm s^{-1}) fluidisation state is $2\times u_{mf}$, while for the small particle size, (u_{mf} = 6 cm s^{-1}, u_o = 31 cm s^{-1}) fluidisation state is $5\times u_{mf}$. Therefore, bed hydrodynamics are different, in particular the bubble size which has a critical influence over mass and heat transfer rates in the bed and reported rates of propane combustion (Dennis et al., 1982). Yet, by maintaining similar fluidisation states the gas residence time is significantly different. As shown here and by others (van der Vaart, 1985; Srinivasan et al., 1998), conversion is a strong function of the gas residence time. The observed effect of particle size for a given excess fluidising velocity may be explained by the increasing minimum fluidisation velocity (u_{mf}) with particle size thus, increasing the relative proportion of gas flowing into the emulsion phase. As combustion rates are slower in the emulsion phase due to competition with char for available oxygen, the resulting outcome is a reduction in conversion with increasing particle size from chemical loss through by-passing in the emulsion phase. Furthermore, char combustion rates change with bed particle size (Schluter et al. 1996; Kulasekaran et al. 1999). In a bubbling fluidised bed, a solids convective heat transfer component exists which acts to increase the heat transfer rate.

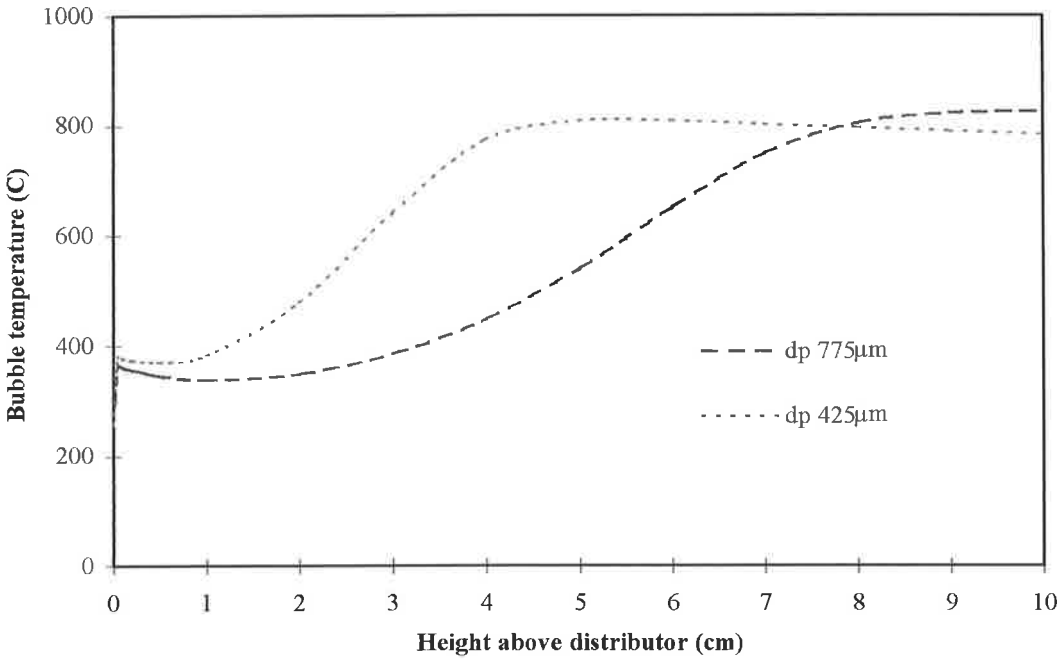

Figure 8.20 Comparison of predicted bubble temperature profiles for a mean bed particle size of 425 µm (u_{mf} = 6 cm s^{-1}) and 775 µm (u_{mf} = 25 cm s^{-1}) at 850°C at a constant excess fluidising velocity of 25 cm s^{-1}.

However, the mass transfer rate depends only on the minimum fluidisation velocity. Thus, for a given heat transfer rate, char combustion rates increase with particle size (u_{mf}) as char particles reside only in the dense phase which is in contact with gas flowing at the minimum fluidisation velocity (Schluter et al. 1996). To support this present view, a comparison of the normalised plot for the predicted reaction rates of oxygen consumed via heterogeneous and homogeneous reactions over the total oxygen consumed as a function of bed height for varying particle size is shown in Figure 8.21. This result clearly identifies an increase in the char combustion rate with increasing particle size lending further support that decreasing the bed particle size increases in-bed combustion efficiency of volatiles. Clearly more work in this area is required. However, this is a factor of concern more so for FBC applications than FBG, as the inert bed particle size is an operating variable, while for a FBG the size distribution is intrinsic to the ash/bed characteristics developed during operation.

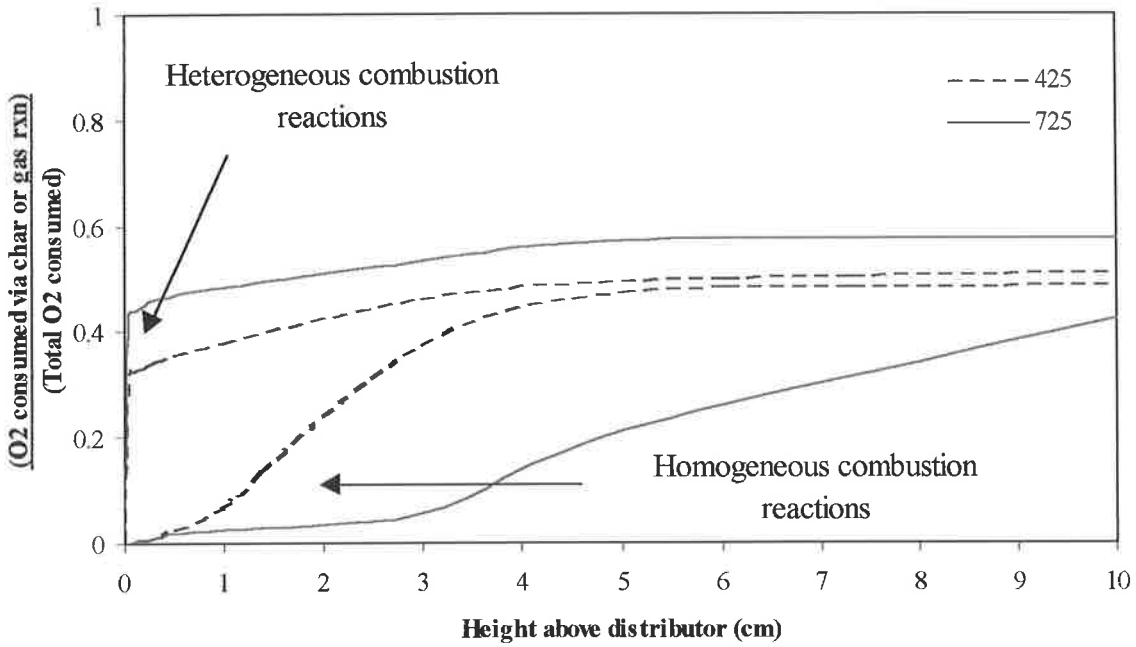

Figure 8.21 Normalised plot for the predicted reaction rates of oxygen consumed via heterogeneous and homogeneous reactions over the total oxygen consumed as a function of bed height for varying particle size.

The results of varying the excess fluidising velocity, $u\text{-}u_{mf}$ of 20 cm s^{-1} (dashed line), 25 cm s^{-1} (broken line) and 30 cm s^{-1} (solid line) at 850°C during the co-gasification of propane and char for a constant bed particle size of 425 μm are shown in Figure 8.22.

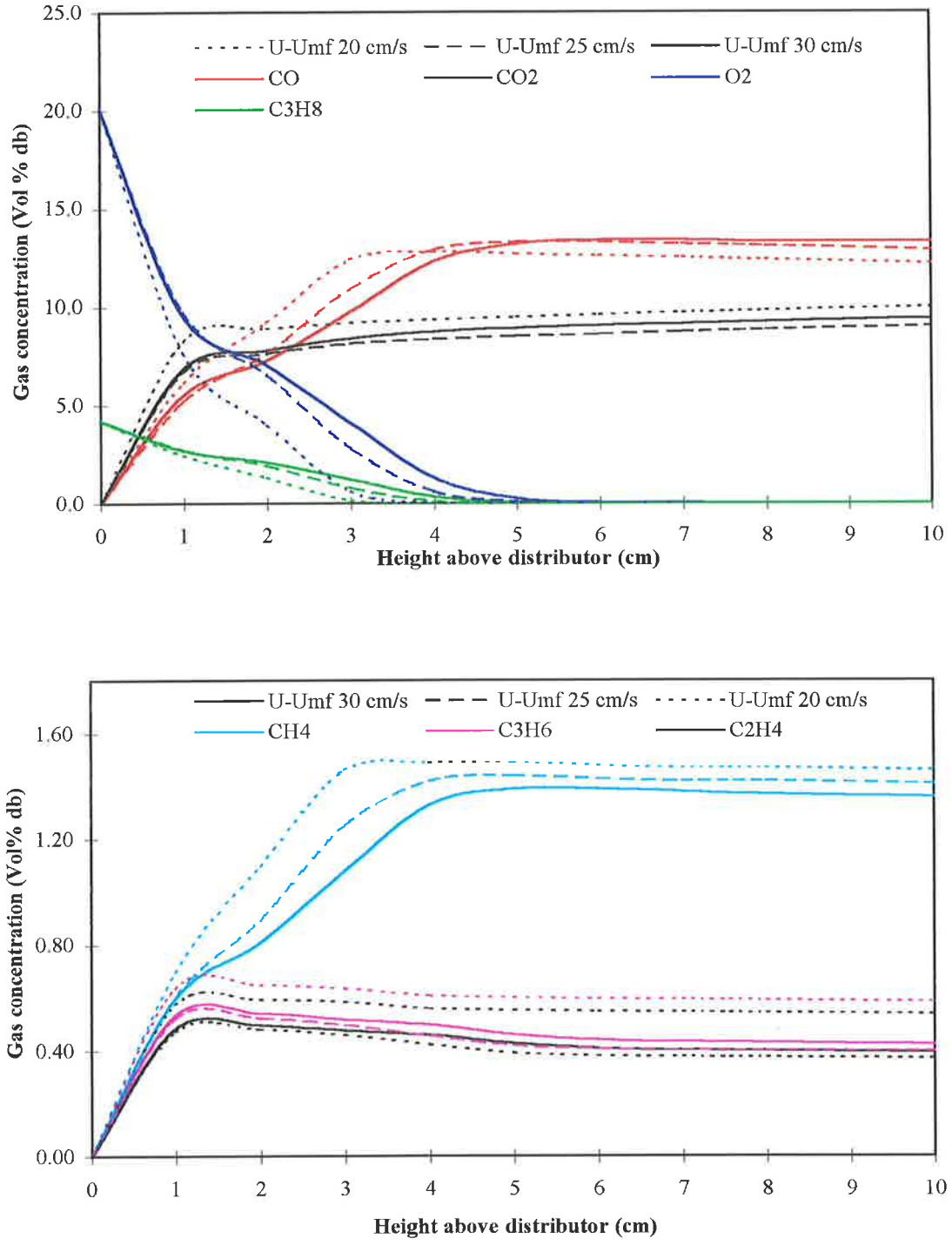

Figure 8.22 Comparison of model predictions of species profiles for various excess fluidisation velocities, u-u_{mf} of 20 cm s^{-1}, 25 cm s^{-1} and 30 cm s^{-1} at 850°C during the co-gasification of propane and char for a constant bed particle size of 425 µm (u_{mf} = 6 cm s^{-1}); (a) major species, (b) minor species.

As the profiles indicate, increased conversion occurs as the excess fluidising velocity is reduced. Once again this was observed experimentally by van der Vaart (1985) for propane combustion in a FBC and predicted in the models developed by van der Vaart, (1985) and Srinivasan et al. (1998).

The reduction in homogeneous combustion reaction rates with increasing excess fluidising velocities primarily decreases the reactant residence time thereby manifested as a decrease in in-bed conversion. The bubble will penetrate further into the bed before heating to an equivalent temperature as compared to a lower fluidising velocity. Furthermore, any increase in gas flow will directly pass through to the bubble phase as emulsion phase gas flow is hydrodynamically capped. This increases the amount of sensible heat required to heat the bubble gas and changes heat and mass transfer rates in the bed due to the increase in bubble volume fraction.

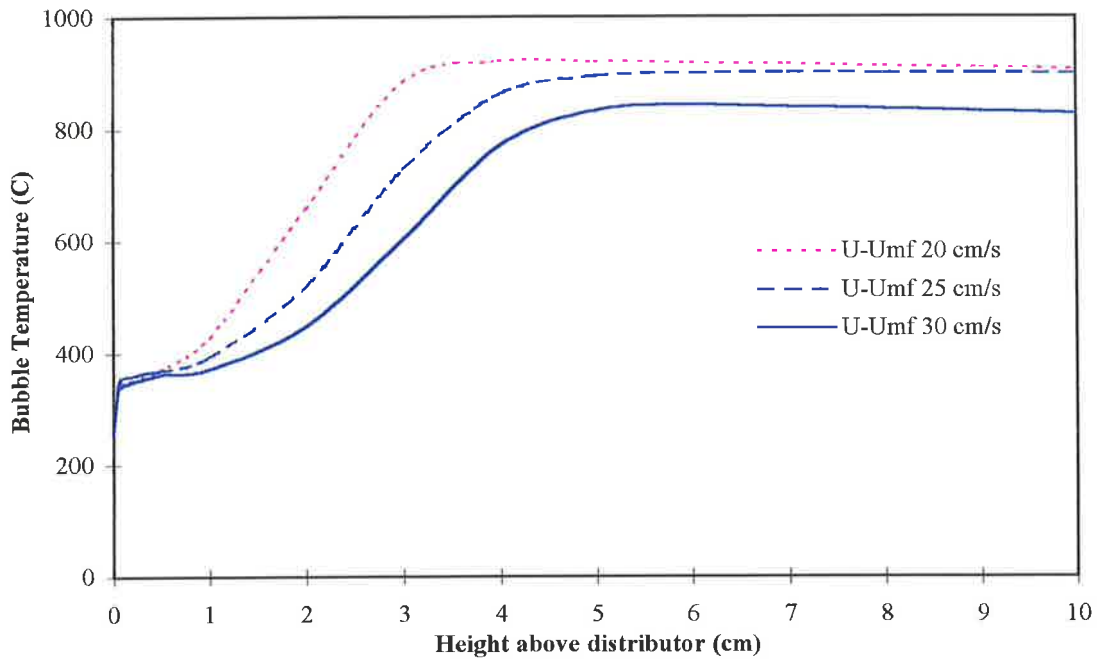

Figure 8.23 Comparison of predicted bubble temperatures for various excess fluidisation velocities, u-u_{mf} of 20 cm s^{-1}, 25 cm s^{-1} and 30 cm s^{-1} at 850°C during the co-gasification of propane and char for a constant bed particle size of 425 µm (u_{mf} = 6 cm s^{-1}).

A summary on the effect of the variation in superficial velocity and bed particle size on model output parameters for co-gasification of propane and char is outlined in Table 8.4. As expected, promoting the in-bed combustion efficiency of volatile matter permits greater availability of char for conversion through gasification reactions. The higher rates of oxygen consumption due to homogeneous reactions close to the distributor influences char combustion conversion rates correspondingly more so than gasification yields. However, this is not surprising given the balance of competition for the complete consumption of oxygen between heterogeneous and homogeneous reactions and that maximal gasification conversion favours the higher operating temperature of 950°C.

Table 8.4 A summary on the effect of the variation in superficial velocity and bed particle size on model output parameters for co-gasification of propane and char.

Parameter	T_{bed} (°C)	850 C	850 C	850 C	850 C
	$u-u_{mf}$ (cm/s)	25	25	20	30
	dp (μm)	775	425	425	425
O_2 consumption by char combustion / Total O_2 consumption rate	%	57.6	50.9	46.2	52.7
Total carbon conversion	%	84.0	80.9	78.8	80.9
Carbon conversion due to gasification reactions	%	26.7	32.4	32.0	30.1
Carbon conversion due to combustion reactions	%	57.3	48.5	46.8	50.8
Excess gas expansion due to 'Net flow'	%	13.0	14.2	13.9	13.5

8.5 SUMMARY

A comparison of the predictions from a non-isothermal model for gas combustion in a fluidised-bed gasifier against experimental data collected for char and co-propane and char gasification at three bed temperatures of 750°C, 850°C and 950°C was presented.

For char gasification conditions, model results under predicted the oxygen consumption rate, primarily due to the uncertainties in the choice of the product distribution coefficient, ϕ, for the CO/CO_2 combustion products in the char partial combustion reaction scheme. The majority of oxygen consumed in the bed, between 78 % to 99 %, was by heterogenous partial combustion reactions of char. At the lowest bed temperature, carbon conversion was dominated by combustion reactions, with an increasing contribution by gasification to the total carbon conversion with increasing temperature.

Sensitivity analysis on the influence of kinetic parameters on the model predictions, found that the kinetic representation of van der Vaart (1985), on which the reaction scheme was based on, resulted in either a poor agreement with experimental data or caused convergence problems for the energy balance equations. It was determined that for all Reactions (9) to (13), representative of the propane and intermediate species decomposition and partial combustion reaction scheme, the reaction rates were too fast. A best-fit kinetic representation for propane combustion at 850°C was subsequently determined through minimisation of the total sum-squared error by changing the pre-exponential factor in accordance with conclusions of van der Vaart (1985). Based on the sensitivity studies, the best set of frequency factors for propane decomposition and combustion kinetic expressions appropriate for the gasification environment is 1.0×10^{10} mol s^{-1} for methane combustion and propane decomposition (Reactions (9) to (11)) and 1.0×10^{11} mol s^{-1} for propylene and ethylene combustion (Reactions (12) to (13)), respectively.

The importance of secondary decomposition reactions on the combustion rates of volatiles was accordingly highlighted, consistent with the experimental findings reported by Cho et al. (1995). In particular, the model predictions were most sensitive

to propane pyrolysis reactions as similarly observed by Srinivasan et al. (1988). In general the model predictions showed excellent agreement for the major species (CO, CO_2, C_3H_8 and O_2), however, the inclusion of a pyrolysis reaction scheme for C_3H_6 and C_2H_2 intermediates would be seen to improve the model for propane combustion in a fluidised-bed.

Model predictions for co-gasification of propane and char were very good for the higher bed temperatures of 850°C and 950°C, associated with stable in-bed combustion of propane. At 750°C, the model predicts significant homogeneous combustion to have occurred, primarily associated with hydrocarbon intermediate species. This contradicts experimental observations reported here and elsewhere in the literature, where little combustion of propane (and intermediates) occurs within the bed at temperatures below the critical bed temperature for propane of 830°C (Hayhurst, 1991; Dennis et al., 1982; Hesketh et al., 1991; van der Vaart, 1985, 1988, 1992).

Most importantly, the addition of propane to simulate the volatile matter released from coal during devolatilisation, results in an increasing proportion of oxygen consumption by homogeneous rather than heterogeneous combustion reactions. This results in an increase in availability of char to undergo gasification reactions, subsequently showing an increase in carbon conversion due to gasification over the sole gasification of char. Thus, the importance of increasing the in-bed combustion efficiency of volatiles upon char combustion and gasification rates and the oxygen consumption distribution between volatiles and char has been successfully demonstrated for the FBG of coal.

Parametric studies on the effect of bed particle size and excess fluidisation velocity have shown that decreasing both parameters favours an increase in the in-bed combustion efficiency of propane. However, the information regarding the measured temperature profiles of gases in the fluidised-bed coal gasifier has been neither measured in the experiments nor found in the literature, and this leads to some difficulties for the verification of the predicted temperature profiles from the model.

CHAPTER 9

CONCLUSIONS AND RECOMMENDATIONS

9.1 SUMMARY

The work presented in this study has been aimed at understanding the behaviour of volatile matter, as simulated by propane, on the performance of a fluidised-bed gasifier. In particular, the competition for oxygen between char and volatile matter and the balance between char combustion and gasification reactions on the total carbon conversion. Chapter 2 reviewed the published literature with respect to in-bed volatile combustion in bubbling fluidised-beds and its subsequent modelling, with particular emphasis on devolatilisation times of mm-sized low-rank coal particles and the combustion behaviour of pre-mixed hydrocarbon gas mixtures. The principal limitations of the present status of research were thus defined. The most distinctive of these areas are:

1. The development of a suitable theory supported by a simple, reliable, quantitative technique to characterise the rate of devolatilisation for low-rank coal particles under a variety of experimental conditions.
2. An immediate need for an experimental investigation to quantify the gas phase reactions of volatiles in environments simulating fluidised-bed gasifiers and its impact on char combustion and gasification rates.
3. The development of a suitable FBG model which can satisfactorily account for homogeneous reactions of volatiles, which otherwise have been either ignored or poorly treated in the literature.

Chapter 3 outlined the experimental apparatus used and the techniques employed in this study. A very significant but largely unreported proportion of time and effort was spent on the development of the experimental system. Four low-rank coals, a Bowmans coal from South Australia and Morwell, Loy Yang and Yallourn coals from Victoria were used in the experimental investigations.

The time taken for a coal particle to devolatilise along with coal particle mixing within the bed determines the locations of volatile release to the bed for subsequent mixing with oxygen and combustion (Stubington et al., 1997). Understanding the effects of various coal and bed properties on the devolatilisation time and the mechanisms controlling devolatilisation of large coal particles pertinent to fluidised-bed applications remains unclear. Chapter 4 outlined a new experimental technique and definition to measure the devolatilisation times of coal particles of various sizes in a fluidised-bed. This was based on measuring the centre particle temperature history during devolatilisation. Furthermore, a new theoretical definition for the devolatilisation time has been presented. This was based on a theoretical treatment that distinguishes between heat transfer and chemical-kinetically controlled regimes during devolatilisation, by comparing the ratio of particle evolution/heat-up times to the ratio of Biot to the modified Damkohler number (Heidenreich, 1999).

As a consequence of the transition of volatile combustion to within the bed as temperature increases, the oxygen distribution and consequently the char combustion reaction rate will be affected. The volatiles compete with char for the available oxygen in the bed. Chapter 5 measured the weight loss of a batch of particles with time. The subsequent particle burn-out times and combustion rate characteristics were evaluated.

Numerous experimental investigations have been conducted to elucidate factors affecting the rate and location of gas phase oxidation reactions of coal volatiles released under FBC conditions. These studies have primarily focused on the introduction of premixed stoichiometric proportions of synthetic volatiles such as propane and methane with air. An in-bed water cooled probe was used to measure steady-state axial concentration profiles of stable chemical species at various bed temperatures with and without char feed to the bed. The experimental results reported here are believed to provide the first comprehensive data on volatiles combustion under fluidised-bed gasification conditions. Such data is required to develop a realistic model of volatile combustion process and to independently test model predictions.

A useful first step to the more complex problem of inclusion of the concentration distribution of volatile release within the bed, is to consider a substitute sub-model of the behaviour of pre-mixed homogeneous combustion of gas in a fluidised-bed as a test for validation of reactor models (Van der Vaart, 1992; Srinivasan et al., 1998). A non-isothermal numerical model of pre-mixed gas combustion under fluidised-bed gasification conditions, based on the two-phase theory of fluidisation incorporating the 'net flow" concept and temperature and concentration dependent thermodynamic properties was developed in Chapter 7 (Yan et al. 1998b, 1999b, 1999c). In Chapter 8, a comparison of model predictions on the variation of O_2, CO, CO_2, C_3H_8, CH_4, C_3H_6 and C_2H_4 concentrations with bed height for char gasification and co-gasification of propane and char is made with experimental data collected in Chapter 6.

9.2 CONCLUSIONS

The following conclusions may be drawn from the results of the work presented in this thesis:

9.2.1 DEVOLATILISATION TIME

- Bed temperature, oxygen concentration, particle size, moisture content and coal rank were found to influence the devolatilisation time.
- The devolatilisation time was found to be directly proportional to the particle diameter when correlated using the classic empirical particle diameter power law relation $t_v = Ad_p^n$
- This result is contrary to current theory based on heat transfer control, which defines a square law relationship.
- From a comparison of the current technique with the flame extinction time and CO_2 profile measurement techniques for the coal devolatilisation time, discrepancies in the reported exponent *n* have been resolved due to differences in the definition of the endpoint.
- The effect of coal type and coal moisture on the variation of reported exponent values have also been highlighted.

- A new theoretical treatment to distinguish between heat transfer and chemical-kinetically controlled regimes of coal devolatilisation based on the ratio between the 95% evolution time, t_{95} and the time required for 95% heating of the particle centre, T_{95}, versus the modified Damkholer number to Biot number ratio has been used to derive an analogous equation to that of the empirical power-law correlation of the form.

$$T_{95} = \left[6250\, t_{95} \left(\frac{r' \rho_0 C_p}{h_o} \right)^{0.94} \right] d_p^{0.94}$$

- The new theoretical treatment directly verifies current experimental observations of the observed proportionality between the devolatilisation time and particle diameter.
- It is now possible to quantitatively define the correlation parameter A, and explain the experimental observations relating to the influence of bed temperature and gas atmosphere upon the devolatilisation time.
- The observed effects of these variables are consistent with that of heat transfer to and within the particle as the rate controlling step for large particle devolatilisation in fluidised-beds.

9.2.2. Influence of Volatiles on the Combustion Rate of Char

- A comparison of the single particle burn-out times of char as a function of bed temperature showed good agreement to the data of Hesketh et al. (1991).
- It was found that the char burnout times increased substantially, between 13 to 88%, as the bed operating temperature was raised from 700°C to 900°C, respectively, upon the introduction of 3% v/v propane into a nitrogen diluted, 10 % v/v oxygen air fluidising stream.
- The increasing difference in the burnout times with increasing bed temperature is associated with the transition of over-bed to in-bed combustion of propane.
- At the highest bed temperature of 900°C, the rate of char combustion is diffusion-controlled
- The influence of chemical kinetics is evident at the lower bed temperatures.

- The ash layer formed during char burn-out does not impose any additional resistance on the char combustion rate.

9.2.3. PRE-MIXED COMBUSTION OF PROPANE IN FBG

- For all conditions studied, propane conversion, whether via thermal cracking or oxidation reactions, increased with increasing bed height and temperature.
- For the lowest bed temperature of 750°C under propane gasification conditions, propane conversion is characterised by a sudden explosive reaction at the bed surface, consistent with the literature results under FBC conditions.
- As the bed temperature is successively increased to 850 and 950°C, propane conversion occurs increasingly throughout the bed to carbon monoxide and carbon dioxide.
- Introduction of char feed to simulate the gasification environment results in the rapid consumption of oxygen by both heterogeneous and homogeneous reactions.
- At the lowest bed temperature of 750°C, char combustion reactions dominates over gasification reactions.
- With increasing bed temperature, gasification reactions play an increasing role, with associated carbon monoxide concentration increasing and final yield being correspondingly higher as compared to char gasification only. This indicates the relative contribution of partial volatile combustion to carbon monoxide yields.
- The char bed was found to enhance secondary decomposition reactions.

9.2.4. MODELLING PRE-MIXED PROPANE COMBUSTION IN A FBG

- For char gasification conditions, model results under predicted the oxygen consumption rate primarily due to the uncertainties in the choice of the product distribution coefficient, ϕ, for the CO/CO_2 combustion products in the char partial combustion reaction scheme.
- The majority of oxygen consumed within the bed was by heterogenous partial combustion reactions.

- At the lowest bed temperature, carbon conversion was dominated by combustion reactions, with an increasing contribution by gasification to the total carbon conversion with increasing temperature.
- Sensitivity analysis on the influence of kinetic parameters on the model predictions found that the kinetic representation of van der Vaart (1985) resulted in poor agreement or caused convergence problems for the energy balance equations.
- The model predictions were most sensitive to propane pyrolysis reactions as similarly observed in the literature (Srinivasan et al., 1988).
- In general the model predictions showed excellent agreement for the major species (CO, CO_2, C_3H_8 and O_2)
- For the minor species, in particular C_2H_4 and C_3H_6 hydrocarbon intermediates, the incorporation of a pyrolysis reaction scheme would be expected to improve the model predictions.
- Model predictions for co-gasification of propane and char were very good for the higher bed temperatures of 850°C and 950°C, associated with stable in-bed combustion of propane.
- At 750°C, the model calculates that a significant proportion of homogeneous combustion occurs within the bed, primarily associated with hydrocarbon intermediate species, contrary to experimental observations.
- Most importantly, the addition of propane resulted in an increasing proportion of oxygen consumed by homogeneous rather than heterogeneous partial combustion reactions. The resultant increase in availability of char to undergo char gasification reactions, leads to an increase in carbon conversion due to gasification.
- The importance of increasing the in-bed combustion efficiency of volatiles upon char combustion and gasification rates and oxygen consumption distribution between volatiles and char has been successfully demonstrated for FBG of coal.
- Parametric studies on the effect of bed particle size and excess fluidisation velocity have shown that decreasing both parameters favours an increase in the in-bed combustion efficiency of propane, consistent with literature findings of van der Vaart (1985) and Srinivasan et al. (1998).

9.3 EVALUATION AND IMPLICATIONS OF THE PRESENT WORK

The present work represents a rigorous investigation and developmental study, which can be seen to improve the present status of knowledge in the following areas;

- The development of an improved technique for measuring the devolatilisation times of large coal particles and a thorough investigation of the role of a number of influencing parameters.
- The development of a new theoretical treatment which directly verifies current experimental observations of the proportionality between the devolatilisation time and particle diameter. Furthermore, for the first time quantitatively defined the correlation parameter A, and explain experimental observations relating to the influence of bed temperature and gas atmosphere upon the devolatilisation time
- The generation of a comprehensive set of experimental data on the combustion and decomposition behaviour of a simulated volatile (propane) and its influence on the carbon conversion balance between char combustion and gasification reactions under FBG conditions.
- A non-isothermal mathematical model based on the two-phase theory of fluidisation accounting for gas combustion in a FBG was successfully developed.
- A thorough validation of the model predictions with experimental data and an alternative kinetic representation for propane combustion was proposed.

The results of this work have a number of implications in terms of the operational behaviour of a fluidised-bed gasifier. The accurate prediction of devolatilisation time will have ramifications relating to coal particle feed spacing in the bed in context to volatile dispersion and subsequent in-bed combustion efficiency of volatiles. The results from the volatile combustion experiments on the influence on char combustion rates and oxygen distribution between heterogeneous and homogeneous combustion reactions have indicated the importance of volatiles to the overall carbon conversion efficiency.

By promoting in-bed combustion of volatile matter, more char undergoes gasification reactions. Thus, the future design and operational parameters of fluidised-bed gasifiers should take into account the consideration of maximising the in-bed combustion efficiency of volatiles to improve carbon gasification efficiency.

It is considered therefore, that this thesis has made a significant contribution to the science of low-rank coal devolatilisation and the behaviour and interaction of volatile matter within a fluidised-bed gasifier.

9.3 RECOMMENDATIONS FOR FUTURE WORK

Based on the experimental and modelling experience and findings of this thesis, the following areas are highlighted for possible future investigations:

- Experimental investigation of secondary decomposition reactions of volatiles in a fluidised-bed environment. In particular, the interaction of bed material on condensation reactions. The influence of various operating parameters upon composition and product yields should be investigated.
- The provision for more experimental validation of volatile matter combustion under fluidised-bed gasification conditions, particularly under high pressure and extension into the combustion behaviour of real coal volatile products.
- Characterisation of the possible catalytic effects of Ca-based desulphurisation sorbents on in-bed volatile combustion efficiency.
- Suitable experimental development to obtain kinetic data and expressions to represent coal volatile matter decomposition and partial combustion in a fluidised-bed.
- The incorporation of particle dispersion and finite devolatilisation sub-models, to form a truly realistic and comprehensive FBG model.
- The determination of the CO/CO_2 product ratio for the char partial combustion reactions under conditions representative of a fluidised-bed gasifier.

NOMENCLATURE

Symbol	Description	Units
a_s	Specific particle surface area	m^2m^{-3}
a_B	Interfacial area between bubble and emulsion phase	$m^2 m^{-3}$
A	Cross-sectional area of bed	m^2
A	Pre-exponential term (Equation 2.1)	$s\ mm^{-n}$
A_p	Surface area of particle	cm^2
Bi	Biot number	
c	Mean volatiles concentration (Equation 2.2)	$g\ cm^{-3}$
C	Gas concentration	$mol\ m^{-3}$
c_a	Mean specific heat of ash	$kJ\ kg^{-1}\ K^{-1}$
c_f	Mean specific heat of fixed carbon	$kJ\ kg^{-1}\ K^{-1}$
c_{v1}	Mean specific heat of primary volatile matter	$kJ\ kg^{-1}\ K^{-1}$
c_{v2}	Mean specific heat of secondary volatile matter	$kJ\ kg^{-1}\ K^{-1}$
C_p	Mean specific heat capacity	$J\ kg^{-1}\ K^{-1}$
$\overline{C}pi$	Mean heat capacity of gaseous component *i*	$J\ mol^{-1}\ K^{-1}$
C_{pi}	Heat capacity of gaseous components at temperature T	$J\ mol^{-1}\ K^{-1}$
d	Particle diameter	m
D	Effective mass diffusivity (Equation 2.2)	$cm^2\ s^{-1}$
D_{crit}	Critical bubble radius (Equation 2.20)	m
D_{gr}	Gas radial dispersion coefficient (Equation 2.18)	$m^2\ s^{-1}$
D_{sr}	Solid radial dispersion coefficient (Equation 2.18)	$m^2\ s^{-1}$
Da′	Modified Damkohler number	
D_{ij}	Binary diffusion coefficient	$m^2 s^{-1}$
Eo	Mean acitivation energy	$J\ mol^{-1}$
e	Emissivity	
f	Molar flow rate	$mol\ s^{-1}$
Fo	Fourier number	
F_c	$1-0.2756\omega + 0.059035\mu_r$ (Equation 6.20)	
h	Convective heat transfer coefficient (Equation 2.3)	$W\ m^{-2}K^{-1}$

h_{BE}	Interface heat transfer coefficient: bubble and emulsion	J m^{-3} K^{-1} s^{-1}
H	Bed height	m
$H_{gi,f}$	Enthalpy of gaseous components entering the bed	J mol^{-1}
$H_{gi,o}$	Enthalpy of gaseous components leaving the bed	J mol^{-1}
$H_{si,f}$	Enthalpy of the solids entering the bed	J mol^{-1}
$H_{si,o}$	Enthalpy of the solids removal rate exiting the bed	J mol^{-1}
h_p	Single particle convective heat transfer coefficient	J m^{-2} s^{-1} K^{-1}
k_{eff}	Effective thermal conductivity (Equation 2.3)	W m^{-1} K^{-1}
k_{BE}	Interface mass transfer coefficient: bubble and emulsion	m s^{-1}
k_c	Mass transfer coefficient	m.s^{-1}
M	Molecular weight	g.mol^{-1}
m_p	Particle mass	g
n	Power law parameter (Equation 2.1)	
n	Number of gas species in the system	
n_i, n_j	Molar fluxes	mol $m^{-2}s^{-1}$
Plu	Plume number	
Q	Enthalpy out due to heat loss	J mol^{-1}
Q_{hhv}	High heating value	kJ kg^{-1}
r′	Modified reaction rate (Equation 2.6)	s^{-1}
r_{Bj}	Homogeneous reaction rate in bubble phase	mol m^{-3} s^{-1}
r_{Di}	Reaction rates of homogenous reactions	mol m^{-3} s^{-1}
r_{Ej}	Homogeneous reaction rate in emulsion phase	mol m^{-3} s^{-1}
r_{Egj}	Rate of gasification reaction j in emulsion phase	mol $m^{-3}s^{-1}$
r_{Ecj}	Rate of char combustion reaction j in emulsion phase	mol $m^{-2}s^{-1}$
r_{Evj}	Rate of devolatilization reaction j in emulsion phase	mol $m^{-3}s^{-1}$
r_{vz}	Radius of volatile containing zone	m
R	Universal gas constant	J $mol^{-1}K^{-1}$
S	Stoichiometric coefficient	
t	Time	s
t_v	Devolatilisation time (Equation 2.1)	s
T	Temperature	K
T_{bi}	Normal boiling point of component i	K

u_b	Bubble rising velocity	m s^{-1}
u_0	Gas superficial velocity	m s^{-1}
u_{mf}	Minimum fluidisation velocity	m s^{-1}
V	Volume of solid phase in bed	m^3
V	Volatile matter evolved	kgkg^{-1} raw coal
V*	Total volatile matter evolved	kgkg^{-1} raw coal
V_p	Particle volume	m^3
V_{bi}	Liquid molar volume at normal boiling point	m^3 mol^{-1}
V_c	Critical volume	cm^3 mol^{-1}
w_i	Weight fraction of component *i* in the coal or char	
y_i, y_j	Mole fraction of gases	
z	Increment of bed height	m

Greek Symbols

α_{ij}	Stoichiometric coefficient of *i*th component in *j*th reaction	
σ	Stefan-Bolzman constant = 5.669×10^{8}	J m^{-2} s^{-1} K^{-4}
σ	Standard deviation in activation energy	J mol^{-1}
σ_i	Collision diameter of component i	A
δ	Volume fraction occupied by dilute phase	
ΔH_{in}	Sensible heat of gaseous components entering control volume	J mol^{-1}
ΔH_{net}	Sensible heat carried by the net flow	J mol^{-1}
ΔH_{out}	Sensible heat of gaseous components leaving control volume	J mol^{-1}
ΔH^0_{Bj}	Heat of reaction at 298 K, 1 atm in the bubble phase	J mol^{-1}
ΔH^0_{Ej}	Heat of reaction at 298 K, 1 atm in the emulsion phase	J mol^{-1}
ΔF	Net flow between phases	mol $m^{-3}s^{-1}$
ε	Volume fraction	
ε_I	Relative strength of intermolecular attraction	
μ	Viscosity	μP
μ_{pi}	Dipole momentum of component i	debyes

μ_r	Dimensionless dipole moment
Ω_v	Viscosity collision integral
Ω_D	Collision integral for diffusion
ω	Acentric factor

Super/Sub-scripts

B	bubble phase
b	bed
b	bulk
c	critical
conv	convective
E	emulsion phase
f	feed inlet
i	components
j	reaction numbers
m	mixture
mf	minimum fluidisation condition
o	product outlet
o	initial condition
p	particle(s)
rad	radiative
s	solid(s)
s	surface
∞	bulk gas

REFERENCES

Achara, N., Horsley, M.E., Purvis, M.R. and Teague, R., *Heat and Mass transfer in Fixed and Fluidised Beds*, ed. van Swaaij, W.P. and Afghan, N.H., 1985, 523.

Adesanya, B.A., and Pham, H.N., Mathematical modelling of devolatilization of large coal particles in a convective environment, *Fuel*, 1995, **74**, (6), 896-902.

Andrei, M.A., Sarofim, A.F. and Beer, J.M., Time-resolved burnout of coal particles in a fluidised bed, *Combustion and Flame*, 1985, **61**, 17-27.

Anthony, D.B., Howard, J.B., Hottel, H.C., and Meissner, H.P., Rapid devolatilization of pulverised coal, *Fifteenth Symposium (International) on Combustion*, The Combustion Institute, Pittsburgh, 1975, 1303.

Anthony, D.B. and Howard, J.B., Coal devolatilisation and hydrogasification, *AIChE*, 1976, **22**, (4), 625.

Agarwal, P.K. and Wildegger-Gaissmaier, A.E., *Chem Eng Res. Des*. 1987, **65**, 431.

Agarwal, P.K., Genetti, W.E. and Lee, Y.Y., Model for devolatilisation of coal particles in fluidised beds, *Fuel*, 1984(a), **63**, 1157.

Agarwal, P.K., Genetti, W.E. and Lee, Y.Y., Model for devolatilisation of coal particles in fluidised beds, *Fuel*, 1984(b), **63**, 1748.

Arthur, J.R., Reactions between Carbon and Oxygen, *Trans. Faraday Soc*., 1950, 164.

Baskakov, A.P., Filippovskii, N.F., Munts, V.A., and Ashikhmin, A.A., Temperature of particles heated in a fluidised bed of inert material, *J Engng Phys*, 1987, **52**, 574-578.

Basu, P., Burning rate of carbon in fluidised beds, *Fuel*, 1977, **56**, 390-392.

Batu. S.P., Shah, B and Talwalkar, A. , *AIChE Sym. Ser*, 1978, **74**, (176), 176-186.

Bautista-Margulis, R.G., Siddall, R.G. and Manzanares-Papayanopoulos, L.Y., Combustion modelling of coal volatiles in the freeboard of a calorimetric fluidised-bed combustor, *Fuel*, 1996, **75**, (15), 1737-1742.

Bhattacharya, S.P., Vuthaluru, H.B., Yan, H. and Kosminski, A., Preliminary results from CFBC pilot plant trials at Osborne, *Proc. 5th annual conf., CRC New Tech. for Power Generation from Low Rank Coal*, 1998, Report 98013, 201-206.

Berber, J., Rice R.L. and Fortney, D., Thermal cracking of low temperature pitch, *I & EC prod. res. devp.*, 1967, **6**, (3), 197-200.

Bi, J., Luo, C., Aoki, K.I., Uemiya, S. and Kojima, T., A numerical simulation of a jetting fluidised bed coal gasifier, *Fuel*, 1997, **76**, 285-301.

Bird, R.B., Stewart, W.E. and Lightfoot, E.N., *Transport Phenomena*, Wiley, New York, 1960, chap. 16.

Blackman, A.U., Smoot, L.D. and Yousefi, P., Rates of oxidation of millimetre sized char particle: simple experiments, *Fuel*, 1994, **73**, 602-612.

Borghi, G., Sarofim, A.F. and Beer, J.M., A model of coal devolatilisation and combustion in fluidised beds, *Combustion and Flame*, 1985, **61**, 1-16.

Brokaw, R.S., *Ind. Eng. Chem. Process Design Develop.*, 1969, **8**, 240.

Brockway, D.J., and Higgins, R.S., *The Science of Victorian Brown Coal: Structure, Properties and Consequences for Utilisation*, Butterworth-Heinemann Limited, Oxford, 1991, 248-273.

Broughton, J., *Applied Energy*, 1975, **1**, 61.

Brunello, I.F., Maissa, P. and Bruyet, B., Kinetic study of char combustion in a fluidised bed, *Fuel*, 1996, **75**, 536-544.

Bruno, C., Walsh, P.M., Santavicca, D.A., Sinha, N. and Yaw, Y., *Combustion Sci. and Tech.*, 1983, **31**, 43.

Bywater R.J., The effects of devolatilisation kinetics on the injector region of fluidised beds, *Int. Conf. Fluidised Bed Comb.*, Atlanta, 1980, **3**, 1092.

Calkins, W.H., Ehagaman and Zeldes, H., Coal flash pyrolysis 1. Indication of the olefin precursors in coal by ^{13}Cnmr spectroscopy, *Fuel*, 1984, **63**, 1113-1118.

Calkins, W.H., Coal flash Pyrolysis 3: An analytical method for polymethylene moieties in coal, *Fuel*, 1984, **63**, 1125-1129.

Caram, H. S. and Amundson, N. R. , *Ind. Eng. Chem. Process Des.Dev*, 1979, ***18***, 80-96.

Carangelo, R.M., Solomon, P.R., and Gerson, D.J., Application of TG-FT-i.r. to study hydrocarbon structure and kinetics., *Fuel*, **66**, 1987, 960-967.

Chatterjee, P. K., Datta, A. B., and Kundu, K. M., *Canadian. J. of Chem. Eng.*, 1995, **73**, 204-210.

Cho, S., Marlow, D. and Niksa, S., Buring Velocities of Multicomponent Organic Fuel Mixtures derived from Various Coals, *Combustion and Flame,* 1995, **101**, 399-410.

Chung, T.H., Lee, L.L. and Starling, K.E., *Ind. Eng. Chem. Fundam.*, 1984, **23**, 8.

Ciesielczyk, E. and Gawdzik, A., *Fuel*, 1994, **73**, 105.

Cliff, D.I., Doolan, K.R., Mackie, J.C. and Tyler, R.J., Products from rapid heating of a brown coal in the temperature range 400-2300°C, *Fuel*, 1984, **63**, 394.

Colin, P.J., Tyler, R.J. and William, M.A., Proton n.m.r. studies of tars from flash pyrolysis of three Australian coals, *Fuel* , 1980, **59**, 479-486.

Dagaut, P., Cathonnet, J., Boettner, J.C. and Gilliard, F., Kinetic modeling of propane oxidation, *Combust. Sci. and Tech*, 1987, **56**, 23-63.

Davidson, J.F.and Harrision, D., *Fluidised Particles*, 1963, Cambridge University Press, London.

Davidson, J.F., Clift, R., and Harrison, D. (ed), *Fluidisation 2nd ed.*, Academic Press, U.S., 1985, 158-338.

Dennis, J.S., Hayhurst, A.N. and Mackle, I.G., The Ignition and Combustion of Propane/Air Mixtures in a Fluidised Bed, *Nineteenth Symposium International on Combustion*, The Combustion Institute Pittsburgh, 1982, 1205-1212.

Derbyshire, F., JagFoyen, M. and Kimber, G., Coal: A resource for the production of carbon materials, *AIE 7th Australian Coal Science Conf.*, Dec. 1996, Gippsland, Australia, 37-44.

Dincer, I., Kilic, Y.A., and Kahveci, N., Heat transfer modelling of spherical particles subject to heating in a fluidized bed, *Int. Commun. Heat Mass Transfer*, 1996, **23**, 5, 705-712.

Doolan, K.R. and Mackie, J.C., Kinetics of pyrolysis of octane in argon-hydrogen mixtures, *Combust. Flame*, 1983, **50**, 29-39.

Eatough, C.N. and Smoot, L.D., Devolatilisation of large coal particles at high pressure, *Fuel*, 1996, **75**, (13), 1601.

Ekinci, E., Yalkin, G., Atakul, H., and Erdem-Senatalar, A., The combustion of volatiles from Turkish coals in a fluidised bed, *Journal Inst. Energy*, 1988, **61**, 189.

Essenhigh, R.H., The influence of coal rank on burning times of single captive particles, *J. Eng. Power*, 1963, **85**, 183.

Farina, L., IGCC: A commerical reality, *The Chem. Eng.*, Jan 1996, 13-14.

Figueiredo, J.L. and Moulijn, J.A., (Ed.), NATO ASI Series, Series E: Applied Sciences- No. 105 *Carbon and coal gasification*, Martinus Nijhoff Publishers, 1986, 181.

Fristrom, R.M. and Westenberg, A.A., Flame structure, 1965, McGraw-Hill USA.

Gavalas, G.R., Coal Pyrolysis, in *Coal Science and Technology*, **4**, Elsevier Scientific Publishing, 1982.

Froberg, R.W. and Essenhigh, R., *Seventeenth Symposium International on Combustion*, The Combustion Institute Pittsburgh, 1978, 179-187.

Gloe, C.S., and Holdgate, G.R., Geology and Resources, in *The Science of Victorian Brown Coal: Structure, Properties and Consequences for Utilisation*, Butterworth-Heinemann Limited, Oxford, 1991, 2-45.

Goyal, A., Retimaf, A., Knowlton, J.M., Leppin, D., Waibel, R.T. and Patel, J.G., *Fuel Processing Tech.*, 1987, **17**, 169-186.

Goyal, A., Byran, B.G. Rehmat, A. and Patel, J.G., *Energy Sources*, 1990, **12**, 161-179.

Griffiths, J., Gasification-here at last, *The Chem. Eng.*, Oct. 1996, 21.

Gururajan, V.S., Agarwal P.K. and Agnew, J.B., Mathematical modelling of fluidised-bed gasifiers, *Trans IChemE*, 1992, **70**, 211-238.

Haslam R.T. , *Ind. Engng. Chem*, 1923, **15**, 679.

Hadler, S. and Saha, R.K., Studies on mechanism of evolution and combustion of volatiles in fluidised bed combustor, *Indian Chem. Eng.*, 1993, **35**, (3), 145.

Haggerty, J. F. and A. H. Pulsifer, Modelling coal char gasification in a fluidised bed, *Fuel*, 1972, **51**, 304-307.

Hautman, D.J., Dryer, F.L., Schug, K.P. and Glassman, I., *Comb. Sci. and Tech.*, 1981, **25**, 219.

Hayhurst, A.N. and Tucker, R.F., *Combust. Flame,* 1990, **79**, 175-185.

Hayhurst, A.N., Does carbon monoxide burn inside a fluidised bed? A new model for the combustion of coal char particles in fluidised beds, *Combust. Flame,* 1991, **85**, 155-168.

Heidenreich, C.A., *Mathematical modelling of large low-rank coal particle devolatilisation*, PhD Thesis, Department of Chemical Engineering, The University of Adelaide, Australia, 1999.

Heisler H.,P., *ASME*, 1947, **69**, 227-236.

Hesp, W.R. and Water, P.L., Thermal cracking of tars and volatile matter from coal, *Ind. Eng. Chem. Prod. Res. Develop.*, 1970, **9**, 194-202.

Hesketh, R.P. and Davidson, J.F., The effect of volatiles on the combustion of char in a fluidised bed, *Chem. Eng. Sci.*, 1991, **46**, 3103-3113.

Hesketh, R.P. and Davidson, J.F., Combustion of methane and propane in an incipiently fluidised bed, *Combust. Flame,* 1991, **85**, 449-467.

Holman, J.P., *Heat Transfer*, 7th Edition, McGraw-Hill Publishing Company, New York, 1990.

IGT Coal Conversion Technical Data Book, 1978

Jeng, R.S. and Altwicker, E.R., Propane combustion in a spouted bed combustor: Experimental and Modeling aspects in the bed region, *AIChE*, 1997, paper 187g.

Jess, A., Mechanisms and kinetics of thermal reactions of aromatic hydrocarbons from pyrolysis of solid fuels, *Fuel*, 1996, **75**, (12), 1441-1448.

Johnson, J.L., *Kinetics of Coal Gasification*, 1979, The Institute of Gas Technology, John Wiley & Sons, New York.

Juntgen, H., Review of the kinetics of pyrolysis and hydropyrolysis in relation to the chemical constitution of coal, *Fuel*, 1984, **63**, 731-737.

Juntgen , H., and van Heek, K.H., *Fuel Processing Technology*, 1979, **2**, 261.

Katheklakis, L., Shi-Lin, Bartle, K.D. and Kandiyoti, R., Effect of freeboard residence time on the molecular mass distributions of fluidised bed pyrolysis tars, *Fuel*, 1990, **69**, 172-176.

Karim, G.A. and Mohindra, D., *Journal of the Institute of Fuel*, 1974, **47**, 219.

Keller, J., Diversification of feedstocks and products: recent trends in the development of solid fuel gasification using the TEXACO and the HTW process, *Fuel Processing Tech.*, 1994, **24**, 247-268.

Kilic, Y.A., Kahveci, N., Dincer, I., and Bardakci, T., An investigation of transient heat transfer between a spherical coal particle and air medium during devolatilization, *Int. Commun. Heat and Mass Transfer*, 1993, **20**, 711-720.

Kobayashi, H., Howard, J.B. and Sarofim, A.F., Coal Devolatilization at High Temperatures, *Eighteenth Symposium (International) on Combustion*, The Combustion Institute, Pittsburgh, 1977, 411.

Kojima, T., Uemiya, S. and Matuskata, M., Analysis and control of local reactions in a fluidised bed gasifier, *Conf. Proc. Energy Conversion and Utilisation*, 1993, B01-12, 69-73.

Kozlov, G.I., *Seventh Symp. (Intl.) on Combustion*, The combustion Institute, Pittsburgh, 1959, **7**, 142.

Kulasekaran, S., Linjewile, T.M., Agarwal P.K., Mathematical modelling of fluidised bed combustion 3. Simultaneous combustion of char and combustible gases, *Fuel*, 1999, 78, 403-417.

Kunii, D. and Levenspiel, O., *Fluidisation Engineering*, 2nd edition, Butterworth-Heinemann, Boston, 1991.

LaNauze, R.D., Coal Devolatilisation in Fluidised-Bed Combustors, *Fuel*, 1982, **61**, 771.

La Nauze, R.D and Jung, K., The kinetics of combustion of petroleum coke particles in a fluidised-bed combustor, *Nineteenth Symposium (International) on Combustion*, The Combustion Institute, Pittsburgh, 1982, 1087-1092.

La Nauze R.D. and Jung, K., Combustion kinetics in a fluidised bed, *Proc. 7th Int. Fluidised Bed Conf.*, DOE/MMCT/83-84, 1983, **2**, 1040-1053.

La Nauze, R.D. Fundamentals of coal combustion in fluidised beds, *Chem. Eng. Res. Des.*, 1985, **63**, 3-33.

Linjewile, T.M., *Temperature of burning carbonaceous particles in a fluidised bed combustor*, Ph.D. Thesis, Department of Chemical Engineering, University of Adelaide, Australia, 1993.

Longwell, J.P. and Weiss, F.J., *Ind. And Eng. Chem*, 1955, **47**(8), 1634.

Lowry, H. H. (editor), *Chemistry of Coal Utilisation*, 1963, Supplementary Volume, John Wiley & Sons, New York, NY.

Lufei, J., Becker, H.A., and Code, R.K., Devolatilization and Char Burning of Coal Particles in a Fluidised Bed Combustor, *Canadian Journal Chem. Eng.* 1993, **71**, 10.

Ma, R. P., Felder R. M., and Ferrell, J. K., *Fuel Processing Tech,* 1988, **19**, 265-290.

Mackay, G., 1996, Geology and Petrology of Coal Deposits, Short course: *The Science and Technology of Low-Rank Coal*, Monash University, Melbourne, Feb 19-22, 1996.

Makhorin, K.E. and Khinkis, P.A., *Heat and Mass transfer in Fixed and Fluidised Beds*, ed. van Swaaij, W.P. and Afghan, N.H., 1985, 545.

Matsui, I., Kojima, T., Kunii, D. and Furusawa, T. , 1987, *Ind. Eng. Chem. Res., 1987,* **26**, 95-100.

Matsukata M., Honda, Y., Yoshitake, H. and Kojima, T., Performance of a fluidised bed coal gasifier with various ways of gas introduction, *Fuel Processing Tech.*, 1993, **36**, 227-233.

McIntosh, M., Technology development for power generation, *CRC for New Technologies for Power Generation from Low-Rank Coal*, 5th Annual Conf., Report No. 98013, 1998, 11-15.

Megalos, N., PhD Thesis, Department of Chemical Engineering, University of Adelaide, Australia, 1998.

Merry, J. M. D., 1975, *AIChE J, 1975,* **21**, (3), 507.

Mitchell, D.R., Coal Preparation, *American Institute of Mining, Metallurgy and Petroleum Engineers*, 1984, New York..

Mori, S. and Wen, C. Y. , 1975, *AIChE Journal , 1975,* **21**, 109-115.

Morris, J.P., and Keairns, D.L., Coal devolatilisation studies in support of the Westinghouse FBCG process, *Fuel*, 1979, **58**, 465.

Neogi, D., Chang, C.C., Walawender, W.P. and Fan, L.T., Study of coal gasification in an experimental fluidised bed reactor, *AIChE J.,* 1986, **32**, 17-28.

Newmann, L.L., *Ind. Eng. Chem.*, 1948, **40**, 559.

Nienow, A.W., Rowe, P.N. and Chiba, T., Mixing and segregation of a small proportion of large particles in gas fluidised beds of considerably smaller ones, *AIChE Symp. Ser.*, 1978, **74**, (176), 45-53.

Ogada, T. and Werther, J., Combustion characteristics of wet sludge in a fluidised bed: Release and combustion of the volatiles, *Fuel*, 1996, **75**, (5), 617-626.

Overturf, B.W. and Reklaitis, G.V., *AIChE Journal* , 1983, **29**, 820.

Panagakis, G., B.E. Thesis, University of New South Wales, 1995.

Park, K.Y. and Edgar, T.F., *Ind. Eng. Chem. Res.*, 1987, **26**, 237.

Park, D., Levenspiel, O. and Fritzgerald, T.J., Plume Model for Large Particle Fluidised Bed Combustor, *Fuel*, 1981, **60**, 295.

Peeler, P.K., personal communication

Perry, R.H. and Green, D., Perry's Chemical Engineers' Handbook, 6th Edition, McGraw Hill Publishers, New York, 1984.

Petrakis, L. and Grandy, D.W., Free radicals in coals and synthetic fuels, *Coal Science and Technology*, **5**, Elsevier Sci. Pub., The Netherlands, 1983, 27-30.

Pillai, K.K., Journal Inst. Energy, 1976, **49**, 200.

Pillai, K.K., The influence of coal type on devolatilisation and combustion in fluidised beds, *Journal Inst. Energy*, 1981, **54**, 142.

Pillai, K.K., A schematic for coal devolatilisation in fluidised bed combustors, *Journal Inst. Energy*, 1982, **55**, 132-133.

Pillai, K.K., Devolatilization and combustion of large coal particles in a fluidised bed, *Journal Inst. Energy*, 1985, **58**, 3.

Prins, W., Fluidised bed combustion of a single carbon particle, PhD Thesis 1987, Twente University, The Netherlands.

Prins, W. Siemons, R. and van Swaaij, W.P.M., Devolatilisation and ignition of coal particles in a two-dimensional fluidised bed, *Combustion and Flame*, 1989, **75**, 57-79.

Pukanic, G. W., Cobb, J. T. , Haynes, W. P., and Strakey, J. P. , *71st Annual AIChE meeting*, Miami, 1978.

Purdy, M. J., Felder, R. M., and Ferrell, J. K. , *Ind. Eng. Chem. Process Des. Dev., 1981, **23**,* 267-293.

Purdy, M. J., Felder, R. M., and Ferrell, J. K. , *Ind. Eng. Chem. Process Des. Dev., 1981, **20**,* 675-682.

Ranz W.E. and Marshall, W.R., *Chem. Eng. Prog*, 1952, ***48***, 173.

Reid, R.C., Prausnitz, J.M. and Poling, B.E., *The properties of gases and liquids*, 1988, 4th Edition, McGraw-Hill, Singapore.

Roberts, P.T., Shiril, L.C. and Cowley, L.T., *Combustion and Flame,* 1987, **69**, 243.

Ross, I.B. and Davidson J.F., The combustion of carbon particles in fluidised bed combustor, *Trans IChemE*, 1981, **59**, 108.

Ross, I.B., Patel, M.S. and Davidson J.F., The temperature of burning carbon particles in fluidised beds, *Trans. Inst. Chem. Eng.*, 1981, **59**(2), 83-88.

Saffer. M., Ocampo, A. and Laguerie, C., *Int. Chem. Eng.,1988,* **28,** 46-61.

Schafer, H.N., Pyrolysis of brown coal. 1. Decomposition of acid groups in coals containing carboxyl groups in the acid and cation forms., *Fuel*, 1979, **58**, 667-672.

Schafer, H.N., Pyrolysis of brown coal. 2. Decomposition of acid groups on heating in the range 100°C to 900°C., *Fuel*, 1979, **58**, 673-679.

Schobert, H.H., The chemistry of hydrocarbon fuels, Butterworth & Co Pub., England, 1990.

Schluter G.B., Zhang, D.K. and Agnew, J.B., Combustion of coal volatiles in a fluidised bed, *Proc. 4th annual conf., CRC Clean Power from Lignite* 1997, Report No. 97008, 91-96.

Schluter, G.B., Zhang, D.K. and Agnew, J.B., Fluidised bed combustion of brown coal char, *Proc. 3rd annual conf., CRC New Technology for Power Generation from Low Rank Coal*, 1996, Report No. 96016, 41.

Schluter, G.B., Linjewile, T.M. and Zhang, D.K., Measurement of CO/CO_2 product ratio from single particle combustion in a incipiently fluidised bed, *3rd Asian-Pacific Int. Symposium on Combustion and Energy Utilisation*, 1995, 366-371.

Sett, A. and Bhattacharya, S. C., *Applied Energy*, 1988, ***30***, 161-186.

Shaw, D.W., Zhu, X., Misra, M.K. and Essenhigh,R.H., Determination of global kinetics of coal volatiles combustion, *Twenty third Symposium (International) on Combustion*, The Combustion Institute, Pittsburgh, 1990, 1155-1162.

Sit, S.P. and Grace, J.R., *Chem. Eng. Sci.* , 1981, **36**, 327-335.

Srinivasan, R.A., Siramulu, S., Kulasekaran, S. and Agarwal P.K., Mathematical modeling of fluidised bed combustion-2: combustion of gases, *Fuel*, 1998, **77**, 1033-1049.

Smoot, L.D., *Coal Combustion and Gasification*, Plenum Press, New York, 1985.

Smoot, L.D. and Thurgood S.H., *Pulverised coal combustion and gasification*, Plenum Publishers, New York, 1979, 83-165

Souza-Santos M.L.de, *Fuel*, 1989, **68**, 1507.

Solomon P.R., and Colket, M.B., Coal Devolatilisation, *Seventeenth Symposium (International) on Combustion*, The Combustion Institute, Pittsburgh, 1979, 131-143.

Solomon, P.R., Fletcher, T.H., and Pugmire, R.J., Progress in coal pyrolysis, *Fuel*, 1993, **72**, 5, 587-597.

Stiles, D., and Kandiyoti, R., Secondary reactions of flash pyrolysis tars measured in a fluidised bed pyrolysis reactor with some novel design features, *Fuel,* 1989, **68**, 275-282.

Stubington, J.F., The role of coal volatiles in fluidised bed combustion, *J. Inst. Energy*, 1980, **53**, 191-195.

Stubington J.F. and Chan, S.W., Development of a simulated coal particle for the study of coal volatiles combustion in a fluidised bed, CHEMECA 86, Adelaide 19th-22nd Aug. 1986.

Stubington, J.F., and Sumaryono, Release of volatiles from large coal particles in a hot fluidized bed, *Fuel*, 1984, **63**, 1013-1019.

Stubington, J.F., and Linjewile, T.M., The effects of fragmentation on devolatilization of large coal particles, *Fuel*, 1989, **68**, 155-160.

Stubington, J.F., and Chan, S.W., On the phase location and rate of volatiles combustion in bubbling fluidized bed combustors, *Trans IChemE*, 68, Part A, 1990, 195-201.

Stubington, J.F., Chan S.W., and Clough, S.J., A Model for Volatile Release into a Bubbling Fluidised Bed Combustor, *AIChE Journal*,1990a, **36**, (1), 75-85.

Stubington J.F. and Chan, S.W. The Interpretation of O_2 probe measurements in fluidised bed combustion, *Journal of the Institute of Energy*, 1990b, 136-142.

Stubington J.F. and S.W. Chan, S.W., Experimental measurements of combustion of simulated coal volatiles in a bubbling fluidised bed combustor, *Fuel*, 1990c, **69**, 678.

Stubington, J.F., Huang, G., and Scaroni, A.W., Devolatilization times of mm-sized coal particles, *Fuel*, 1991, **70**, 1105-1108.

Stubington, J.F., Chui, T.Y. and Saisthidej, S., Experimental factors affecting coal devolatilisation time in fluidised bed combustion, *Fuel Sci. Tech. Int.*, 1992, **10**, (3). 397.

Stubington J.F. and Chan, S.W., Multiple discrete diffusion flame model for fluidised bed combustion of volatiles, *12th Int. FBC. Conf.* 1992.

Stubington, J.F., Ng, K.W., Moss, B., an Peeler, P.K., 1997, Comparison of experimental methods for determining coal particle devolatilisation times under fluidised bed combustor conditions, *Fuel*, **76**, (3), 1997, 233-240.

Sundaresan, S. and Amundson, N. R., *Chemical Engineering Science,* 1979b, **34**, 355-358.

Suuberg, E.M., Peters, W.A., and Howard, J.B., Product compositions and formation kinetics in rapid pyrolysis of pulverised coal - implications for combustion, *Seventeenth Symposium (International) on Combustion*, The Combustion Institute, Pittsburgh, 1979, 117-127.

Tia, S., Bhattacharya, S.C., and Wibulswas, P., Pyrolysis and volatile combustion of a single large lignite particle, *Energy*, 1991, **16**, (8), 1131-1146.

Toei, R., Matsuno, R., Hotta, H. and Fujine, Y.J., *Chem Engng Jpn.*, 1972, **25**, 219.

Tomeczek, J., and Kowol, J., Temperature field within a devolatilising coal particle, *Can. J. Chem. Eng.*, 1990, **69**, 286.

Tyler, R.J., Flash pyrolysis of coals. 1. Devolatilization of a Victorian brown coal in a small fluidised bed reactor, *Fuel*, 1979, **58**, 680-686.

Tyler, R.J., Flash pyrolysis of coals 2. Devolatilisation of bituminous coals in a small fluidised bed reactor, *Fuel*, 1980, **59**, 218-226.

Urkan, M.K., and Arikol, M., Burning times of volatiles from Turkish coals during fluidised bed combustion, *Fuel*, 1994, **73**, (5), 768.

Van der Vaart, D.R., The combustion of gas in a fluidised bed, *PhD Thesis*, University of Cambridge, England, 1985.

Van der Vaart, D.R., The chemistry of premixed hydrocarbon/air combustion in a fluidised bed, *Combustion and Flame*, 1988, **71**, 35-39.

Van der Vaart, D.R., Mathematical modelling of methane combustion in a fluidised bed, *Ind. Chem. Res.* 1992, **31**, 999-1007.

Van der Vaart, D.R. and Davidson, J.F., *Fifth Engineering Foundation Conference on Fluidisation*, 1986, 539.

Van Heek, K.H. and Hodek, W., Structure and pyrolysis behaviour of different coals and relevant model substances, *Fuel*, **73**, No. 6, 1994, 886-896.

Van der Honing, G., *Volatile and char combustion in large scale fluidised bed combustors*, PhD Thesis, University of Twente, The Netherlands, 1991.

Van Liere, J. and van der Burgt, M., Gasification-an alternative to natural gas, *The Chem. Eng.*, Jan. 1996, pp 15-18.

Wang, S.C. and Wen, C.Y., *AIChE. Journal*, 1972, **18**,1231.

Weimer, A. W. and Clough, D. E., 1981, *Chemical Engineering Science*, 1981, **36**, 549-567.

Wen, C.Y. and Tseng, H.P., *72nd Annual AIChE Meeting*, 1979, San Francisco, CA.

Wilke, C.R., *J. Chem. Phys.*, 1950, **18**, 517.

Wilson, J.S., Hallow, J. and Ghate, M.R., *Chem Tech.*, 1988, **18**, 123-128.

Winter, F., Prah, M.E., and Hofbauer, H., Temperature in a fuel particle burning in a fluidized bed: the effect of drying, devolatilization, and char combustion., *Combustion and Flame*, 1997, **108**, 302.

Woskobenko, F., Stacy, W.O. and Raisbeck, D., Physical structure and properties of brown coal in *The Science of Victorian Brown Coal: Structure, Properties and Consequences for Utilisation*" editied by R.A. Durie, Butterworth-Heinemann Ltd., Great Britain, 1991, 152-235.

Xu Y. and Tomita, A., The effects of temperature and residence time on the secondary reactions of volatiles from coal pyrolysis, *Fuel Processing Tech.*, 1989, **21**, 25-37.

Yanata, I., Makorin, K.E. and Glukhomanyuk, A.M., *Intl. Chem. Engng.*, 1975, **15**, 68.

Yan, H. M., Heidenreich, C. and Zhang, D. K, Mathematical modelling of a bubbling fluidised-bed coal gasifier and the significance of 'net flow', *Fuel,* 1998b, **77,** 1067.

Yan, H.M, Mathematical modelling of a bubbling fluidised-bed coal gasifier, CRC Report No. 99012, 1999.

Yan, H. M., Heidenreich, C. and Zhang, D. K, Modelling of bubbling fluidised-bed coal gasifiers, *Fuel*, 1999b, **78**, 1027-1047.

Yan, H. M., Heidenreich, C. and Zhang, D. K, Mathematical modelling of a bubbling fluidised-bed coal gasifier: Development of a non-isothermal model, *6th CRC annual conf., CRC New Technology for Power Generation from Low Rank Coal*, Report No. 99011, 1999c, pp79-84.

Yan, H. M. and Zhang, D. K, Modelling of fluidised-fed coal gasifiers: Elimination of char combustion product distribution coefficient by considering homogeneous combustion, *Chem. Eng. Proc.*, 1999d, (accepted for publication).

Yan, H. M. Heidenreich, C., and Zhang, D. K, Mathematical Modelling of a Bubbling Fluidized-Bed Coal Gasifier, *Proceedings, 7th Australian Coal Science Conference*, 1996, *287-293.*

Yan, H.M. and Rudolph, V., *Twenty sixth Symposium (International) on Combustion,* The Combustion Institute, Pittsburgh, 1995.

Yates, J.G., MacGilliver, M. and Cheesman, D.J., Coal Devolatilisation in Fluidised-Bed Combustors, *Chem. Eng. Sci.*, 1981, **35**, 2360.

Ye, D.P., Agnew, J.B. and Zhang, D.K., Gasification of two Australian Lignites with Carbon Dioxde and Steam, (submitted to *FUEL* for publication Nov. 1996).

Yoshida, K. and D. Kunii, Complex reaction in fluidised beds - simulation of gasification, *Journal of Chem. Eng. of Japan*, 1974, **7**, (1), 34-39.

Zhang, D.K., Jackson, P.J. and Vuthaluru, H.B., Low-rank coal and advanced technologies for power generation, *Engineering Foundation Conference: Impact of mineral Impurities in solid fuel combustion*, Hawaii, 2-7 November, 1997.

Zhang, J.Q., Becker, H.A., and Code, R.K., Devolatilisation and Combustion of Large Coal Particles in a Fluidised Bed, *Canadian Journal Chem. Eng.* 1990, **68**, 1010.

PUBLICATION LIST

REFEREED JOURNAL PUBLICATIONS

Ross, D.P., Laurent, P.J., Schluter G.B., and Zhang, D.K., The influence of volatilies on the combustion rate of Loy Yang char in a fluidised-bed, *Dev. Chem. Eng. Mineral Process*, 1999, **7**(5/6), 577-591.

Ross, D.P, Heidenreich, C.A. and Zhang, D.K., Devolatilisation times of large coal particles in a fluidised-bed, *Fuel*, 2000, **79**(8), 873-883.

Ross, D.P, Yan, H.M. and Zhang, D.K., An experimental study of propane combustion in a fluidised-bed gasifier, *Combustion and Flame*, 2000, (in press).

Ross, D.P, Yan, H.M. and Zhang, D.K., Modelling of a laboratory-scale bubbling fluidised-bed gasifier with feeds of both char and propane, *Fuel*, 2000, (submitted for publication).

EXTERNAL CONFERENCE PAPERS

Ross, D.P., Laurent, P.J., Schluter G.B., and Zhang, D.K., The influence of volatilies on the combustion rate of Loy Yang char in a fluidised-bed, Joint Tech. Workshop Thermal Energy Eng. & Environment, Wuhan, P.R. China, April, 1999, 2.

Ross, D.P, Yan, H.M. and Zhang, D.K., Mathematical modelling of propane combustion in a fluidised-bed gasifier, 9th Australian Coal Science Conference, Aust. Inst. Energy, 26th-29th November, Brisbane, Australia, 2000.

Yan, H.M., **Ross, D.P.**, Jackson, P.J. and Zhang, D.K., Development of a Non-Isothermal Model for Bubbling Fluidised Bed Coal Gasifiers, a paper offered to the 28th Symposium on Combustion, University of Edinburgh, 2000.

Zhang, D.K., **Ross, D.P.,** and Yan, H.M., Behaviour of propane combustion in a $H_2O/O_2/N_2$ environment in a fluidised-bed gasifier, a paper offered to the 28th Symposium on Combustion, University of Edinburgh, 2000.

Ross, D.P. and Zhang, D.K., The effective thermal conductivity of ceramic die coats used in low pressure die casting, *Chemeca 96*, Proc. 24th Aust. & N.Z. Chem. Eng. Conf., Sydney Australia 1996, Vol 1, pg 19.

CRC Annual Conference Papers

Ross, D.P. Yan, H.M. and Zhang, D.K., Mathematical modelling of propane combustion in a fluidised-bed gasifier, Seventh Annual Conference, Waite Campus, University of Adelaide, 2000, June 21-23.

Ross, D.P. and Zhang, D.K., Devolatilisation times of large Bowman and Morwell coal particles, Sixth Annual Conference, Monash University, Melbourne, 1999, June 22-23, 139-144.

Ross, D.P. and Zhang, D.K., The influence of volatiles on the combustion rate of char, Fifth Annual Conference, Monash University, Melbourne, 1998, June 25-26, 121-126.

Ross, D.P. and Zhang, D.K., The fate of coal voltiles in fluidised-bed gasification of low-rank coal, Fourth Annual Conference, Swinburne University of Technology, Melbourne, 1997, June 26-27, 121-128.

Ross, D.P. and Zhang, D.K., Devolatilisation and volatile matter combustion under fluidised bed gasification conditions, Third Annual Conference, Waite Campus, University of Adelaide, Adelaide, 1996, June 20-21, 81-87.